ANALYSIS AND DESIGN OF THE LR55 TRACK SYSTEM

BY

FOUAD ABBAS MOHAMMAD

BSc MSc (Civil Eng) MSc (Structural Design)

A THESIS SUBMITTED TO LIVERPOOL JOHN MOORES UNIVERSITY FOR THE DEGREE OF DOCTOR OF PHILOSOPHY

LIVERPOOL JOHN MOORES UNIVERSITY
SCHOOL OF THE BUILT ENVIRONMENT
LIVERPOOL
UNITED KINGDOM

JUNE 1998

PAGE/PAGES EXCLUDED UNDER INSTRUCTION FROM UNIVERSITY

FOR THE MEMORY OF MY FATHER

AND

THE LOVE OF MY MOTHER

ACKNOWLEDGEMENT

The author wishes to express his sincere gratitude to Dr H. Al-Nageim, Prof. L. Lesley and Dr D. Pountney for their continual guidance, valuable discussions and advice throughout the whole period of this project.

Special thanks are reserved to Prof. D. Jaggar for providing generous research facilities and support all the time.

The author also wishes to record his indebtedness to Prof. Peter Morgan, Director of the School of Built Environment, and the other members of staff for their help and encouragement.

The author highly appreciates the collaboration and assistance of the Material Testing and Structural Laboratory technicians during the preparation of the experimental work involved in this project.

Finally, the author is very grateful to his family and friends for their understanding and moral support.

ABSTRACT

In this thesis, an attempt was made to analyse and design a new light rail track system known as the low profile rail LR55 track system. The main components of the LR55 track system are: low profile steel rail, elastomeric pad and concrete trough. This innovative system is a solution to overcome the drawbacks of the existing light rail track systems due to its main characteristics and unique features.

The result of the investigation concerning the analysis phase was the development of a mathematical model, where the LR55 track system was treated as multilayer beams on elastic foundations. This model was solved both analytically using a classical calculus method and numerically using one dimensional finite element method. At the design phase, a nonlinear optimisation technique based on the Complex method was adopted to find the minimum area of a pre-tensioned prestressed concrete trough section satisfying the serviceability and ultimate states as per BS 8110 and Tarmac Precast Concrete Limited requirements for the most critical loading and boundary conditions. The performance of the rail, elastomeric pad and track base were routinely examined and found to be satisfactory under the same critical loading and boundary conditions.

The mathematical model was then validated experimentally through a series of static non-destructive tests on a full-scale 6 m long LR55 track model including the case of 1 m collapsed foundation simulation. The results obtained from these experiments compared well with the theoretical solution. The experimental work also ensured the safety of the theoretical design of the LR55 track system as no sign of failure occurred to any of the track components when the track model was subjected to a maximum service load around 100 kN.

A number of purpose written computer programs in FORTRAN 77 for P.C. machines were set up to process all the calculations involved during the analysis and design procedures of the LR55 track system with high level of efficiency in terms of speed and accuracy. These programs were validated through comparison with the works of others and with commercially available finite element packages.

CONTENTS

LIST OF FIGURES

LIST OF TABLES

LIST OF SYMBOLS

A = cross-sectional area of the element

A_b = area of the base contributed by each spring

A_c = cross-sectional area of the concrete trough based on gross uncracked section

A_f = surface area of the formwork per metre length of the concrete trough

A_p = contact area between the pad and the rail contributed by each spring

A_{ps} = total area of the prestressing tendons

A_{sv} = total area of shear reinforcement (links) at the neutral axis, at a section

A_1 = cross-sectional area of the rail section

A_2 = cross-sectional area of the rail section

B = total width of the concrete trough section

b = breadth of the section at the level where shear stress v is calculated

b_{cj} = width of concrete strip

b_v = breadth of the member, or for T-, I- and L-beams, the breadth of the rib

b_1 = part of width dimension of the concrete trough section as defined in Fig.(3.3)

b_2 = part of width dimension of the concrete trough section as defined in Fig.(3.3)

b_3 = part of width dimension of the concrete trough section as defined in Fig.(3.3)

b_4 = part of width dimension of the concrete trough section as defined in Fig.(3.3)

b_5 = part of width dimension of the concrete trough section as defined in Fig.(3.3)

C_c = unit cost of the concrete material

C_f = unit cost of the formwork

C_{ps} = unit cost of the prestressing tendons

C_{sv} = unit cost of the shear reinforcement

D = total depth of the concrete trough section

d = distance from the extreme compression fibre to the centroid of the tendons in the tension zone, i.e. effective depth of the concrete section

d_j = distance from tendon layer j to the extreme compression fibre

d_m = maximum distance between any two points of the design variables

d_t = distance from the extreme compression fibre either to the longitudinal bars or to the centroid of the tendons which is ever is greater

d_1 = part of depth dimension of the concrete trough section as defined in Fig. (3.3)

d_2 = part of depth dimension of the concrete trough section as defined in Fig. (3.3)

d_3 = part of depth dimension of the concrete trough section as defined in Fig. (3.3)

E = Young's modulus of the beam

E_{ci} = Young's modulus of concrete at transfer (initial)

EI_1 = bending rigidity of the upper beam (rail)

EI_2 = bending rigidity of the lower beam (concrete trough)

E_p = Young's modulus of the pad

E_{ps} = Young's modulus of prestressing tendon

E_1 = Young's modulus of the rail material

E_2 = Young's modulus of the concrete

e = eccentricity of centroid of tendons from centroid of section

e_j = eccentricity of tendon layer j

F_c = total compressive force resisted by concrete

F_{cj} = axial compressive force resisted by concrete strip j

F_{pj} = force resisted by tendon layer j

F_{ps} = total force resisted by the whole prestressing tendons

f_{ci} = characteristic cube strength of concrete at transfer (initial)

f_{cj} = average stress of concrete strip j

f_{cp} = concrete compressive stress at the location of maximum shear stress within the section due to effective prestress only

f_{co} = concrete compressive stress at the centroid of prestressing tendon

f_{cs} = allowable compressive stress at service

f_{ct} = allowable compressive stress at transfer

f_{cu} = characteristic cube strength of concrete at service (at 28 days)

f_{pb} = design effective prestress in the tendons

f_{pbj} = stress at the centroid of tendon layer j

f_{pe} = design effective prestress in the tendons after all losses

f_{pi} = initial prestressing stress in the tendons before losses

f_{pt} = concrete compressive stress at the extreme tension fibre due to effective prestressing force

f_{pu} = characteristic strength of a prestressing tendon

f_t = maximum design principal tensile stress

f_{ts} = allowable tensile stress at service

f_{tt} = allowable tensile stress at transfer

f_{yv} = characteristic yield strength of shear reinforcement

f_1 = stress at the extreme bottom fibre of the concrete trough

f_2 = stress at the extreme top fibre of the concrete trough

$g_j(\{x\})$ = behavioural (implicit) constraint

h = depth below the face of sleeper (inches) as defined in eq. (2.12), or
= total depth of a prestressed concrete rectangular, T-, I- and L-section as defined in eq. (4.57)

h_p = thickness of the pad

I = moment of inertia of the beam

I_1 = moment of inertia of the rail

I_2 = moment of inertia of the concrete trough

I_X = moment of inertia of the section about the X-axis

I_{XY} = product moment of inertia of the section about X, Y axes

I_Y = moment of inertia of the section about Y-axis

I_c = moment of inertia of the section about the centroidal axis

I_{max} = maximum moment of inertia of the section

I_{min} = minimum moment of inertia of the section

I_x = moment of inertia of the section about the x-axis

I_{xy} = product moment of inertia of the section about x, y axes

I_y = moment of inertia of the section about the y-axis

I_1 = moment of inertia of the rail section

I_2 = moment of inertia of the concrete trough section

K = a factor determined by experiment

K_t = a coefficient for the type of tendon

K_{1h} = stiffness of pad horizontal spring

K_{2h} = stiffness of track base horizontal spring

K_{1v} = stiffness of pad vertical spring

K_{2v} = stiffness of track base vertical spring

k = track foundation modulus

k_b = foundation modulus of the soil corresponding to full size foundation

k_{plate} = modulus of subgrade reaction of the soil obtained from plate-load test

k_{sh} = modulus of horizontal (shear) reaction of the base

k_1 = pad modulus

k_2 = track base modulus

[K] = global stiffness matrix of the structure

$[K]_{1h}$ = stiffness matrix of pad horizontal spring

$[K]_{1v}$ = stiffness matrix of pad vertical spring

L = length of the precast concrete trough unit

L_e = length of a track element

L_{eff} = effective length (unsupported length) of the member

L_j = jth component of the lower limit vector {L}

L_p = portion of pad length allocated for each hypothetical spring

{L} = lower limit vector of the design variable point {x}

M = design bending moment at the section due to ultimate load

M_c = resisting moment of concrete compression area

M_{cj} = moment resisted by concrete strip j

M_L = Bending moment at the left end of the element

M_{max} = maximum bending moment of the beam

M_o = bending moment necessary to produce zero stress in the concrete at the extreme tension fibre

M_{pj} = moment resisted by tendon layer j

M_{ps} = resisting moment of the prestressing steel

M_R = Bending moment at the right end of the element

M_s = bending moment due to external applied load including self weight at service

M_t = bending moment due to self weight of the member at transfer

M_u = ultimate moment capacity of concrete section

M_x = Bending moment about x-axis, sagging positive

$(M_{s+})_{app}$ = applied positive (sagging) moment of the section at service

$(M_{s-})_{app}$ = applied negative (hogging) moment of the section at service

$(M_{t+})_{app}$ = applied positive (sagging) moment of the section at transfer

$(M_{t-})_{app}$ = applied negative (hogging) moment of the section at transfer

$(M_{s+})_{pro}$ = provided positive (sagging) moment of the section at service

$(M_{s-})_{pro}$ = provided negative (hogging) moment of the section at service

$(M_{t+})_{pro}$ = provided positive (sagging) moment of the section at transfer

$(M_{t-})_{pro}$ = provided negative (hogging) moment of the section at transfer

$(M_{s+})_1$ = provided positive (sagging) moment of the section controlled by bottom fibre stress at service

$(M_{s+})_2$ = provided positive (sagging) moment of the section controlled by top fibre stress at service

$(M_{s-})_1$ = provided negative (hogging) moment of the section controlled by bottom fibre stress at service

$(M_{s-})_2$ = provided negative (hogging) moment of the section controlled by top fibre stress at service

$(M_{t+})_1$ = provided positive (sagging) moment of the section controlled by bottom fibre stress at transfer

$(M_{t+})_2$ = provided positive (sagging) moment of the section controlled by top fibre stress at transfer

$(M_{t-})_1$ = provided negative (hogging) moment of the section controlled by bottom fibre stress at transfer

$(M_{t-})_2$ = provided negative (hogging) moment of the section controlled by top fibre stress at transfer

M_1 = bending moment of the upper beam (rail)

$M_{1, max}$ = maximum bending moment of the upper beam (rail)

M_2 = bending moment of the lower beam (concrete trough)

$M_{2, max}$ = maximum bending moment of the lower beam (concrete trough)

N = axial force, compression positive

N_L = axial force at the left end of the element

N_R = axial force at the right end of the element

N_s = axial force in the section due to external applied load at service

N_t = axial force in the concrete trough section due self weight developed during lifting

n_c = total number of concrete strips in the compression zone

n_p = number of prestressing tendon layers within the concrete section

P = point load as defined in eq. (2.2), or

= prestressing force at the section considered at transfer (initial) as defined in eq. (4.4)

P_a = uniform bearing pressure (psi) over the sleeper face centreline

P_e = effective prestressing force at the section considered after all losses take place

P_x = pressure (psi) in the ballast at any distance x (inches) from the centreline

p = pressure on the soil due to applied load

p_1 = pressure on the upper foundation (rail pad)

p_2 = pressure on the upper foundation (track base)

{P} = applied load vector on the structure

Q = first moment of area above or below the level where shear stress v is calculated, taken about the centroidal axis of the section

Q_v = first moment of area above or below the level where maximum shear stress occurs, taken about the centroidal axis of the section

q = line force acting under the beam

q_1 = line force acting under the upper beam (rail)

q_2 = line force acting under the lower beam (concrete trough)

q_{max} = maximum line force acting under the beam

r_{max} = maximum radius of gyration of the section

r_{min} = minimum radius of gyration of the section

r = radius of gyration of the section

$r_{i,j}$ = a random number in the range 0 to 1

r_x = radius of gyration of the section with respect to x-axis

r_y = radius of gyration of the section with respect to y-axis

S_i = stiffness coefficient

s = variance for a set of design variable points

s_v = spacing of links along the member

t_c = thickness of concrete strip

U_j = jth component of the upper limit vector {U}

{U} = upper limit vector of the design variable point {x}

V = shear of the beam at any point x from the point load as defined in eq.(2.5), or = design shear force at the section due to ultimate load

V_c = design ultimate shear resistance of the concrete trough section

V_{co} = design ultimate shear resistance of the concrete trough section uncracked in flexure

V_{cr} = design ultimate shear resistance of the concrete trough section cracked in flexure

V_L = Shear force at the left end of the element

V_R = Shear force at the right end of the element

V_{max} = maximum shear force of the beam

V_{per} = maximum permitted shear force by the concrete trough section necessary to to prevent web crushing

V_{sv} = volume of shear reinforcement per metre length

V_1 = shear force of the upper beam (rail)

$V_{1, max}$ = maximum shear force of the upper beam (rail)

V_2 = shear force of the lower beam (concrete trough)

$(V_s)_{app}$ = applied shear force at service

v = shear stress at any level along the section measured from the centroidal axis of the section

v_{max} = maximum shear stress in the concrete trough section

W_r = rail width

w = uniformly distributed load

w_c = unit weight of the concrete trough section per metre run

w_s = unit weight of steel

X_i = X-coordinate of vertex i

X_{max} = X-coordinate of the extreme right fibre of the section

X_{min} = X-coordinate of the extreme left fibre of the section

X' = X-coordinate of the section centroid

x = x-coordiante of any point along the beam measured from the point load P as defined in eq. (2.1), or

= distance from the neutral axis to the point where stress is required, measured normal to the y-axis as defined in eq. (3.1), or

= depth of the neutral axis measured from extreme compression fibre as defined in eq. (4.26)

x_i = design variable

$x_{i,j}$ = jth component of point $\{x\}_i$

$x_{r,j}$ = jth component of point $\{x\}_r$

$\{x\}$ = vector of design variables

Y_i = Y-coordinate of vertex i

Y_{max} = Y-coordinate of the extreme top fibre of the section

Y_{min} = Y-coordinate of the extreme bottom fibre of the section

Y' = Y-coordinate of the section centroid

y = deflection of the beam in the vertical direction as defined in eq. (2.2), or
= distance from the neutral axis to the point where stress is required, measured normal to the x-axis as defined in eq. (3.1)

y_{cj} = distance from the neutral axis to the centroid of concrete strip j

y_{max} = maximum deflection of the beam

y_v = location of the maximum shear stress within the concrete trough section measured from the centroidal axis

y_1 = deflection of the upper beam (rail)

$y_{1, max}$ = maximum deflection of the upper beam (rail)

y_2 = deflection of the lower beam (concrete trough)

$y_{2, max}$ = maximum deflection of the lower beam (concrete trough)

Z = objective function

$Z_{x, bot}$ = elastic section modulus for the extreme bottom fibre

$Z_{y, left}$ = elastic section modulus for the extreme left fibre

$Z_{y, right}$ = elastic section modulus for the extreme right fibre

Z_1 = elastic section modulus for the bottom fibre of the concrete trough

Z_2 = elastic section modulus for the top fibre of the concrete trough

l_t = transmission length of the prestressing tendon

α = reflection factor

α_e = modular ratio

α_t = coefficient of thermal expansion of the material forming the element

β = angle between the lifting sling and the horizontal axis

Δf_{pcr} = loss in prestressing stress due to creep of concrete

Δf_{pes} = loss in prestressing stress due to elastic shortening

Δf_{psh} = loss in prestressing force due to shrinkage of concrete

ΔT = change in temperature, increase in temperature is positive

δ = deflection (settlement) of the soil due to applied load

δ_i = camber (instantaneous deflection) of the concrete trough unit due to initial prestressing

$\{\delta\}$ = displacement vector of the structure

ε_c = strain of concrete

ε_{cj} = strain of concrete strip j

ε_s = strain of prestressing steel

ε_{pbj} = total strain in tendon layer j

ε_{pe} = strain in the tendons due to effective prestressing

ε_{rj} = residual strain in tendon layer j

ε_s = strain of prestressing steel

ε_{sh} = shrinkage strain of the concrete

ε_{uj} = concrete strain at ultimate condition at the level of tendon layer j

ε_1 = tendon strain at stress of 0.8 f_{pu} /γ_m

ε_2 = tendon strain at stress of f_{pu} /γ_m

ϕ = wire or strand diameter

ϕ_{cr} = creep coefficient

γ = ratio of the overhang span to the total span length of the concrete trough unit

γ_m = partial safety factor for strength of materials;

= 1.5 (for concrete)

= 1.15 (for prestressing steel)

θ = slope of the beam at any point x from the point load

σ_{cri} = critical buckling stress

σ_z = bending stress at any point within the section, compression positive

ξ_i = convergence criterion

ψ = angle between x-axis and the principal axis corresponding to I_{max}

CHAPTER ONE
INTRODUCTION

1.1 General

Cities around the world are getting bigger and increasing in number. As living standards rise, more people purchase private automobiles and seek to use them for daily travel needs. This means that there is always a conflicting problem associated with the increasing volume of traffic generated in large cities and rising levels of economic activities. The impact of such a problem can be reduced by improving the public transport in light of the following schemes, (Lesley 1991 and 1993):

1. Applying market forces, i.e. charging for access to particular roads within the city centre. This will lessen the demand for road space and generate revenue to invest in improving the transport system. The tolled access (road pricing) has recently been introduced in Singapore, and Oslo and Bergen in Norway. However, since the political will to tax traffic congestion has always been weak, directed market forces are likely to be the least effective approach to improve public transport.
2. Employing traffic management schemes such as speed and parking controls and building new urban roads. Some big cities like Paris affirm the effectiveness of this method where new metro and regional railway lines have been built and bus lanes provided, thus increasing the speed of all traffic. Although the construction of new metro lines with tunnels away from traffic congested roads would be ideal, they are unfortunately very expensive and hence financially unfeasible to achieve particularly with cities around the world grappling with public expenditure cuts.
3. Using light rail transits in city streets, which can significantly help in improving the traffic flow. This is because a light rail track system can provide a capacity of 15,000 passengers per hour per single road lane whereas a private car road offers a maximum capacity of 2,250 passengers per hour per single road lane. In other words, around 650% increase in passenger flow can be gained with the case of light rail track system in comparison to private car only road, (Lesley 1991). Besides reducing traffic congestion, light rail systems in major cities can provide opportunities for minimising serious environmental problems, such as the level of

noise, vibration and air pollution. In this context, they might be genuinely regarded as environmentally friendly means of transport, i.e. "green transport".

To this end, opening a new light rail line is not cheap as the capital cost of constructing the track is high, especially those laid in public highways shared by road vehicles and requiring foundation of 500 - 700 mm deep excavation. In addition, there is the disruption to the urban fabric as city centre roads are closed for months while the tracks are installed, (Lesley 1991 and 1993). Therefore, a new light rail track system offering a competitive capital cost to conventional systems, and accelerating the construction period should be very attractive.

As a result of thorough examination of the existing street running track systems, a new light rail track system known as low profile rail LR55 track system was proposed by Professor Lewis Lesley of Liverpool John Moores University in 1989, (Lesley 1989). He stated that the development of this new system promises to shorten installation period, minimise disruption to highway pavements and underground services, expedite restoration to traffic and, more importantly, reduce the total construction cost as compared to the conventional ones, (Lesley 1991).

The main components of the LR55 track system are: low profile steel rail, elastomeric pad and concrete trough. After a few experiments and desk analysis, based on a practical experience of the team initially involved with the design of the LR55 track system, the shape and size of the rail was fixed and a tentative geometrical cross section was suggested for the concrete trough, (Lesley 1993 and 1994).

However, there is a need for an elaborate theoretical investigation supported by extensive experiments including full-scale tests in order to develop confidence in its operational service and gain public acceptance for this new light rail track system.

Accordingly, the work presented in this thesis is an important step in exploring in depth both at theoretical and experimental levels, the structural behaviour of the LR55 track system and its responses under the effect of applied loads, and consequently to provide

safe and adequate design of the track system that could be competitive to the conventional ones.

1.2 Purpose and Scope

The purpose of the work described in this thesis is to develop a mathematical model for the analyse and design of the LR55 track system and then to validate it experimentally using full scale laboratory tests on a physical 6 m long track model.

A further important and closely related goal to the main objective was accomplished, which is the development of a number of purpose built computer programs written in FORTRAN 77 for P.C. machines. These programs might be regarded as an integrated package for processing all the calculations involved during the analysis and design procedures of the LR55 track system with high efficiency in terms of speed and accuracy. The list of the programs is as follows:

- SECT: A program for determining the cross-sectional properties of any shape including the LR55 rail, concrete trough and voided sections.
- TROUGH: A program for calculating all the characteristics of a given pre-tensioned prestressed concrete trough section that satisfies the serviceability (transfer and service) and ultimate limit states requirements of BS 8110 (1985) and Tarmac Precast Concrete Limited.
- MLBOEF: A program for the analysis of the LR55 track system modelled as multilayer beams on elastic foundations, based on the analytical solution of the governing differential equation of the system.
- LR551D: A program for the analysis of the LR55 track system modelled as mulitlayer beams on elastic foundations, based on the numerical solution of one dimensional finite element idealisation of the suggested mathematical model.
- OPTIM: A nonlinear structural optimisation program based on the Complex method, for finding the minimum cross-sectional area of a pre-tensioned prestressed concrete trough precast units satisfying all the imposed constraints due to the serviceability (transfer and service) and ultimate limit states requirements of BS 8110 (1985) and

Tarmac Precast Concrete Limited for the most critical loading and boundary conditions experienced by the track system.

The scope of this project broadly falls into two parts: theoretical study and experimental work as briefly described below.

Chapter two discusses the basics of railway track engineering including the historical development of railway systems, types and characteristics of rail supports, the concept and the various kinds of light rail track systems and the sources of track loading. A literature review covering the analytical and numerical methods of track analysis is also presented in this chapter.

Chapter three presents the general description and unique features of the low profile rail LR55 track system and its components namely, the LR55 rail, elastomeric pad and concrete trough. A full description of the computer program SECT is given in this chapter.

Chapter four deals with the derivations of the necessary equations required for determining the characteristics of a pre-tensioned prestressed concrete trough section at transfer, service and ultimate conditions according to BS 8110 (1985) and Tarmac Precast Concrete Limited requirements. Due to the non-standard shape of the concrete trough, a numerical procedure was developed to calculate the ultimate moment capacity (sagging and hogging) of the section. The method is so general that it can be easily employed to solve a wide range of geometrical shapes such as rectangular, T- and U-sections. The computer program TROUGH is presented in this chapter.

Chapter five is concerned with the development of a mathematical model where the LR55 track system was treated as multilayer beams on elastic foundations. The governing differential equation of the system was solved analytically using classical calculus, and the computer program MLBOEF was set up accordingly. Several examples were demonstrated to visualise the response of the track system in terms of deflection, moment, shear and pressure under single and multiple axle loads and for a range of base and pad moduli.

The mathematical model of the track system was extended in chapter six to include a numerical solution based on one dimensional finite element method and the development of the computer program LR551D for this particular purpose. This numerical technique has special features by which a wide range of practical track problems can be efficiently tackled such as nonlinearity due to track base separation (uplift), existence of a soft patch or cavity underneath the track system, combined effect of vertical wheel load, horizontal traction load, track self weight and temperature variation. Several examples were solved for two specific reasons: First, to prove the correctness of the LR551D program through comparing the numerical results with those obtained from the analytical solution (MLBOEF program) and commercially available finite element packages ANSYS and ABAQUS. Second, to define the most critical load cases that govern the design of the LR55 track components.

Chapter seven involves with the design of the LR55 track system. A nonlinear structural optimisation technique based on the Complex method was followed to find the minimum area of the pre-tensioned prestressed concrete trough section satisfying the serviceability and ultimate limit states as per BS 8110 (1985) and Tarmac Precast Concrete Limited requirements for the most critical loading and boundary conditions experienced by the track system. The rail, elastomeric pad and track base were systematically checked and found to be satisfactory under the same critical loading and boundary conditions.

The experimental work, including a series of plate-load tests and full-scale tests on a 6 m long track model, is described in chapter eight. A comparison between the experimental and theoretical results was made which proved the validity of the mathematical model and hence ensuring the safety and adequacy of the proposed design of the LR55 track system.

Finally, chapter nine summarises the main conclusions of this thesis and recommends a number of areas for further research and investigation.

CHAPTER TWO
RAILWAY TRACK ENGINEERING

2.1 Definition

A railway track system can be defined as a load-distributing structure, which conventionally consists of a discrete system made up of rails, sleepers, ballast and subgrade. Thus, its main function is to support traffic loading safely on the principle of stress reduction, layer by layer. The greatest stress occurs between the wheel and the rail. The rail absorbs and distributes wheel loads to the sleepers through a base plate or resilient pad with diminished pressure. The sleepers distribute the load to the ballast, the ballast distributes the load to the subgrade and eventually the load is distributed to the natural ground in which the stresses will be several orders smaller than that at the contact area between the wheel and rail. Fig. (2.1) shows a typical cross-section of a conventional track system.

A railway track has several other functions. It acts as a guidance system to the trains, a carrier of signalling messages and a return path for current in electrified systems. For this reason a wide range of parties both within and without railway engineering organisation itself, take an interest in track design.

Track systems have been built for a variety of purposes, some economic and others as part of a country's military establishment. Today railways play a vital role in shaping the infrastructure and constitute the backbone of the transportation system of many countries.

2.2 Historical View

Railway tracks have taken various forms and their development across history came mostly through trial and error and incremental improvement. The following summarises the evolution of track systems since the early ages.

Wooden railways with horse-drawn wagons were the first types of track systems used in coal mines during the early sixteenth century. It is most likely that German miners brought this idea to the collieries of Northumberland in Britain about 1600, (Kirby et al 1956).

By the 1670's, timber railways were laid from the colliery to the river exactly straight and parallel. The rails were formed of oak, and connected to cross timbers of the same material. The rails were 101.6 mm (4 in) deep, and 101.6 - 127 mm (4 - 5 in) wide, laid parallel, 914.4 - 1219.2 mm (3 - 4 ft) apart, in length of 1.829 m (6 ft). The cross sleepers were 1.829 m (6 ft) long by 101.6 - 127 mm (4 - 5 in) deep and 127 mm (5 in) wide, laid about 609.6 mm (2 ft) apart between centres. The rapid abrasion and wear of rails led to the placing of an additional rail upon the first one. The second rail became the wearing piece, and could be renewed with facility; whilst the increased depth afforded by it allowed for the covering of the sleepers by the soil, and their protection from the horses' feet. The wearing rails were made of hard wood 1.829 m (6 ft) long by 101.6 - 152.4 mm (4 - 6 in) deep. The under rails were at first made of oak and were subsequently made of fir. The next achievement was the introduction of renewable metal strips made of wrought iron, fastened to the timber rails, (Clark 1894). Fig. (2.2) shows some forms of timber railway at the early days.

In 1789, rails like beams were made of cast iron, but given a deeper section in the middle of their span between sleepers in order to sustain heavier loads. From their appearance, they were known as fish-belly rails, (Kirby et al 1956, Morgan 1971). The early development of iron rail is presented in Fig. (2.3).

The first railway chartered for the use of the public was built from the Thames River at London southward 12.875 km (8 miles) to Croydon, opened in 1803, later extended and maintained until 1846, (Cope 1993).

In 1821 George Stephenson was planning the world's first Steam-hauled passenger carrying railway from Stockton to Darlington and this was opened to the public in 1825. The rails were 4.572 m (15 ft) long carried in chairs on stone sleepers set at 914.4 mm (3 ft) spacing and weighed 13.89 kg/m (28 lb/yd). These rails were T-shaped, 50.88 mm (2

in) deep at their ends and bullied to a depth of 82.55 mm (3.25 in) in the middle of the space between the sleepers. The dimensions between the running edges of the rails, i.e. track gauge, was determined to be 1435 mm (4 ft 8.5 in) which became the standard world gauge accepted these days, (Kirby et al 1956).

In 1830 the Liverpool and Manchester Railway was opened, following a somewhat similar form of construction to that used for the Stockton and Darlington Railway. The rails weighed 17.36 kg/m (35 lb/yd). Later, a 24.8 kg/m (50 lb/yd) rail was introduced and eventually replaced by a 37.2 kg/m (75 lb/yd) rail. The justification for using heavier and hence stronger rails was the rapid growth of larger, more powerful and therefore heavier locomotives, (Rolt 1968).

Since 1830's, the construction of railway system got under way gradually in several European countries. In 1831, the Lyons-St. Etienne Railway was introduced using steam locomotives. By 1842, the French government was planning 9 lines, 7 to radiate from Paris. German lines began with the Nürnberg-Fürth road in Bavaria, opened in 1835. Holland joined Amsterdam and Harmelen in 1839. Russia, Austria, Italy and Spain also laid similar plans during that period. Most of these early equipment and the contractors for these European projects were British, (Kirby et al 1956).

In the United States, 4.828 km (3 mile) railway in Quincy, Massachusetts was one of the first railroads built in 1826 to carry granite from the quarry to the wharf. The first American tramway was the New York and Harlem Line, opened in 1832, (Clark 1894).

In 1835 Joseph Locke, one of Stephensons pupils, designed the double-headed rail with both heads of the same dimensions. This rail was first put into service on the Grand Junction Railway that linked Liverpool and Manchester with Birmingham. Locke's idea was that when one rail head had worn down under traffic the rails could be turned upside down in the chairs and the other head used. In practice, however, it was found that the lower head could not be used satisfactorily, because it had become indented where it rested in the chairs. So the design of the rail was changed. Instead of a symmetric section, the upper head was enlarged to give the longest possible life under traffic, while the lower head was reduced to a small foot which rested in the chair. This type of the

rail was known as "bull-head" (BH), see Fig. (2.4). The Shropshire Union Railway, opened in 1848 was probably the first line to use BH rails, (Cope 1993).

In 1836 Charles Vignoles designed a different type of rail which bears his name to this day. This is similarly shaped head, but below it is spread out into a wide, flat foot. For this reason it is often called a "flat-bottomed" (FB) rail, see Fig. (2.5). The main advantage of the FB rail over the BH rail of equivalent weight is its greater lateral stiffness. It was also recognised that the fastenings available for FB track were more effective than the crude dog spikes of earlier years. This is why the FB rail has been accepted as a standard type of section in British railways since 1948, (Cope 1993).

As heavier rail sections were finding favour so too were longer rails, primarily to reduce the number of joints. By the turn of the century the bulk of the mileage was laid with 13.716 m (45 ft) lengths. By 1910, the London and North Western Railway had standardised on a rail length of 18.288 m (60 ft), (Cope 1993).

The next big improvement in the railway was the substitution of steel for wrought iron rails due to the continuing increase of weight and speed of the trains. In 1857 the first steel rails were laid on a busy crossover of the Midland Railway at Derby. The traffic at this point was so heavy that it had been necessary to replace wrought iron rails every 3 months, whereas the new steel rails lasted for 16 years, (Rolt 1968, Cope 1993).

The first stretch of continuously welded rails (CWR) over 1.609 km (1 mile) in length was laid in 1955 by the Southern Region on the West of England main line near Crewkerne. Such a success was attributed to the invention of electric arc welding and the production of a relatively higher strength rail that was capable of safely sustaining thermal stresses developed during hot weather without buckling. By the mid 1960's the CWR were introduced in all suitable main lines of the British Rail. The change to CWR was accompanied by the effective abandonment of softwood sleepers in favour of either prestressed monoblock concrete sleepers or hardwood sleepers. At the same time the spike fastenings came to be regarded as obsolete, and after many trials Pandrol fastenings became standard, (Rolt 1968, Cope 1993).

2.3 Rail Supports

The rails are basically supported by structures made of timber, steel or concrete. The main functions and requirements of these structures are:

1. Providing support and fixing possibilities for the rail and fastenings.
2. Sustaining rail loads and transferring them as uniformly as possible to the track bed.
3. Ensuring lateral and longitudinal stability of the track system.
4. Maintaining track gauge and rail alignment both horizontally and vertically.
5. Providing adequate electrical insulation between the rails.
6. Being capable of resisting weathering effect over a long period of time.

The main types of the rail supports and their characteristics are presented briefly in the following sections.

2.3.1 Timber Sleepers

Timber sleepers have been used for rail support since the early days of railways. Timber sleepers are prismatic in shapes and are generally 250 - 300 mm wide, 125 - 175 mm deep and 2500 - 2700 mm long. The weight of an individual timber sleeper is about 100 kg, which is an advantage as it can be replaced manually. The timber sleeper spacing is usually between 550 - 700 mm. The total service life of timber sleepers ranges between 5 - 50 years depending on the species of the timber (oak, pine, fir .. etc.), the traffic loading, weather condition, type of treatment against vegetative and insect enemies, the quality of track construction including type of rail, fastenings and track base and the standard of the track maintenance, (Hay 1982, Esveld 1989, Cope 1993).

2.3.2 Steel Sleepers

Steel sleepers are widely used in Africa, South America, Asia and in some parts of Europe. They are first made of flat plates rolled into trough shapes. Fig. (2.6) shows some types of steel sleepers produced by British Steel Track. Steel sleepers have some notable advantages which are, (Esveld 1989, Cope 1993):

1. The average service life of steel sleeper is well over 50 years.
2. When steel sleepers are damaged for any reason, they can readily be repaired by pressing and/or welding, i.e. they have positive residual value.

3. Steel sleepers have great dimensional accuracy and give high consistency of track gauge both at installation and during subsequent service.
4. They provide good anchorage to the track because of their inverted trough shapes where the ballast is packed inside as well as around them.
5. Steel sleepers pack neatly into bundles and thus simplify all handling and transport operations.
6. Steel sleepers do not burn or suffer from exposure to dry heat and they are free from decay and insect attack which is extremely beneficial in tropical climates.

However, steel sleepers are now only used on a very small scale due to the following disadvantages (Esveld 1989, Cope 1993):

1. Relatively high price.
2. Need for special tamping and lining machines owing to the hollow shape of the cross-section and the spaded ends.
3. Subject to rust and wear around the fastenings in which the latter become loose and require frequent bolt tightening and renewal.
4. Indispensable need for high quality electrical insulations which is relatively expensive.
5. Tendency to degrade soft ballast more rapidly than wooden sleepers, hence the use of hard stone is preferred to steel sleepers.

2.3.3 Concrete Sleepers

The first experiment with reinforced concrete sleepers was made over 100 years ago. Concrete sleepers were initially designed in France in 1884. The first recorded use of concrete sleepers in the United States was 1893, (Weber 1969, Hanna 1979). In Britain, trials with reinforced concrete sleepers were made at various times up to the Second World War. In 1941, two designs of reinforced concrete sleepers were made and put in a branch near Derby. In the next year, 100 reinforced concrete sleepers were put in the mainline near Watford and survived for just 10 days since they could not withstand the dynamic loading from main line trains, (Scott 1976, Taylor 1993).

Under the pressures of timber shortages during the Second World War and owing to the introduction of continuously welded rail, the advent of prestressing techniques and

improvement in concrete technology, a programme was set up in the UK for developing prestressed concrete sleepers. The first precast pre-tensioned concrete sleepers in the world were produced and put in the west coast at Cheddington in 1943. This achievement enabled the go-ahead to be given for the building of the first factory in the world at Tallington for the large scale commercial production of prestressed concrete sleepers in 1943-1944, (Browne 1985). It is worthwhile to mention that the factory was originally managed by Dow Mac and has been taken over recently by Tarmac Precast Concrete Limited. The latter is also involved with the production of the concrete trough sample for experimental purposes conducted in the present work.

The first use of prestressed concrete sleepers on American railways was in 1960 when 500 were installed on the Atlantic Coastline Railroad and 600 on the Seaboard Air Line Railroad, (FIP 1987).

In the past 20 some years concrete sleepers have gained wider international acceptance for several reasons including, (Weber 1969, Hanna 1979, Esveld 1989, Cope 1993):

1. Experience to date indicates that the use of concrete sleepers are desirable for economic reasons as well as for the superior structural properties that add considerably to the overall stability and performance of the track structure.
2. The enhanced stability of concrete sleepered track reduces the incidence of derailments and their severity is reduced by modern fastenings that hold gauge well during derailment.
3. Increased use of mechanised track-laying and renewal equipment has overcome the difficulty of handling heavy concrete sleepers. In fact, it has been established that the heavy weight sleeper (200 - 300 kg) is used to advantage in connection with stability of continuously welded rail (CWR) track.
4. Softwood sleepers are often unable to withstand the stresses in modern main-line track and good quality hardwood is increasingly expensive and difficult to obtain. Moreover, concrete sleepers have a generally longer service life than their wooden counterparts.
5. Concrete sleepers are relatively simple and cheap to manufacture with a great freedom of design and construction as compared to steel sleepers.

6. Once installed, there is little preventative maintenance required for concrete sleepers, though the fastenings may need periodic attention. The higher labour costs and intensive track use nowadays necessitate reduced frequency of maintenance cycles.
7. Whilst concrete is a semiconductor, adequate insulation for track circuits can be achieved by incorporating appropriate insulation components into the fastenings without difficulty and at relatively low cost.

2.3.3.1 Pre-tensioned Concrete Monoblock Sleepers

Pre-tensioned concrete monoblock sleepers are normally produced by a long line method in which several moulds are set end to end on a prestressing bed. The prestressing tendons are positioned and tensioned between two abutments located at the ends of the bed. Then concrete is placed in the forms, vibrated and cured. After the concrete has reached a specified strength, the tendons are cut, thus transferring the tension in the tendons into the concrete as a compressive load. This method is seen as ideal for mass production, but it needs high investment, (FIP 1987, Cope 1993).

Pre-tensioned concrete monoblock sleepers are today the most widely used type and account for about 80 per cent of the world's annual prestressed concrete sleeper production, (Hanna 1979). A typical diagram for a pre-tensioned monoblock sleeper is shown in Fig. (2.7).

2.3.3.2 Post-tensioned Concrete Monoblock Sleepers

Post-tensioned concrete monoblock sleepers are produced by an instant demoulding method in which the concrete is cast in a mould and is provided with a duct. When the concrete has attained the required strength, high tensile steel bars are inserted into the duct, tensioned and anchored to the ends of the sleeper by some form of locking system. Finally, the ducts are filled with cement grout to protect the steel bars from corrosion. This method of manufacture requires less capital-investment than the case for a pre-tensioned sleeper, and lends itself to relatively small scale production, (FIP 1987, Cope 1993).

Post-tensioned sleepers were originally developed in Germany and the principal users today are Germany, Austria, Finland, Italy, India, Turkey and Mexico, (FIP 1987). Fig. (2.8) presents a diagram for a typical post-tensioned sleeper.

2.3.3.3 Twin-block Concrete Sleepers

Twin-block concrete sleepers consist of two reinforced concrete blocks connected together by a steel tie bar. The latter is made of normal quality rail steel to provide adequate resistance to fatigue and corrosion. Twin-block sleepers are produced by an instant demoulding method similar to post-tensioned sleepers except that the tie bar is surrounded by a steel spiral and reinforcement grids positioned above and below the tie bar are placed in a mould. Low workability concrete is then cast in the mould around each end of the tie bar and vibrated thoroughly. When compaction is complete the sleeper is demoulded and cured. Normally a steam chamber is used for curing to avoid premature drying of the exposed concrete surface.

A twin-block sleeper was initially developed in 1949 by Roger Sonneville while he was the chief engineer for the French National Railways (SNCF). This is why it is often designated as the RS sleeper, (Hay 1982). Today, France, Belgium, Denmark, Netherlands, Portugal, Spain India, Japan, Algeria, Tunisia, Brazil and Mexico are the main users of twin-blocks, (FIP 1987). A recent example of using the twin block in Britain is the ballasted track part of the South Yorkshire Supertram, (Baxter 1993). A diagrammatic representation of a twin block sleeper is shown in Fig. (2.9).

2.3.4 Concrete Slab

Concrete slab is another type of rail support which is quite common and suitable for underground railways primarily in tunnels, light rail transits and street running tramways. It comprises an in-situ paved reinforced concrete slab, thus the name paved concrete track (PACT). The slab can be laid by especially made slip form paver. The rail may be continuously supported by a resilient elastomeric pad and secured in position by elastic fasteners. Alternatively, base plates may be used which are bolted through holes drilled into the slab, (Baxter 1997). An example of PACT slab is the installation of the street running track part of South Yorkshire Supertram as shown in Fig. (2.10), (Boak 1995).

In some applications, precast units such as monoblock concrete sleepers (either with prestressed or plain reinforcement) or twin blocks are embedded into an in-situ reinforced concrete slab. In this form of construction either ballast may be used as in the Barbican Station for London Underground Limited (LUL), (Cope 1993), or the slab takes the place of ballast, hence the name non-ballasted track such as that adopted in the Channel Tunnel as shown in Fig. (2.11), (Kirkland 1995).

In locations where it is necessary to reduce vibration and noise transmission from the track into adjacent properties, the concrete slab is mounted on resilient bearings to form a floating slab track as that used for Dockland Light Railway in London, (Baxter 1997). A typical cross-section of floating slab track is shown in Fig. (2.12).

The benefits of a concrete slab track can be summarised as follows:

1. It provides accurate and stable track geometry.
2. The maximum pressure on the track formation is reduced due to larger contact area. Consequently it is possible to use the concrete slab to minimise track formation problems.
3. The day-to-day maintenance cost of a slab track is very low.
4. The hazard of track buckling either vertically or laterally is eliminated.
5. Because the slab track offers the possibility of continuous support to the rail, the bending stresses developed in the rail due to train loading is much lower than that of conventional track (e.g. with monoblock concrete sleepers). This means a lighter rail section can be used or transferring more metal into the rail head to provide for extra wear before replacement.

The main drawbacks of slab track are:

1. The installation cost of slab track is more expensive than that for conventional track.
2. The laying of slab track is much slower than that of conventional track.
3. The slab track makes the maintenance requirements for the underlying services of pipes, cables and ducts extremely difficult and costly.
4. Changes at a later stage are difficult to implement.

2.4 Light Rail Tracks

Light rail tracks (LRT) are often described as modern tramways where they are laid in the public highways shared by road vehicles. Thus, several conflicting requirements are expected for such systems. Firstly, they must withstand the train loads and maintain the track gauge so that the railway vehicles can operate safely. Secondly, they must not jeopardise the structural integrity of the highway and thus be capable for supporting the loads imposed by passing vehicles along and across rail tracks. Thirdly, they usually provide the return path for electrical current in case of electrical vehicles. Lastly, they must not cause a nuisance to road users by having ridges or sharp troughs which might cause accidents or damage road vehicles, (Lesley 1993 and 1994).

The existing track systems used for light rail transits and street running tramways can be classified according to the type of rail profile, namely:

1. High profile rail system
2. Low profile rail system

2.4.1 High Profile Rail System

The high profile rail system includes the German, French and Dresden track systems in which a girder type of rail is used such as the Phoenix grooved Vignoles rail, e.g. Ri59, which is 180 mm high and weighs 59 kg/m as shown in Fig. (2.13).

In German track system, the rails are mechanically fixed, directly, or over a rubber pad to a concrete slab. Whereas with French track system the rails are fixed either to conventional monoblock or more usually twin-block concrete sleepers in which the latter is installed on ballast and buried in the road. The road is then made up on both sides and between the rails using materials that sustain load from rubber tyred road vehicles.

The main drawback of these systems is that the required depth of the track foundation is so high that it disturbs all the apparatus below the road surface. Therefore, when new tracks are going to be installed in existing roads, all the underground services of pipes, cables and ducts have to be removed and relocated again once the track is constructed. The recent construction of Manchester Metro Link has demonstrated that diverting or

relocating the underground public utilities at certain locations demanded a huge amount of money per metre length of the track.

In Dresden track system, a completely different approach is followed where the rails are embedded into 20 m long precast concrete panels. These prefabricated panels are taken to the site and mechanically installed, with the rails being continuously welded. While this system is shown to be relatively fast and more labour productive, it restricted the development and flexibility of the tracks, (Lesley 1991).

2.4.2 Low Profile Rail System

Budapest track system is an example of low profile rail system. It consists of 20 m concrete panels with a precast steel channel. The panels are installed in the street then a special low profile rail 70 mm high is fitted into the panels, and held in place with mechanically injected rubber gaskets, see Fig. (2.14). This system has already been used in 20 cities in 8 European countries. The main advantage of Budapest system is that it can negotiate complex curves by means of short panels formed as tangents around curves.

In 1989 a new low profile rail (LR55) track system was developed by Prof. Lewis Lesley of Liverpool John Moores University. It has a novel concepts and revolutionary solution to the drawbacks and limitations so far related with the existing low as well as high profile rail systems, (Lesley 1989 and 1991). As mentioned earlier, the main objective of the present work is to study the structural aspects of the LR55 track system. The subsequent chapters cover in detail the analysis and design of this system to ensure it's capability for sustaining various loading expected during it's service as light rail track system.

2.5 Track Loadings

2.5.1 Source of Loadings

The loads acting on a track system (mainline or light rail) can be considered from three main directions:

1. Vertical

2. Longitudinal, i.e. horizontal and parallel to the track
3. Lateral, i.e. horizontal and transverse to the track

The main source of loading in the vertical direction is the wheel load of the train and the passing road vehicles in the case of street running tramways. The vertical track loading is dependent upon:

1. Type of traffic, i.e. passenger, freight .. etc.
2. Number and spacing of axles
3. Train speed-dynamic loading considerations
4. Density, i.e. number and frequency of load applications

Main sources of longitudinal loading on the track are:

1. Thermal forces due to temperature changes
2. Braking and accelerating load
3. Shrinkage forces resulted from welding of rails in the track

Lateral loading of the track can occur due to

1. Hunting, rocking and rolling of rail vehicles
2. Centrifugal force on curved track
3. Rotational acceleration of the vehicle body due to curvature changes
4. Impact due to irregular rail alignment or configuration
5. Braking and accelerating of vehicles passing across the track

2.5.2 Design Axle Load

The actual loads acting on a track system are transient dynamic and random in nature, and are characterised by rapid fluctuations. In order to design the structural components of a track system, it is idealistic to perform full dynamic analysis including track-vehicle interaction and correlating this with actual strain measurements obtained from extensive laboratory or field tests. However, this approach is not always practical for it is too complicated and economically unfeasible.

Therefore, an alternative technique has to be used, which is commonly practised by railway organisations all over the world, including for instance, British Rail (BR),

Association of American Railroads (AAR), German Federal Railways (DB) and French National Railways (SNCF), ..etc. In this method, a static design axle load is obtained from augmenting the nominal static weight applied by the cars or trains by a factor known as Dynamic Load Factor (DLF) to account for the impact effect of the traffic loading, i.e.:

Design axle load = Nominal axle load x (1 + DLF)

2.5.2.1 Nominal Axle Load

The nominal axle load is calculated by dividing the static vehicle weight by the number of axles, assuming an equal distribution of the weight to each axle. Table (2.1) lists typical maximum static nominal axle loads for main lines as recommended by various countries, (FIP 1987).

For light rail transits and street running tramways, the nominal axle loads are much less than those for main line. For example, in the case of Manchester Metro Link the maximum nominal axle load is 108 kN (11 tonne). In North America, about 106 kN (10.8 tonne) axle load is suggested, (Selig and Waters 1994). The new system of Kuala Lumpur light rail transit is designed for 118 kN (12 tonne) axle load, (Vandenbril 1997).

2.5.2.2 Dynamic Load Factor (DLF)

The DLF is normally expressed as a percentage of the nominal axle load and generally ranges between 0.5 to 1.5, (Hanna 1979). The main factors which affect the magnitude of the DLF are, (Hay 1982, Frederick and Round 1984, Stewart and O'Rourke 1988):

1. Vehicle characteristics including type of truck, car weight, axle suspension, number and spacing and wheel diameter
2. Operation conditions including running speed, braking and acceleration
3. Irregularities in the roundness of the wheels including wheel flats
4. Track characteristics including track geometry, quality and stiffness of track structural components
5. Irregularities in track profile both horizontally and vertically and irregular track stiffness due to variable characteristics and settlement of track bed
6. Irregularities in the rail due to welds, joints and corrugations

There is no entirely adequate way which has been devised to account for all the above mentioned effects. Instead, several empirical formulae for the DLF are suggested by various railway organisations, largely based on experience and rule of thumb. Taylor (1993) presented 12 different formulae for the DLF in one diagram as shown in Fig. (2.15), relating the factor to the vehicle speed and the type of railway being used as main line or light rail systems. He emphasised that one must be led by experience in deciding on the value of DLF as it is greatly influenced by the maintenance of the whole railway. Fig. (2.15) reveals that the DLF is, in most cases, linearly proportional to the train speed, exceptions being the Peterson formula for steam locomotive and German formula.

2.6 Methods of Track Analysis

Analysis of a track system is mainly required for the rational and economical design of it's components, e.g. rail, sleeper, fastenings and track bed. It also provides the basis for maintenance procedures. This problem has been addressed by numerous researchers working in the field of railway engineering. Hence, different types of mathematical models have been proposed ranging from simple one dimensional representation of the track system to a more elaborate three dimensional case. In any of these models, the elements of a track system are interrelated in a specific functional manner such that their complex interactions are simplified on the grounds of certain assumptions. The main objective of these models is to determine the effect of traffic and environmental loads on the track responses in terms of deflections, stresses and strain. Generally speaking, there are two methods to analyse a track system which are presented below.

2.6.1 Analytical Methods

A conventional railway system which consists of rail, base plate or pad, transverse sleepers, ballast and subgrade, lends itself admirably to be modelled as a one dimensional beam on an elastic foundation as shown in Fig. (2.16). In this case, the rail is considered as a continuous beam while the rest of the track components are represented as one homogeneous elastic foundation of Winkler type. Winkler foundation is characterised by the fact that the pressure at every point in the foundation is linearly proportional to the deflection occurring at the point, and is unaffected by the deflection of adjacent points.

This implies that the foundation material is unable to transfer shear, (Selvadurai 1979, Dulacska 1992).

The first analytical solution of the track problem was carried out by Zimmermann in 1888. The track was modelled as a continuous beam of infinite length supported by a homogeneous elastic foundation. The concept of track foundation modulus was introduced in his analysis to calculate the deflection and bending moment of the rail, (Clarke 1957, Tayabji 1976). The track foundation modulus is defined as the load per unit length of the rail necessary to produce a deflection of the track foundation equal to unity, (Cope 1993). The governing differential equation of this model is:

$$EI\, d^4y/dx^4 + ky = 0 \qquad (2.1)$$

The solution of eq. (2.1) for an infinitely long track subject to single point load P is, see for example (Hetenyi 1946):

Deflection: $y = (\lambda P/k)(\cos \lambda x + \sin \lambda x)\, e^{-\lambda x}$ (2.2)

Slope: $\theta = (\lambda^2 P/k)(\sin \lambda x)\, e^{-\lambda x}$ (2.3)

Moment: $M = (P/4\lambda)(\cos \lambda x - \sin \lambda x)\, e^{-\lambda x}$ (2.4)

Shear: $V = (-P/2)(\cos \lambda x)\, e^{-\lambda x}$ (2.5)

where

E = Young's modulus of the beam (rail)

I = moment of inertia of the beam (rail)

P = point load

x = x-coordiante of the beam measured from the point load P

k = track foundation modulus

$\lambda = (k/4EI)^{1/4}$ (2.6)

y = deflection of the beam (rail) at any point x from the point load P

θ = Slope of the beam (rail) at any point x from the point load P

M = Moment of the beam (rail) at any point x from the point load P

V = Shear of the beam (rail) at any point x from the point load P

The line force acting under the beam (rail) is:

$$q = y\, k \qquad (2.7)$$

By inspection, the maximum values of deflection, moment, shear and line force occur directly beneath the point load P, i.e. at x = 0. These are found to be:

$$y_{max} = P\lambda/2k \tag{2.8}$$

$$M_{max} = P/4\lambda \tag{2.9}$$

$$V_{max} = P/2 \tag{2.10}$$

$$q_{max} = y_{max}\, k$$

$$= P\lambda /2 \tag{2.11}$$

Talbot and his joint committee applied the same theory of a beam on an elastic foundation to analyse a track system. He studied the problem more extensively and produced a steady stream of work from 1918 to 1940, (AREA 1980). Talbot found out that the theoretical results of rail deflections, bending moments and stresses were very close to those observed in field tests. He also managed to estimate the percentage of the static rail load carried by an individual sleeper. By correlating the analytical results with the experimental work, Talbot developed the following empirical formula for the vertical pressure at any depth in the ballast below the sleeper face and at any distance to the left or right of the sleeper centreline, (Hay 1982):

$$P_x = 16.8\ (10)^K\ P_a/h^{1.25} \tag{2.12}$$

where

P_x = pressure (psi) in the ballast at any distance x (inches) from the centreline

P_a = uniform bearing pressure (psi) over the sleeper face centreline

h = depth below the face of sleeper (inches)

K = a factor determined by experiment;

$$= -6.05\ x^2/h^{2.5} \tag{2.13}$$

Eq. (2.12) is found to be accurate within 1 - 2% of observed field measurements for depths between 100 and 750 mm (4 and 30 in).

Timoshenko and Langer (1932) hypothesised that a track with closely spaced sleepers could be analysed by the same theory of a beam on an elastic foundation. Their work included the effect of single and multiple axle load on the track responses in terms of deflection and stresses. They concluded that the weight of the rail was directly

proportional to the axle load of the train running over it. They also compared the theoretical results due to vertical, lateral and eccentric loading with those obtained from laboratory and field tests. Both results were found to be in a reasonable agreement.

Clarke (1957) examined analytically the previous work of Zimmermann and Talbot. He discussed elaborately the parameters that affect the track design including type of locomotive, axle load magnitude and spacing and sleeper characteristics. He reached a conclusion that doubling the number of sleepers per mile of track would reduce rail stresses by only 19 per cent. It follows that if rail stresses were too high for a given load, it would be more economical to increase the weight of the rail to be used than consider increasing the number of sleepers per mile. He also tried to develop some useful charts to facilitate calculations during the design process of a track system.

2.6.2 Numerical Methods

Numerical methods such as the finite element method (FEM) are now more widely used due to the vast development of computational mathematics and in particular the advent of relatively inexpensive computers with high specifications. The main advantage of employing numerical techniques is their capability for solving a wide range of problems that cannot be easily treated analytically such as tracks with different boundary conditions and load combinations, nonlinearity due to soil separation, material yielding and large displacement, ..etc.

Tayabji and Thompson (1976) developed a quasi three dimensional finite element model known as ILLITRACK to analyse a conventional railway track system subject to static vertical load. This model consisted of two pseudo-plane strain two dimensional finite element analysis, one longitudinal and the other transverse. The output from the longitudinal analysis was employed as input to the transverse analysis. In a pseudo-plane strain technique, the finite element thickness was permitted to increase with depth to simulate the three dimensional load dissipation.

In the first stage of the track analysis by ILLITRACK, a two dimensional finite element model for the longitudinal section of the track was suggested. The rail was represented by beam elements and the sleepers by vertical springs of equivalent structural

characteristics, attached to the rail beam elements. The track base components of ballast, sub-ballast and subgrade were represented by 4-node rectangular plane strain elements. The thickness of the elements directly below the sleepers was based on the concept of effective bearing length, which was conservatively assumed equal to 457 mm (18 in). The thickness of the rest of the elements was allowed to linearly increase with depth at an angle of distribution (10 - 30°) to account for the load spread in the direction perpendicular to the plane, see Fig. (2.17). This is what was meant by pseudo-plane strain technique.

In the second stage, a two dimensional finite element model was developed for the transverse section of the track system. The sleeper could be represented either as 4-node rectangular elements or beam elements resting on the ballast. The loading data to the transverse model was taken from the longitudinal analysis stage as nodal loads or prescribed nodal displacements acting along the top of the sleeper. Nonlinear analysis was carried out by incorporating the stress path dependent behaviour of the track base materials (ballast, subballast and subgrade) into the transverse model. Similar to the longitudinal analysis, the thickness of the elements directly under the sleeper was taken equal to the effective bearing length which was, for this stage, equal to the width of the sleeper. The thickness was then increased at an angle of distribution between 10 to 30° to consider the three dimensional effect of load spread with depth, see Fig. (2.18).

The main advantage of this model is that the three dimensional nature of the actual track system has been simulated with two pseudo-plane strain two dimensional finite element analysis. Hence, the complexity and inordinate cost associated with actual three dimensional finite element formulations is avoided. The main disadvantage of this model is that the results might be affected by factors such as bearing length and spacing of sleepers, and angle of distribution since the model is only a two dimensional approximation to the actual three dimensional problem. Thus it should be used with care and judgement, (Desai and Siriwardane 1982, Selig and Waters 1994). For more details of ILLITRACK model one should refer to Tayabji (1976).

Desai and Siriwardane (1982) presented three different formulations based on a one, two and three dimensional idealisation of a railway track system. Material nonlinearity due to

elasto-plastic behaviour of the track bed was taken into consideration and the load was applied by increments during the analysis.

For the one dimensional model, a given length of rail supported by equivalent springs representative of the semi-infinite foundation was treated as a beam on a nonlinear foundation. The rail was represented by beam elements with six degrees of freedoms, three translations and three rotations at each end. The transverse displacements are approximated by using cubic Hermitian interpolation functions, and the axial and torsional displacements are assumed to be linear, (Zienkiewicz 1977). Track base separation was taken into account by redistributing the excess tensile stresses to the beam and the springs in compression, (Siriwardane 1980).

For the two dimensional model, plane strain idealisation with uniform thickness of the section was suggested. Eight-node quadratic isoparametric elements were used for all the components of the track system. Special thin interface elements were used to simulate the interface conditions between various track components, see Fig. (2.19).

The three dimensional case involved using hexahedral elements with 21 nodes for the sleeper, ballast, subballast and subgrade whereas thin interface elements were used to represent the junctions between the different parts of the track, see Fig. (2.20). The procedure had been verified by solving a number of track support structures and comparing the results with field observations, analytical, and other numerical methods including the ILLITRACK model presented previously. Detailed explanation for these finite element formulations was given by Siriwardane (1980).

Chang et al. (1980) developed a three dimensional multilayer model named GEOTRACK for determining the elastic response of railroad track system under wheel load. In this model, the stress-dependent material properties for the ballast, subballast and subgrade, and the sleeper-ballast separation had been taken into account.

The rails were represented as linear elastic beams supported by a number of concentrated reactions, one at each rail-sleeper intersection. The rails spanned 11 sleepers and were free to rotate at the end, and at each sleeper. Each connection between the rails and

sleepers was represented by a linear spring. Each sleeper was divided into 10 equal rectangular segments of linear elastic properties and with the underlying ballast reaction represented as a concentrated force in the centre of each segment. These forces were applied to the ballast surface as a uniform pressure over a circular area, whose diameter was related to the sleeper segment dimensions. The ballast, subballast and underlying subgrade were represented as a series of linear elastic layers of infinite horizontal extent. The model permitted the track bed to be divided into as many layers as possible to account for the variation of the properties with depth. The bottom layer was assumed of infinite depth. Each layer was specified by a separate Young's modulus and Poisson's ratio. Perfect bond was assumed to exist at the layer interfaces, i.e. no slip was permitted between the layers.

The model only permitted the vertical component of wheel load. Single or multiple axle load could be used with a maximum number of four load applications. A possibility for unequal axle load could also be accommodated. The weight of the rails and the sleepers were also considered.

The output of GEOTRACK included rail seat reaction, sleeper-ballast reactions, rail and sleeper deflections and bending moments. In addition, it also provided output of the vertical deflection and the complete three dimensional stress states at selected locations within the track bed layers (ballast, sub-ballast and subgrade), sleeper and rail. The advantage of this method is that the soil layers can be extended to semi-infinite space, with a substantial reduction of computing cost over the other three-dimensional solutions. The main disadvantage of this model, though it is a three dimensional representation of the track system, is that the effect of lateral and longitudinal loads can not be taken into consideration. The model was set up to account for vertical load only. Fig. (2.21) shows the track components and forces proposed in the GEOTRACK model. A detailed explanation of this model was presented by Adegoke (1979).

Profillidis (1986) proposed a three dimensional FEM to study the track response in terms of stresses and strains in the rail, sleeper and track bed. A typical discretised mesh of the track system is shown in Fig. (2.22). Nonlinear analysis was performed by considering the material elasto-plastic behaviour and the interface conditions between the track

components. Parametric study was conducted to account for the influence of sleeper type (timber, prestressed concrete and reinforced concrete), thickness of the track bed, and quality of the soil forming the subgrade (bad, medium, good and very good) on the stresses and deformations of the track system. It was found that the parameter with predominant influence was the quality of subgrade. The thickness of the track bed had an important influence, but secondary compared to that of the subgrade quality. The influence of the sleeper type on the stress values was more distinct compared to the deflection values.

Raymond (1991) described a procedure for a three dimensional FEM capable for analysing railway track system subject to static load. A family of isoparametric elements with a choice of 8-node hexahedral and 6-node pentahedral elements or 20-node hexahedral and 15-node pentahedral elements was used, see Fig. (2.23). All the materials forming the track system were assumed to be isotropic and elastic. Nonlinearity was employed in the model by accounting for the ballast lack of ability to sustain tension and the stress path dependence. A special computer program called ARTS was developed for this purpose. The program was written in FORTRAN IV. A sample analysis was selected to solve a track supporting a heavy gantry crane using ARTS program. The analytical results were compared with those of a field test. It was noted that the ballast lack of resisting tension has important effect on the results.

Table (2.1): Typical maximum static nominal axle load for various main lines in the world.

Country	Maximum static nominal Axle Load	
	(kN)	(Tonne)
Australia	245	25.0
Canada	292	29.7
China	245	25.0
Germany	221	22.6
Hungary	202	20.5
India	220	22.5
Italy	221	22.6
Japan	164	16.7
South Africa	221	22.6
Sweden	221	22.6
UK	245	25.0
USA	321	32.7

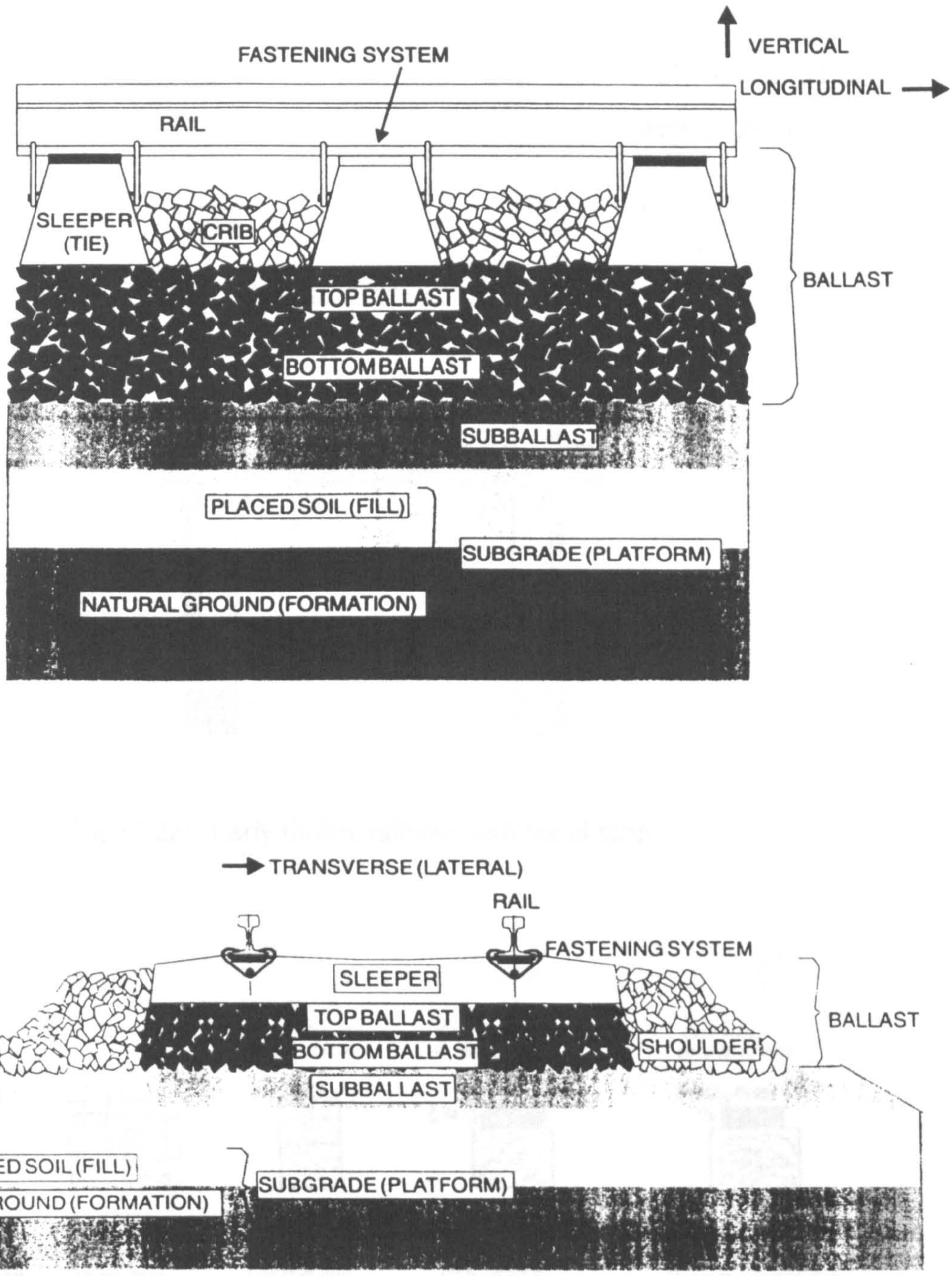

Fig. (2.1): A typical cross section of a conventional railway track system.

Fig. (2.2a): Early timber railway.

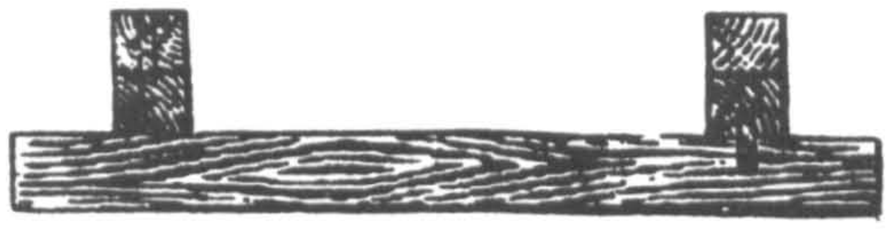

Fig. (2.2b): Early timber railway, with double rail.

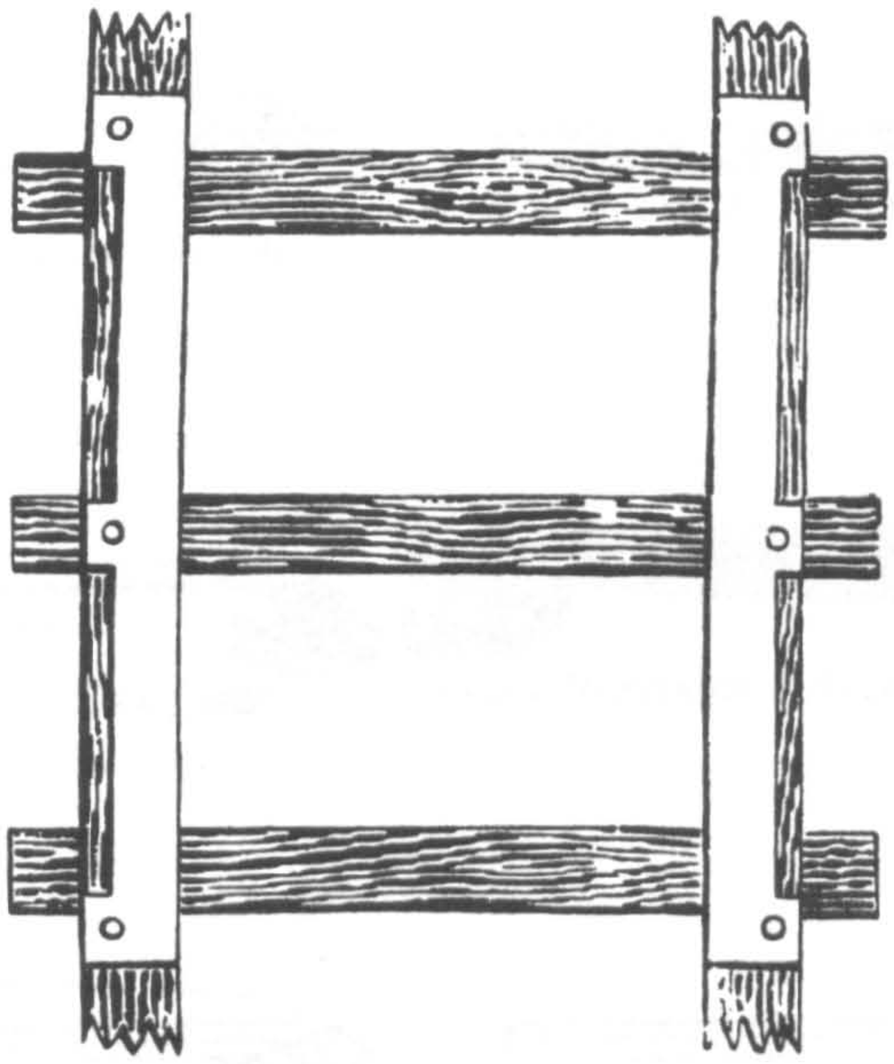

Fig. (2.2c): Early timber railway with metal strip.

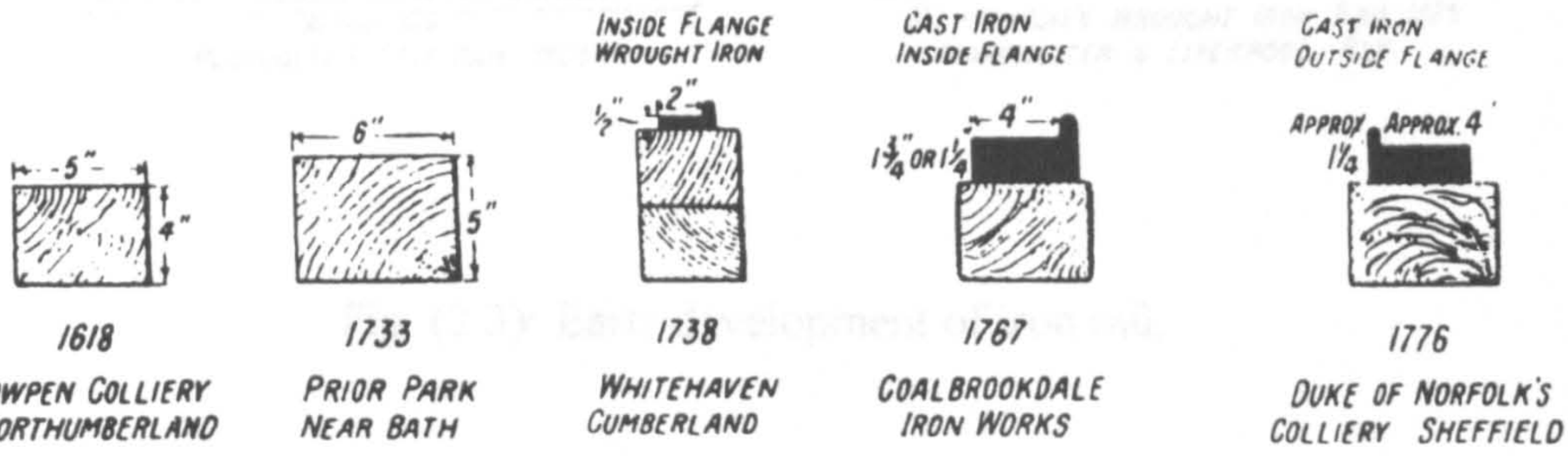

Fig. (2.2d): Early timber rail cross sections.

Fig. (2.2): Development of early timber railway.

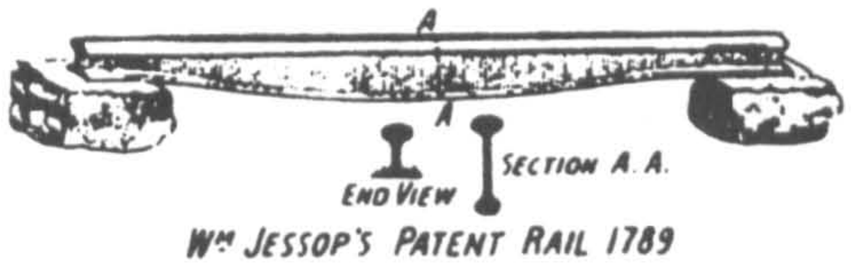

Wm JESSOP'S PATENT RAIL 1789

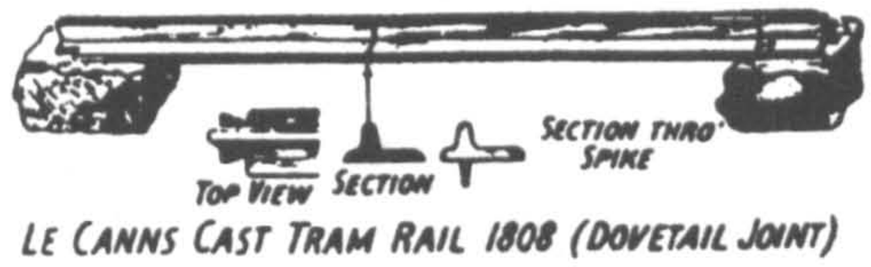

LE CANNS CAST TRAM RAIL 1808 (DOVETAIL JOINT)

LAWSON COLLIERY NEWCASTLE-ON-TYNE 1797

LORD CARLISLE'S WROUGHT IRON RAIL 1811

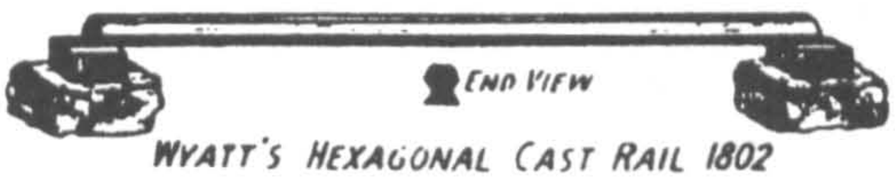

WYATT'S HEXAGONAL CAST RAIL 1802

LOSH & STEPHENSON'S PATENT CAST RAIL 1816

CAST TRAM RAIL SURREY IRON RLY. 1803

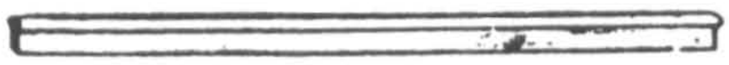

WROUGHT IRON RAIL PATº BY JOHN BIRKENSHAW 1820

WOODHOUSE'S CAST RAIL 1803

STEPHENSON'S WROUGHT IRON RAIL 1829
MANCHESTER & LIVERPOOL RLY.

Fig. (2.3): Early development of iron rail.

Fig. (2.5): Flat Bottom rail section, identification no. 90 A according BS 11 (1985).

Fig. (2.6): Steel sleepers and their cross-sectional properties, produced by British Steel Track.

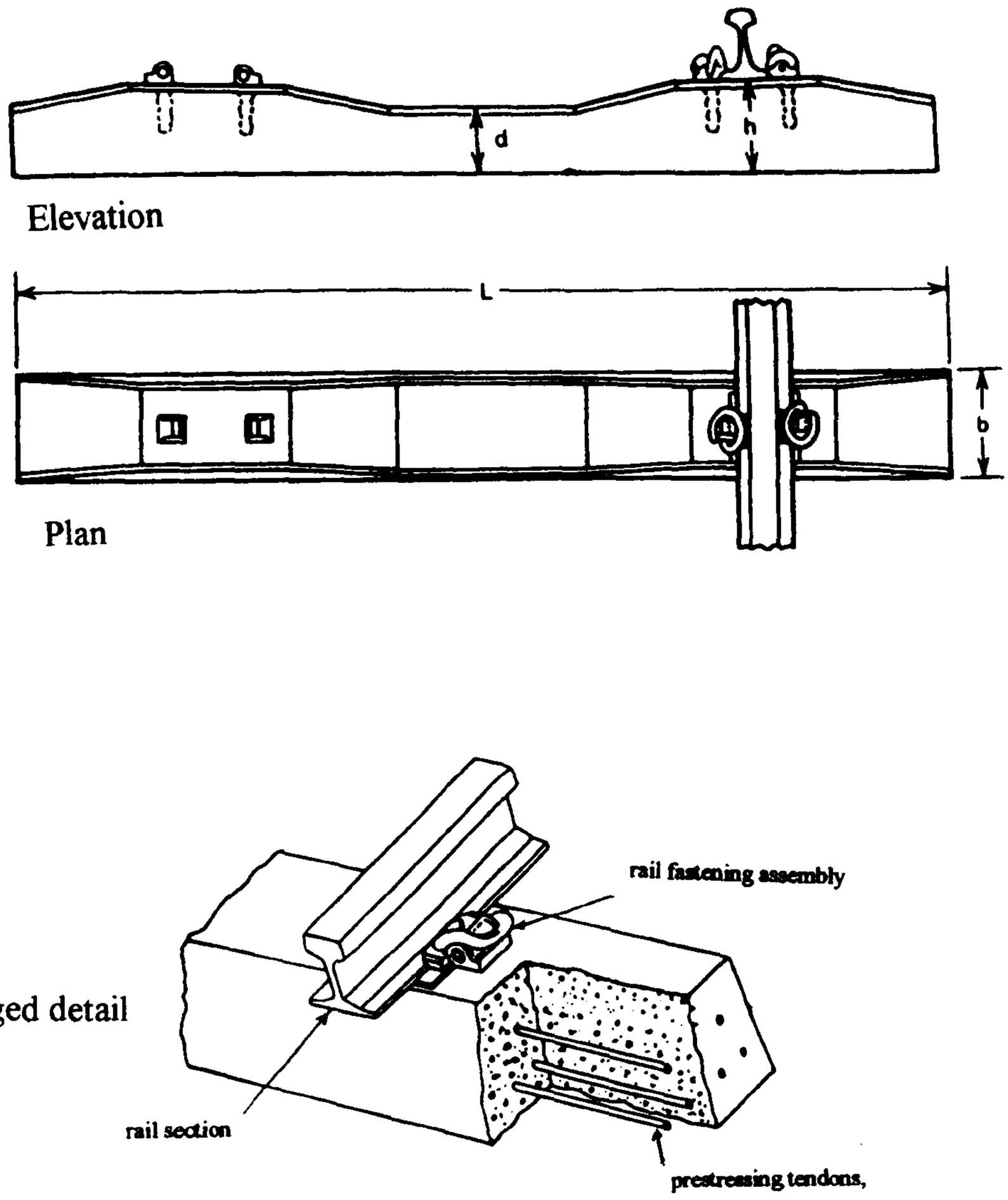

Fig. (2.7): Pre-tensioned concrete monoblock sleepers.

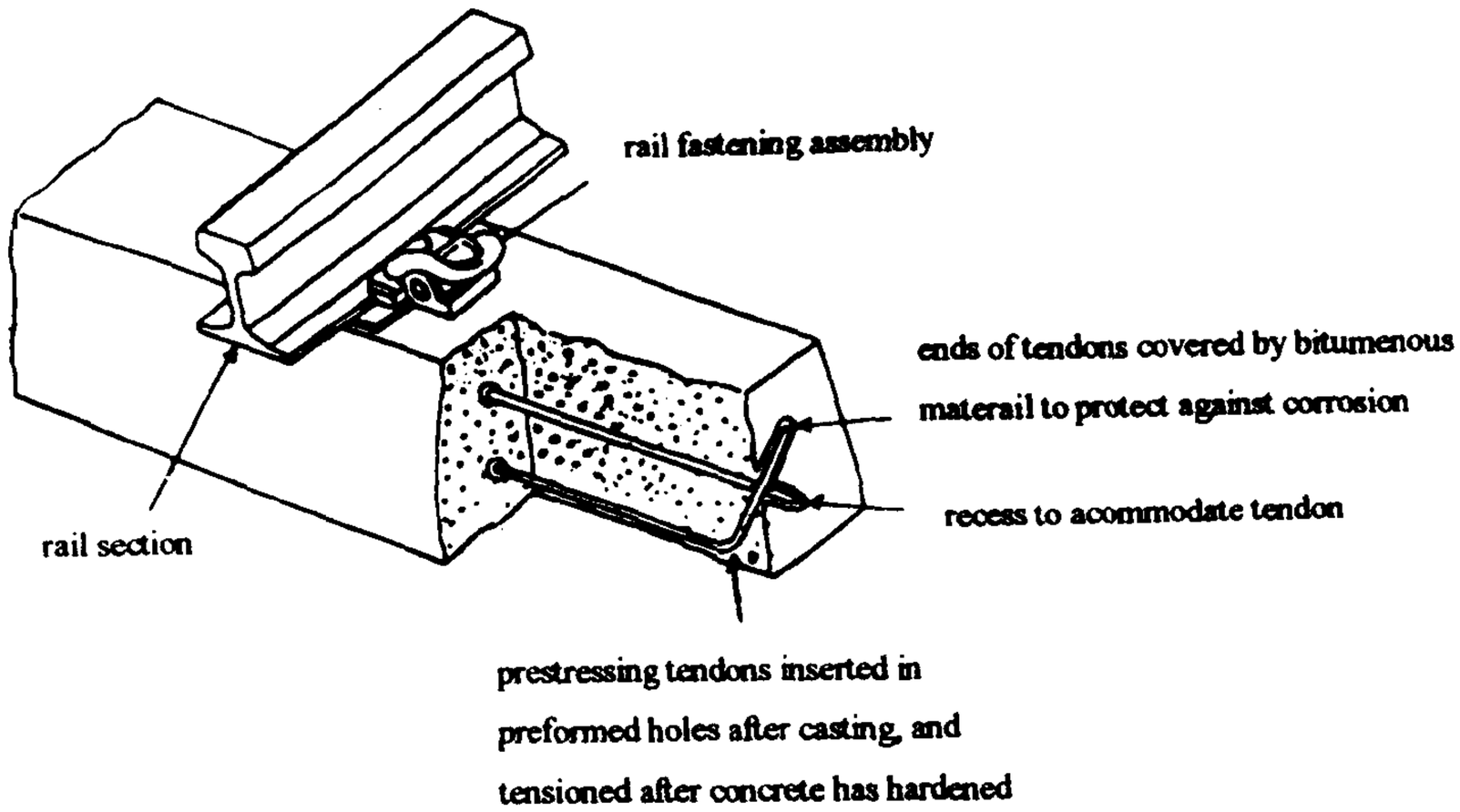

Fig. (2.8): Post-tensioned concrete monoblock sleepers.

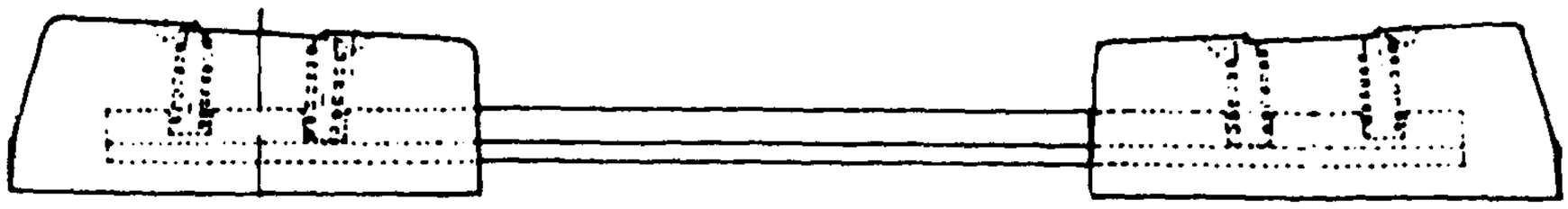

Elevation

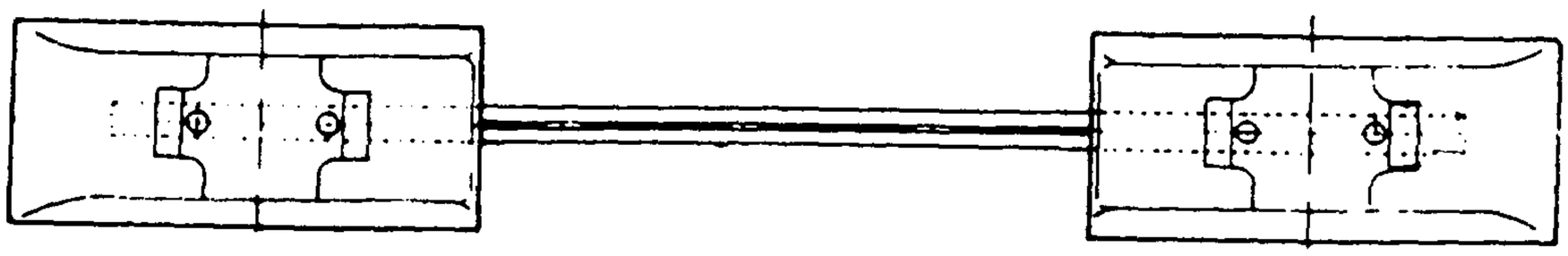

Plan

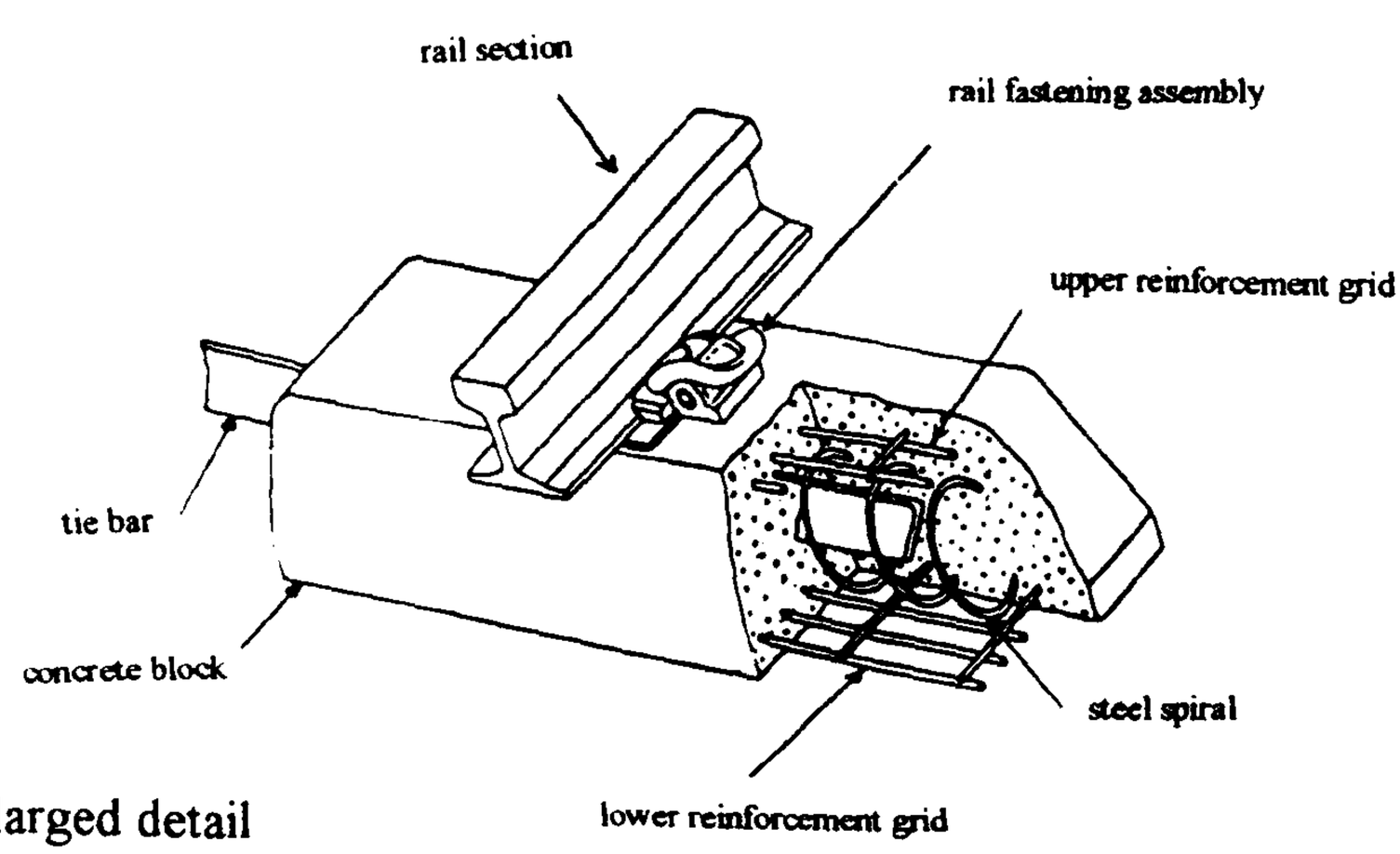

Enlarged detail

Fig. (2.9): Twin-block concrete sleepers.

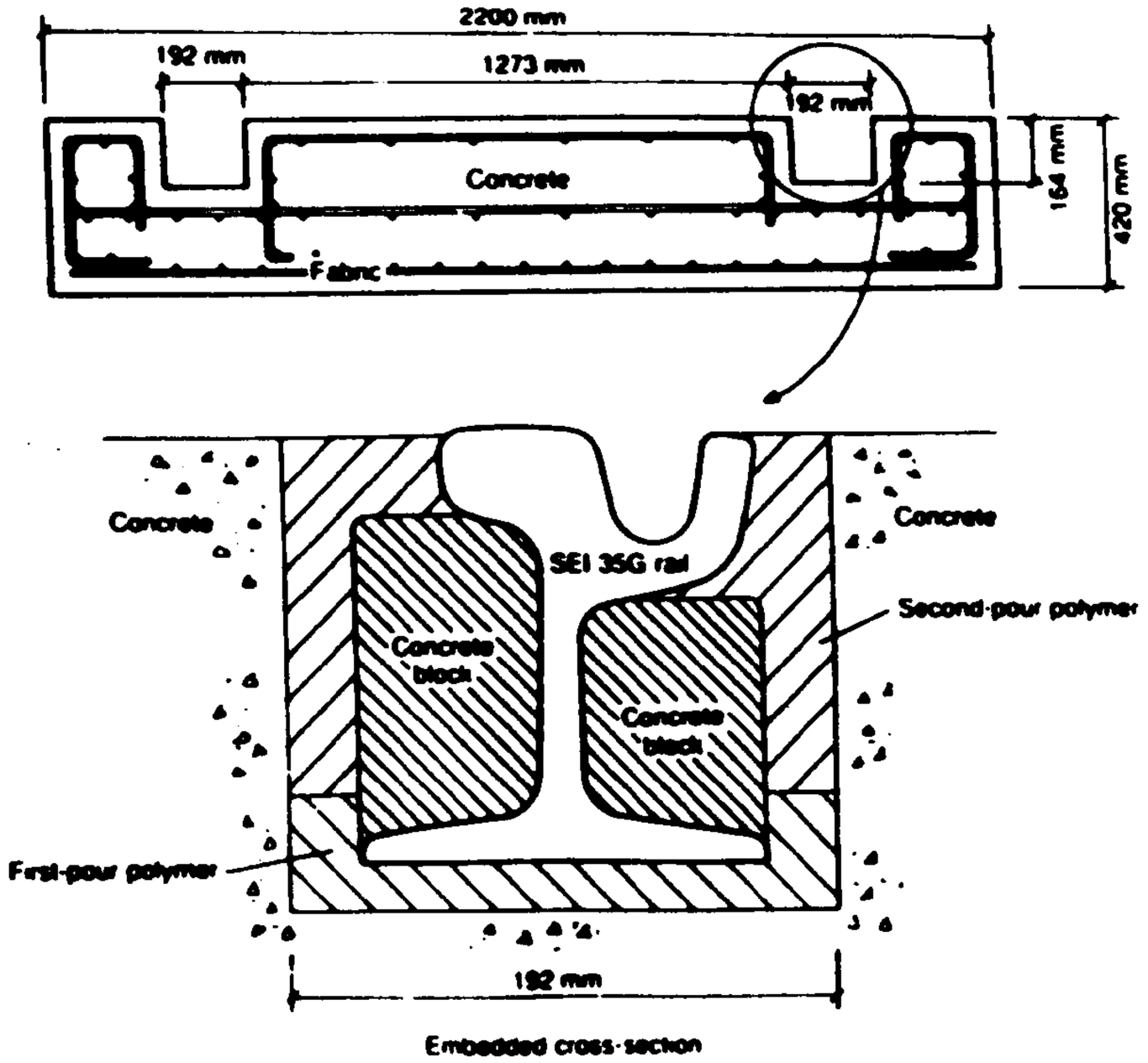

Fig. (2.10): Paved concrete slab track (PACT) used for South Yorkshire Supertram.

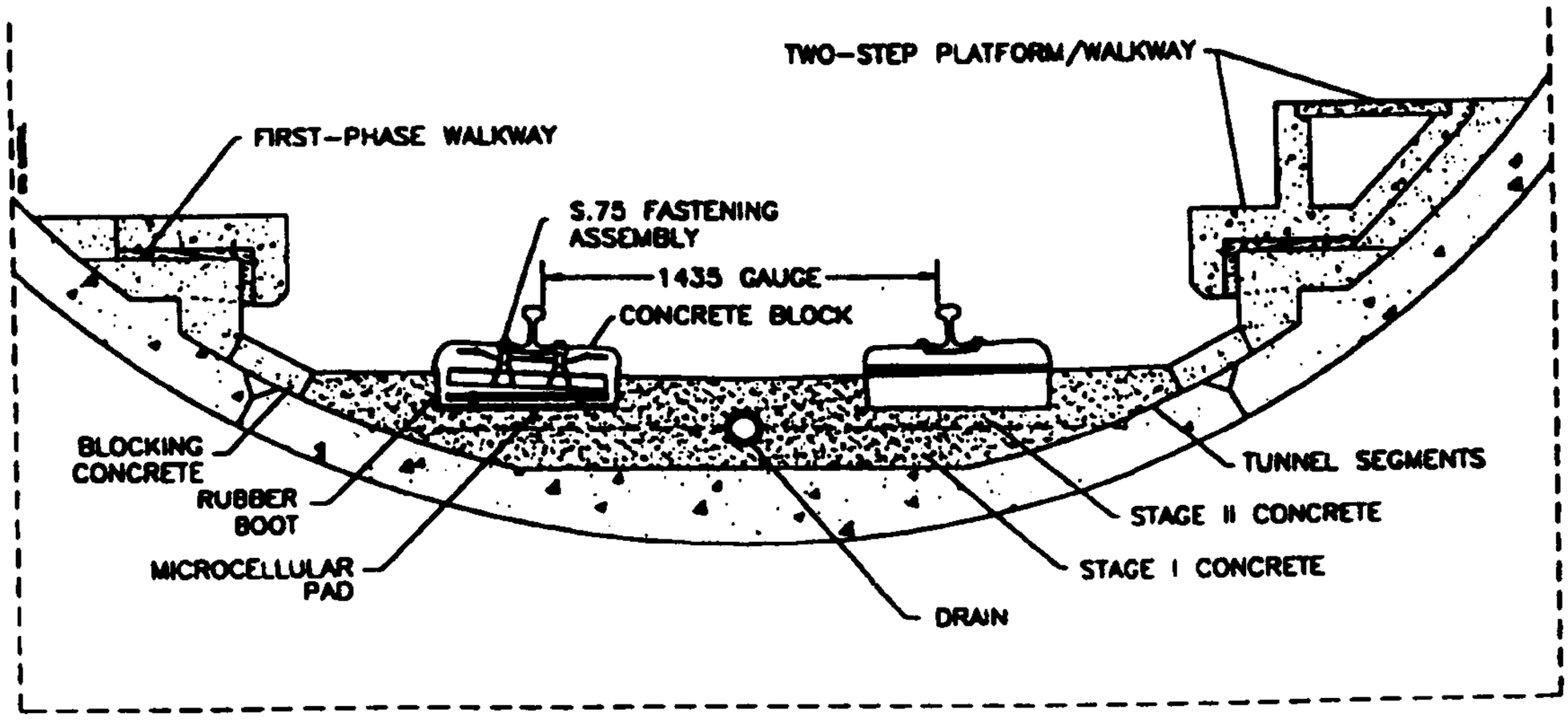

Fig. (2.11): Paved concrete slab track (PACT) with the rail supported by twin-block, used for the Channel Tunnel.

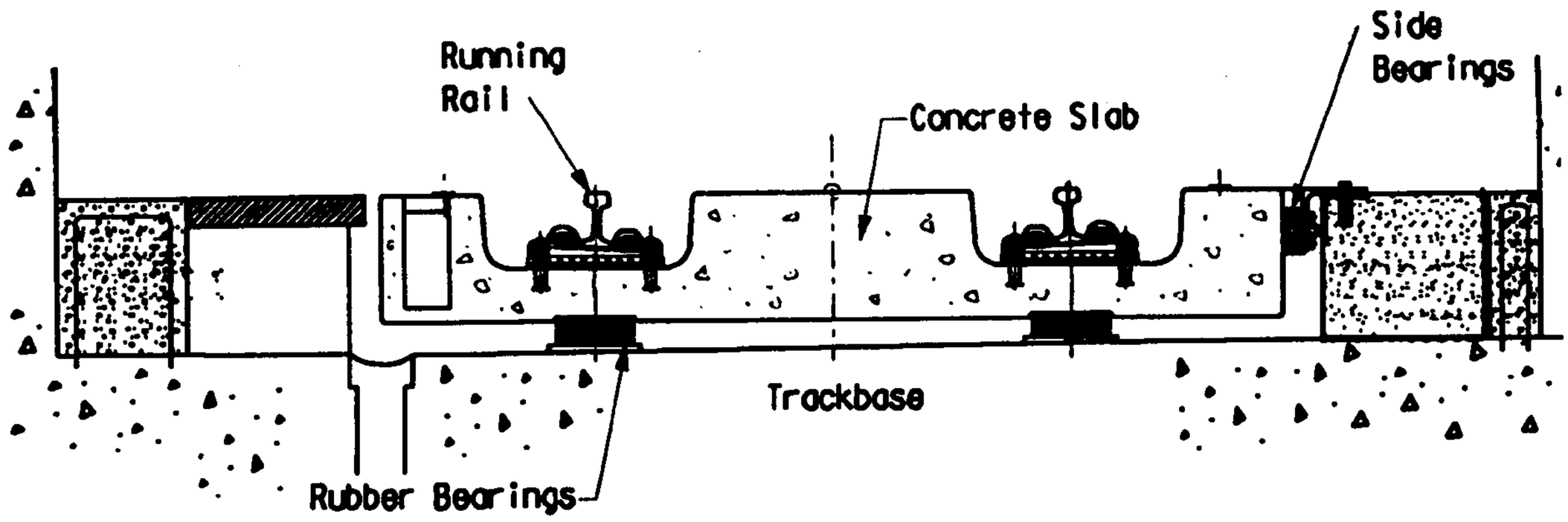

Fig. (2.12): Typical cross section of a floating concrete slab track.

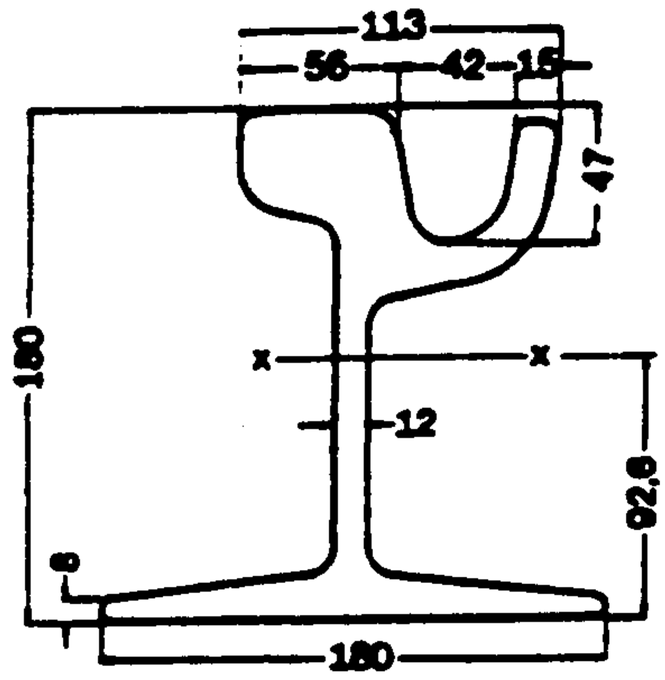

Fig. (2.13): High profile rail, Ri59 rail used for Manchester Metrolink.

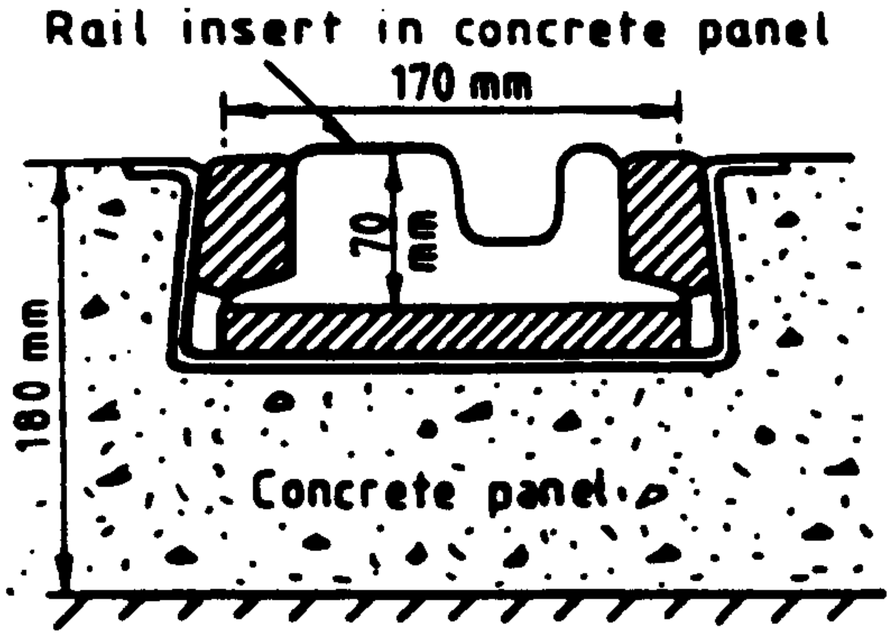

Fig. (2.14): Low profile rail used for Budapest track system.

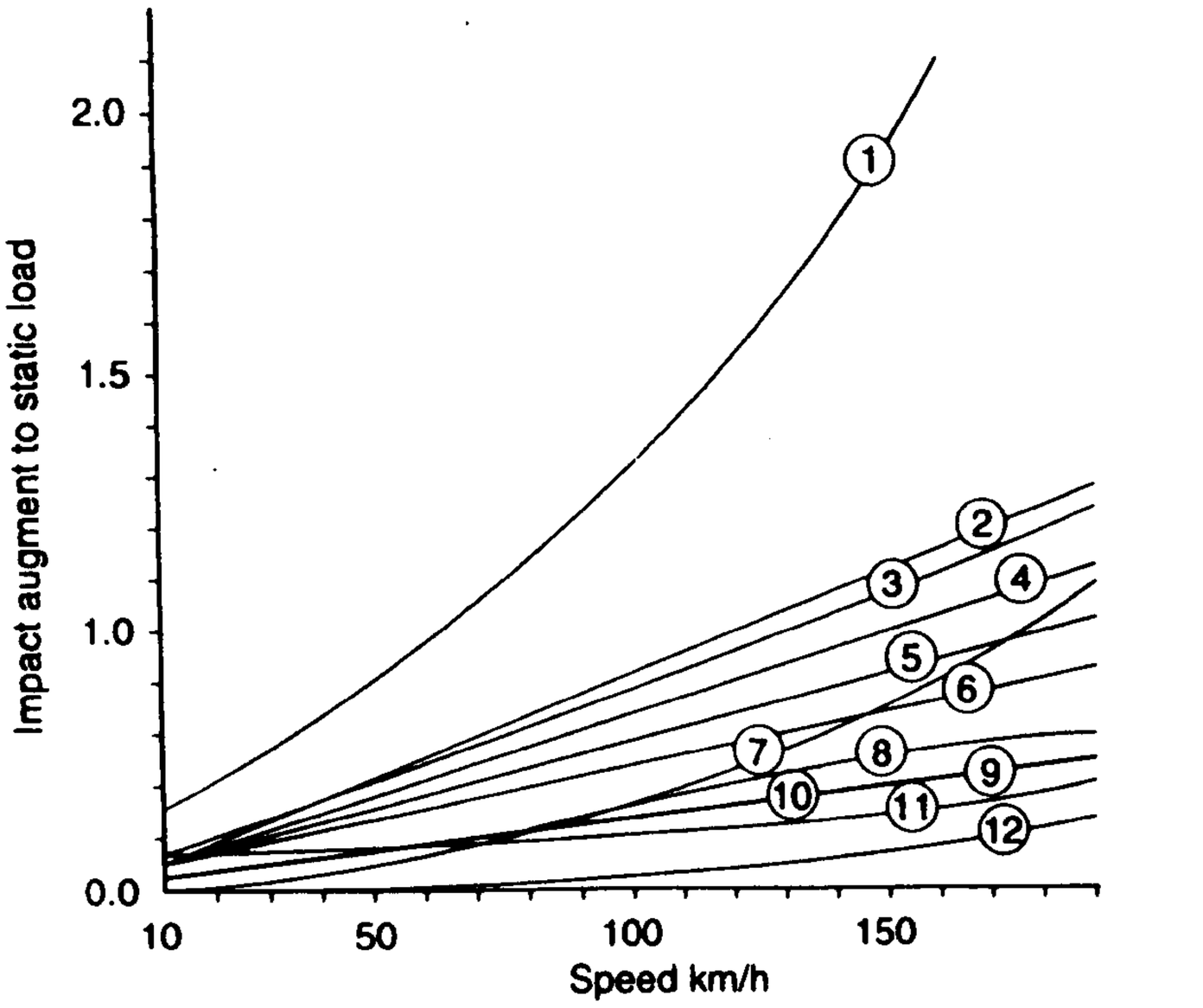

1 Steam loco, Peterson formula
2 Clark formula high end of range
3 Diesel loco, Peterson formula
4 Indian formula for light track 1
5 AAR formula for diesel locos 1
6 Indian formula for light track 2
7 German formula
8 Schram
9 Clark formula
10 AAR formula for steam locos 2
11 Ore 071 formula 1
12 Ore 071 formula 2

Fig. (2.15): Dynamic load factor (DLF) formulae as function of railway type and vehicle speed.

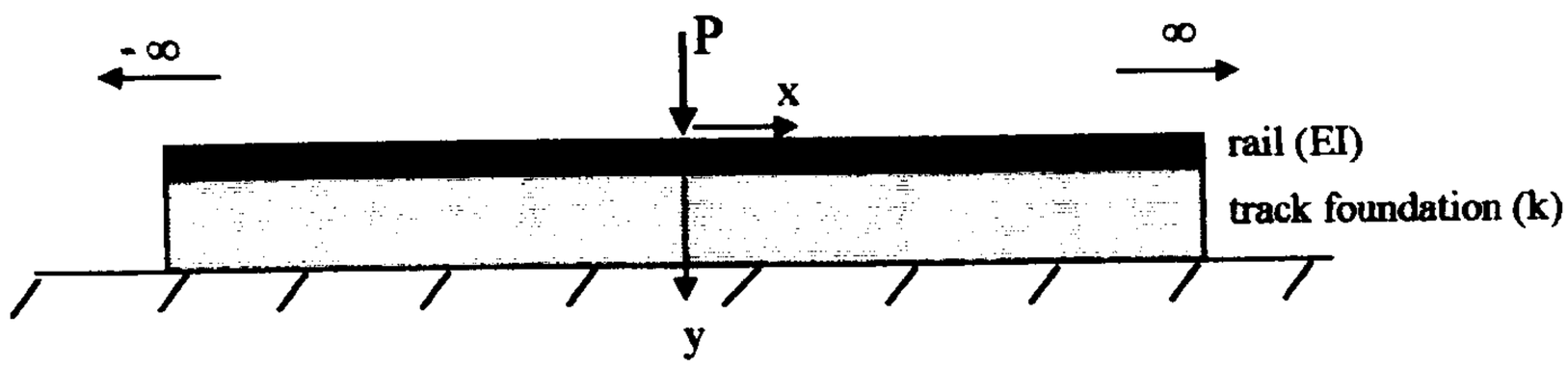

Fig. (2.16): Conventional track system modelled as single layer beam on an elastic foundation.

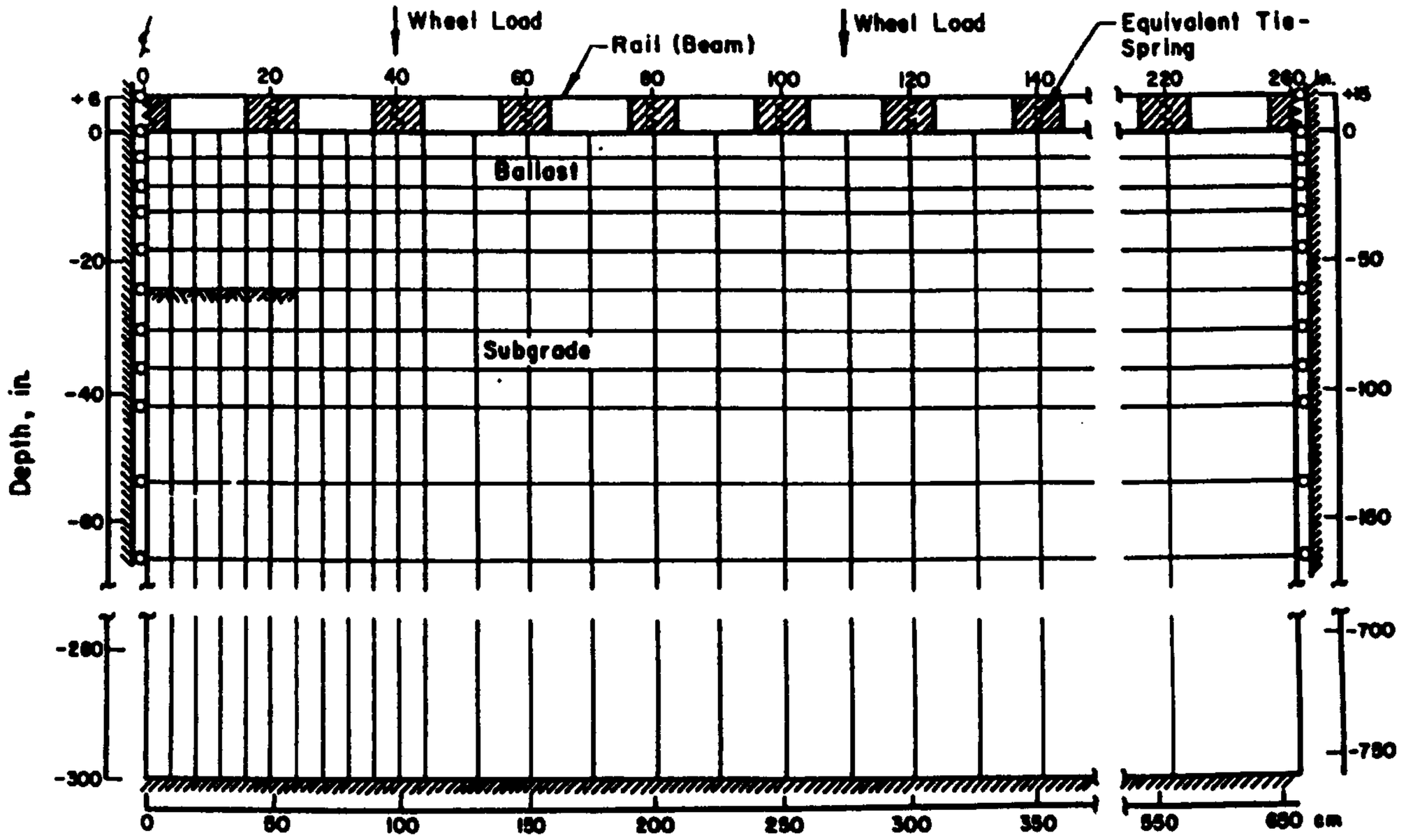

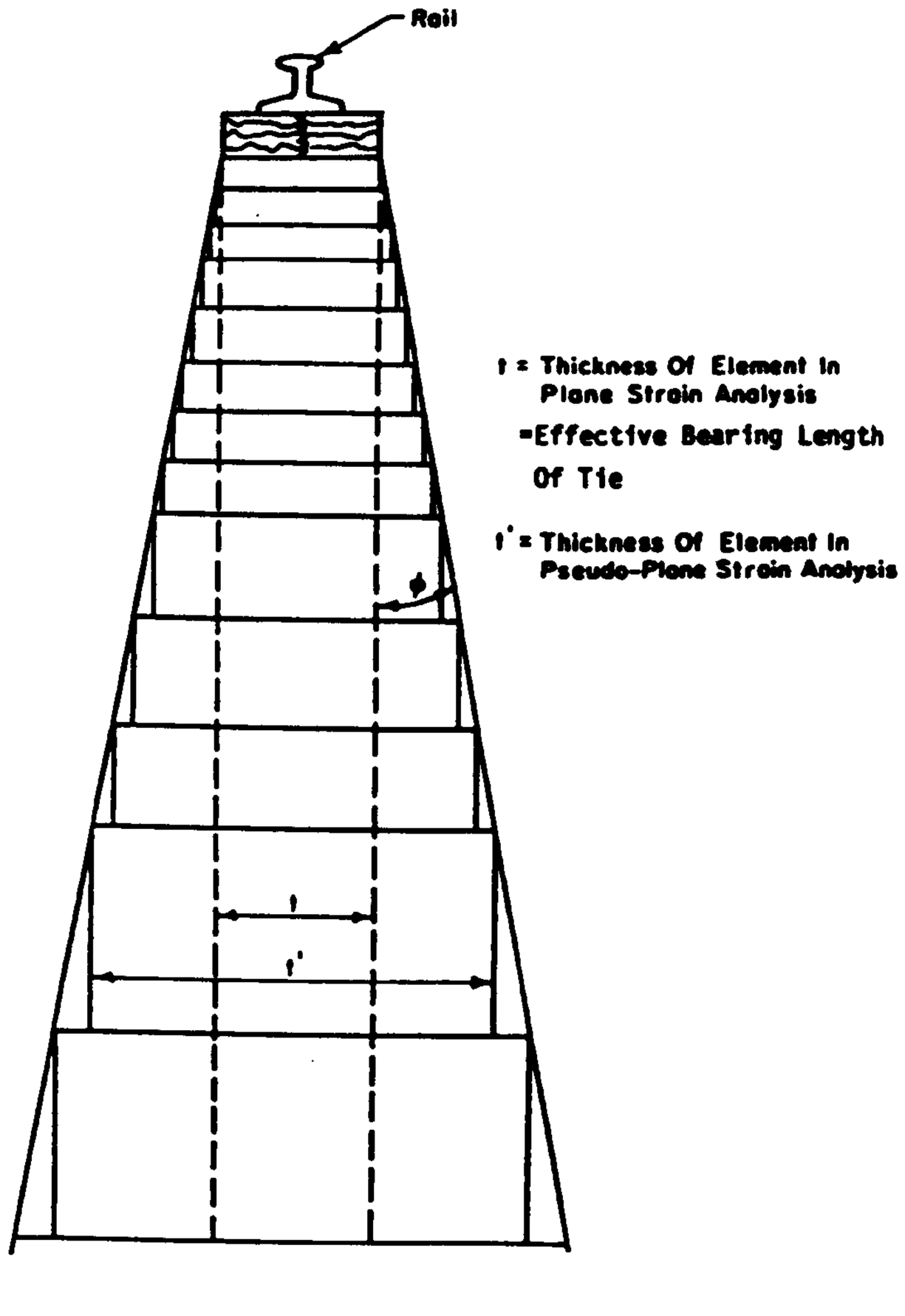

Fig. (2.17): Typical two dimensional finite element mesh for longitudinal analysis by ILLITRACK model.

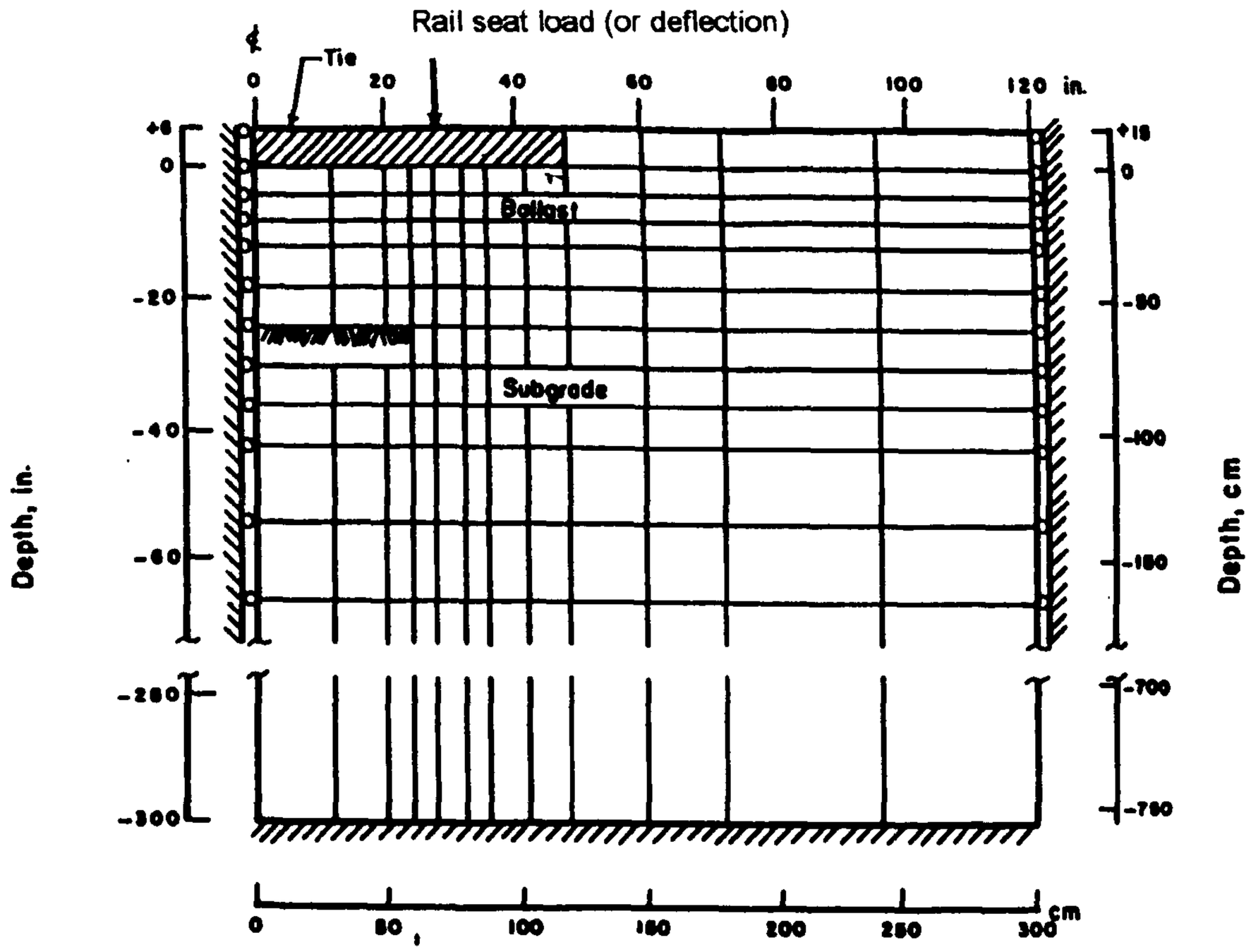

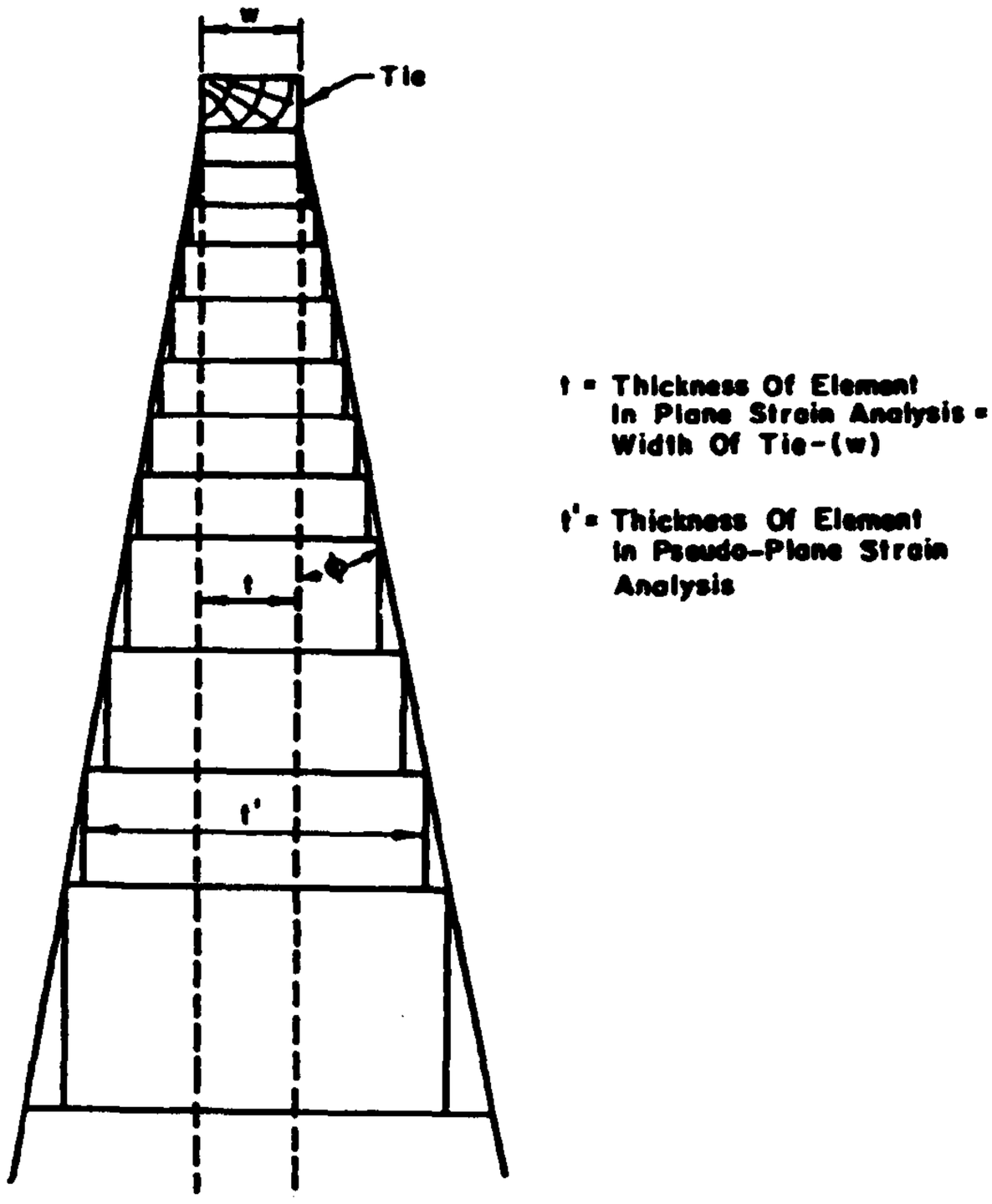

Fig. (2.18): Typical two dimensional finite element mesh for transverse analysis by ILLITRACK model.

Fig. (2.19a): 8-node isoparametric element.

Fig. (2.19b): Two dimensional interface element.

Fig. (2.19c): Finite element mesh.

Fig. (2.19): Two dimensional finite element idealisation for track analysis by Desai and Siriwardane (1982).

Fig. (2.20a): 21-node hexahedral element.

Fig. (2.20b): Three dimensional interface element.

Fig. (2.20c): Finite element mesh.

Fig. (2.20): Three dimensional finite element idealisation for track analysis by Desai and Siriwardane (1982).

Fig. (2.21a): Components of a conventional track system.

Fig. (2.21b): Forces and elements of a conventional track system used by GEOTRACK model.

Fig. (2.21): Three dimensional multilayer modelling of a conventional track system by GEOTRACK model.

Fig. (2.22a): Finite element mesh for the rail.

Fig. (2.22b): Finite element mesh of the track and track bed structures.

Fig. (2.22): Three dimensional finite element idealisation for track analysis by Profillidis (1986).

Fig. (2.23a): 8-node hexahedral element.

Fig. (2.23b): 20-node hexahedral element.

Fig. (2.23c): 6-node pentahedral element.

Fig. (2.23d): 15-node pentahedral element.

Fig. (2.23): Family of isoparametric elements used for track analysis by Raymond (1991).

CHAPTER THREE

LR55 TRACK SYSTEM

3.1 Introduction

As mentioned previously in chapter 2, by the end of the nineteenth century a considerable mileage of tramways and light rail tracks had been laid through the streets of the towns in Britain and other countries of the world. At first the trams had been drawn by horses; then steam locomotives were introduced. The latter were speedily replaced by electric tramcars.

Unfortunately, tramways disappeared from the streets of British towns some 40 years ago. The reason for this demise was that the infrastructure of tramways suffered heavily in the wartime, with the result that substantial amounts of money were required to repair and renew both the tracks and vehicles. In addition to that, the idea of light rail vehicles and tramways running through the streets was treated with suspicion and the traditional tram was remembered as rattling, slow moving and generally inadequate. In Europe the story was somewhat different as tramways were seen as a town friendly mode of transport and worth the investment. Many of these towns expanded systems in the 1950's and 60's.

Today, people in Britain begin to view the modern tramway and light rail system in a positive way, learning from their European colleagues. They have realised that a well designed tramway system can be a viable mean of reducing traffic congestion in major cities and lowering the level of noise, vibration and air pollution; i.e. can be truly considered as "green transport".

Therefore, the opportunity and need for the use of light rail transit that gains public acceptance have been seriously discussed for the last few years in Britain. Consequently, cities in the UK have started to re-introduce tramways. Manchester Metrolink was the first of a new generation of street-running light rail system opened in 1992, (Cope 1993).

It was then followed by South Yorkshire Supertram in Sheffield, (Boak 1995). Such systems have already been proposed for several other cities in Britain.

3.2 LR55 Track System

Low profile rail LR55 track system is entirely a new concept, developed by Professor Lewis Lesley of Liverpool John Moores University in 1989, (Lesley 1989). The main components of the LR55 track system are: low profile steel rail, elastomeric rail pad and concrete trough as shown in Fig. (3.1). This innovative system is meant to be a solution to overcome the drawbacks and limitations of the existing light rail track systems and street running tramways due to it's main characteristics and unique features. They are:

1. The mechanism of load transfer is utilised in a completely different way in comparison to all the existing track systems. The load is transmitted from the upper surface rather than the flat bottom of the rail. Such a criterion promises a shallower foundation depth, hence, little disturbance to the pavement or the underground services of cables, ducts, pipes ... etc. This will contribute to a certain extent to a reduction in the initial construction cost of a track system.
2. The LR55 track system is believed to meet the requirement of the environmental agencies that have set stringent noise and vibration limits. This is due to the following facts. Firstly, the LR55 rail has no web and it is well known that most of the noise and vibration are generated from flimsy thin webs, as it is the case for the conventional girder type of rail, i.e. Ri59 rail. Secondly, the LR55 rail has no mechanical joints and fasteners. Thirdly, the LR55 rail is fixed to the supporting structure by an elastomeric adhesive pad, which has been used as an extremely efficient acoustic isolator. These points make the LR55 track system much quieter than other existing track systems.
3. The LR55 track system is carefully designed to have high quality electrolysis control such that stray traction current does not get onto other structures, such as steel frame buildings or metallic pipes, which may result in electrolytic corrosion. This quality is provided by embedding the LR55 rails in the elastomeric compound, which has an excellent electrical insulation and can help prevent stray current leakage.

4. The LR55 track system satisfies the Department of Transport requirements for high standards of ride quality and passenger comfort, a feature that is essential to make the system attractive to the user. This is owing to the factors: a) The system has continuously welded rails (CWR) which improve the alignment of the rails and offer smooth and superior ride characteristics than jointed track. b) The rails are continuously supported by a resilient elastomeric pad, which has good damping quality and thus can effectively absorb the effect of impact load, noise and vibration caused by the running wheels. c) The robust design of the concrete trough as a main track structural support system does much to aid the required standards of ride quality through ensuring small track deflection and low pressure on the track base and hence less permanent settlement (these aspects will be covered separately in detail in due course).
5. The LR55 track system is expected to provide a long life, low maintenance system which offers a competitive whole life cost. Additionally, maintenance frequency is a critical issue not only for the light rail transit (LRT) operation, but will also minimise the impact of works on the city streets and their other users. This might be attributed to the following points: a) The rails are supported longitudinally by two continuous concrete troughs along its entire length. This will substantially enhance the lateral stiffness of the track and hence greatly improving the stability of the track which will result in a minimum risk of longitudinal or lateral buckling or derailment incidence. b) Using the concept of precast concrete trough elements will facilitate the process of construction and the replacement of any damaged units should it happen during service. c) Maintenance problems which are coherent with the mechanical fastenings as in the case of conventional track system, do not exist at all in the LR55 track system such as tightening the loose bolts or base plate fracture due to crack initiation at the roots of the joints as they are good source of stress concentration.

3.3 Elements of LR55 Track System

3.3.1 LR55 Rail

The LR55 rail has a squat shape of a total width of 165 mm and height of 80 mm as shown in Fig. (3.2). It is worthwhile to mention that the shape and size of the rail was

decided on after a few laboratory tests and desk analysis carried by the team initially involved with the design of the LR55 track system, (Lesley 1993 and 1994). The principle characteristic of the LR55 rail is that the wheel load is basically transmitted to the underlying supporting layers through the top flanges of the rail. Moreover, as the LR55 rail has no web, a quieter track than a conventional system is expected.

The geometrical properties of the rail section are presented in Table (3.1). These were determined by a special computer program called SECT developed for this purpose as will be explained later. The material used for the LR55 rail is made of rolled low carbon austenitic manganese alloy rail steel. It is regarded as a normal grade rail steel whose mechanical properties are shown in Table (3.2), (British Steel Track 1992, Cope 1993).

3.3.1.1 Bending Stresses of LR55 rail

The LR55 rail has no axis of symmetry. For such a section, the bending stresses resulting from pure moment about x-axis might be calculated from simple beam theory using the following formula, (see for example Benham and Warnock 1976):

$$\sigma_z = M_x (yI_y - x I_{xy}) / (I_y I_x - I_{xy}^2) \qquad (3.1)$$

where

σ_z = bending stress at any point within the section, compression positive

M_x = Bending moment about x-axis, sagging positive

x = distance from the neutral axis to the point where stress is required, measured normal to the y-axis

y = distance from the neutral axis to the point where stress is required, measured normal to the x-axis

I_x = moment of inertia of the section about the x-axis

I_y = moment of inertia of the section about the y-axis

I_{xy} = product moment of inertia of the section about x, y axes

Although the LR55 rail section seems to be very unsymmetrical, its product moment of inertia (I_{xy}) is found to be very small compared to I_x and I_y as shown in Table (3.1). The value of I_{xy} gives an indication about how symmetric the section is. For instance, when $I_{xy} = 0$ it means the section is perfectly symmetric.

Therefore, it is interesting to see that the maximum bending stresses in the rail section, which are of most practical importance, can be calculated with reasonable accuracy using the simple bending formula for symmetrical section about y-axis, (Benham and Warnock 1976), i.e.:

For top fibre stress: $\sigma_z = M_x / Z_{x,\,top}$ (3.2)

For bottom fibre stress: $\sigma_z = M_x / Z_{x,\,bot}$ (3.3)

where

$Z_{x,\,top}$ = elastic section modulus for the extreme top fibre

$Z_{x,\,bot}$ = elastic section modulus for the extreme bottom fibre

To illustrate this statement, assume that there is an applied sagging moment M_x of 10 kN m acting on the rail section. According to eq. (3.1), the maximum compressive stress has been found to occur at a distance x = 47.641 mm and y = 37.143 mm from the centroid of the section. Substituting the values of x and y, and from Table (3.1) the values of I_x, I_y and I_{xy} into eq. (3.1) gives,

$(yI_y - x\,I_{xy}) = 37.143 \times 834.634 \times 10^4 + 47.641 \times 43.702 \times 10^4$

$= 3.30828 \times 10^8$ mm^5

$(I_y\,I_x - I_{xy}^2) = 834.634 \times 377.328 \times 10^8 - 43.702 \times 43.702 \times 10^8$

$= 313020.913 \times 10^8$ mm^8

$\sigma_z = M_x\,(yI_y - x\,I_{xy}) / (I_y\,I_x - I_{xy}^2)$

$= 10 \times 10^6 \times 3.30828 \times 10^8/(313020.913 \times 10^8)$

$= 105.689$ N/mm^2

By considering the simpler approach, the maximum compressive stress due to sagging moment M_x = 10 kN m can be approximately calculated by substituting the value of $Z_{x,\,top}$ obtained from Table (3.1) into eq. (3.2), i.e.:

$\sigma_z = 10 \times 10^6/(98.994 \times 10^3)$

$= 101.016$ N/mm^2

Thence,

% accuracy = 100 x 101.016/105.689

= 95.58%

Similarly, according to eq. (3.1) the maximum tensile stress has been found to occur at a distance x = - 27.296 mm and y = - 41.841 mm from the centroid of the section, which is:

$(yI_y - x I_{xy}) = - 41.841 \times 834.634 \times 10^4 - 27.296 \times 43.702 \times 10^4$

$= - 3.61148 \times 10^8 \text{ mm}^5$

$(I_y I_x - I_{xy}^2) = 313020.913 \times 10^8 \text{ mm}^8$

$\sigma_z = M_x (yI_y - x I_{xy}) / (I_y I_x - I_{xy}^2)$

$= - 10 \times 10^6 \times 3.61148 \times 10^8/(313020.913 \times 10^8)$

$= -115.375 \text{ N/mm}^2$

$= 115.375 \text{ N/mm}^2$ tension

When eq. (3.3) is implemented, then the maximum tensile stress occurs at the bottom, and by substituting the value of $Z_{x,\,bot}$ taken from Table (3.1) into eq. (3.3), it will approximately be:

$\sigma_z = 10 \times 10^6/(90.146 \times 10^3)$

$= 110.931 \text{ N/mm}^2$

Thence,

% accuracy = 100 x 110.931/115.375

= 96.15%

From the above calculations one can conclude that the bending stresses in the rail can be determined from the detailed eq. (3.1) to obtain exact results. Alternatively, one can use, for sake of simplicity, eqs. (3.2) and (3.3) to obtain approximate results, but without affecting the accuracy significantly.

3.3.2 Rail Pad

The LR55 rail is bonded to the concrete trough using elastomeric adhesive pad. The elastomeric grout is initially pourable, but cures to a resilient rubber type material.

The term elastomers is derived from elastic polymers. Elastomers are produced from crude rubbers in which a variety of compounding ingredients are incorporated. This is

accomplished by the process of vulcanisation, i.e. curing, which usually takes place under pressure at elevated temperatures. In this process the chain molecules are fastened together at various points along their lengths by cross-links. These cross-links prevent slippage of chains past each other. Initially, the obtained rubber mixtures are usually tacky, thermoplastic and soluble in strong solvents. The final product exhibits a high degree of elastic recovery, loses its tackiness, becomes insoluble in solvents and infusible when heated and is more resistant to deterioration caused by ageing factors, (Nagdi 1993).

The first and foremost property of elastomers is elasticity. All elastomers have the ability to deform substantially by stretching, compression or torsion and then return back to their original shape after removal of the force causing the deformation. The majority of elastomers possess other useful properties such as low permeability to air, several gases, water and steam, good electrical and thermal insulation and the capability of adhering to various fibres, metals, and rigid plastics, (Gent 1993, Nagdi 1995).

In the 1980's, ALH Systems produced their "Series Six" elastomer which comprises a two component modified polyurethane encapsulant and a one component urethane based primer. It has been used successfully since then as a sealant material for underground gas pipes. The material has proved to meet all the requirements of the gas industry under all climatic conditions of temperature and humidity. Series Six has also been utilised in other applications for example water sealing between concrete slabs, encapsulation of concrete pipe joints, and has demonstrated to be ideal for site application where long term resistance to the environment and flexibility are paramount, (ALH 1992).

SikaRail KC 330 is another example of elastomer which is a product of Sika Limited. It is a flexible, two component polymer grout based on a modified polyurethane-epoxy resin combination. It is designed as vibration-absorbing grout for undersealing and fixing track supports to rigid surfaces such as bridge decks, road crossings and tunnels, (Sika 1990). It has already been applied successfully in light rapid transit track work such as Manchester Metrolink, South Yorkshire Supertram and Sydney Light Rail, (Roberts 1996). It was also used for the LR55 track model during the initial laboratory work and

the field test at the Rotherham Bus Station in Sheffield, (Lesley 1993, Lesley and Al-Nageim 1996).

Elastomer such as Series Six or KC 330 has the following advantages which make it a suitable grout and fixation material for light rail transits and street running tramways, (Sika 1990, ALH 1992 and 1996):

1. Liquid applied by pouring or injection. This implies there is no need to level irregular substrates and allows greater casting tolerances on concrete substrates.
2. Resilient grout absorbs considerable vibration which reduces structure borne and vehicle generated noise and vibration, hence providing the track system with a quieter and smoother ride.
3. Excellent mechanical properties including superior tensile and tear strength, high resistance to abrasion and significant absorption of impact and static loading.
4. High adhesion to steel and concrete surfaces which prevent underflow of water and pumping, hence avoiding corrosion of the underside of the rail. More importantly, it can eliminate the need for any anchor bolts.
5. High chemical resistance to fuel oils, de-icing salts, dilute acids, alkalis, water and weather.
6. Excellent electrical resistance characteristics prevent stray currents.
7. Quick cure allows early trafficking in maintenance situations.
8. It can be provided with various coloured surface finishes and anti-skid surfaces.

The most important mechanical properties of Series Six and KC 330 elastomeric grout are presented in Table (3.3). They are based on extensive experimental works carried by Muhr and Gough (1991), ALH (1992), and Mohammad (1997).

Laboratory tests on the Series Six elastomer were also performed under extreme temperatures of 60 and -10 °C. It was demonstrated that over a wide range of temperature between 20 and 60 °C the mechanical properties of the elastomer changes only slightly. This reveals that the elastomeric pad is stable within this range of temperature. At temperatures below zero the material becomes stiffer and shows higher strength and modulus. For more details about these tests, see (Mohammad 1997). The

temperature at which the elastomer becomes glass-like material, i.e. very brittle is round -46 °C. This is known as glass transition temperature, (Nagdi 1995, ALH 1996).

Several samples of the LR55 track system of 1 m length were submerged under 10 mm of water. The rail was fixed to the concrete trough using the resilient grouting KC330 produced by Sika Limited. Tests were undertaken to observe the effectiveness of the bonding material between the rail and the concrete trough. During the tests no water penetration or swelling of the grout material had occurred and no sign of bonding failure was observed, (Lesley and Al-Nageim 1996). In addition, ALH (1996) stated that the immersion of 6 mm thick sample of the Series Six elastomer in water for 7 days caused swelling or water absorption of less than 0.1 %, (ALH 1996).

Due to the above mentioned advantages and high quality performance of these elastomers as proved through rigorous laboratory tests as well as the past experience gained from real practical application of such elastomers, one can strongly recommend the use of such elastomeric pads like Series Six or KC 330 for the LR55 track system as an excellent rail embedment material.

3.3.3 Concrete Trough

The main supporting structural members for the LR55 rails are two separate concrete troughs, placed longitudinally along the rails. A tentative cross-sectional geometry and dimensions of the concrete trough is shown in Fig. (3.3a). This had been initially based on a desk analysis carried out by the team involved with the LR55 track system, (Lesley 1991 and 1993). Then, for ease of stripping the concrete casting moulds and pouring the elastomeric pad, it was suggested to slightly modify the shape as shown in Fig. (3.3b). The main characteristics of the concrete trough are:

1. It has a very high resistance to longitudinal movement resulting from traction or braking loads since it is laid continuously parallel to the axis of the rail.
2. It has high lateral stiffness which is favourable in connection with horizontal forces and track stability.
3. Due to its continuous support to the rail, the bending stresses developed in the rail and pressure on the track formation are expected to be lower than those of

conventional track system where the rail is supported by concrete sleepers at discrete points.

The concrete trough section could be either reinforced or prestressed concrete. In the case of reinforced concrete section, it would be ideal to follow cast in-situ production using a slipform technique in order to reduce construction time. Whereas, in case of prestressed concrete section, it might be produced efficiently in large quantities using the long line method described in section (2.3.3.1), chapter 2.

Prestressed concrete section does offer a number of distinct advantages over the reinforced one, namely; (Naaman 1982, Kong and Evans 1989, Lin and Burns 1995):

1. In a fully prestressed concrete section, the whole area of the concrete acts to resist bending, unlike reinforced concrete where the concrete in the tension zone provides negligible contribution to the stiffness of the section. Hence for a given span and loading it is possible to have a shallower depth in the case of prestressed section. This means a prestressed concrete trough will definitely help to achieve the most paramount goal promised from the design of LR55 track system where the depth of foundation, hence excavation is desired to be as minimum as possible.
2. A prestressed concrete element is a crack free structure and made of quality materials (concrete and tendons) as compared to a reinforced concrete section. This means that the risk of the tendons being corroded is minimised, the structure is more durable and has longer span life and hence less maintenance is required. Therefore, having a prestressed concrete trough will contribute to a large extent in satisfying another viable target expected from the design of LR55 track system where the overall maintenance cost is required to be minimised.
3. A prestressed concrete section has higher impact and fatigue resistance than reinforced concrete section. Such a criterion is quite preferable and important for a structure which is primarily under repetitive dynamic loading such as the case with a track system. Past experience demonstrated that reinforced concrete sleepers performed very poorly under the effect of dynamic loads of the passing vehicles, (FIP 1987, Taylor 1993).

However, there are some limitations related with the production of prestressed concrete elements. They are, (Naaman 1982, Lin and Burns 1995):

1. As higher strength concrete and higher grade steels are used in the case of prestressed concrete, the initial cost of producing concrete units will be relatively high, despite the fact that less material is used as compared with a reinforced concrete member.
2. The cost of prestressing the tendon will add to the overall cost of the concrete unit.
3. The prestressing operation necessitates a reasonable level of skill and supervision than is otherwise necessary in conventional reinforced concrete construction.

According to the author's point of view as well as the partners who are dealing with the LR55 track project, it has been found that the advantages of using a prestressed concrete trough outweigh its drawbacks.

Having decided on a prestressed concrete trough section, the pre-tensioning method is found to be more practical and suitable than a post-tensioning method for the following reasons:

1. Pre-tensioned concrete trough units have no locking device at their ends. So, there is no difficulty in connecting these units together along the track in practice. On the contrary, if a post-tensioning method is adopted, it would be extremely difficult and expensive to maintain these locking systems once the track system is installed and made flush with the top surface of the road.
2. A pre-tensioning method can be achieved in mass production more efficiently and economically than the case with a post-tensioning method as explained previously in section 2.3.3, chapter 2.
3. Tarmac Precast Concrete Limited is the largest leading company in Britain for producing pre-tensioned concrete sleepers and has long term experience over 50 years in this field. Furthermore, Tarmac Precast Concrete Limited is one of the partners involved in the current project as the company manufactured and supplied the prestressed concrete trough sample for experimental purpose conducted in this work. Tarmac Precast Concrete Limited is very keen on the idea of a pre-tensioned concrete trough and strongly support it for feasibility and commercial purposes.

Accordingly, pre-tensioned prestressed precast concrete trough units sound to be ideal for the LR55 track system. In case of straight line tracks, these precast elements will be provided in standard lengths of 6 m for handling and transportation convenience and will be connected together by simple construction joints (hinges) along the track system.

Owing to the reasons presented above, it was decided to investigate and study the analysis and design of a pre-tensioned prestressed concrete trough for the LR55 track system in the present work. This will be discussed in more detail in the following chapters.

3.4 Design Wheel Load

From the literature survey it has been found that the light rail transits are designed to axle loads between 108 - 118 kN (11 - 12 tonne), see section 2.5.2.

In 1993, a 10 m length of the LR55 track model was embedded at the entrance road of Rotherham Bus station in Sheffield in order to carry out some field experiments. During the tests, it had been noticed that round 5000 buses per day with axle load up to 108 kN (11 tonne) passed over the LR55 track, (Lesley 1993). This reveals that the occurrence of axle loads experienced by a street running track system are quite frequent such that the overall annual tonnage carried by the system is very high. A factor which has to be taken into consideration for long term performance of the track system such as fatigue criteria and total accumulated settlement with time.

Additionally, through the personal communication between the author and Lewis Lesley (Professor of Transport Science in Liverpool John Moores University), Lesley mentioned that the recorded axle loads in British roads are as great as 128 kN (13 tonne).

Thus, street running track systems are subject to a maximum axle load ranging between 108 - 128 kN (11 - 13 tonne) with high annual tonnage. Therefore, a static nominal axle load of 122.6 kN (12.5 tonne) is assumed for the analysis and design of the LR55 track system in the present work in order to be on the safe side. It is interesting to mention

that this assumed axle load is half the maximum axle load for the British Rail main lines, (Cope 1993).

The maximum speed of light rail transit is normally between 70 - 80 km/h, and sometimes reaches up to 100 km/h. According to Fig. (2.15), the DLF for light rail transits that corresponds to a speed of 100 km/h, ranges between 0.48 and 0.7. In the present work, the value of the DLF is taken as 0.7. In fact, the DLF could be most likely assumed a value higher than 0.7 as it depends not only on the traffic speed, but also on experience and largely on the maintenance requirement. The latter is a very serious and important issue to be taken into account for street running rail systems since any maintenance operation would be very expensive and nuisance as it would cause disruption to all the users of the street. However, the value of DLF is kept as 0.7 on the basis of assuming a slightly conservative axle load.

Accordingly, the design axle load for the LR55 track system will be:

Design axle load = Nominal axle load x (1 + DLF)

= 122.6 x (1 + 0.7)

= 208.42 kN

The design wheel load will be:

Design wheel load = (Design axle load)/2

= 208.42/2

= 104.21 kN

3.5 Computer Program SECT

During the design process of a member having non-standard section such as the LR55 rail or the concrete trough, it is usually necessary to determine its geometric properties. This can be a tedious task involving a great deal of manual arithmetic manipulations. To avoid this, a special computer program called SECT was coded in FORTRAN 77 for P.C. machines to carry out these calculations with high speed and accuracy. The program is based on a simple numerical procedure where any geometrical figure can be treated as

a polygon of n vertices (n sides). Expressions can then be easily derived for the properties of shapes with polygonal boundaries as presented below:

Consider a polygon of n vertices whose coordinates are measured with respect to X, Y axes, and numbers are successively given in anticlockwise direction as shown in Fig. (3.4). The area, centroid and moment of inertia of the polygon is the algebraic sum of the corresponding geometrical properties of the trapezia formed by the sides of the polygon and their projections on to the X and Y axes, (Cope et al 1982). Thus:

$$A = \sum_{i=1}^{n} (X_i - X_{i+1})(Y_i + Y_{i+1})/2 \tag{3.4}$$

$$Y' = \sum_{i=1}^{n} (X_i - X_{i+1})(Y_i^2 + Y_iY_{i+1} + Y_{i+1}^2)/6A \tag{3.5}$$

$$X' = \sum_{i=1}^{n} (Y_{i+1} - Y_i)(X_i^2 + X_iX_{i+1} + X_{i+1}^2)/6A \tag{3.6}$$

$$I_X = \sum_{i=1}^{n} (X_i - X_{i+1})(Y_i^3 + Y_i^2Y_{i+1} + Y_iY_{i+1}^2 + Y_{i+1}^3)/12 \tag{3.7}$$

$$I_Y = \sum_{i=1}^{n} (Y_{i+1} - Y_i)(X_i^3 + X_i^2X_{i+1} + X_iX_{i+1}^2 + X_{i+1}^3)/12 \tag{3.8}$$

$$I_{XY} = \sum_{i=1}^{n} (X_i - X_{i+1})[X_i(9Y_i^2 + 6Y_iY_{i+1} + 3Y_{i+1}^2) + X_{i+1}(3Y_i^2 + 6Y_iY_{i+1} + 9Y_{i+1}^2)]/72 \tag{3.9}$$

where

X_i = X-coordinate of vertex i

Y_i = Y-coordinate of vertex i

A = area of the section

X' = X-coordinate of the section centroid

Y' = Y-coordinate of the section centroid

I_X = moment of inertia of the section about X-axis

I_Y = moment of inertia of the section about Y-axis

I_{XY} = product moment of inertia of the section about X, Y axes

The moment of inertia of the polygon about x, y axes passing through the centroid can be calculated using the parallel axis theorem, (Cope et al 1982):

$$I_x = I_X - AY'^2 \tag{3.10}$$

$$I_y = I_Y - AX'^2 \tag{3.11}$$

$$I_{xy} = I_{XY} - AX'Y' \tag{3.12}$$

where

I_x = moment of inertia of the section about x-axis

I_y = moment of inertia of the section about y-axis

I_{xy} = product moment of inertia of the section about x, y axes

The maximum and minimum moments of inertia and inclination of the principal axes can be determined by the standard formula as, (Cope et al 1982):

$$I_{max} = [(I_x + I_y) + \{(I_x - I_y)^2 + 4I_{xy}^2\}^{1/2}]/2 \tag{3.13}$$

$$I_{min} = [(I_x + I_y) - \{(I_x - I_y)^2 + 4I_{xy}^2\}^{1/2}]/2 \tag{3.14}$$

$$\tan(\psi) = (I_x - I_{max})/I_{xy} \tag{3.15}$$

where

I_{max} = maximum moment of inertia of the section

I_{min} = mimimum moment of inertia of the section

ψ = angle between x-axis and the principal axis corresponding to I_{max}

The elastic section moduli and radii of gyration of the section can be found as, (Gere and Timoshenko 1985):

$$Z_{x,\,bot} = I_x/(Y' - Y_{min}) \tag{3.16}$$

$$Z_{x,\,top} = I_x/(Y_{max} - Y') \tag{3.17}$$

$$Z_{y,\,left} = I_y/(X' - X_{min}) \tag{3.18}$$

$$Z_{y,\,right} = I_y/(X_{max} - X') \tag{3.19}$$

$$r_x = (I_x/A)^{1/2} \tag{3.20}$$

$$r_y = (I_y/A)^{1/2} \tag{3.21}$$

$$r_{max} = (I_{max}/A)^{1/2} \tag{3.22}$$

$$r_{min} = (I_{min}/A)^{1/2} \tag{3.23}$$

where

X_{max} = X-coordinate of the extreme right fibre of the section

X_{min} = X-coordinate of the extreme left fibre of the section

Y_{max} = Y-coordinate of the extreme top fibre of the section

Y_{min} = Y-coordinate of the extreme bottom fibre of the section

$Z_{x, bot}$ = elastic section modulus for the extreme bottom fibre

$Z_{x, top}$ = elastic section modulus for the extreme top fibre

$Z_{y, left}$ = elastic section modulus for the extreme left fibre

$Z_{y, right}$ = elastic section modulus for the extreme right fibre

r_x = radius of gyration of the section with respect to x-axis

r_y = radius of gyration of the section with respect to y-axis

r_{max} = maximum radius of gyration of the section

r_{min} = minimum radius of gyration of the section

The flow chart of the computer program SECT shown in Fig. (3.5) summaries the steps involved for calculating the section properties by employing eqs. (3.4) – (3.23). The program SECT can be utilised to cater for any irregular shape including voided sections and sections with curved boundaries. In case of a voided section, the hollow item within the section is given a weight factor = -1. For a curved boundary figure such as the LR55 rail, a number of small connected lines, depending on the level of accuracy aimed, can be used to simply represent the curved edge.

The cross sectional properties of the universal beam section UB203 x 133 x 30 were determined by the SECT program as shown in Table (3.4). The results were compared with those given by British Steel tables for standard sections, (British Steel 1996). The maximum difference is less than $\pm$ 0.1%. In addition to that, the area of the LR55 rail is 67.155 cm^2 as calculated by SECT program. The same section was solved by AutoCAD Release 12 and the area is found to be 66.894 cm^2, i.e. a difference of – 0.3% only. These two cases confidently prove the correctness of the SECT program.

Table (3.1): Section properties of the LR55 rail.

Description	Value
Area (cm^2)	67.155
Weight (kg/m)	52.76
Centroid (mm):	
x_c from far left	78.4
x_c from far right	86.6
y_c from far top	38.1
y_c from far bottom	41.9
Moment of inertia (cm^4):	
I_x	377.328
I_y	834.634
I_{xy}	-43.702
I_{max}	838.773
I_{min}	373.189
Elastic section modulus (cm^3):	
$Z_{x,\ bot}$	90.146
$Z_{x,\ top}$	98.994
$Z_{y,\ left}$	106.51
$Z_{y,\ right}$	96.332
Radius of gyration (mm):	
r_x	23.7
r_y	35.2
r_{max}	35.3
r_{min}	23.6

Table (3.2): Mechanical properties of the LR55 rail as normal grade steel.

Description	Value
Young's modulus (N/mm^2)	200 000
Yield strength based on 0.2% proof stress (N/mm^2)	467
Minimum tensile strength (N/mm^2)	700
Elongation (%)	10 - 12
Coefficient of thermal expansion per 1 °C	12×10^{-6}

Table (3.3): Mechanical properties for the elastomeric pad at normal room temperature.

Description	Range of value
Tensile Young's modulus (N/mm^2)	2.5 - 3.5
Tensile strength (N/mm^2)	2.8 - 4.0
Maximum tensile strain	150 - 250 %
Compressive Young's modulus (N/mm^2)	13.5 - 15.5
Compression (Pressure) resistance (N/mm^2)	up to 3.2 - 5 without failure
Compressive stain	up to 40% without failure
Shear modulus (N/mm^2)	1 - 2.6
Shear strength (N/mm^2)	1.9 - 2.1
Maximum shear strain	200 - 300%
Poisson's ratio	0.47 - 0.4996

Table (3.4): Section properties of the UB203 x 133 x 30 as found by SECT program and British Steel (1996).

Description	SECT program	British Steel	% Difference
Area (cm^2)	38.24	38.2	+ 0.1%
Moment of inertia (cm^4):			
I_x	2898	2896	+ 0.06%
I_y	384.67	385	- 0.1%
Elastic section modulus (cm^3):			
$Z_{x, bot}$	280.27	280	+ 0.1%
$Z_{x, top}$	280.27	280	+ 0.1%
$Z_{y, left}$	57.46	57.5	- 0.07%
$Z_{y, right}$	57.46	57.5	- 0.07%
Radius of gyration (mm):			
r_x	8.71	8.71	0%
r_y	3.17	3.17	0%

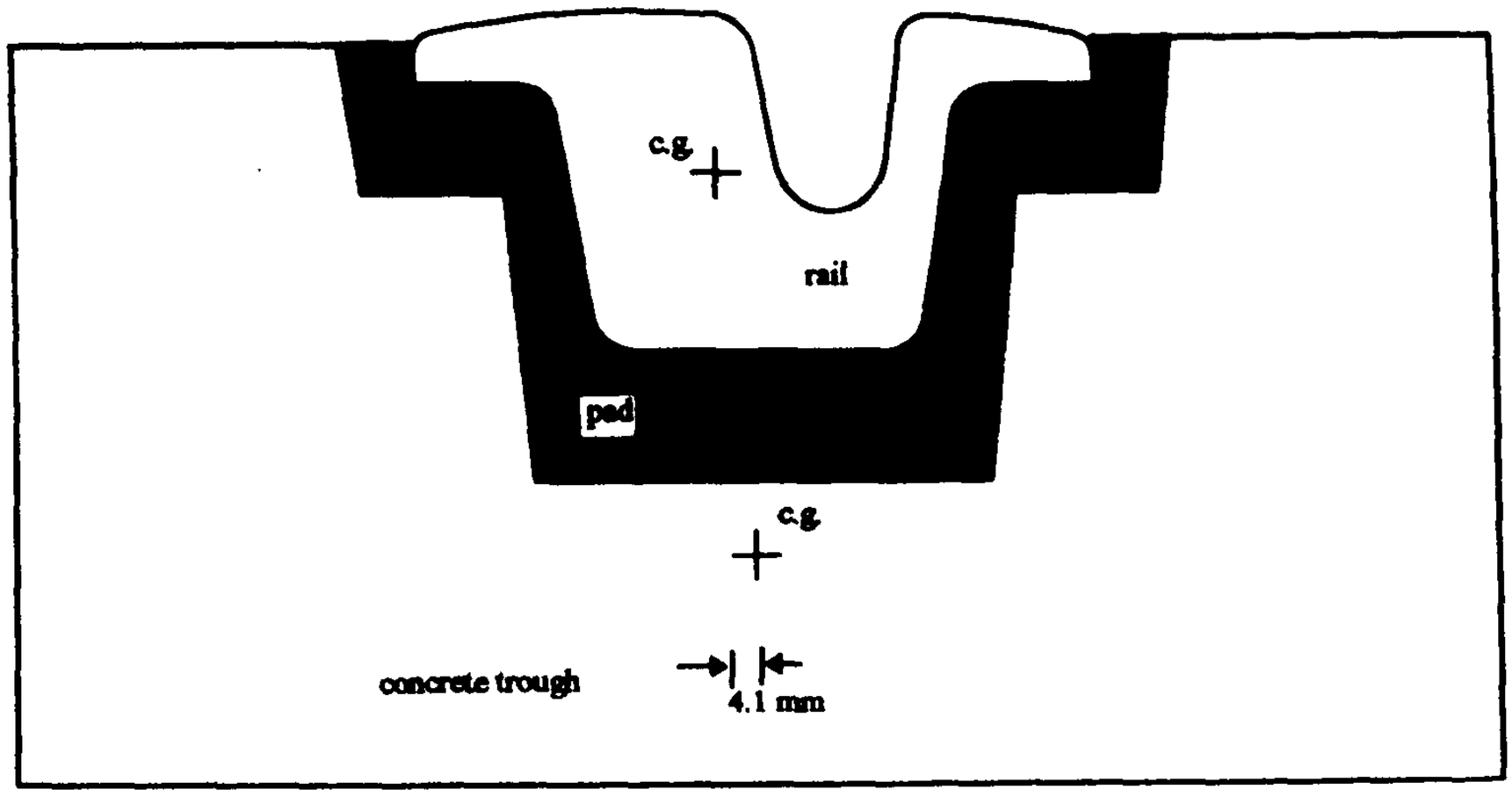

Fig. (3.1): Components of the LR55 track system.

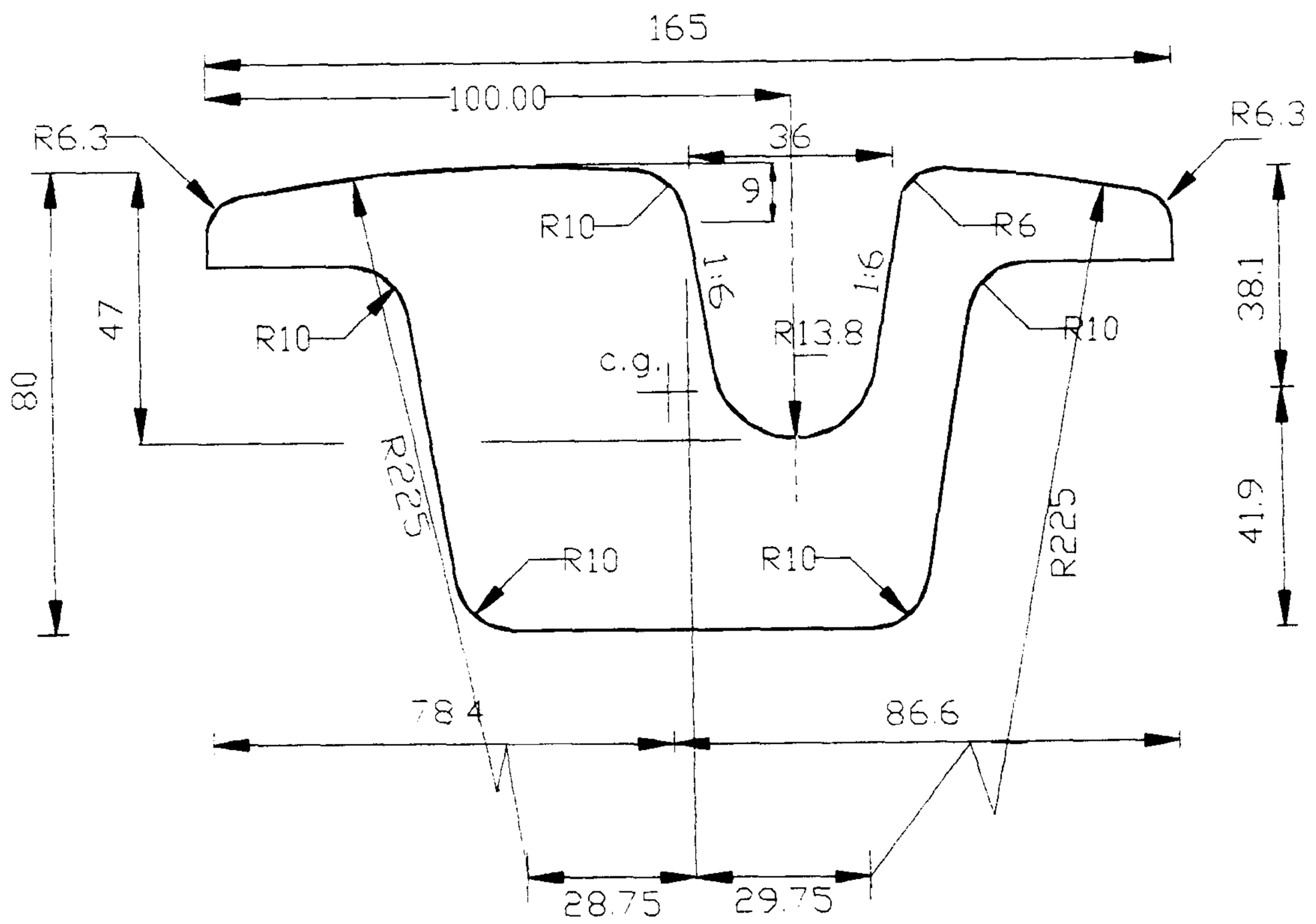

All dimensions are in mm.

Fig. (3.2): LR55 rail.

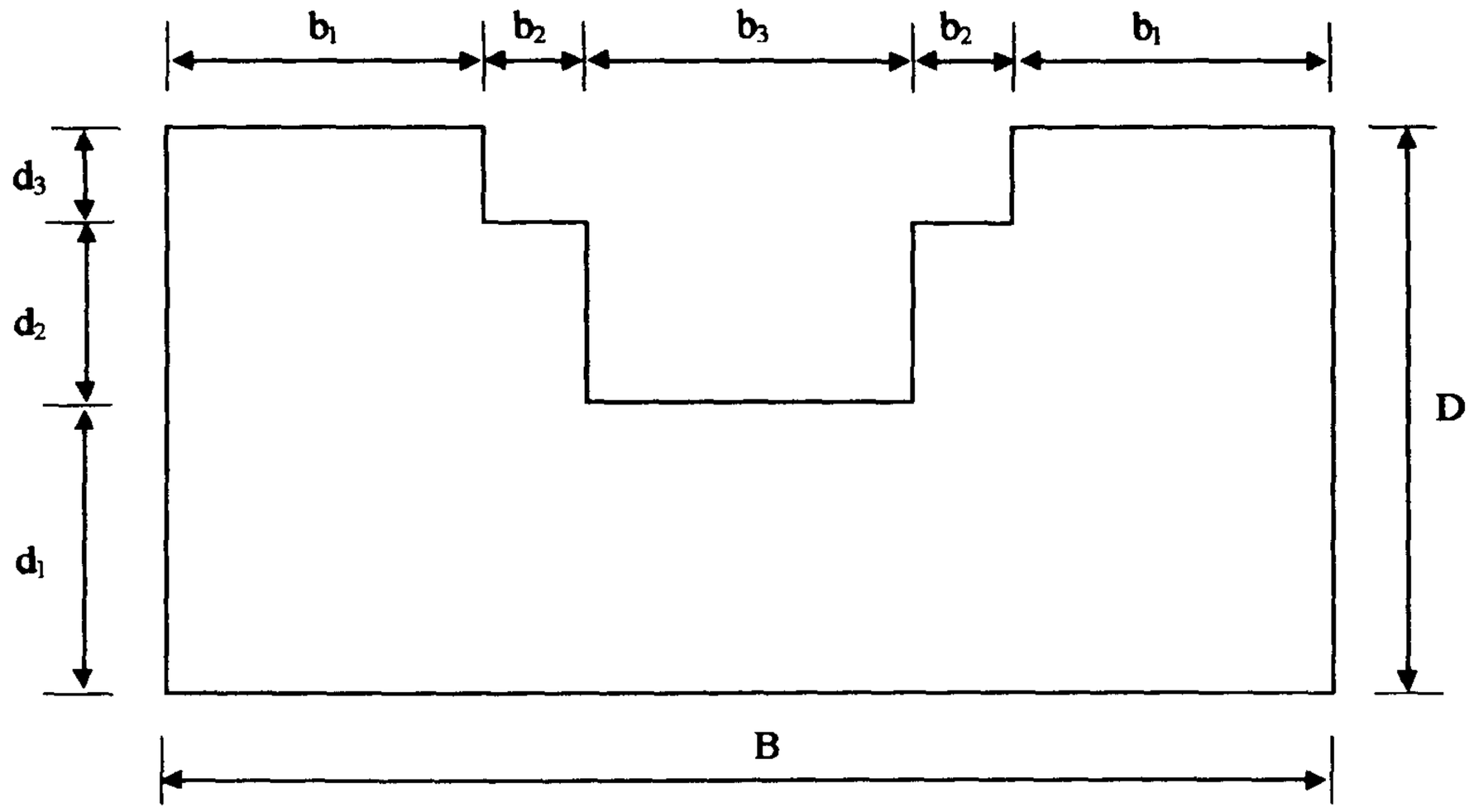

$b_2 = 35$, $b_3 = 130$
$d_2 = 60$, $d_3 = 25$

Fig. (3.3a): Initial proposed concrete trough shape.

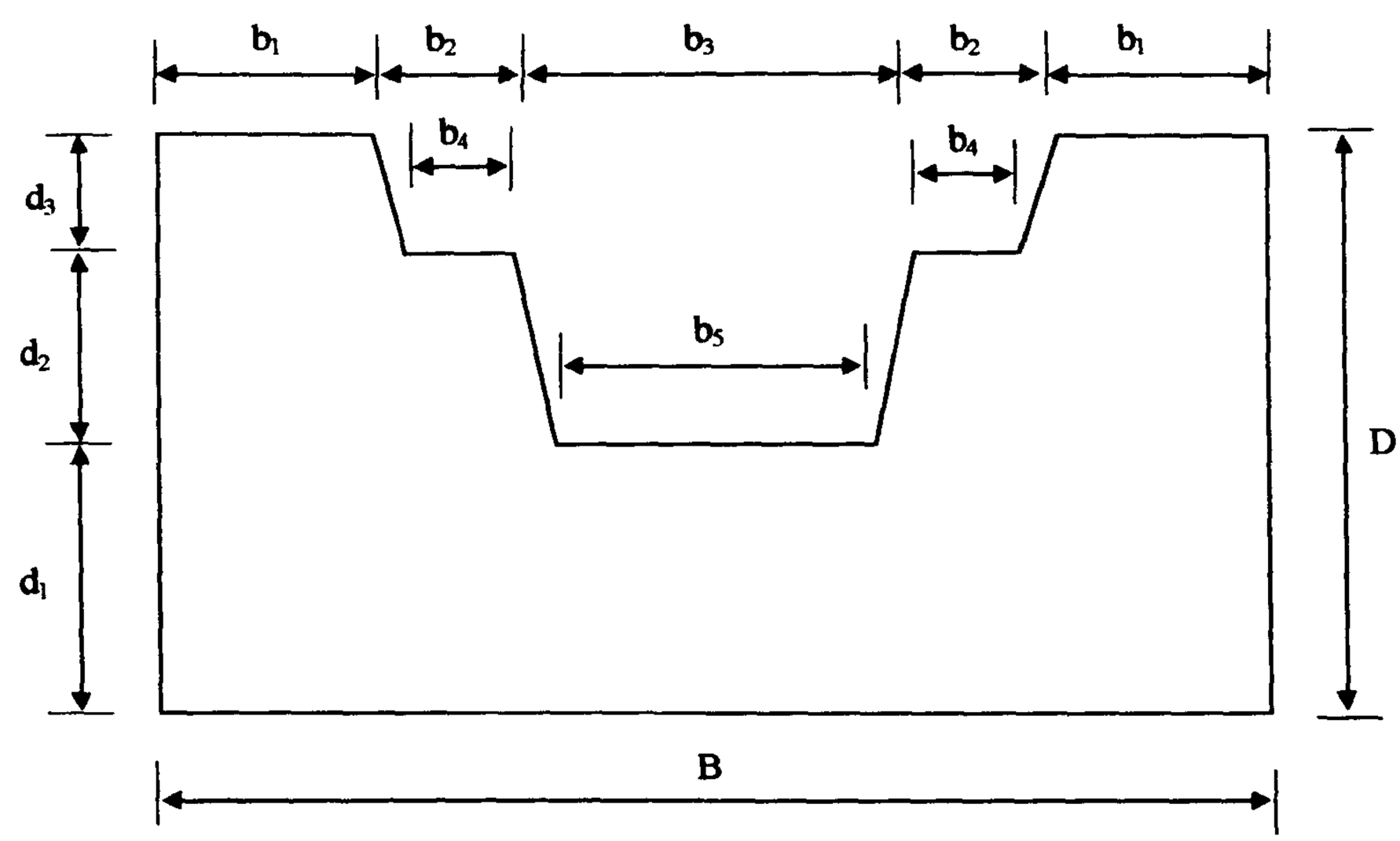

$b_2 = 43$, $b_3 = 138$, $b_4 = 38$, $b_5 = 120$
$d_2 = 70$, $d_3 = 35$

All dimensions are in mm.

Fig. (3.3b): Final proposed concrete trough shape.

Fig. (3.3): Concrete trough cross-sectional shape.

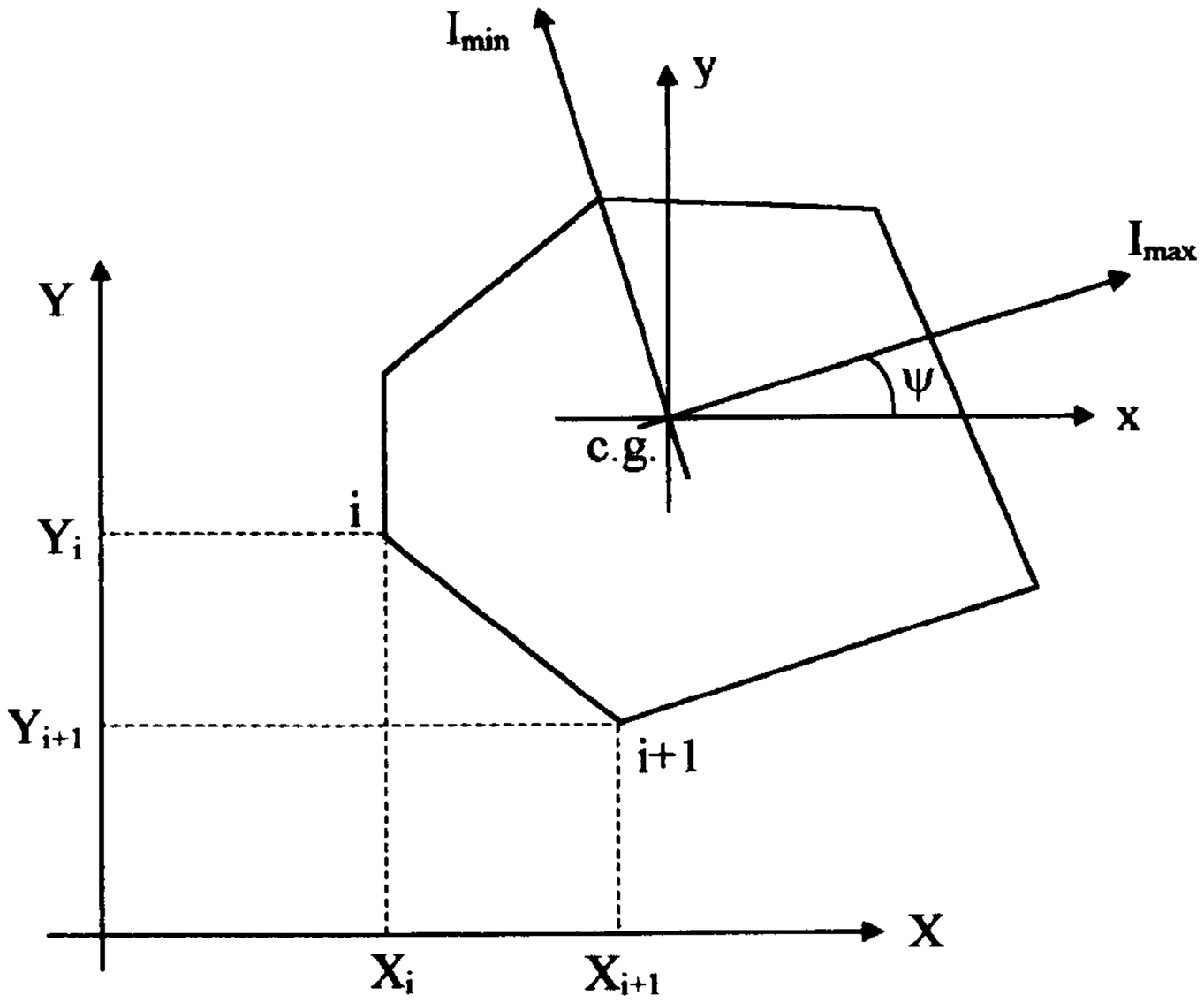

Fig. (3.4): Properties of a polygon determined by SECT program.

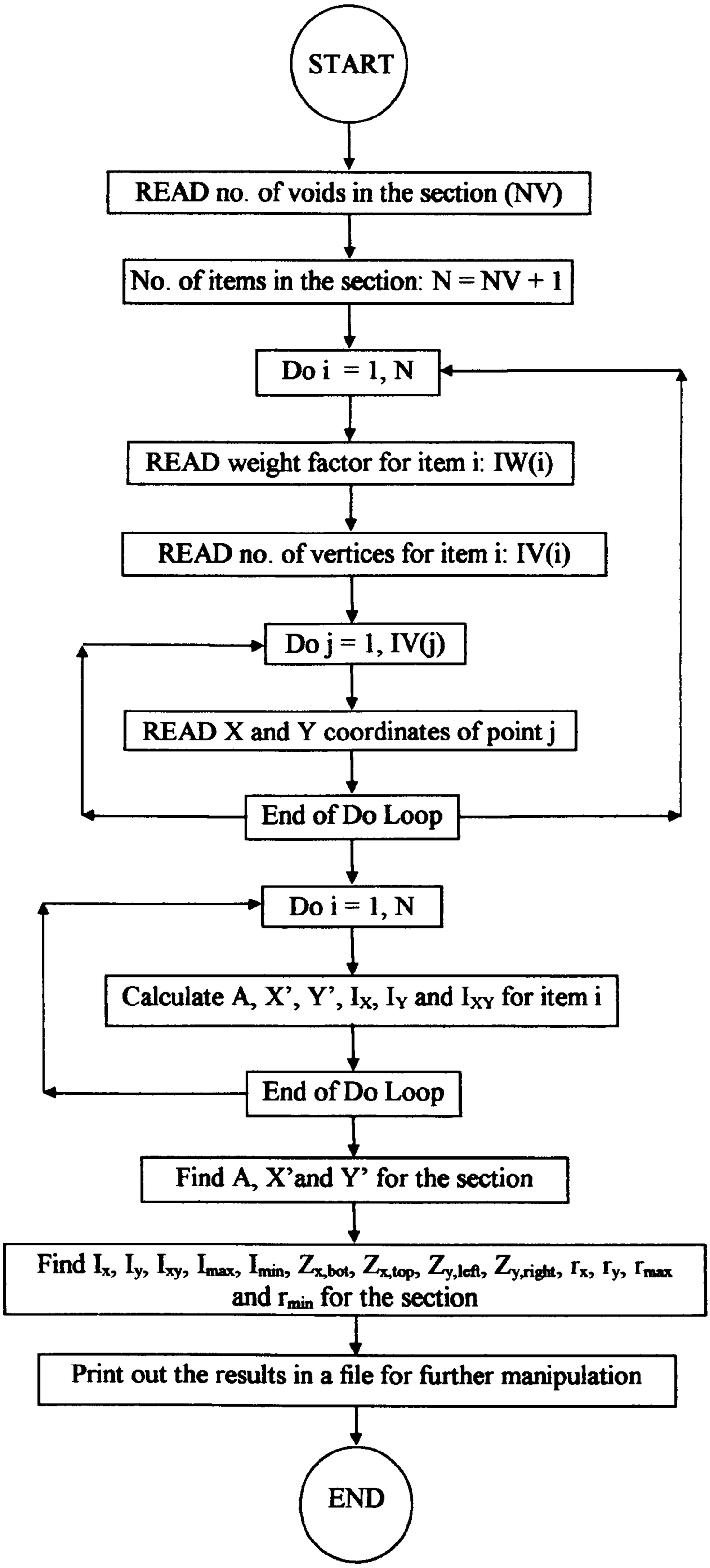

Fig. (3.5): Flow chart for the computer program SECT.

CHAPTER FOUR

PRESTRESSED CONCRETE TROUGH

4.1 Introduction

Prestressing involves the deliberate introduction of permanent internal stresses into a concrete structure during its construction to improve its performance under normal conditions. Prestressing the concrete would produce compressive stresses, either uniform or non-uniform, which will counteract tensile stresses induced by external loadings. Depending on the amount of prestressing, the tensile stresses can be entirely eliminated, thus producing a crack-free structure during its service life. Alternatively, a limited tensile stress with or without controlled cracking is permitted in the structure in a way similar to reinforced concrete.

4.2 Methods of Prestressing

The most common methods of prestressing involve the use of tensioned steel tendons, consisting of high strength wires, strands or bars incorporated permanently into the structure. The tendons may be tensioned before the concrete is placed (pre-tensioned) or after the concrete has hardened (post-tensioned). The choice of the method is governed largely by the type and size of member and the need for precast or in-situ construction. A description for both methods is well covered in the literature, see for example (Abeles and Bardhan-Roy 1981, Lin and Burns 1995). However, a brief explanation of these methods will be presented for sake of convenience and completeness.

4.2.1 Pre-tensioning

In pre-tensioning the prestressing tendons such as wires or strands are stretched to a predetermined tension between temporary anchorages. The concrete is then poured around the tendons in moulds. When the concrete has hardened and gained sufficient strength, the force in the tendons is released from the temporary anchorages and transferred to the concrete. As the bond between the tendons and the concrete resists the shortening of the tendons, the concrete gets compressed.

Pre-tensioning may be used where large numbers of similar precast units are required. Thus it is ideal for factory production of standard units such as concrete sleepers for conventional railway systems and the concrete trough for the LR55 track system. In this case a long line-production is arranged in which the tendons pass through appropriate holes in the stop-ends of each unit and are simultaneously or individually tensioned. Mould assembly and reinforcement fixing is completed and concrete is placed and compacted around the tensioned tendons. When the concrete has achieved sufficient strength, the force in the tendons is released from the abutments and transferred to the concrete. The tendons are then cut between the units, the stop-ends removed and the projecting tendons cut or burnt off.

Depending on the pre-tensioned structural elements produced, the tendon profile may be either straight such as in concrete sleepers for railway systems or deflected at one or two points such as in bridge girders.

4.2.2 Post-tensioning

This method involves the use of wire, strands or bars which are tensioned and anchored at the ends of the concrete member after the member has attained sufficient strength. The tendons are normally contained within one or more ducts placed along the member before concrete casting. After stressing and anchoring, the void between each tendon and its duct is normally filled with mortar grout to ensure effective bonding of the tendon to the surrounding concrete and prevent corrosion of the tendons. In some structures the ducts are filled with grease instead of grout to prevent the bond throughout the length of the tendon. This leads to debond tendons which have particular application in slab systems with several bays for its economy and efficiency, (Namman 1982).

Post-tensioning may be used in precast concrete operation such as the production of monoblock post-tensioned sleepers, (Taylor 1992). However, it is the most suitable for in-situ construction where large structures such as bridge girders cannot be transported.

The concrete trough for the LR55 track system considered in this work is a pre-tensioned prestressed element. Therefore the analysis and design of a pre-tensioned

member will only be explained in the following sections and no further attention will be given to post-tensioning structures.

4.3 Prestressing Steel

In pre-tensioned prestrressed concrete elements, high strength steel wires and strands are commonly used. They are produced in the UK to meet the specification of BS 5896 (1980).

Cold drawn steel wires are produced by drawing hot-rolled, steel rods through dies to produce wires of the required diameter. The drawing process cold works the steel, thereby altering its mechanical properties and increasing its strength. The wires are then stress relieved by a process of continuous heat treatment to improve its mechanical properties. The wire surfaces are initially smooth but may be indented or crimped by a subsequent process to improve their bond characteristics. The mechanical properties of cold-drawn wires are presented in Tables (4) and (5) of BS 5896 (1980).

Strands consist of a number of prestressing wires which are woven together to suit the dimensions and strength of the end product. The outer wires are spun into a helical form to lie firmly together and around a straight core wire. Due to this mechanical forming process, there are some stresses. Therefore, the strand is finally given a stress-relieving treatment similar to the one previously described for cold-drawn wire. The mechanical properties of 7-wire strands are given in Table (6) of BS 5896 (1980).

It is worthwhile to mention that all pre-tensioned concrete sleepers were initially made with wires, but strands are being increasingly used these days. This is mainly for production advantage in that less strands need to be run and stressed for the same force as that provided by many wires. For example, 6-ϕ 9.3 mm (ϕ means diameter) 7-wire strand is roughly equivalent to 18-ϕ5 mm wires, (Taylor 1992).

4.4 Transmission Length

In pre-tensioned members, once the tendons are cut, and the pre-tensioning force released, the transfer of force usually occurs at the end of the member. The stress in the

steel varies from zero at the end part of the member to the full prestress value at some distance from the end. The distance over which the effective prestressing force is transferred to the concrete is called the transmission length (l_t). The main factors that contribute to the effective anchorage are the chemical adhesion, friction and mechanical interlocking between concrete and steel.

The transmission length (l_t) is influenced by many factors which can be summarised in the following points, (Zia and Mostafa 1977, Tabatabai and Dickson 1993, Buckner 1995):

1. Type of tendon (wires versus strands)
2. Method of release the prestressing force (sudden versus gentle release)
3. Surface conditions of tendon (smooth, deformed, clean or rusty)
4. Size of tendon
5. Steel stress level
6. Concrete compressive strength
7. Degree of compaction of concrete
8. Amount of concrete coverage around steel

Zia and Mostafa (1977) showed that the transmission lengths usually fall within the range of 50-160 times the tendon diameter. The American Concrete Institute Building Code, ACI 318-89 (1989) suggests an assumption of 50 and 100 diameters for the transmission length of strands and wires respectively. Kong and Evan (1989) stated that the transmission length is roughly about 65 diameters for crimped wires and 25 diameters for strands. The reason that strands have lower transmission length is due to their twisted shape which provides a good mechanical bond in addition to friction.

A short transmission length is an essential feature of pre-tensioned concrete sleepers. Therefore, 5 mm wire and 9.3 mm 7-wire strands are the most widely used tendons. Smaller diameter wires down to 2.11 mm and 3-wire strands down to 6.3 mm have also been used in certain countries, (Hanna 1979, FIP 1987).

BS 8110 (1985) recommends the following equation for the calculation of the transmission length (l_t) provided that the initial prestressing force is less than 75% of the characteristic strength of the tendon:

$$l_t = K_t \phi/\sqrt{f_{ci}} \qquad (4.1)$$

where

ϕ = wire or strand diameter

f_{ci} = characteristic cube strength of concrete at transfer (initial)

K_t = a coefficient for the type of tendon. Typical values are:

= 600 for plain or indented wire including crimped wire with a small wave height

= 400 for crimped wire with a total wave height not less than 0.15 ϕ

= 240 for 7-wire strand or super strand

= 360 for 7-wire drawn strand

For instance, when the prestressed concrete trough is designed to have f_{ci} = 30 N/mm^2 and 7-wire strands of 9.3 mm diameter, then by using eq. (4.1) the transmission length (l_t) will be:

$$l_t = (240)(9.5)/\sqrt{30}$$

= 408 mm

It is a common practice for calculation purposes at the serviceability limit state that the development of prestressing force is assumed to be linear over the transmission length (l_t). This means that the prestressing force is zero at the ends of the prestressed element and linearly increasing to its full value at distance l_t from either ends of the member.

4.5 Serviceability Limit State

There are two distinct stages when the stress conditions for the serviceability limit state at critical sections have to be considered. The first stage is at transfer (initial) and the second one is at service. The resultant stress of any fibre within the section will be the combined effect of the prestressing force and the applied load at each stage.

4.5.1 Sign Convention

The sign convention adopted in this work to derive the stresses in the prestressed concrete trough section is as follows:

1. Sagging moment due to applied load is positive.
2. Hogging moment due to applied load is negative.
3. Axial compression due to applied load is positive.
4. Axial tension due to applied load is negative.
5. Compressive stress within the section is positive.
6. Tensile stress within the section is negative.
7. Downward eccentricity of the tendon is positive.
8. Upward eccentricity of the tendon is negative.

4.5.2 Basic Assumptions

The following assumptions were made in order to find the stresses within the section due to prestressing and any applied load at serviceability limit state:

1. Plane transverse sections before deformation remain plane and normal to the longitudinal axis after deformation.
2. Stress-strain relationships of the materials forming the section are linear.
3. Section properties (area, moment of inertia and section modulus) are based on the gross concrete cross-section.
4. Bending occurs about a principal axis.

4.5.3 Stresses at Transfer

The stress distribution in the concrete trough section at transfer is a combination of that due to prestressing and the self weight only. There are two cases to be considered at this stage which are:

Case 1: simply supported

When the precast concrete trough unit is prestressed, it will deflect due to prestressing eccentricity in such away that it spans between the ends. As a result a bending moment due to the self-weight of the member occurs. Using simple beam bending theory, the stresses at the extreme bottom fibre (fibre 1) and the top fibre (fibre 2) can be calculated as:

$$\text{Bottom fibre:} \quad f_1 = P/A_c + P\,e/Z_1 - M_t/Z_1 \tag{4.2}$$

$$\text{Top fibre:} \quad f_2 = P/A_c - P\,e/Z_2 + M_t/Z_2 \tag{4.3}$$

where:

f_1 = stress at the extreme bottom fibre of the concrete trough

f_2 = stress at the extreme top fibre of the concrete trough

P = prestressing force at the section considered at transfer (initial)

A_c = cross-sectional area of the concrete trough based on gross uncracked section

e = eccentricity of centroid of tendons from centroid of section

Z_1 = elastic section modulus for the bottom fibre of the concrete trough

Z_2 = elastic section modulus for the top fibre of the concrete trough

M_t = bending moment due to self weight of the member at transfer

For a pre-tensioned prestressed concrete trough with straight fully bonded tendons, the critical sections at transfer occur at the end of transmission length (l_t) where M_t can be calculated from simple static analysis, see Fig. (4.1):

$$M_t = w_c (L - l_t) l_t /2 \qquad (4.4)$$

where

w_c = unit weight of the concrete trough section per metre run

L = length of the precast concrete trough unit

The bending moment diagram and the stress distribution at transfer for this case is presented in Fig. (4.1).

Case 2: two ends overhang due to lifting

A few days after prestressing, the concrete trough unit has to be removed from the production line and transported to the storage area. The stresses induced in the concrete trough during the lifting process may be important and worth considering. The critical sections will be at the lifting points where the bending moment M_t (hogging) and the axial force N_t (compression) can be easily determined from simple static analysis as, see Fig. (4.2):

$$M_t = - w_c (\gamma L)^2/2 \qquad (4.5)$$

$$N_t = w_c L /(2 \tan \beta) \qquad (4.6)$$

where

γ = ratio of the overhang span to the total span length of the concrete trough unit

N_t = axial force in the concrete trough section due to self weight developed during lifting

β = angle between the lifting sling and the horizontal axis

As the distance γL is practically round 300 - 500 mm, it can approximately assumed to be equal to the transition length ($l_t \approx 400$ mm). The lifting angle β could be any value between 30 to 60 °. According to eq. (4.6) the lower the value of angle β the higher the value of axial force N_t would be. Therefore, eqs. (4.5) and (4.6) can be re-written as:

$$M_t = - w_c l_t^2/2 \quad (4.7)$$

$$N_t = w_c L /(2 \tan 30^\circ)$$

$$= 0.866 w_c L \quad (4.8)$$

The resultant stresses for this case due to prestressing and self weight at the extreme bottom and top fibres will be:

$$\text{Bottom fibre: } f_1 = P/A_c + P e/Z_1 - M_t/Z_1 + N_t/A_c \quad (4.9)$$

$$\text{Top fibre: } f_2 = P/A_c - P e/Z_2 + M_t/Z_2 + N_t/A_c \quad (4.10)$$

The stress distribution along the cross section for this case is shown in Fig. (4.2).

4.5.4 Stresses at Service

After transfer, there will be some losses in the prestressing force due to relaxation of steel and shrinkage and creep of the concrete. Therefore, effective prestress will be acting on the section. In addition to the self weight of the structure, bending moments and axial forces occur at the section as a result of load application during the service life of the track system. These loads are mainly due to the wheel load of the train and passing vehicles as well as temperature effect. Therefore, the final stresses in service at the extreme fibres will take the form:

$$\text{Bottom fibre: } f_1 = P_e/A_c + P_e e/Z_1 - M_s/Z_1 + N_s/A_c \quad (4.11)$$

$$\text{Top fibre: } f_2 = P_e /A_c - P_e e/Z_2 + M_s/Z_2 + N_s/A_c \quad (4.12)$$

where

P_e = effective prestressing force at the section considered after all losses take place

M_s = bending moment due to external applied load including self weight at service

N_s = axial force in the section due to external applied load at service

Fig. (4.3) shows the stress distribution along the section at service. The critical sections where M_s and N_s occur depend on the loading condition (wheel load magnitude and location, temperature effect), boundary condition (existing of hinges, cavity, ...etc.) and track characteristics (pad and base moduli). Therefore, all the possible realistic combinations of these parameters have to be investigated in searching the worst cases that govern the design of the concrete trough at service as will be shown in subsequent chapters.

4.5.5 Design Criteria

At the serviceability limit state, a number of stress limits called permissible or allowable stresses has to be assigned. These permissible stresses are not to be exceeded by actual stresses at the critical sections during the transfer and service stages. There are four permissible stresses on the concrete section which must be considered in the design process: namely two for the transfer loading (tension and compression) and two for the most severe service loading (tension and compression). Therefore, the design criteria at serviceability limit state will be as follows:

- At transfer

  Bottom fibre: $f_{tt} \le f_1 \le f_{ct}$

  Top fibre: $f_{tt} \le f_2 \le f_{ct}$

- At service

  Bottom fibre: $f_{ts} \le f_1 \le f_{cs}$

  Top fibre: $f_{ts} \le f_2 \le f_{cs}$

where

f_1 = stress at the extreme bottom fibre of the concrete trough section

f_2 = stress at the extreme top fibre of the concrete trough section

f_{ct} = allowable compressive stress at transfer

f_{tt} = allowable tensile stress at transfer

f_{cs} = allowable compressive stress at service

f_{ts} = allowable tensile stress at service

BS8110 (1985) limits the allowable stresses according to the class of prestressing required which are Class 1, 2 and 3 members. The concrete trough could be designated as Class 2 members for the following reasons:

1. In Class 2 members, tensile stresses up to the design flexural tensile strength of the concrete are permitted at service, whereas no tension is allowed in Class 1 members. Hence, a more economical section is obtained with Class 2 stress limits.
2. In Class 3 members, cracking is permissible, though with limited width. As the concrete trough is in close contact to harsh environment, cracking will allow water ingress and salt attack to the section and hence tendon corrosion and material disintegration will occur with time. In addition to that, a deliberate presence of cracking is undesirable for structures specifically under dynamic and cyclic loading such as is the case with the concrete trough. This is due to the fact that stress concentration will develop at the vicinity of the crack tip, which may cause unexpected brittle failure of catastrophic nature. These consequences related with crack existence will definitely lead to a high maintenance cost due to frequent repair or even possibly premature failure of the concrete trough units. Therefore, Class 3 stress limit is not a suitable decision for the concrete trough.

Tarmac Precast Concrete Limited is one of the leading companies in the UK who produce concrete sleepers for railway systems. Due to their long term experience over 50 years in this field, they implement their own stress limits according to the type of sleepers, (Taylor 1993). Furthermore, Tarmac Precast Concrete Limited is one of the partners involved in the LR55 track project as they manufactured and supplied the prestressed concrete trough sample for experimental purposes conducted in this work. As the LR55 track system is meant for light rail transit and street running tramway, Tarmac Precast Concrete Limited stress limits specified for light rail sleeper (type EF29S) would be suitable to consider for the design of the concrete trough.

The Class 2 stress limits suggested by BS 8110 and those employed by Tarmac Precast Concrete Limited for light rail sleepers are presented in Table (4.1). It is clear that the permissible stresses at service of BS 8110 are more conservative than those of Tarmac

Precast Concrete Limited which means the latter gives more economical design. Therefore, allowable stresses of Tarmac Precast Concrete Limited will be considered for the design of the concrete trough section in the present work.

4.5.6 Flexure Design Formulae

The provided (resistant) moment of the concrete trough section can be obtained when the stress at the bottom or top fibre reaches the limiting stress. As the positive (sagging) moment induces tensile stress at the bottom fibre and compressive stress at the top, therefore the provided positive moment of the concrete trough is controlled either by the permissible tensile stress at the bottom fibre or compressive stress at the top fibre. On the contrary, the provided negative (hogging) moment of the concrete trough is governed either by the allowable compressive stress at the bottom fibre or tensile stress at the top fibre. Accordingly, the provided positive moment of the section transfer can be derived as follows:

By making the bottom fibre stress (f_1) defined by eq. (4.2) equal to the permissible tensile stress (f_{tt}) and solving for the moment gives:

$$(M_{t+})_1 = Z_1 (P/A_c + P\ e/Z_1 - f_{tt}) \tag{4.13}$$

or, by making the top fibre stress (f_2) defined by eq. (4.3) equal to the permissible compressive stress (f_{ct}) and solving for the moment gives:

$$(M_{t+})_2 = Z_2 (f_{ct} - P/A_c + P\ e/Z_2) \tag{4.14}$$

The lower of the two values obtained by eqs. (4.13) and (4.14) must be taken as the provided positive moment of concrete trough section at transfer, i.e.:

$$(M_{t+})_{pro} = \min \{(M_{t+})_1, (M_{t+})_2\} \tag{4.15}$$

where

$(M_{t+})_{pro}$ = provided positive (sagging) moment of the section at transfer

$(M_{t+})_1$ = provided positive (sagging) moment of the section controlled by bottom fibre stress at transfer

$(M_{t+})_2$ = provided positive (sagging) moment of the section controlled by top fibre stress at transfer

Similarly, the provided negative moment of the concrete trough section at transfer can be obtained by using the bottom fibre stress given by eq. (4.9) and permissible compressive stress, i.e.

$$(M_{t-})_1 = Z_1 (P/A_c + P\ e/Z_1 + N_t/A_c - f_{ct}) \quad (4.16)$$

or by making use of eq. (4.10) for the top fibre stress and permissible tensile stress, i.e.

$$(M_{t-})_2 = Z_2 (f_{tt} - P/A_c + P\ e/Z_2 - N_t/A_c) \quad (4.17)$$

The provided negative moment of the section at transfer is, therefore, the smaller of the two values defined by eqs. (4.16) and (4.17), i.e.:

$$(M_{t-})_{pro} = \min \{(M_{t-})_1, (M_{t-})_2\} \quad (4.18)$$

where

$(M_{t-})_{pro}$ = provided negative (sagging) moment of the section at transfer

$(M_{t-})_1$ = provided negative (hogging) moment of the section controlled by bottom fibre stress at transfer

$(M_{t-})_2$ = provided negative (hogging) moment of the section controlled by top fibre stress at transfer

Following similar approach, the provided positive moment of the concrete trough at service can be derived from eqs. (11) and (12), i.e.:

$$(M_{s+})_1 = Z_1 (P/A_c + P\ e/Z_1 + N_s/A_c - f_{ts}) \quad (4.19)$$

$$(M_{s+})_2 = Z_2 (f_{cs} - P/A_c + P\ e/Z_2 - N_s/A_c) \quad (4.20)$$

$$(M_{s+})_{pro} = \min \{(M_{s+})_1, (M_{s+})_2\} \quad (4.21)$$

where

$(M_{s+})_{pro}$ = provided positive (sagging) moment of the section at service

$(M_{s+})_1$ = provided positive (sagging) moment of the section controlled by bottom fibre stress at service

$(M_{s+})_2$ = provided positive (sagging) moment of the section controlled by top fibre stress at service

The provided negative moment of the concrete section at service will be:

$$(M_{s-})_1 = Z_1 (P/A_c + P\ e/Z_1 + N_s/A_c - f_{cs}) \quad (4.22)$$

$$(M_{s-})_2 = Z_2 (f_{ts} - P/A_c + P\ e/Z_2 - N_s/A_c) \quad (4.23)$$

$$(M_{s-})_{pro} = \min \{(M_{s-})_1, (M_{s-})_2\} \quad (4.24)$$

where

$(M_{s-})_{pro}$ = provided negative (hogging) moment of the section at service

$(M_{s-})_1$ = provided negative (hogging) moment of the section controlled by bottom fibre stress at service

$(M_{s-})_2$ = provided positive (sagging) moment of the section controlled by top fibre stress at service

4.5.7 Deflection

The initial prestressing of the concrete trough element causes an instantaneous deflection, i.e. camber due to the eccentricity of prestressing force. For a precast concrete trough unit of length L and provided with straight tendons located at eccentricity e, the maximum upward deflection (camber) occurs at the centre of the span and its value is, (Kong and Evan 1989):

$$\delta_i = -P\, e\, L^2/(8E_{ci}\, I_c) + 5\, w_c L^2/(384E_{ci}\, I_c) \quad (4.25)$$

where

E_{ci} = Young's modulus of concrete at transfer (initial)

I_c = moment of inertia of the section about the centroidal axis

BS 8110 (1985) does not specify any limitation on maximum camber. However, for the case of concrete trough structure, it is good practice to have a small value of camber. This is because excessive camber will create difficulties in setting the vertical alignment of the concrete trough units along the track system. Tarmac Precast Concrete Limited suggests that the camber should preferably be less than 1 mm for the 6 m long concrete trough unit and this figure will be used as a limit during the design of the concrete trough unit.

The deflection of the concrete trough due to applied load at service depends on the location of the wheel load with respect to the construction joints, existing of soft patch or cavity underneath the wheel load and the magnitude of pad and base moduli. Therefore, the interaction of all these parameters has to be examined for finding the maximum deflection of the concrete trough at service. This can be achieved by the

appropriate mathematical model developed for the LR55 track system as presented in chapters 5 and 6.

The maximum permissible track deflection at service is limited to 4.0 - 5.0 mm according to British practice (Sperring 1992, Cope 1993) or 6.4 mm according to American practice (Tayabji 1976).

4.6 Ultimate Limit State: Bending

Having checked the concrete trough section for the requirement of serviceability limit state, it is necessary to check that the ultimate limit state requirement for flexure is satisfied too.

4.6.1 Basic Assumptions

The derivation of moment capacity of the concrete trough section due to ultimate load is based on the following assumptions:

1. Plane sections before deformation remain plane after deformation. This implies that the strain in concrete and in prestressing tendons is linearly proportional to the perpendicular distance from the neutral axis.
2. The ultimate limit state of collapse is reached when the concrete strain at the extreme compression fibre reaches a value of 0.0035.
3. The stresses in the concrete in compression are derived from the idealised parabolic-rectangular design stress block recommended by BS 8110 (1985) as shown in Fig. (4.4).
4. The stresses in the prestressing tendons are derived from the idealised stress-strain curve proposed by BS 8110 (1985) as shown in Fig. (4.5).
5. The partial safety factors for materials are those recommended by BS 8110 (1985) for the ultimate limit state.
6. Full bonding exists between concrete and steel.
7. Tensile strength of concrete is neglected.
8. The area of concrete displaced by prestressing tendons in compression is so small that it has not been taken into account.
9. Buckling does not occur before the ultimate load is attained.

4.6.2 Mathematical Model

The fundamental approach for finding the ultimate moment of resistance of a prestressed concrete section is to assume a certain depth of the neutral axis. For such a position, the strains, stresses and hence the forces in the concrete and prestressing steel are calculated. If it happens that the forces in the concrete and steel are in a state of internal equilibrium, then the assumed depth of the neutral axis will be correct. Finally, the ultimate moment of resistance can be determined by taking moment about a datum, for instance the neutral axis. This approach can be tackled either analytically or numerically.

With a concrete trough section having a non-standard shape and a parabolic-rectangular stress block, the rigorous analytical technique is possible, but requires a careful manipulation of mathematical expressions. Therefore, more flexible numerical procedure is preferable. In the present work, an efficient numerical method is developed to find the moment capacity of the concrete trough.

4.6.3 Numerical Analysis

The main concept of the numerical technique followed in this work is that for any assumed depth of neutral axis x, the concrete compression zone is subdivided horizontally into a finite number of thin strips. To achieve sufficient accuracy, the assumed initial depth of the neutral axis x is taken as 1/100th the overall depth of the section, i.e. x = 0.01 D, then increased by a small increment of 0.01 D. Furthermore, a small thickness is assumed for each strip as it is usually taken around 1 mm.

In practice, the prestressing tendons are placed in a minimum of two layers (levels) within the concrete trough section to cater for both sagging and hogging moment. In this numerical model, any number of tendon layers between 1 and 10 can be assumed.

4.6.3.1 Ultimate Sagging Moment

Consider a pre-tensioned prestressed concrete trough subject to an ultimate sagging moment M acting upon the x-axis as shown in Fig. (4.6).

The determination of the compressive force F_c resisted by concrete and the tensile force F_{ps} resisted by the prestressing tendons can be described as follows:

The number of strips (n_c) in the concrete compression zone may be defined as:

$$n_c = \text{int}(x) + 1 \tag{4.26}$$

The thickness of each strip (t_c) is:

$$t_c = x/n_c \tag{4.27}$$

The distance from the neutral axis to the centroid of strip j (y_{cj}) is:

$$y_{cj} = (j - 0.5)\, t_c \qquad \text{for } 1 \le j \le n_c \tag{4.28}$$

The width of strip j (b_{cj}) depends on the depth of the neutral axis x and the distance from the centroid of strip j to the neutral axis y_{cj}. It can be easily obtained from similarity of triangles and geometrical relationships, see Fig. (4.6):

for $0 < x \le d_3$ and $0 < y_{cj} \le x$

$$b_{cj} = 2\,[b_1 + (b_2 - b_4)(x - y_{cj})/d_3] \tag{4.29}$$

for $d_3 < x \le d_2 + d_3$ and $0 < y_{cj} \le x - d_3$

$$b_{cj} = 2\,[(b_1 + b_2) + 0.5\,(b_3 - b_5)(x - d_3 - y_{cj})/d_2] \tag{4.30}$$

for $d_3 < x \le d_2 + d_3$ and $x - d_3 < y_{cj} \le x$

b_{cj} is the same as defined in eq. (4.29)

for $d_2 + d_3 < x \le D$ and $0 < y_{cj} \le x - d_2 - d_3$

$$b_{cj} = B \tag{4.31}$$

for $d_2 + d_3 < x \le D$ and $x - d_2 - d_3 < y_{cj} \le x - d_3$

b_{cj} is the same as defined in eq. (4.30)

for $d_2 + d_3 < x \le D$ and $x - d_3 < y_{cj} \le x$

b_{cj} is the same as defined in eq. (4.29)

From the strain diagram, the strain of strip j (ε_{cj}) is:

$$\varepsilon_{cj} = 0.0035\ y_{cj}/x \tag{4.32}$$

The average stress of strip j (f_{cj}) can be obtained from stress-strain diagram shown in Fig. (4.4):

for $\varepsilon_{cj} < 2.4 \times 10^{-4}(f_{cu}/\gamma_m)^{0.5}$

$$f_{cj} = 5500\ [(f_{cu}/\gamma_m)^{0.5} - (5500/2.64)\ \varepsilon_{cj}]\ \varepsilon_{cj} \tag{4.33}$$

for $\varepsilon_{cj} \geq 2.4 \times 10^{-4}(f_{cu}/\gamma_m)^{0.5}$

$$f_{cj} = 0.67\ (f_{cu}/\gamma_m) \tag{4.34}$$

where

f_{cu} = characteristic cube strength of concrete at service (at 28 days)

γ_m = partial safety factor for strength of materials; for concrete:

= 1.5

The axial force resisted by strip j (F_{cj}) is equal to the average stress f_{cj} times the area of the strip j, i.e.:

$$F_{cj} = f_{cj}\ b_{cj}\ t_c \tag{4.35}$$

The total compression force resisted by the concrete F_c is simply the summation of all strip forces in the concrete compression zone, i.e.:

$$F_c = \sum_{j=1}^{n_c} F_{cj} \tag{4.36}$$

The total strain in tendon layer j (ε_{pbj}) at ultimate condition can be expressed as:

$$\varepsilon_{pbj} = \varepsilon_{pe} + \varepsilon_{uj} + \varepsilon_{rj} \tag{4.37}$$

where

ε_{pe} = strain in the tendons due to effective prestressing;

$$= f_{pe}/E_{ps} \tag{4.38}$$

f_{pe} = design effective prestress in the tendons after all losses

E_{ps} = Young's modulus of prestressing tendon

ε_{uj} = concrete strain at ultimate condition at the level of tendon layer j;

$$= 0.0035\ (d_j - x)/x \tag{4.39}$$

d_j = distance from tendon layer j to the extreme compression fibre

ε_{rj} = residual strain in tendon layer j. It can be defined as the prestressing steel stress after losses divided by the elastic modulus for prestressing tendon E_{ps}, i.e.

$$= (P_e/A_c + P_e\, e\, e_j/I_c)/E_{ps} \qquad (4.40)$$

e_j = eccentricity of tendon layer j

From stress-strain relationship for prestressing tendons shown in Fig. (4.5), the stress at the centroid of tendon layer j (f_{pbj}) is:

for $\varepsilon_{pbj} \le \varepsilon_1$

$$f_{pbj} = E_{ps}\, \varepsilon_{pbj} \qquad (4.41)$$

for $\varepsilon_1 < \varepsilon_{pbj} \le \varepsilon_2$

$$f_{pbj} = 0.8\, f_{pu}/\gamma_m + (f_{pu}/\gamma_m - 0.8\, f_{pu}/\gamma_m)(\varepsilon_{pbj} - \varepsilon_1)/(\varepsilon_2 - \varepsilon_1)$$

$$= 0.8\, f_{pu}/\gamma_m + (0.2\, f_{pu}/\gamma_m)(\varepsilon_{pbj} - \varepsilon_1)/(\varepsilon_2 - \varepsilon_1)$$

$$= 0.2\, f_{pu}/\gamma_m + [4 + (\varepsilon_{pbj} - \varepsilon_1)/(\varepsilon_2 - \varepsilon_1)] \qquad (4.42)$$

for $\varepsilon_{pbj} > \varepsilon_2$

$$f_{pbj} = f_{pu}/\gamma_m \qquad (4.43)$$

where

f_{pu} = characteristic strength of a prestressing tendon

ε_1 = tendon strain at stress of $0.8\, f_{pu}/\gamma_m$ as shown in Fig, (4.5);

$$= (0.8\, f_{pu}/\gamma_m)/E_{ps} \qquad (4.44)$$

ε_2 = tendon strain at stress of f_{pu}/γ_m as shown in Fig. (4.5);

$$= (f_{pu}/\gamma_m)/E_{ps} \qquad (4.45)$$

γ_m = partial safety factor for strength of materials; for prestressing steel:

= 1.15

The force resisted by tendon layer j (F_{pj}) is equal to the stress f_{pbj} times the area of tendons in layer j (A_{psj}), i.e.:

$$F_{pj} = f_{pbj}\, A_{psj} \qquad (4.46)$$

The total force resisted by the whole prestressing tendons F_{ps} is simply the summation of forces F_{pj} over all tendon layers, i.e.:

$$F_{ps} = \sum_{j=1}^{n_p} F_{pj} \tag{4.47}$$

where

n_p = number of prestressing tendon layers within the concrete section

Having calculated the compressive force in the concrete F_c and the tensile force in the tendons F_{ps}, the equilibrium condition of the horizontal forces has to be checked, i.e. to see if the term $(F_c - F_{ps})$ is zero. For a small value of the neutral axis the compressive force F_c is smaller than the tensile force F_{ps}. This means the value of the term $(F_c - F_{ps})$ is negative. As the neutral axis depth increases the compressive force F_c will increase as the tensile force F_{ps} decreases and hence the term $(F_c - F_{ps})$ will eventually become positive. When the term $(F_c - F_{ps})$ changes from negative to positive, the search for the value of the neutral axis depth x, at which the term $(F_c - F_{ps})$ is zero, can be carried out using smaller intervals. At this stage, the iteration procedure is repeated, commencing with the value of x from the previous iteration, but, with a very small increment of D/5000 to obtain a more accurate estimate of the neutral axis depth that will satisfy equilibrium condition.

Once the appropriate value of the neutral axis has been found, the moment resisted by the concrete M_c and the prestressing tendons M_{ps} can be calculated as follows:

By taking moment about the neutral axis, the moment resisted by concrete strip j (M_{cj}) can be defined as:

$$M_{cj} = F_{cj}\, y_{cj} \tag{4.48}$$

The resisting moment of the concrete compression area M_c is the summation of all strip moments in the concrete compression zone, i.e.:

$$M_c = \sum_{j=1}^{n_c} M_{cj} \tag{4.49}$$

Similarly, by taking moment about the neutral axis, the moment resisted by tendon layer j (M_{pj}) may be found as:

$$M_{pj} = F_{pj} (d_j - x) \tag{4.50}$$

The resisting moment of the prestressing steel M_{ps} is the summation of all tendon layers moments, i.e.:

$$M_{ps} = \sum_{j=1}^{n_p} M_{pj} \tag{4.51}$$

Th ultimate sagging moment of the concrete trough will be the sum of the concrete moment M_c and prestressing moment M_{ps}, i.e.:

$$M_u = M_c + M_{ps} \tag{4.52}$$

4.6.3.2 Ultimate Hogging Moment

The procedure for deriving the ultimate hogging moment capacity of the concrete trough is exactly the same as for the sagging moment but with slight modifications. This is because the hogging moment makes the bottom fibre under compression whereas the top fibre under tension. It means that the neutral axis and the effective depth will be referred to with respect to the bottom fibre. Examining the steps presented previously, one can see that only the equations for the width of the concrete strip have to be reconsidered in the case of hogging moment as they will be subjected to different set of constraints as shown below, see Figs. (4.7):

for $0 < x \le d_1$ and $0 < y_{cj} \le x$

$$b_{cj} = B \tag{4.53}$$

for $d_1 < x \le d_1 + d_2$ and $0 < y_{cj} \le x - d_1$

$$b_{cj} = 2\,[(b_1 + b_2) + 0.5\,(b_3 - b_5)(d_1 + d_2 - x + y_{cj})/d_2] \tag{4.54}$$

for $d_1 < x \le d_1 + d_2$ and $x - d_1 < y_{cj} \le x$

b_{cj} is the same as defined in eq. (4.53)

for $d_1 + d_2 < x \le D$ and $0 < y_{cj} \le x - d_1 - d_2$

$$b_{cj} = 2\,[b_1 + (b_2 - b_4)(D - x + y_{cj})/d_3] \tag{4.55}$$

for $d_1 + d_2 < x \leq D$ and $x - d_1 - d_2 < y_{cj} \leq x - d_1$

b_{cj} is the same as defined in eq. (4.54)

for $d_1 + d_2 < x \leq D$ and $x - d_1 < y_{cj} \leq x$

b_{cj} is the same as defined in eq. (4.53)

The rest of equations mentioned in the previous section will be exactly as they were originally defined.

It is quite obvious that the procedures presented above for both the ultimate sagging and hogging moment are too laborious to be handled manually. Therefore, a special subroutine called ULTMOM was written in FORTRAN 77 for P.C. machines to perform this numerical analysis. To the author's knoweldge, neither the numerical procedure nor the subroutine program has been done elsewhere. The subroutine ULTMOM and the other ones developed for the analysis and desing of prestressed concrete trough section are described concisely in section 4.9. It is worthwhile to mention that the method presented is so general that it can be applied for shapes other than the concrete trough, simply by manipulating the input data of the dimensions b_2, b_3, b_4, b_5, d_2 or d_3 as shown in Fig. (4.8). For instance, assigning a very small value to d_2 and d_3, i.e. $d_2 = d_3 = 0.0001$ mm, then a solution for rectangular shape can be achieved. By making $b_3 = b_5$ and $b_2 = b_4 = 0.0001$, then a U-shape will be obtained.

4.6.4 Examples

Three different examples are demonstrated in order to prove the validity of the numerical technique and the correctness of the developed subroutine ULTMOM.

In the first two examples, the concrete trough dimensions and prestressing tendon arrangement do not represent practical ones. However, they are selected deliberately in such a way that they can be solved by the method explained in BS 8110, clause 4.3.7 for rectangular and flanged sections, in order to compare the results.

The purpose of the third example is to show the generality of the numerical procedure developed by solving a rectangular prestressed section which was already solved analytically by Hulse and Mosley (1987).

4.6.4.1 Example 1: Ultimate Sagging Moment of a Concrete Trough Section

A concrete trough with the dimensions shown in Fig. (4.9) has 208 mm^2 of prestressing steel at a distance of 40 mm from the bottom. It is required to determine the ultimate sagging moment of the section if the tendon characteristic strength f_{pu} = 1770 N/mm^2, initial prestress $f_{pi} = 0.75\ f_{pu}$, total losses = 20%, concrete characteristic strength f_{cu} = 60 N/mm^2.

Using the present numerical procedure with the aid of the subroutine ULTMOM, the output is:

Neutral axis depth x	= 65.44 mm	
Concrete compressive force F_c	= 299.3 kN	
Prestressing steel tensile force F_{ps}	= 299.27 kN ≈ 299.3 kN	O.K.
Ultimate sagging moment M_u	= 39.41 kN m	

Using BS 8110 method:

The procedure of BS 8110, clause 4.3.7 is based on equivalent rectangular stress block. Assume the neutral axis is less than 80 mm. This assumption implies the width of concrete in compression area is:

b = 200 mm

The effective depth d is:

d = 200 - 40

= 160 mm

$f_{pu}\ A_{ps}/(f_{cu}\ b\ d) = (1770 \times 208)/(60 \times 200 \times 160)$

$= 0.1917$

$f_{pe} = (1 - 0.2)\ f_{pi}$

$= 0.8 \times 0.75\ f_{pu}$

$= 0.6\ f_{pu}$

For $f_{pu}\ A_{ps}/(f_{cu}\ b\ d) = 0.1917$ and $f_{pe} = 0.6\ f_{pu}$, using Table (4.4) of BS 8110 gives:

$$x/d = 0.3868 \quad \text{and} \quad f_{pb}/0.87\ f_{pu} = 0.9316$$

i.e.

$$x = 0.3868\ d$$
$$= 0.3868 \times 160$$
$$= 61.89 \text{ mm}$$

Since 61.89 < 80 mm, then the assumption of b = 200 mm is correct.

$$f_{pb}/0.87\ f_{pu} = 0.9316$$

i.e.

$$f_{pb} = 0.9316 \times 0.87 \times f_{pu}$$
$$= 0.9316 \times 0.87 \times 1770$$
$$= 1434.49 \text{ N/mm}^2$$

Using eq. (4.1) of BS 8110 gives:

$$M_u = f_{pb}\ A_{ps}\ (d - 0.45x)$$
$$= 1434.49 \times 208 \times (160 - 0.45 \times 61.89) \times 10^{-6}$$
$$= 39.43 \text{ kN m} \approx 39.41 \text{ kN m} \qquad \text{O.K.}$$

This slight difference between the results is mainly due to the design stress block assumed in each method.

4.6.4.2 Example 2: Ultimate Hogging Moment of a Concrete Trough Section

It is required to determine the ultimate hogging moment for the concrete trough of example 1 except that the prestressing steel area is placed at a distance of 40 mm from the top as shown in Fig. (4.10).

Using the present numerical procedure with the aid of the subroutine ULTMOM, the output is:

Neutral axis depth x	= 35.0 mm
Concrete compressive force F_c	= 320.19 kN
Prestressing steel tensile force F_{ps}	= 320.14 kN ≈ 320.19 kN O.K.

Ultimate sagging moment M_u = 46.37 kN m

Using BS 8110 method:

Assume the neutral axis depth is less than 60 mm. This assumption implies the width of concrete in compression area is:

b = 400 mm

d = 200 - 40

= 160 mm

$f_{pu} A_{ps}/(f_{cu} b d) = (1770 \times 208)/(60 \times 400 \times 160)$

= 0.0959

$f_{pe} = 0.6 f_{pu}$ (from example 1)

For $f_{pu} A_{ps}/(f_{cu} b d) = 0.0959$ and $f_{pe} = 0.6 f_{pu}$, using Table (4.4) of BS 8110 gives:

$x/d = 0.2109$ and $f_{pb}/0.87 f_{pu} = 1.0$

i.e.

$x = 0.2109 d$

$= 0.2109 \times 160$

$= 33.748$ mm

Since 33.75 < 60 mm, then the assumption of b = 400 mm is correct.

$f_{pb}/0.87 f_{pu} = 1.0$

i.e.

$f_{pb} = 1.0 \times 0.87 \times f_{pu}$

$= 1.0 \times 0.87 \times 1770$

$= 1539.9$ N/mm^2

Using eq. (4.1) of BS 8110 gives:

$M_u = f_{pb} A_{ps} (d - 0.45x)$

$= 1539.9 \times 208 \times (160 - 0.45 \times 33.75) \times 10^{-6}$

= 46.38 kN m ≈ 46.37 kN m O.K.

4.6.4.3 Example 3: Ultimate Sagging Moment of a Concrete Rectangular Section

A rectangular prestressed concrete section of 400 mm width and 1200 mm depth has 3000 mm^2 of prestressed tendon located at distance 400 mm from the bottom. It is required to determine the ultimate sagging moment of the section if total estimated loss of the prestressing force is 25 per cent, f_{pu} = 1650 N/mm^2, f_{cu} = 60 N/mm^2 and initial prestressing = 0.70 f_{pu}.

In order to solve this problem using the current numerical procedure, we have to assume a concrete trough section with the dimensions d_2 and d_3 which are very small and the total width B = 400 mm and overall depth D = 1200 mm. So, one may assume the following dimensions, see Fig. (4.11):

b_1 = 100 mm

b_2 = 35 mm

b_3 = 130 mm

b_4 = 35 mm

b_5 = 130 mm

d_1 = 1199.9998 mm

$d_2 = d_3$ = 0.0001 mm

Using the present numerical procedure with the aid of the subroutine ULTMOM, the output is:

Neutral axis depth x	= 408.48 mm
Concrete compressive force F_c	= 3736.28 kN
Prestressing steel tensile force F_{ps}	= 3734.11 kN ≈ 3736.28 kN O.K.
Ultimate sagging moment M_u	= 2327.85 kN m

This example was solved by Hulse and Mosley (1987) based on BS 8110 (1985). They found that the ultimate sagging moment of the section is:

Ultimate sagging moment M_u = 2355.1 kN m ≈ 2327.85 kN m O.K.

The percentage difference between the two results is only 1.16%. This can be attributed to different stress block assumed in each method.

4.7 Ultimate Limit State: Shear

The adequacy of the prestressed concrete trough section to resist shear force due to ultimate load must be checked and, if necessary, additional shear reinforcement has to be provided.

The usual design procedure according to BS 8110 (1985) consists of determining the shear force resistance of the uncracked and cracked sections at the critical points along the length of the member. The lower of the two values obtained must be taken as shear resistance at the point concerned, i.e.:

$$V_c = \min (V_{co}, V_{cr}) \tag{4.56}$$

where

V_c = design ultimate shear resistance of the concrete trough section

V_{co} = design ultimate shear resistance of the concrete trough section uncracked in flexure

V_{cr} = design ultimate shear resistance of the concrete trough section cracked in flexure

4.7.1 Section Uncracked in Flexure

The design ultimate shear resistance of a prestressed concrete rectangular, T-, I- and L-section uncracked in flexure as per BS 8110 (1985) is:

$$V_{co} = 0.67\, b_v\, h\, [f_t^2 + 0.8\, f_{cp}\, f_t]^{0.5} \tag{4.57}$$

where

b_v = breadth of the section, (for T-, I- and L-beams, the breadth of the rib)

h = total depth of a prestressed concrete rectangular, T-, I- and L-section

f_t = maximum design principal tensile stress

f_{cp} = concrete compressive stress at the location of maximum shear stress within the section due to effective prestress only. In case of a rectangular section it will be at the centroidal axis

Kong and Evan (1989) stated that the assumption for deriving eq. (4.57) is based on a rectangular section only. They also proved that eq. (4.57) is still applicable on T-, I- and L-sections with an acceptable percentage of error.

However, the concrete trough section has, unfortunately, none of these standard cross-sectional shapes. Therefore, its ultimate shear resistance uncracked in flexure has to be derived from the basic principles as follows:

From the elementary mechanics of material, see for example (Gere and Timoshenko 1985), the distribution of shear stress across a section due to shear force V can be computed as:

$$v = V\,Q/(I_c\,b) \tag{4.58}$$

where

v = shear stress at any level along the section measured from the centroidal axis of the section

Q = first moment of area above or below the level where shear stress v is calculated, taken about the centroidal axis of the section

I_c = moment of inertia of the section about the centroidal axis

b = breadth of the section at the level where shear stress v is calculated

Examining eq. (4.58) reveals that the maximum shear stress v_{max} and its location depends on values of Q and b, knowing that for any particular section the quantities V and I_c are constant. Due to the cross-sectional geometry of the concrete trough, the location of the maximum shear stress v_{max} cannot be guessed easily *a priori*. In the present study, a precise location of the maximum shear stress is determined by solving eq. (4.58) for the shear stress at several different levels across the depth D with an increment of 0.01 D, and then searching for the maximum one. One may assume that v_{max} has been found such that:

$$v_{max} = V\,Q_v/(I_c\,b_v) \tag{4.59}$$

where

b_v = breadth of the concrete trough section where the maximum shear stress occurs. As the width of the concrete trough responsible for resisting shear force is not uniform along the depth, it will be more conservative to be taken as the smallest web width of the section, i.e.

$= 2\,b_1$

Q_v = first moment of area above or below the level where maximum shear stress occurs, taken about the centroidal axis of the section

The compressive stress f_{cp} due to effective prestressing force P_e only at the location of maximum shear stress can be computed as:

$$f_{cp} = P_e/A_c + P_e\, e\, y_v/I_c \qquad (4.60)$$

where

P_e = effective prestressing force at the section considered after all losses take place

A_c = cross-sectional area of the concrete trough based on gross uncracked section

e = eccentricity of centroid of tendons from centroid of section

y_v = location of the maximum shear stress within the section measured from the centroidal axis

Using the Mohr circle analysis, the maximum principal tensile stress f_t at the location of maximum shear stress can be determined as, (Rees 1990):

$$f_t = [(f_{cp}/2)^2 + v_{max}^2]^{0.5} - (f_{cp}/2) \qquad (4.61)$$

Combining eqs. (4.59) and (4.61) and rearranging terms results in:

$$V = (I_c\, b_v/Q_v)[f_t^2 + f_{cp}\, f_t\,]^{0.5} \qquad (4.62)$$

When the maximum principal tensile stress becomes equal to the design tensile strength of the concrete of $0.24\ \sqrt{f_{cu}}$ as stated by BS 8110 (1985), then the applied shear force V will be corresponding to the design ultimate shear resistance of the section uncracked in flexure V_{co}. Furthermore, BS8110 recommends that f_{cp} should be multiplied by 0.8 to take into account the partial safety factor for concrete material. Hence eq. (4.62) will finally take the form:

$$V_{co} = (I_c\, b_v/Q_v)\,[f_t^2 + 0.8 f_{cp}\, f_t\,]^{0.5} \qquad (4.63)$$

4.7.2 Section Cracked in Flexure

The design ultimate shear resistance of the concrete trough section cracked in flexure V_{cr} may be calculated using the following empirical formula suggested by BS 8110 (1985):

$$V_{cr} = (1 - 0.55\, f_{pe}/f_{pu})v_c\, b_v\, d + M_o\, V/M \quad \geq\ 0.1\, b_v\, d \qquad (4.64)$$

where

f_{pe} = design effective prestress in the tendons after all losses

f_{pu} = characteristic strength of a prestressing tendon

v_c = design concrete shear stress as defined by Table (3.9) of BS 8110 (1985)

b_v = width of the member. In case of the concrete trough, as defined earlier can be conservatively taken as

$= 2\ b_1$

d = distance from the extreme compression fibre to the centroid of the tendons in the tension zone, i.e. effective depth of the concrete section

M = design bending moment at the section due to ultimate load

M_o = bending moment necessary to produce zero stress in the concrete at the extreme tension fibre; in this calculation only 0.8 of the stress due to prestress should be taken into account.

It is worthwhile to mention that the calculation of M_o in eq. (4.64) depends on the sign of the design ultimate moment M acting at the section where shear capacity is being investigated. In the case of positive (sagging) moment M, then:

$$M_o = 0.8\ f_{pt}\ Z_1 \qquad (4.65)$$

and

$$f_{pt} = P_e/A_c + P_e\ e/Z_1 \qquad (4.66)$$

where

f_{pt} = concrete compressive stress at the extreme tension fibre due to effective prestressing force

In the case of negative (hogging) moment M, then:

$$M_o = 0.8\ f_{pt}\ Z_2 \qquad (4.67)$$

and

$$f_{pt} = P_e/A_c - P_e\ e/Z_2 \qquad (4.68)$$

4.7.3 Shear Reinforcement

Once the design ultimate shear resistance of the concrete trough section V_c has been determined, the adequacy of the section and requirement for shear reinforcement as per BS 8110 (1985) may be summarised as follows:

1. If $V > \min (0.8\ b_v\ d\ \sqrt{f_{cu}}\ ,\ 5\ b_v\ d)$

then the section resistance is inadequate to web crushing. Therefore, change the section by increasing the width b_v, depth d or both accordingly.

2. If $V < 0.5\ V_c$

then shear reinforcement need not be provided.

3. If $0.5\ V_c \leq V \leq (V_c + 0.4\ b_v\ d)$

then minimum shear reinforcement is required according to the following formula:

$$A_{sv} = 0.4\ s_v\ b_v\ /(0.87\ f_{yv}) \tag{4.69}$$

4. If $V > (V_c + 0.4\ b_v\ d)$

then shear reinforcement is required according to the following formula:

$$A_{sv} = (V - V_c)\ s_v/(0.87\ f_{yv}\ d_t) \tag{4.70}$$

where

A_{sv} = total area of shear reinforcement (links) at the neutral axis, at a section

s_v = spacing of links along the member

f_{yv} = characteristic yield strength of shear reinforcement

d_t = distance from the extreme compression fibre either to the tendons in tension zone or to the centroid of the tendons which ever is the greater

5. Spacing of shear links should satisfy the following formula:

$$s_v \leq \{0.75d_t, (0.5d \text{ if } V > 1.8\ V_c), 4b_v\} \tag{4.71}$$

4.8 Prestress Losses

The prestressing force of a prestressed concrete member continuously decreases with time. The various sources that contribute to the loss of prestress in case of pre-tensioned prestressed units are:

1. Elastic shortening of the concrete
2. Shrinkage of the concrete
3. Creep of the concrete
4. Relaxation of the prestressing tendons

Elastic shortening is known as short term loss because it takes place immediately after transfer, whereas the other three types of losses occur over a period of time and hence the name long term losses.

The total stress reduction during the life span of the member is known as the total prestress loss. It is essential to predict the amount of the total prestress loss in order to find the magnitude of the effective prestressing force required for the design.

4.8.1 Loss due to Elastic Shortening

When the prestressing force is applied to the concrete, an elastic shortening of the concrete takes place. This is accompanied by an equal and simultaneous reduction in the length of the steel, with a consequent reduction in the prestressing force.

The initial prestressing force after elastic shortening P can be defined as:

$$P = A_{ps} (f_{pi} - \Delta f_{pes}) \tag{4.72}$$

where

A_{ps} = total area of the prestressing tendons

f_{pi} = initial prestressing stress in the tendons before losses

Δf_{pes} = loss in prestressing stress due to elastic shortening

The corresponding concrete compressive stress at the centroid of prestressing tendon f_{co} due to prestressing is:

$$f_{co} = P/A_c + P\ e\ e/I_c$$

$$= P/A_c (1 + e^2/r^2) \tag{4.73}$$

where

r = radius of gyration of the section, defined as:

$$= \sqrt{(I_c/A_c)} \tag{4.74}$$

At the level of the tendon, the concrete and the tendon shorten by the same amount, i.e.

$$\varepsilon_c = \varepsilon_s \tag{4.75}$$

From stress-strain relationship, eq. (4.75) will be:

$$f_{co}/E_{ci} = \Delta f_{pes}/E_{ps} \quad (4.76)$$

or

$$\Delta f_{pes} = (E_{ps}/E_{ci})\, f_{co} \quad (4.77)$$

or

$$\Delta f_{pes} = \alpha_e\, f_{co} \quad (4.78)$$

where

α_e = modular ratio

$$= E_{ps}/E_{ci} \quad (4.79)$$

E_{ps} = Young's modulus of prestressing tendon

E_{ci} = Young's modulus of concrete at transfer (initial)

Substituting eq. (4.78) into eq. (4.72) gives:

$$P = A_{ps}\,(f_{pi} - \alpha_e\, f_{co}) \quad (4.80)$$

Combining eq. (4.73) and (4.80) and rearranging terms gives:

$$f_{co} = f_{pi}\,(A_{ps}/A_c)(1 + e^2/r^2)/[1 + \alpha_e\,(A_{ps}/A_c)(1 + e^2/r^2)] \quad (4.81)$$

If the effect of self weight is taken into consideration then eq. (4.81) will be:

$$f_{co} = f_{pi}\,(A_{ps}/A_c)(1 + e^2/r^2)/[1 + \alpha_e\,(A_{ps}/A_c)(1 + e^2/r^2)] - M_i\, e/I_c \quad (4.82)$$

Substituting eq. (4.82) into eq. (4.78) gives:

$$\Delta f_{pes} = \alpha_e\,\{f_{pi}\,(A_{ps}/A_c)(1 + e^2/r^2)/[1 + \alpha_e\,(A_{ps}/A_c)(1 + e^2/r^2)] - M_i\, e/I_c\} \quad (4.83)$$

Normally the losses are expressed as percentage of the initial prestressing stress. Therefore,

$$\%\ \text{Loss due elastic shortening} = 100\ \Delta f_{pes}/f_{pi} \quad (4.84)$$

4.8.2 Loss due to Shrinkage of Concrete

Shrinkage of concrete is influenced by parameters including mix proportions of the concrete ingredients, relative humidity of the environment, surface area from which moisture can be lost relative to the volume of concrete and curing history, (Naaman

1982, BS 8110 1985). The loss of prestress associated with concrete shrinkage may be expressed as, (Kong and Evans 1989):

$$\Delta f_{psh} = \varepsilon_{sh} E_{ps} \tag{4.85}$$

where

Δf_{psh} = loss in prestressing force due to shrinkage of concrete

ε_{sh} = shrinkage strain of the concrete; for outdoor exposure such as the case for the concrete trough, it may be taken as, BS 8110 (1985):

$= 100 \times 10^{-6}$

Defining the shrinkage loss as percentage means:

$$\% \text{ Loss due concrete shrinkage} = 100\ \Delta f_{psh}/f_{pi} \tag{4.86}$$

4.8.3 Loss due to Creep of Concrete

The sustained compressive stress on the concrete will also cause a long term shortening due to creep, which will similarly reduce the prestress force. The creep strain of the concrete depends on many factors such as age of loading, time, relative humidity ..etc., (BS 8110 1985, Lin and Burns 1995). The determination of the loss of prestress due to the creep of concrete is given as, (Kong and Evan (1989):

$$\Delta f_{pcr} = \alpha_e \phi_{cr} f_{co} \tag{4.87}$$

where

Δf_{pcr} = loss in prestressing stress due to creep of concrete

ϕ_{cr} = creep coefficient. BS 8110 (1985) suggests:

= 1.8 for transfer within 3 days

= 1.4 for transfer between 3 and 28 days

f_{co} = concrete compressive stress at the centroid of the prestressing tendons at transfer; see eq. (4.82)

Substituting eq. (4.82) into eq. (4.87) results in:

$$\Delta f_{pcr} = \alpha_e \phi_{cr} \{f_{pi} (A_{ps}/A_c)(1 + e^2/r^2)/[1 + \alpha_e (A_{ps}/A_c)(1 + e^2/r^2)] - M_i e/I_c\} \tag{4.88}$$

Defining the loss due to concrete creep as percentage gives:

$$\% \text{ Loss due concrete creep} = 100\ \Delta f_{pcr}/f_{pi} \tag{4.89}$$

4.8.4 Loss due to Steel Relaxation

Relaxation of the prestressing tendons is a long term loss of prestressing force in tendons. It is similar to creep in concrete and depends upon the initial tendon load relative to its breaking load, duration of loading and the temperature. The relaxation values are normally quoted in BS 5896 (1980) for class 1 (normal) and class 2 (low) relaxation wires and strands. Typical values are presented in Table (4.2). These values are based on standard tests carried out for a period of 1000 hours at nominal temperature of 20 °C from initial stresses of 60%, 70% and 80% of the actual strength. BS 8110 (1985) requires that these values are further multiplied by a factor of 1.5 and 1.2 in case of pre-tensioning of normal and low relaxation wires respectively.

4.9 Computer Program TROUGH

It has already been shown that the analysis and design of a prestressed concrete trough section involves a great deal of mathematical expressions. These are too laborious and time consuming to tackle manually and in particular the numerical procedure for determining the ultimate moment capacity as explained in section 4.6.3. To avoid this, a purpose built computer program called TROUGH was developed to process the whole steps required for determining the characteristics of a prestressed concrete section with high speed and accuracy. It was written in FORTRAN 77 for P.C. machines and its flow chart is presented in Fig. (4.12). It contains two subroutines, which are:

- SECT: This subroutine determines the cross-sectional properties (area, centroid, elastic section modulus, moment of inertia ...etc) of any geometrical shape. A full description of subroutine SECT is presented in section 3.5 of chapter 3.
- PRESTR: This subroutine calculates the characteristics of a given pre-tensioned prestressed concrete trough section that satisfies the serviceability (transfer and service) and ultimate limit states requirements of BS 8110 and Tarmac Precast Concrete Limited. The flow chart of PRESTR subroutine is shown in Fig. (4.13). This subroutine will be part of another important program developed for the optimum design of the concrete trough section as will be presented in chapter 7. The subroutine PRESTR, in turn, incorporates a number of subroutines as listed below.

- PRLOSS: A subroutine for calculating the short term losses (elastic shortening) and long term losses (concrete shrinkage and creep and steel relaxation) as explained in section 4.8. Its flow chart is given in Fig. (4.14).
- TRAMOM: A subroutine for finding the characteristics of a prestressed concrete trough section at transfer. These are the stresses at extreme fibres due to applied sagging or hogging moment, the provided (resistant) sagging and hogging moment and the camber (instantaneous deflection) due initial prestressing force as described in sections 4.5.3, 4.5.6 and 4.5.7 respectively. Its flow chart is given in Fig. (4.15).
- SERMOM: A subroutine for finding the characteristics of a prestressed concrete trough section at service which are the stresses at extreme fibres due to applied sagging or hogging moment and the provided sagging and hogging moment as per sections 4.5.4 and 4.5.6 respectively. Its flow chart is given in Fig. (4.16).
- ULTMOM: A subroutine for calculating the sagging and hogging moment of a prestressed concrete trough section at ultimate limit states. This subroutine is based on the numerical technique presented in section 4.6.3 and its flow chart is illustrated in Fig. (4.17). The subroutine ULTMOM contains another two subroutines which are:
  - FORSCON: A subroutine for finding the resisting forces (axial and bending) of the concrete compression zone within the section due to applied ultimate moment. Its flow chart is shown in Fig. (4.18).
  - FORSAPS: A subroutine for finding the resisting forces (axial and bending) of the prestressing tendons due to applied ultimate moment. Its flow chart is shown in Fig. (4.19).
- ULTSHR: A subroutine for determining the shear capacity and the necessary shear reinforcement if it is required for a prestressed concrete trough section due to applied shear at ultimate limit state as explained in section 4.7. Its flow chart is shown in Fig. (4.20).

To the author's knowledge, the program TROUGH has not been developed elsewhere and it is an important novel parts of this thesis. The application of this program will be

utilised in chapter 7 where the optimum design of a prestressed concrete trough section is explored in detail.

Table (4.1): Allowable stresses of the concrete as per BS 8110 and Tarmac Precast Concrete Limited.

Case	BS 8110 (1985)	Tarmac Precast Concrete Limited
At transfer:		
Allowable compressive stress (f_{ct})	0.5 f_{ci}	0.5 f_{ci}
Allowable tensile stress (f_{it})	-0.45 $(f_{ci})^{0.5}$	0
At service:		
Allowable compressive stress (f_{cs})	0.4 f_{cu}	0.48 f_{cu}
Allowable tensile stress (f_{ts})	-0.45 $(f_{cu})^{0.5}$	-0.64 $(f_{cu})^{0.5}$

Table (4.2): Typical relaxation values for strands as quoted in BS 5896.

Initial strand load (% of actual breaking load)	% relaxation for Relaxation Class	
	Class 1	Class 2
60	4.5	1.0
70	8.0	2.5
80	12.0	4.5

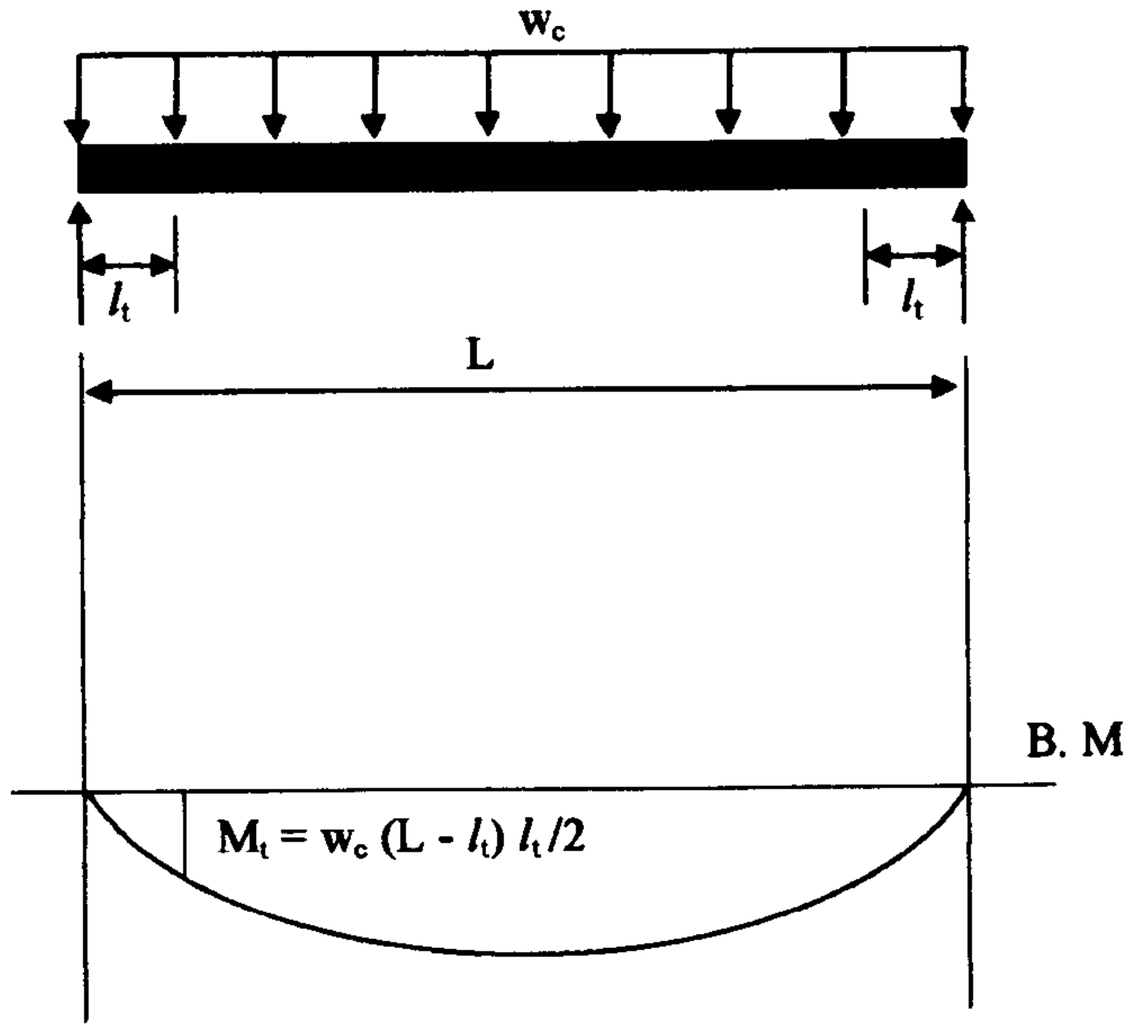

Fig. (4.1a): Bending moment diagram for the concrete trough unit as simply supported due to self weight.

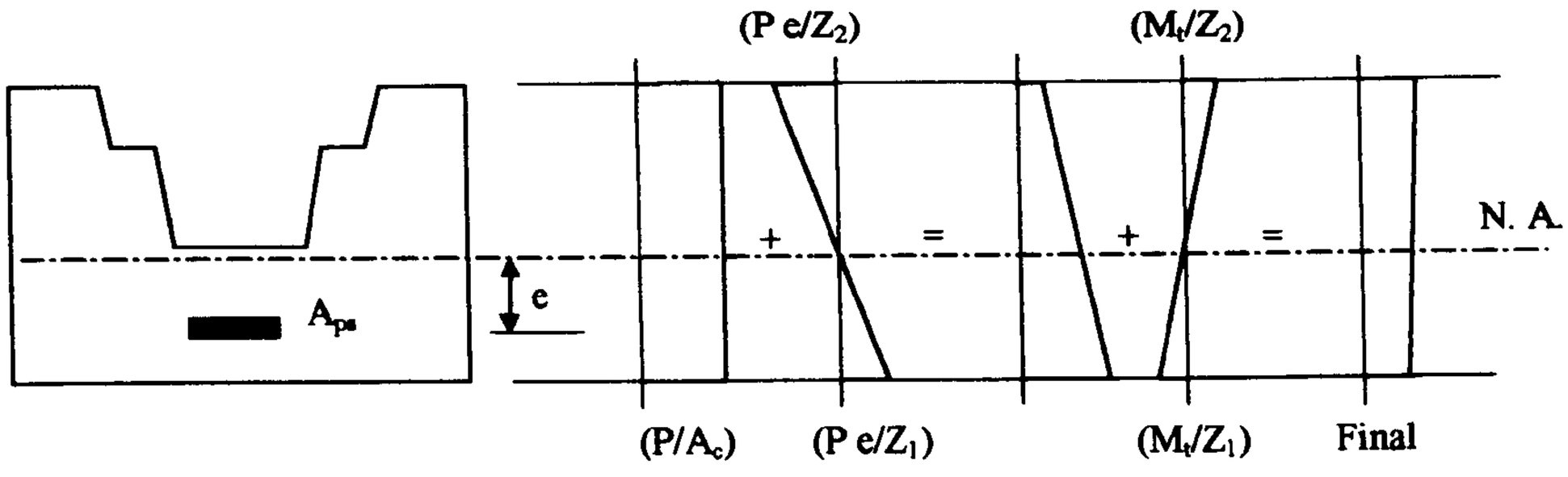

Fig. (4.1b): Stress distribution due to initial prestressing and self weight.

Fig. (4.1): Bending moment and stress distribution at transfer for the concrete trough due to case 1 (simply supported).

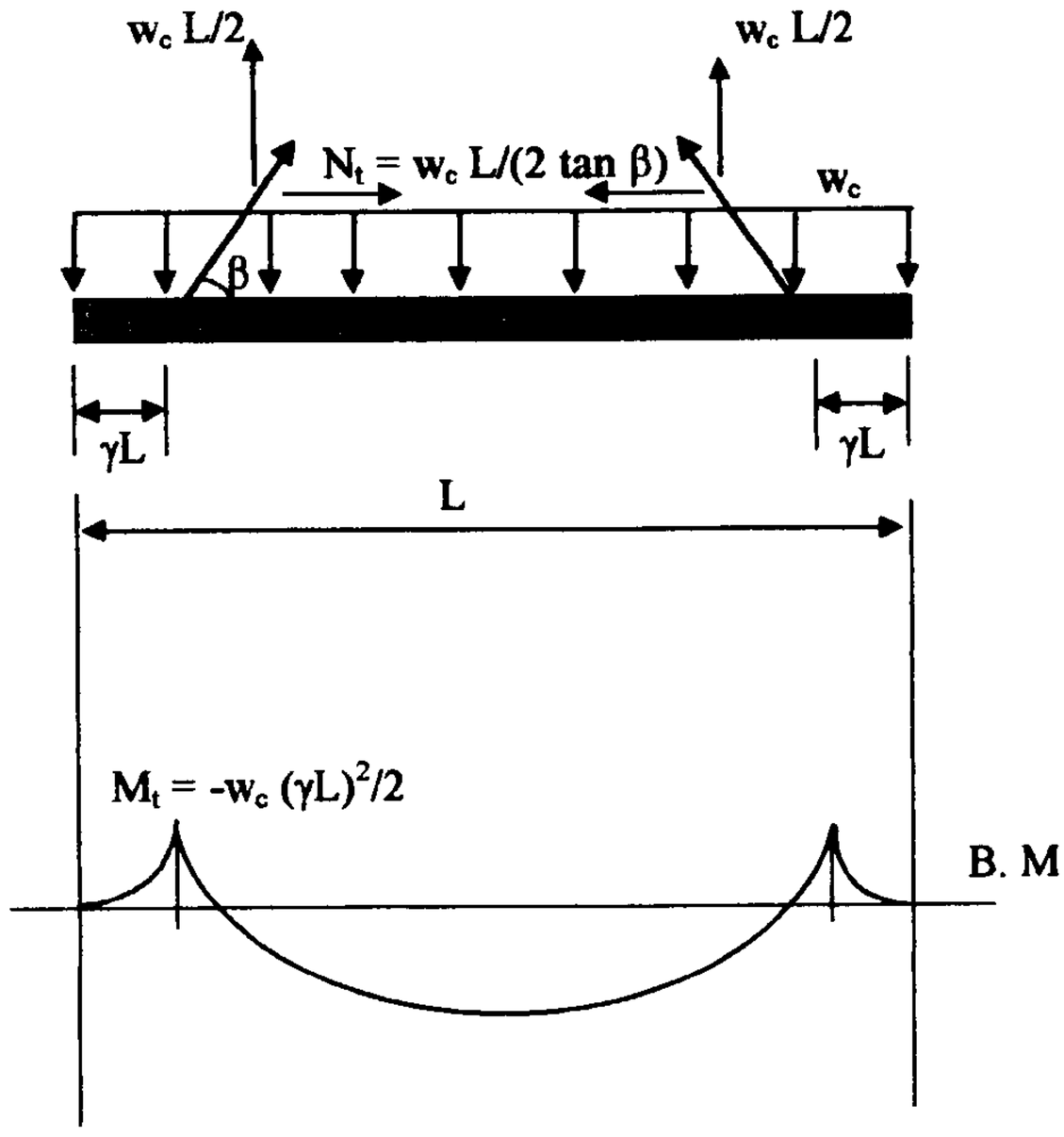

Fig. (4.2a): Bending moment diagram for the concrete trough unit as two ends overhang due to lifting.

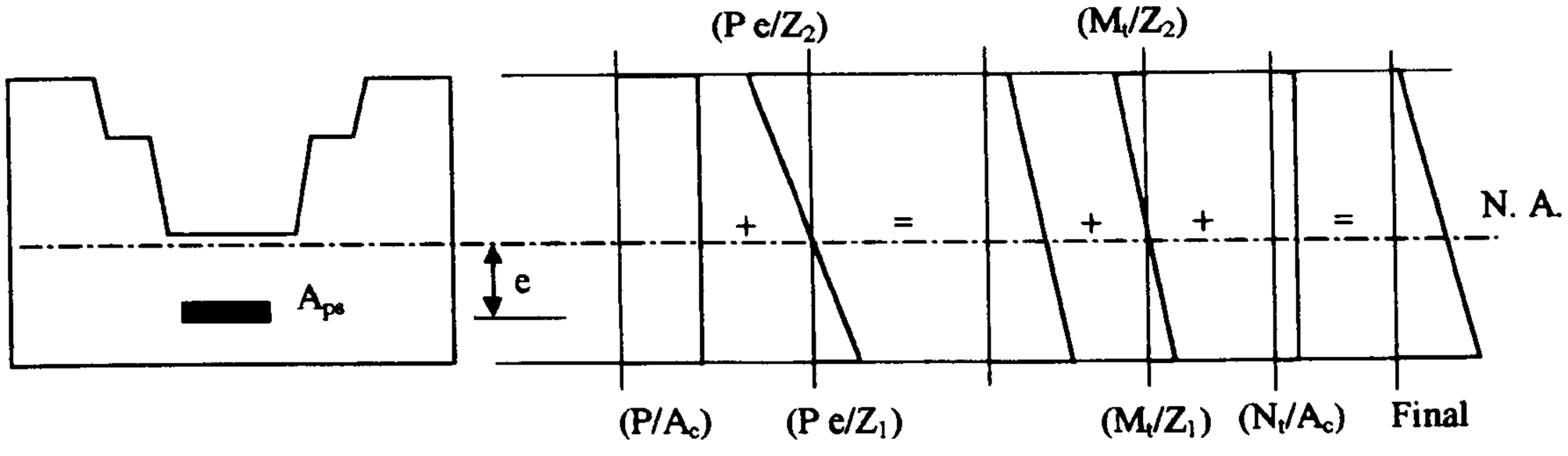

Fig. (4.2b): Stress distribution due to initial prestressing and self weight.

Fig. (4.2): Bending moment and stress distribution at transfer for the concrete trough due to case 2 (lifting).

Fig. (4.3): Stress distribution for the concrete trough at service.

Fig. (4.4): Short term design stress-strain curve for normal weight concrete according BS 8110 (1985).

Fig. (4.5): Short term design stress-strain curve for prestressing tendons according BS 8110 (1985).

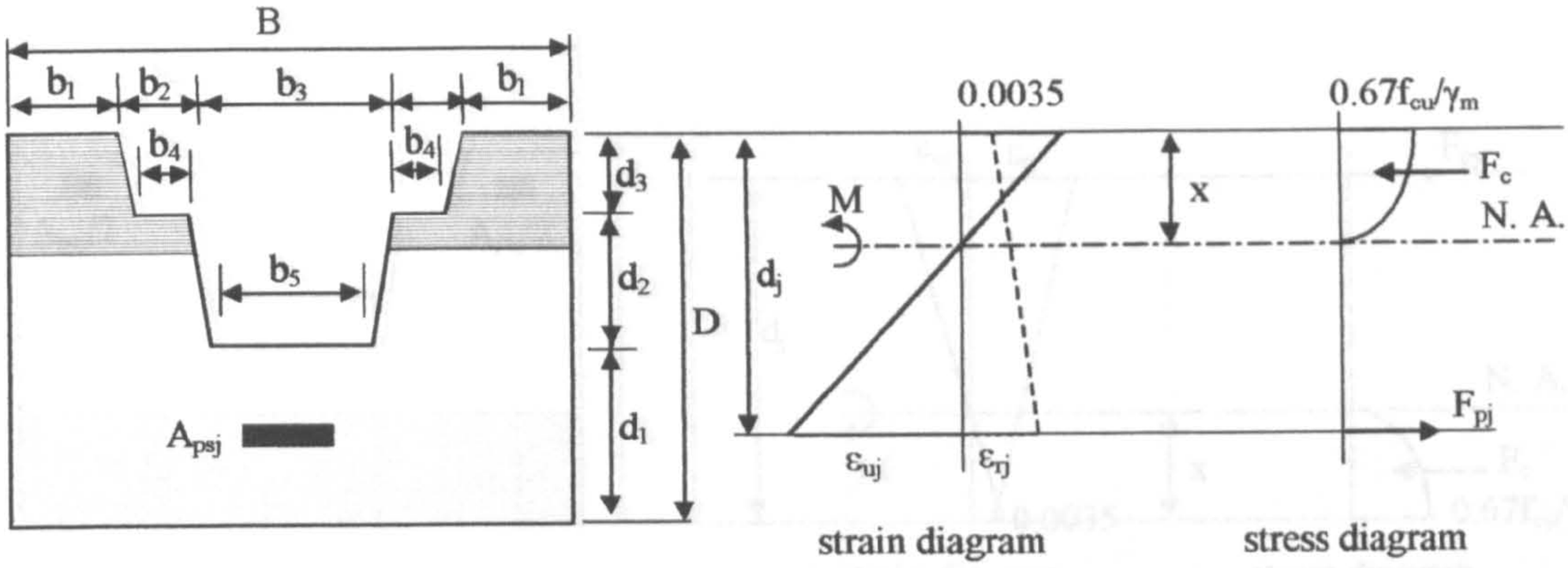

Fig. (4.6a): Strain and stress diagrams of the concrete trough due to ultimate sagging moment.

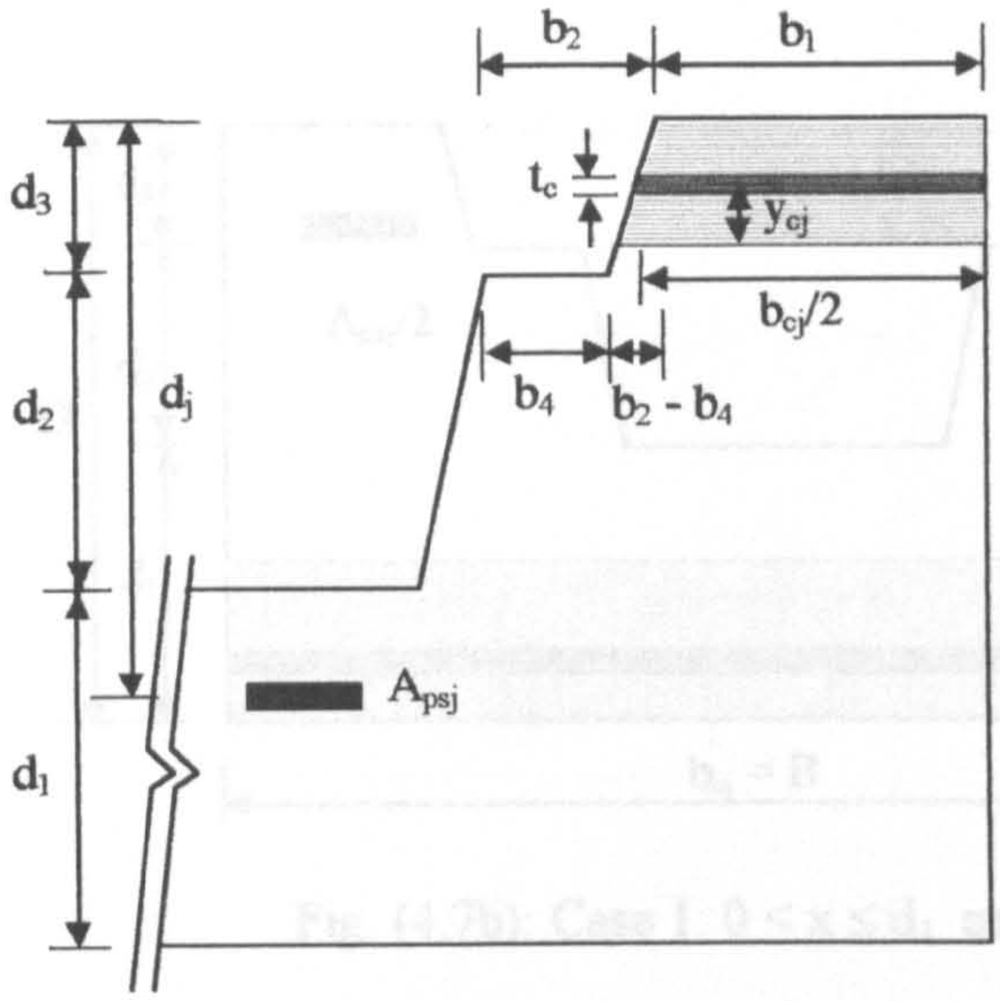

Fig. (4.6b): Case 1: $0 < x \leq d_3$ and $0 < y_{cj} \leq x$.

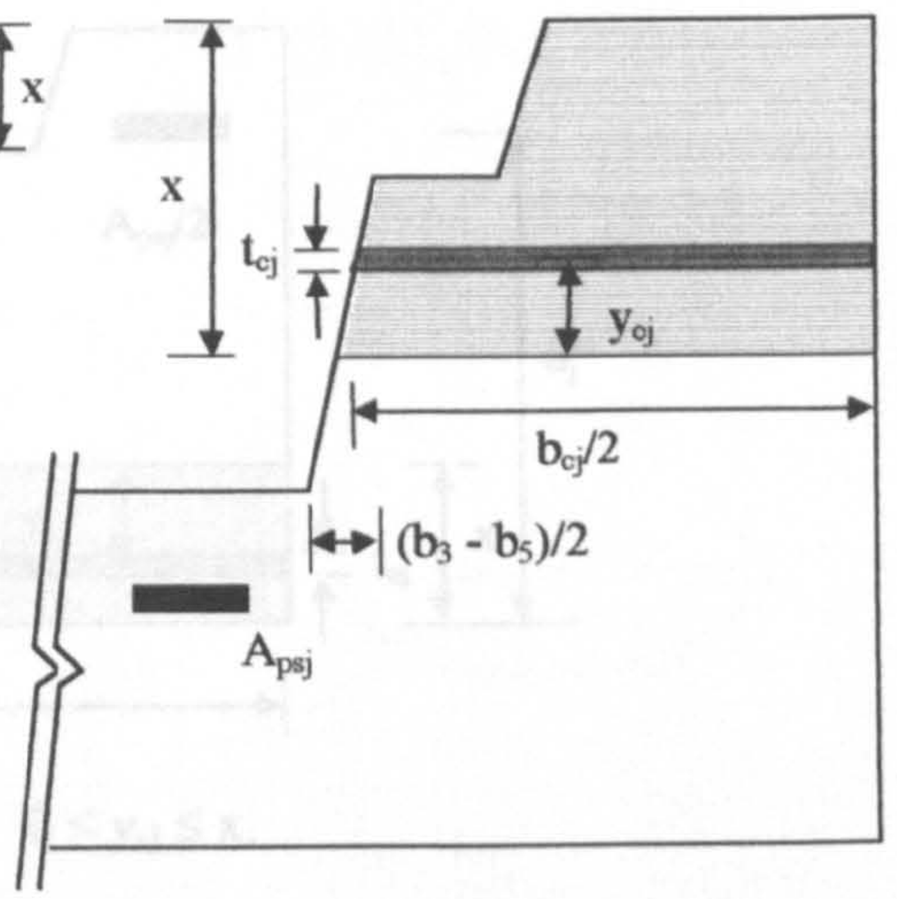

Fig. (4.6c): Case 2: $d_3 < x \leq d_2 + d_3$ and $0 < y_{cj} \leq x - d_3$.

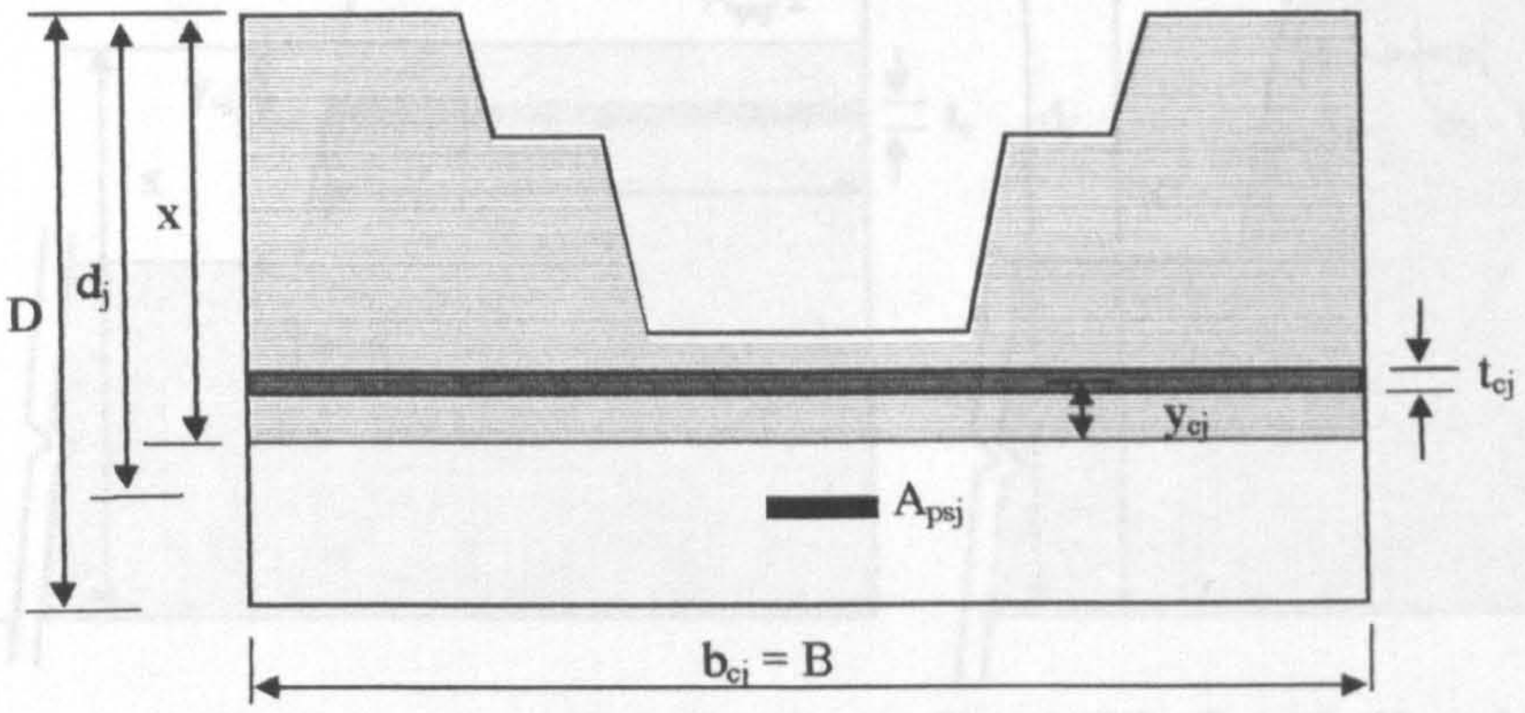

Fig. (4.6d): Case 3: $(d_2 + d_3) < x \leq D$ and $0 < y_{cj} \leq x - d_2 - d_3$.

Fig. (4.6): Concrete trough section subject to sagging moment at ultimate limit state.

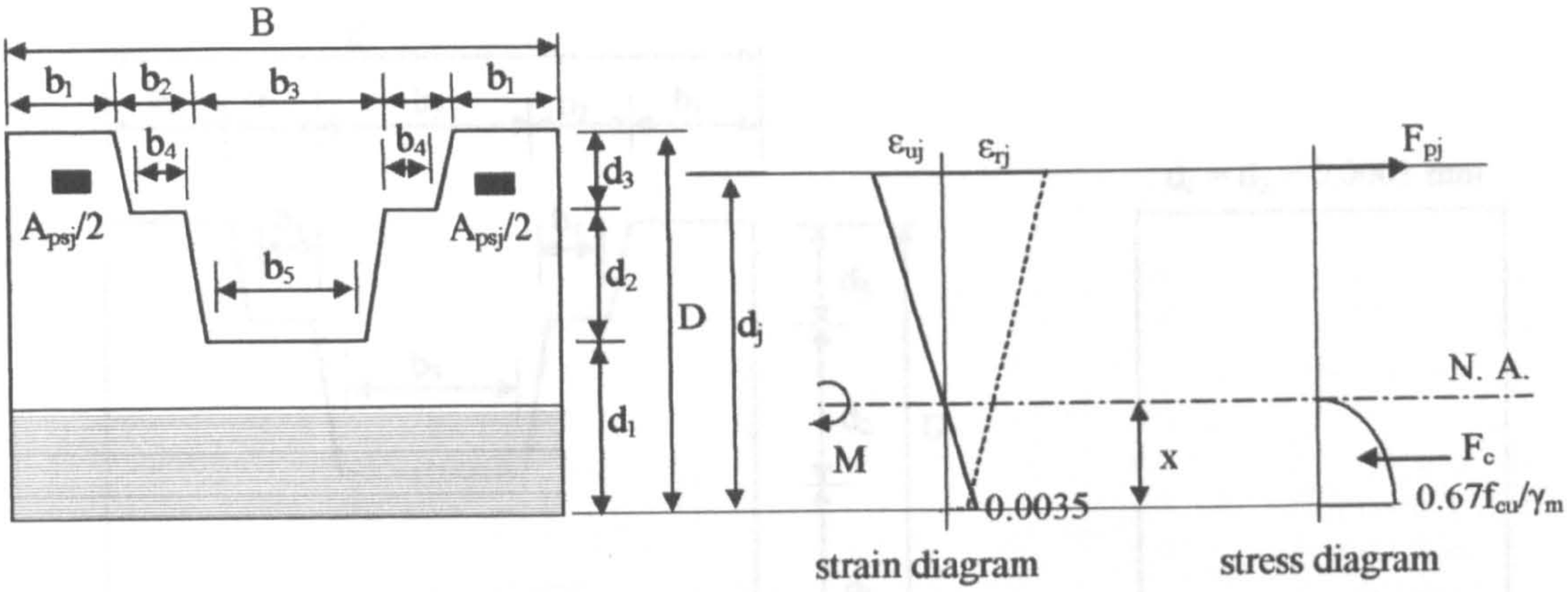

Fig. (4.7a): Strain and stress diagrams of the concrete trough due to ultimate hogging moment.

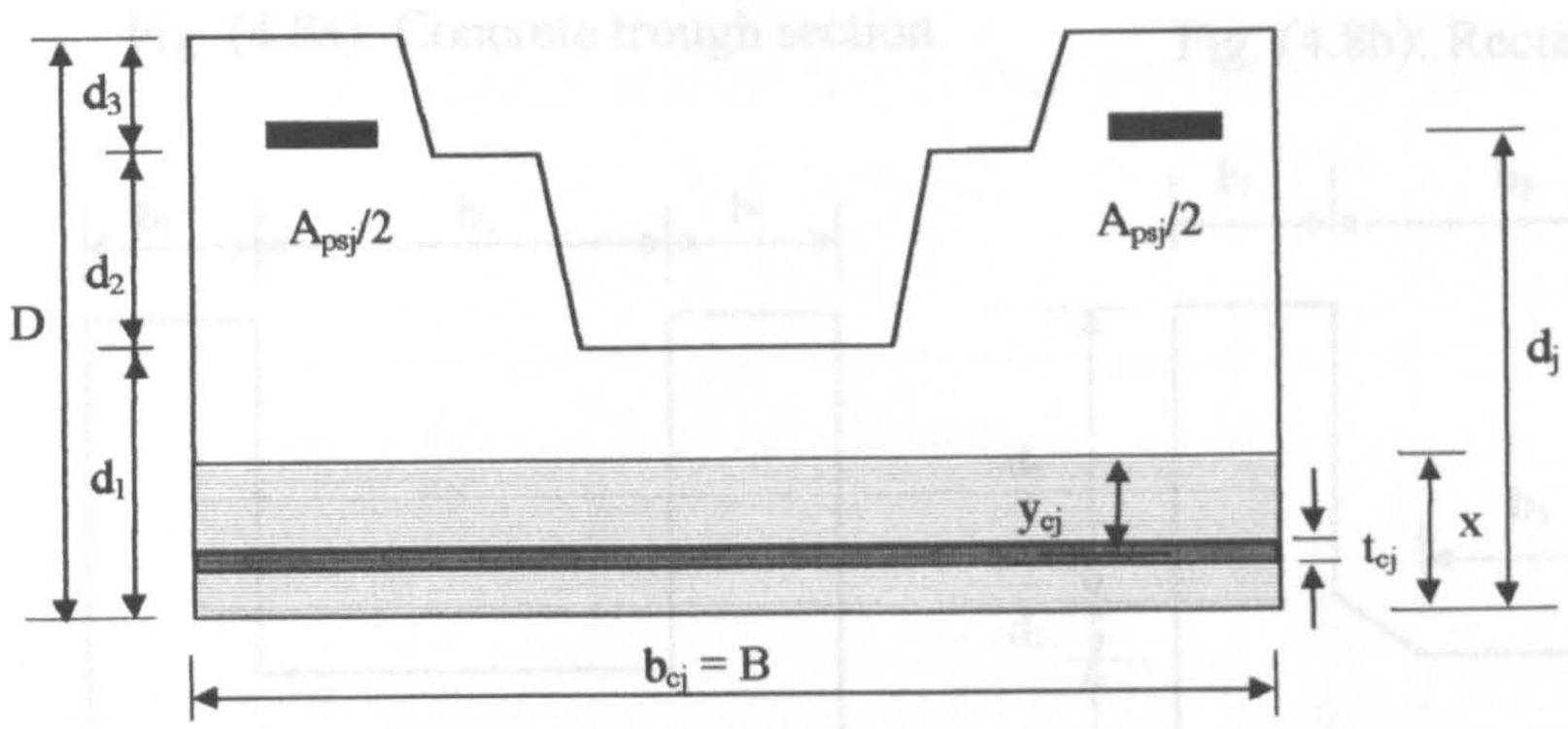

Fig. (4.7b): Case 1: $0 < x \leq d_1$ and $0 < y_{cj} \leq x$.

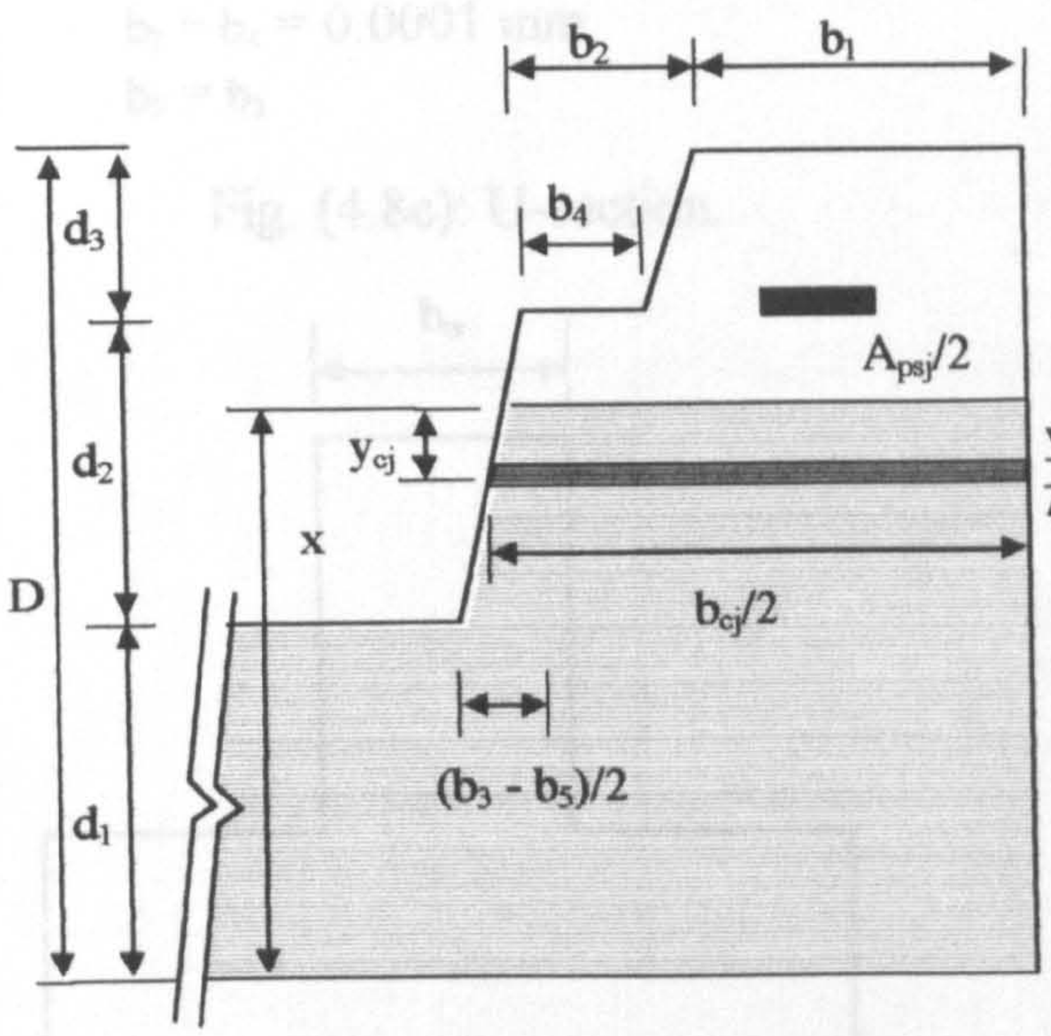

Fig. (4.7c): Case 2: $d_1 < x \leq (d_1 + d_2)$ and $0 < y_{cj} \leq x - d_1$.

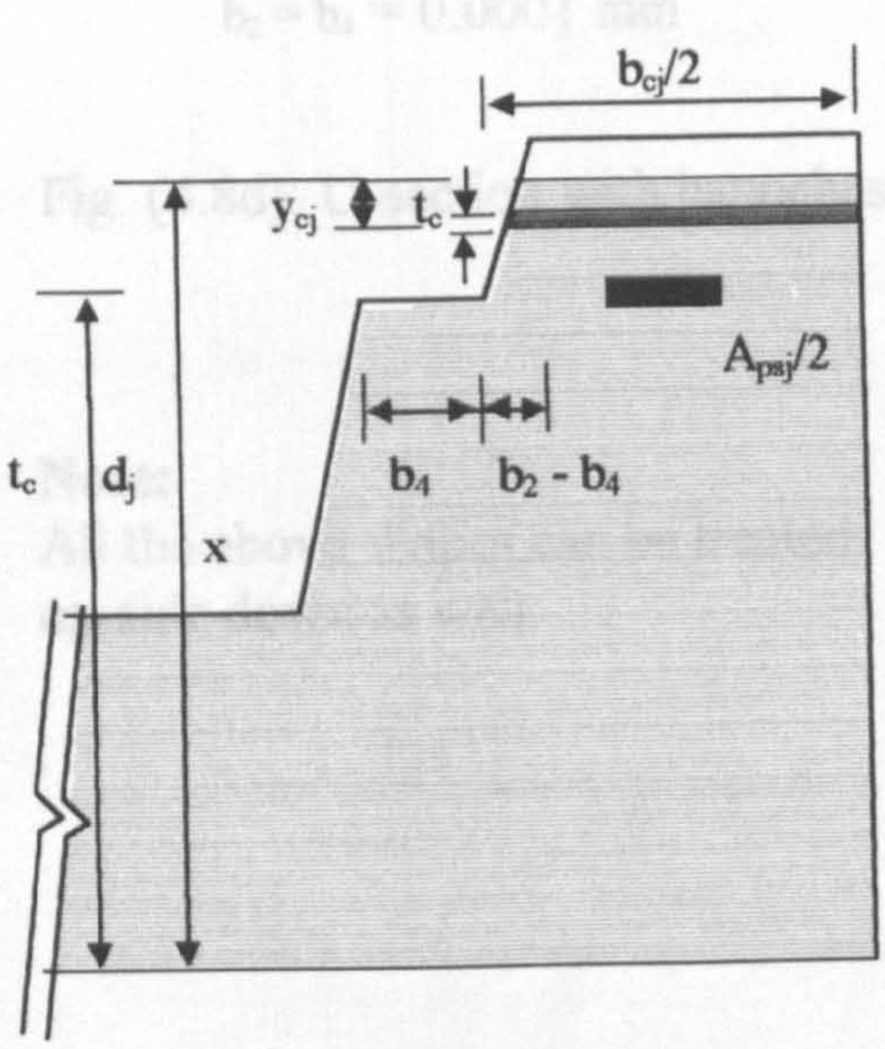

Fig. (4.7d): Case 3: $(d_1 + d_2) < x \leq D$ and $0 < y_{cj} \leq x - d_1 - d_2$.

Fig. (4.7): Concrete trough section subject to hogging moment at ultimate limit state.

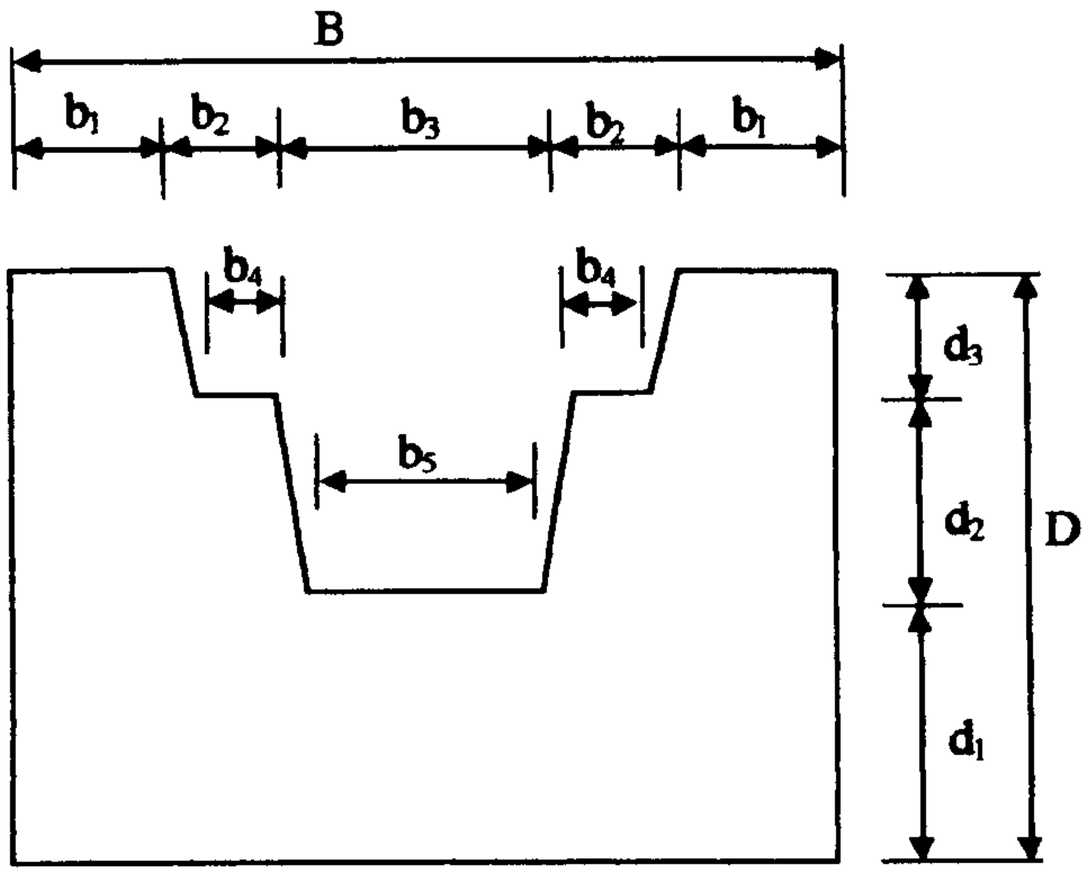

Fig. (4.8a): Concrete trough section.

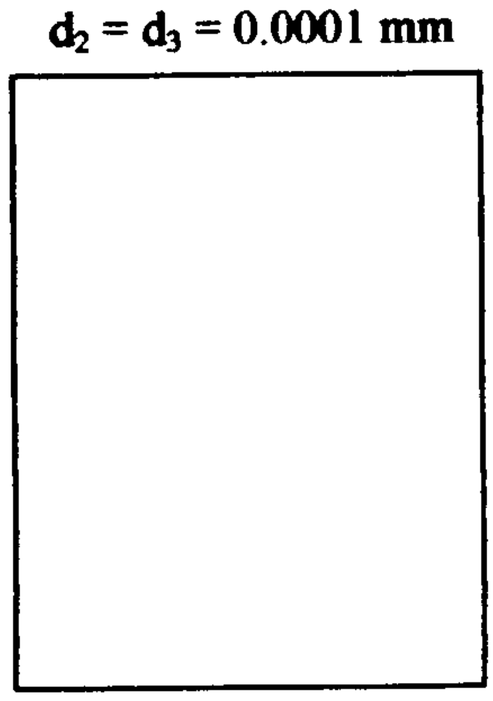

Fig. (4.8b): Rectangular section.

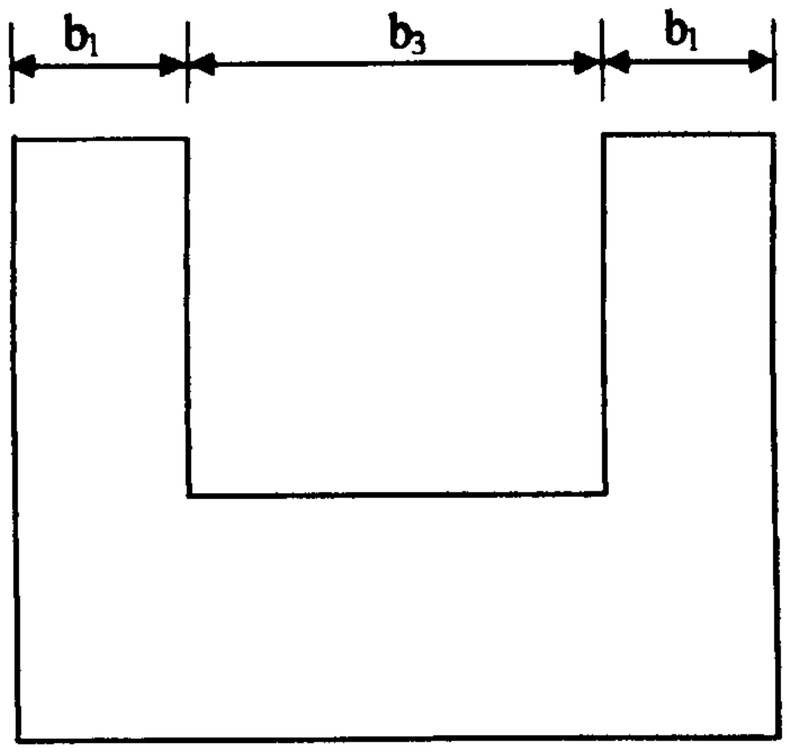

$b_2 = b_4 = 0.0001$ mm,
$b_5 = b_3$

Fig. (4.8c): U-section.

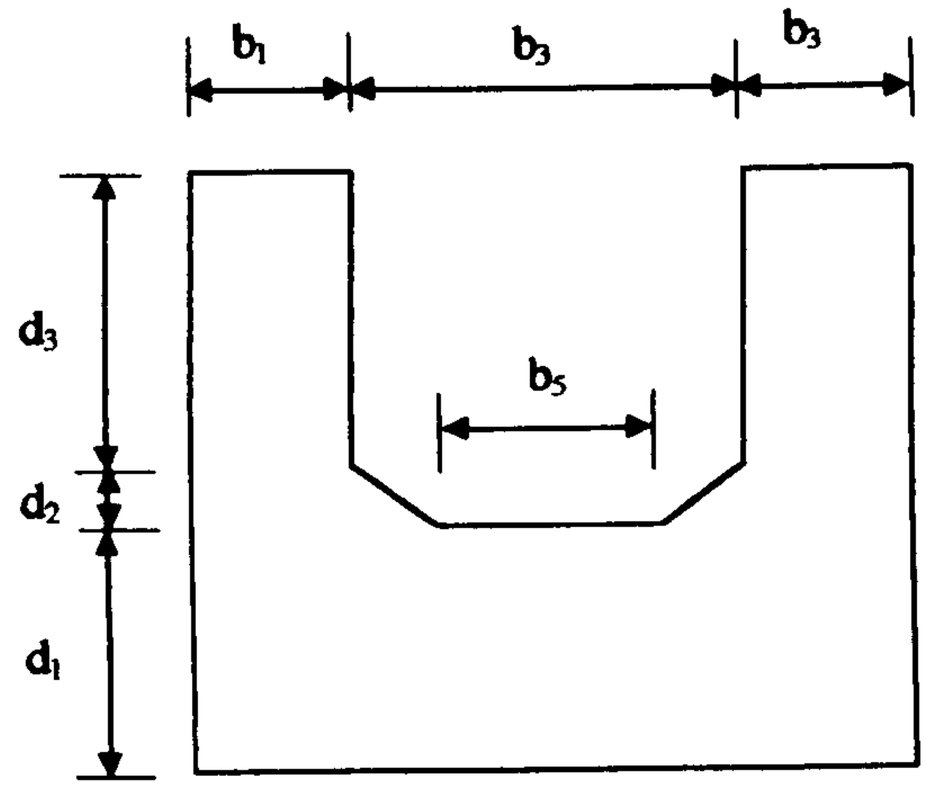

$b_2 = b_4 = 0.0001$ mm

Fig. (4.8d): U-section with haunches.

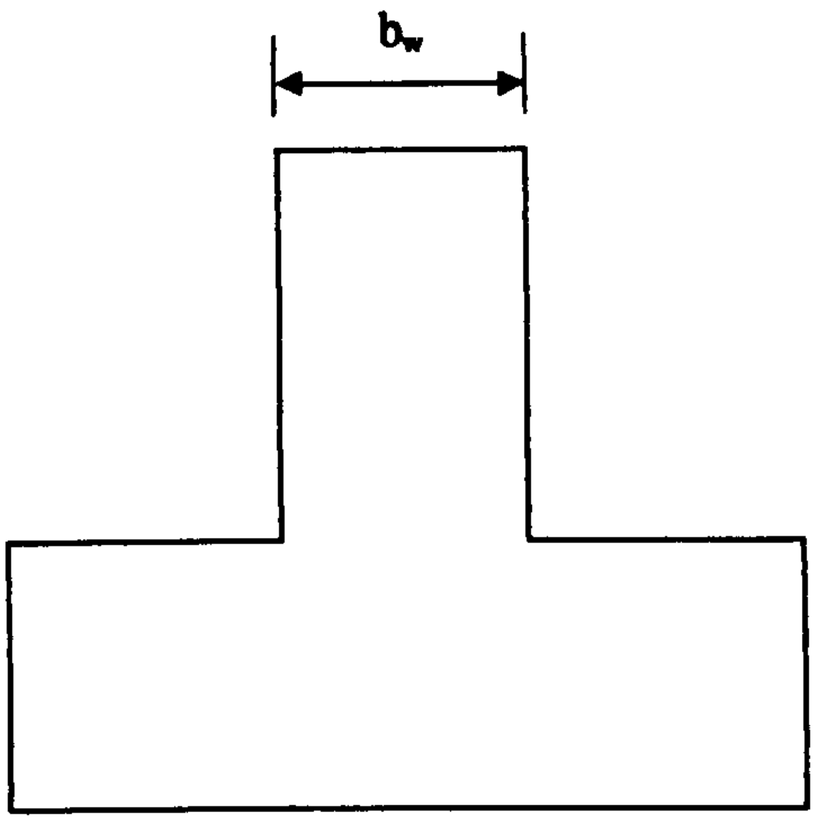

Fig. (4.8e): T-section; to be treated as U-section in Fig. (4.8c) with $b_1 = b_w/2$.

Note:
All the above shapes can be treated up-side down as well.

Fig. (4.8): Various shapes generated from the original concrete trough.

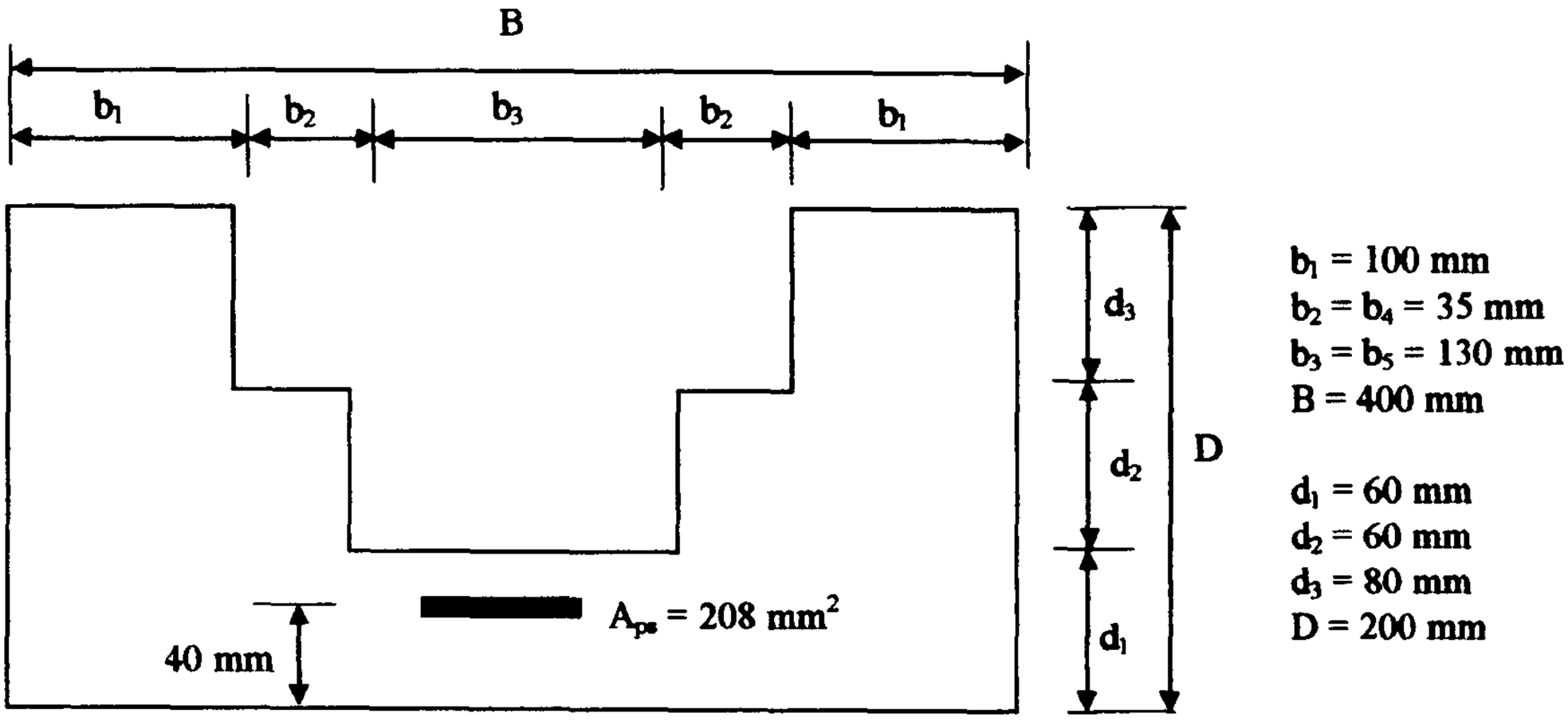

Fig. (4.9): Concrete trough cross-sectional properties for example 1.

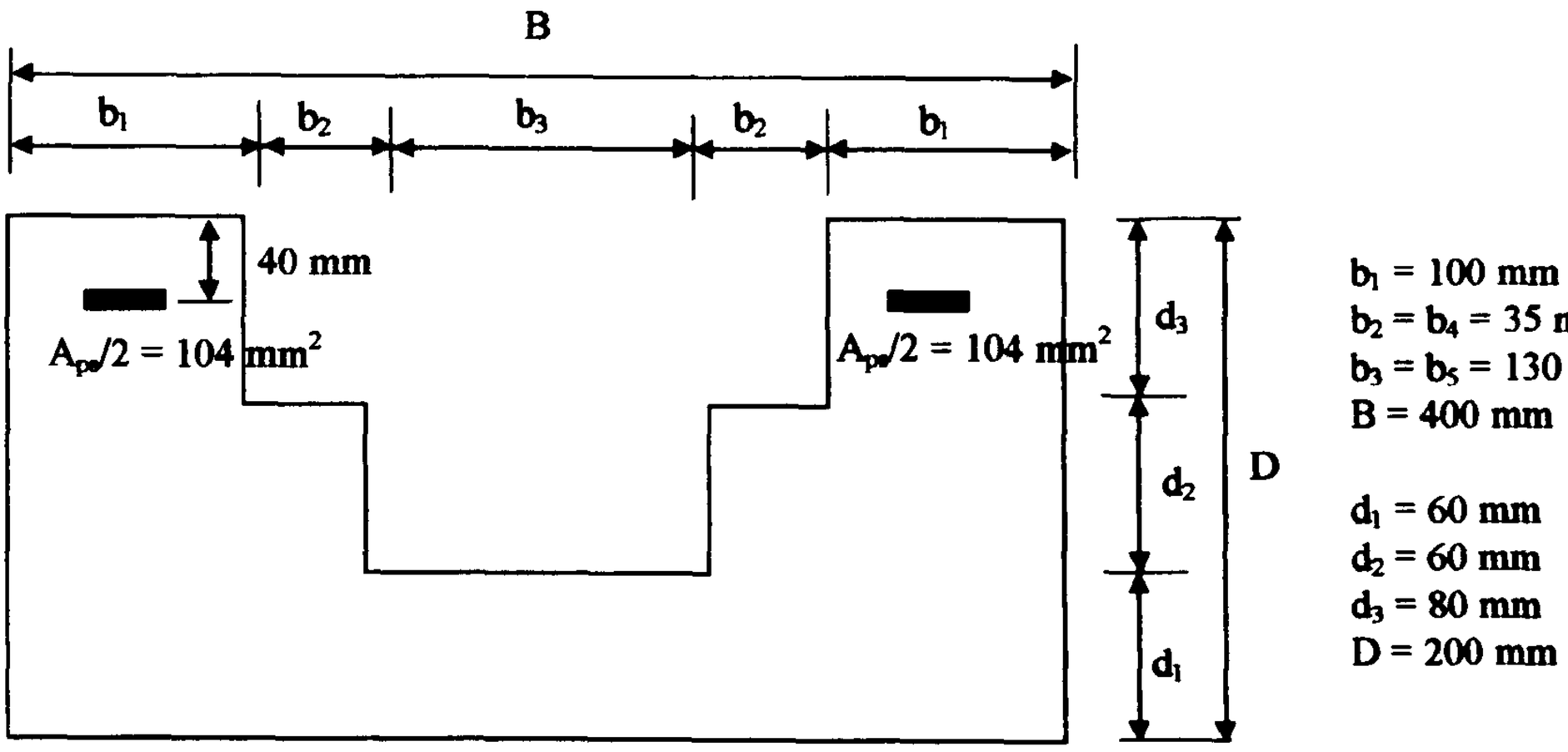

Fig. (4.10): Concrete trough cross-sectional properties for example 2.

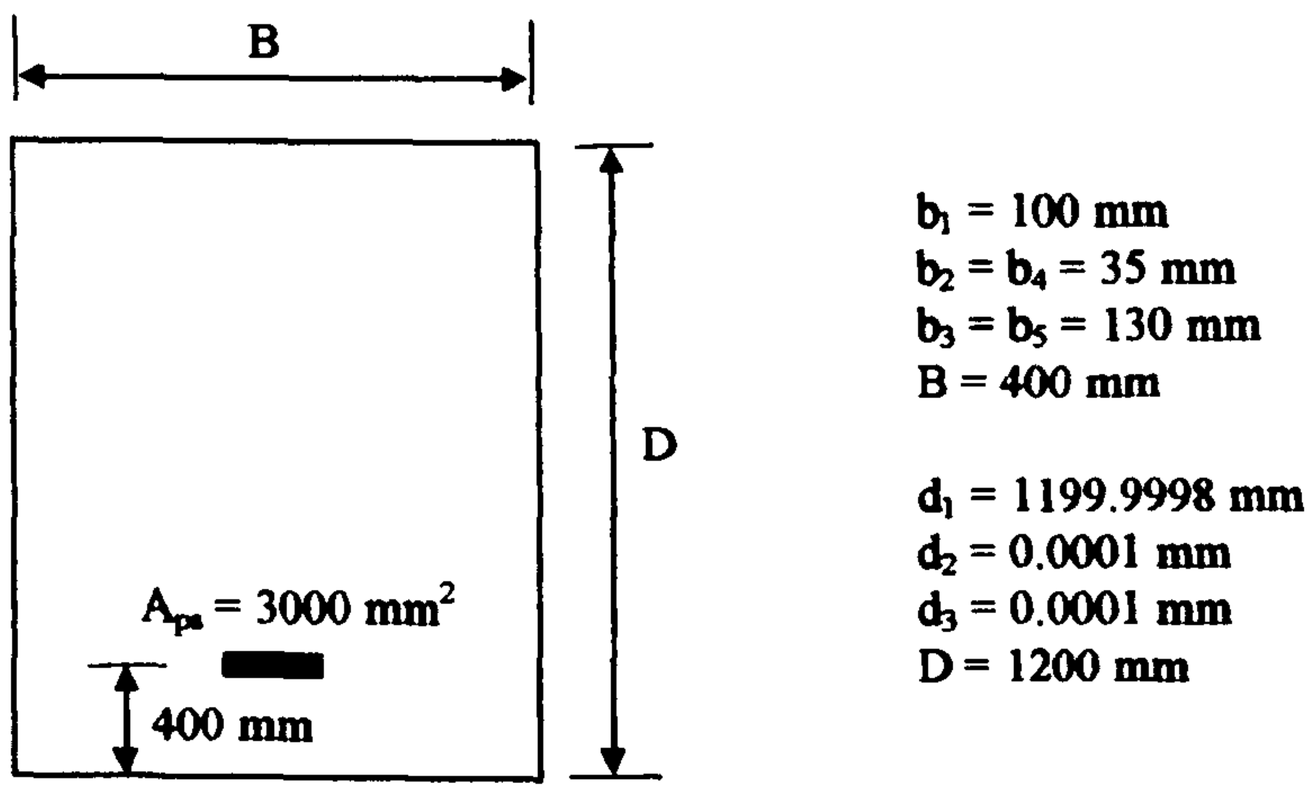

Fig. (4.11): Rectangular cross-sectional properties for example 3; it is generated from a concrete trough shape.

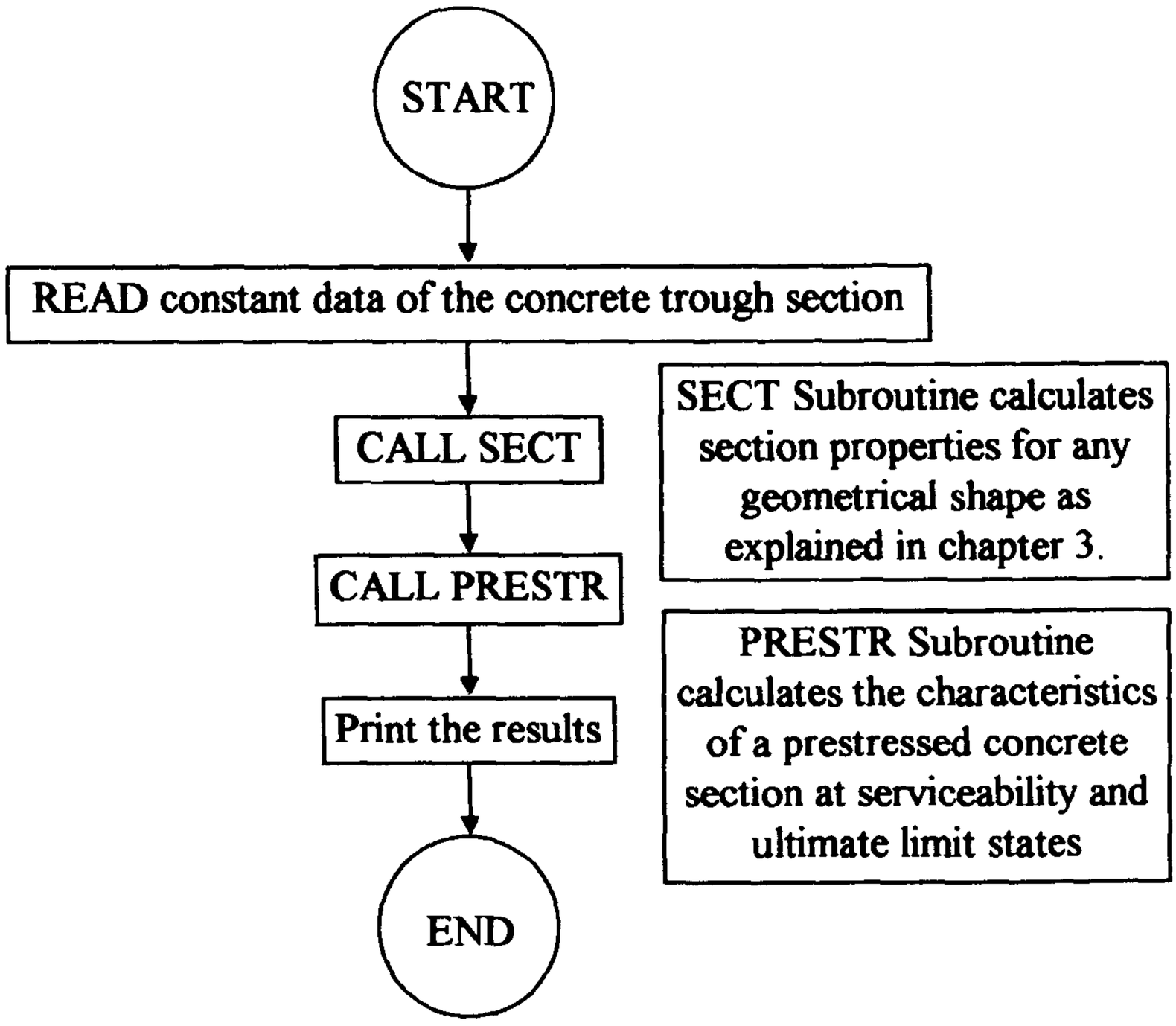

Fig. (4.12): Flow chart for the computer program TROUGH.

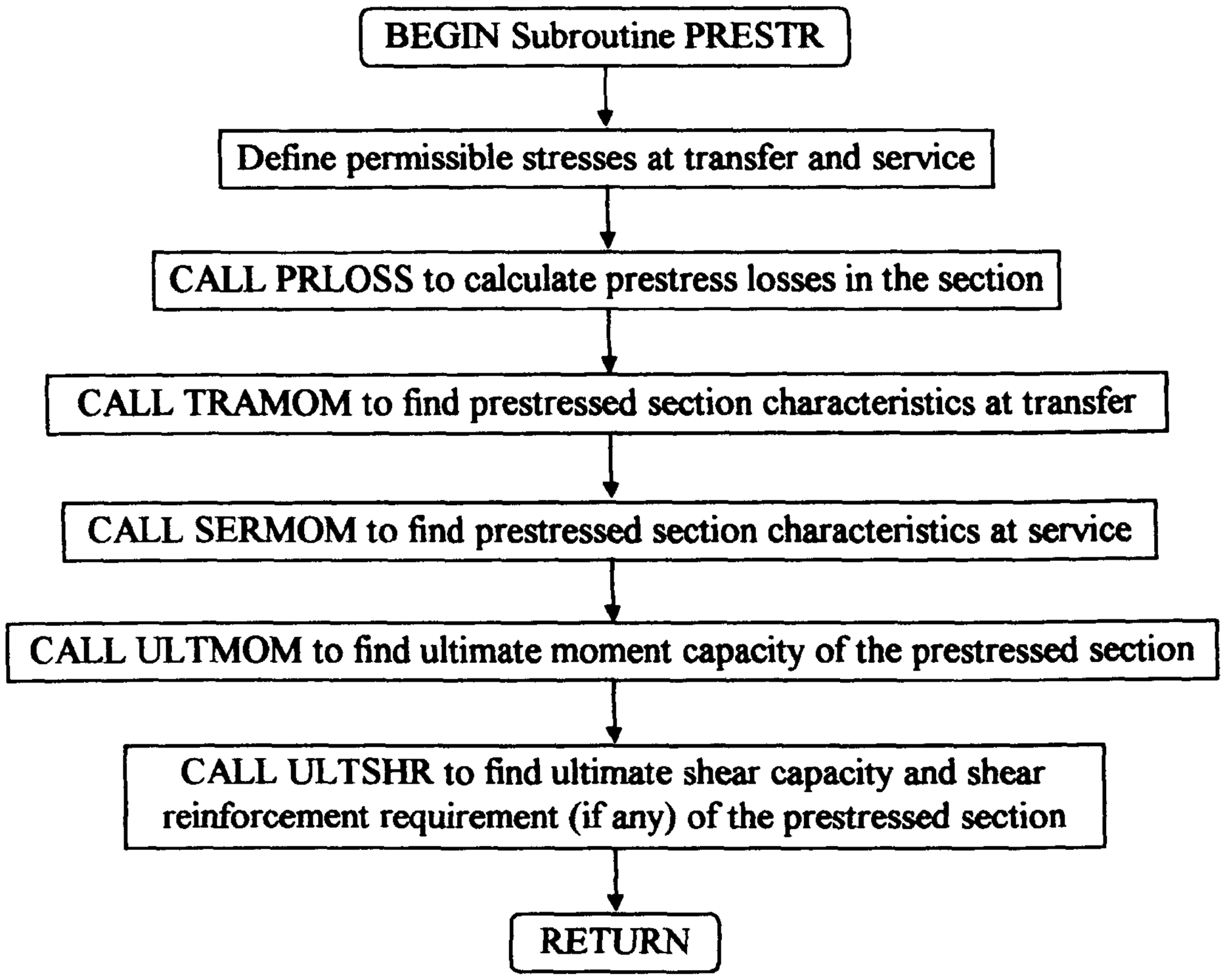

Fig. (4.13): Flow chart for subroutine PRESTR.

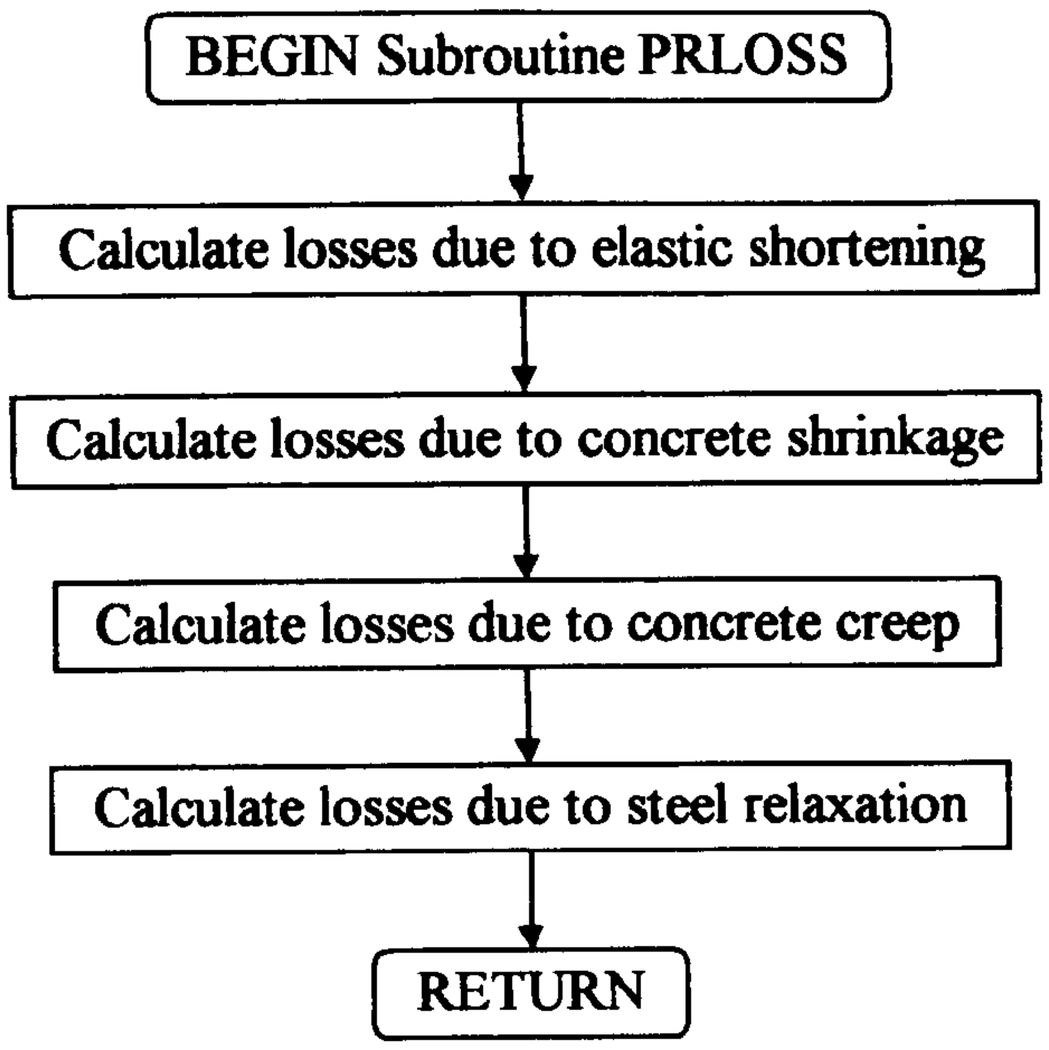

Fig. (4.14): Flow chart for subroutine PRLOSS.

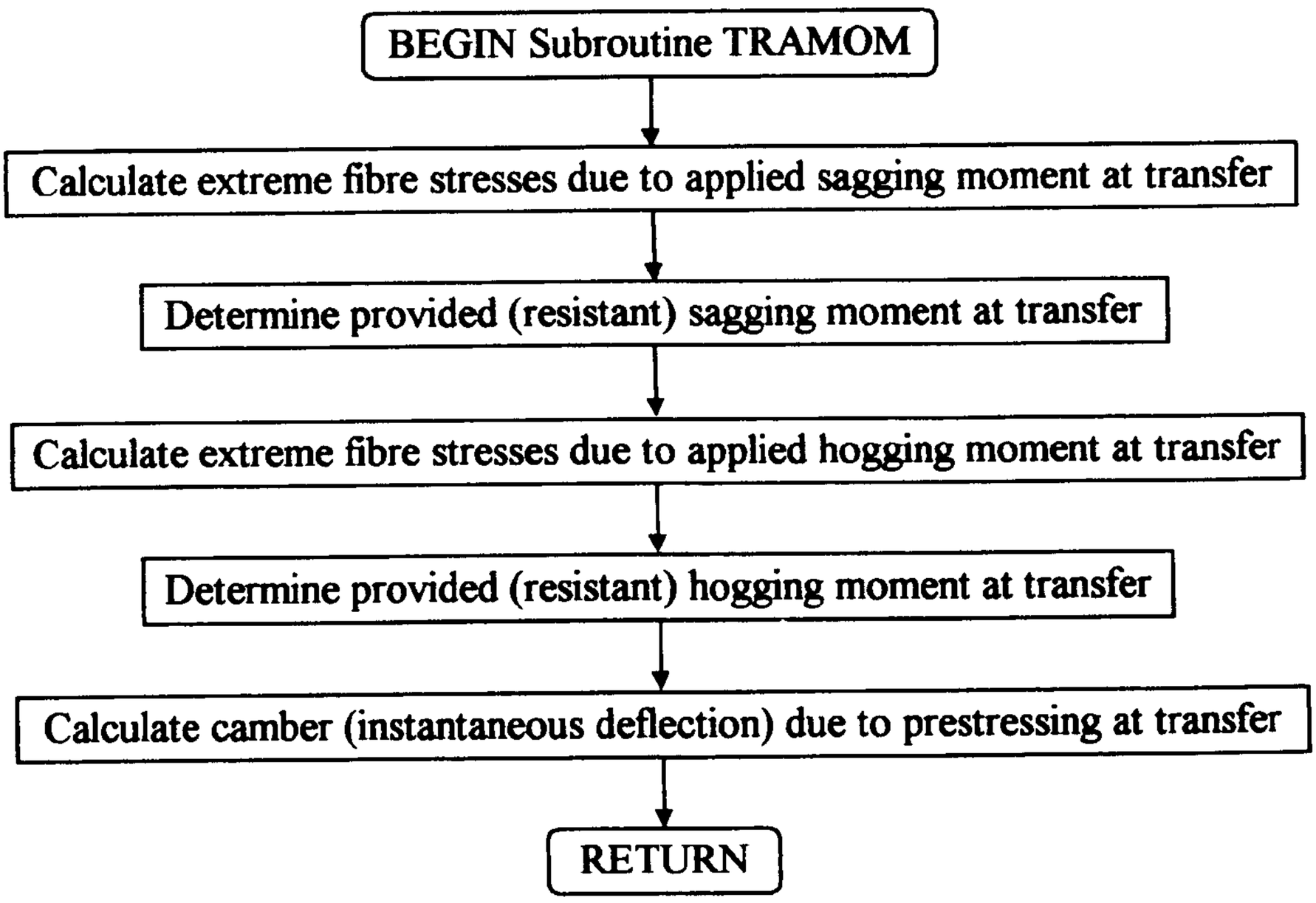

Fig. (4.15): Flow chart for subroutine TRAMOM.

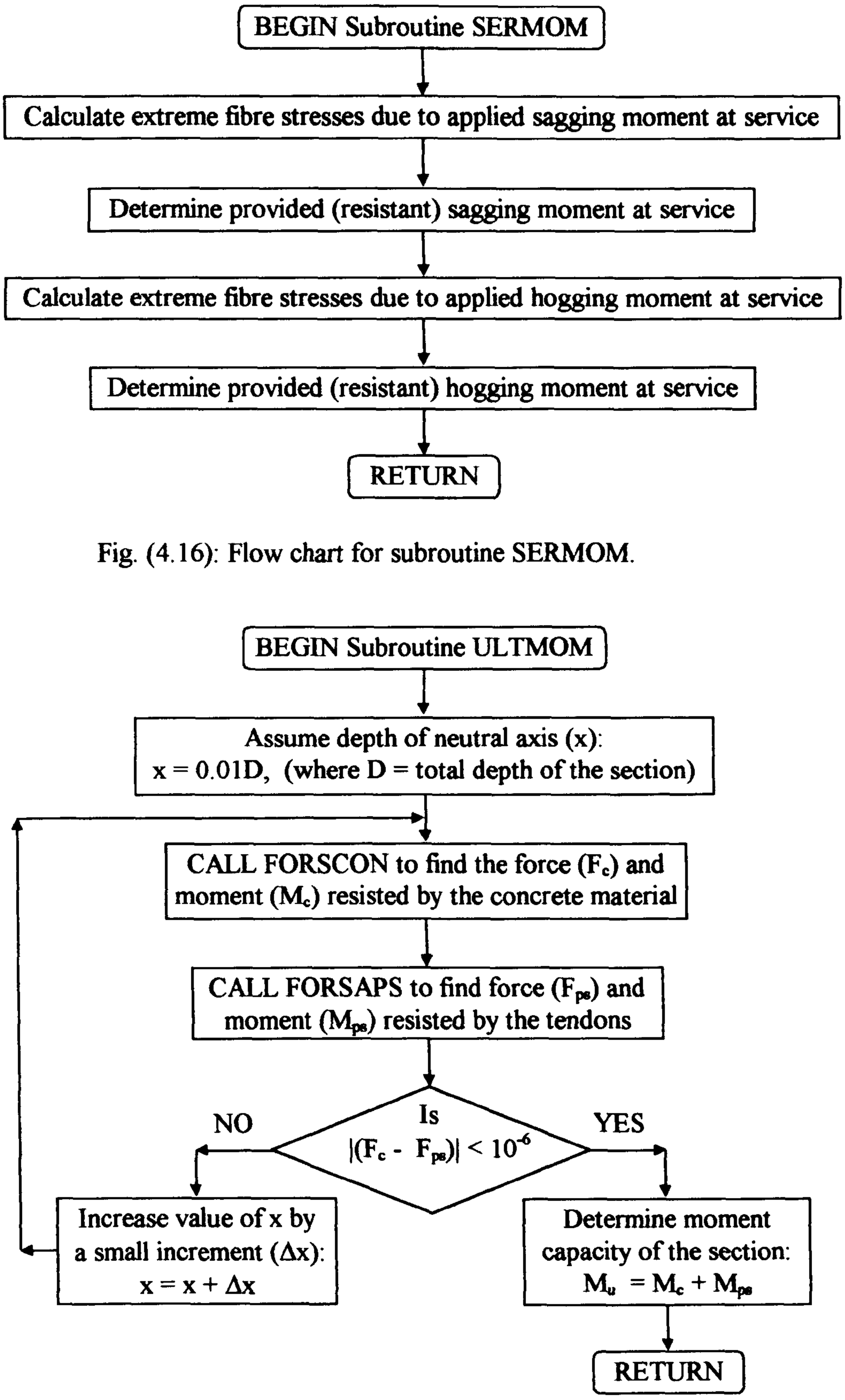

Fig. (4.16): Flow chart for subroutine SERMOM.

Fig. (4.17): Flow chart for subroutine ULTMOM.

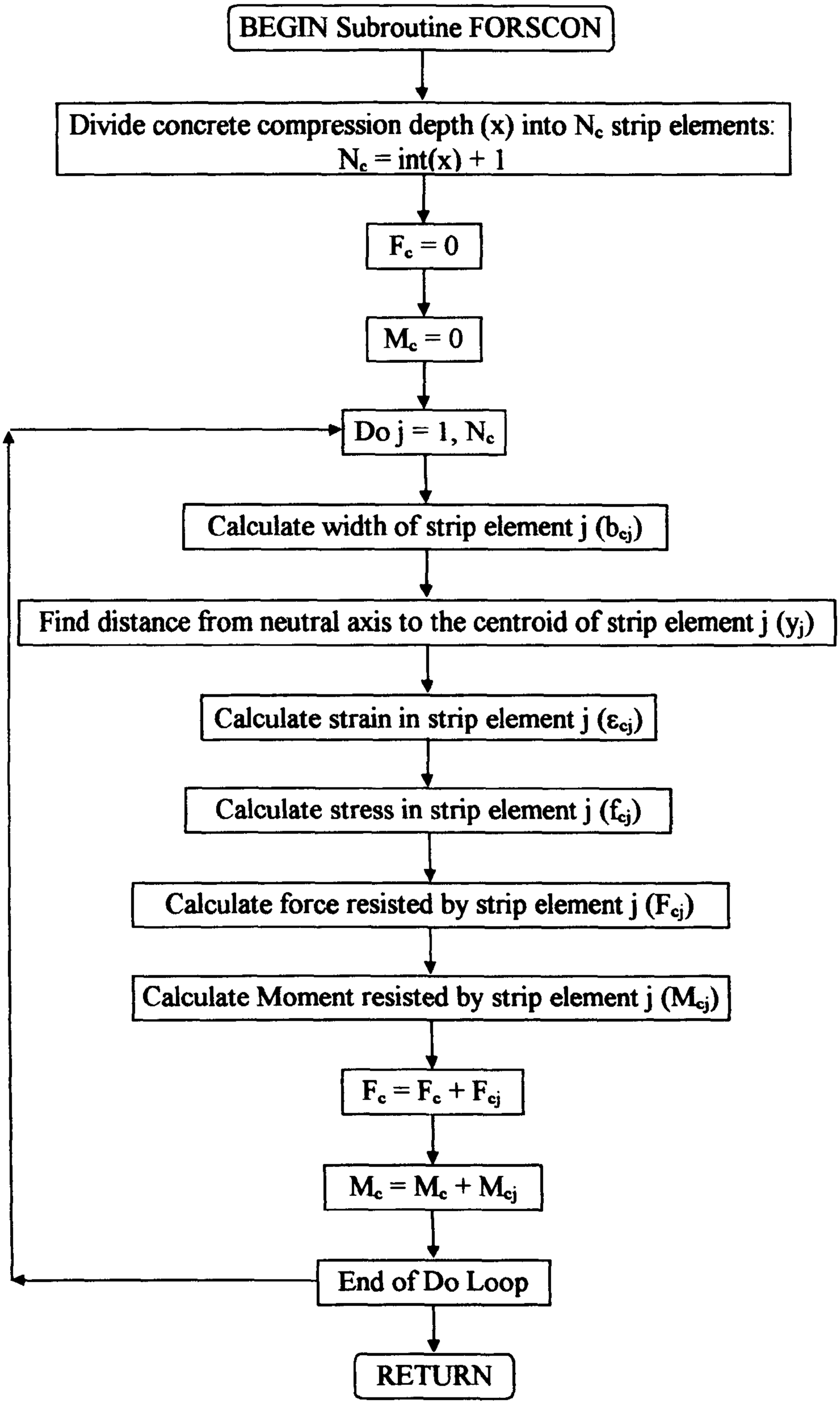

Fig. (4.18): Flow chart for subroutine FORSCON.

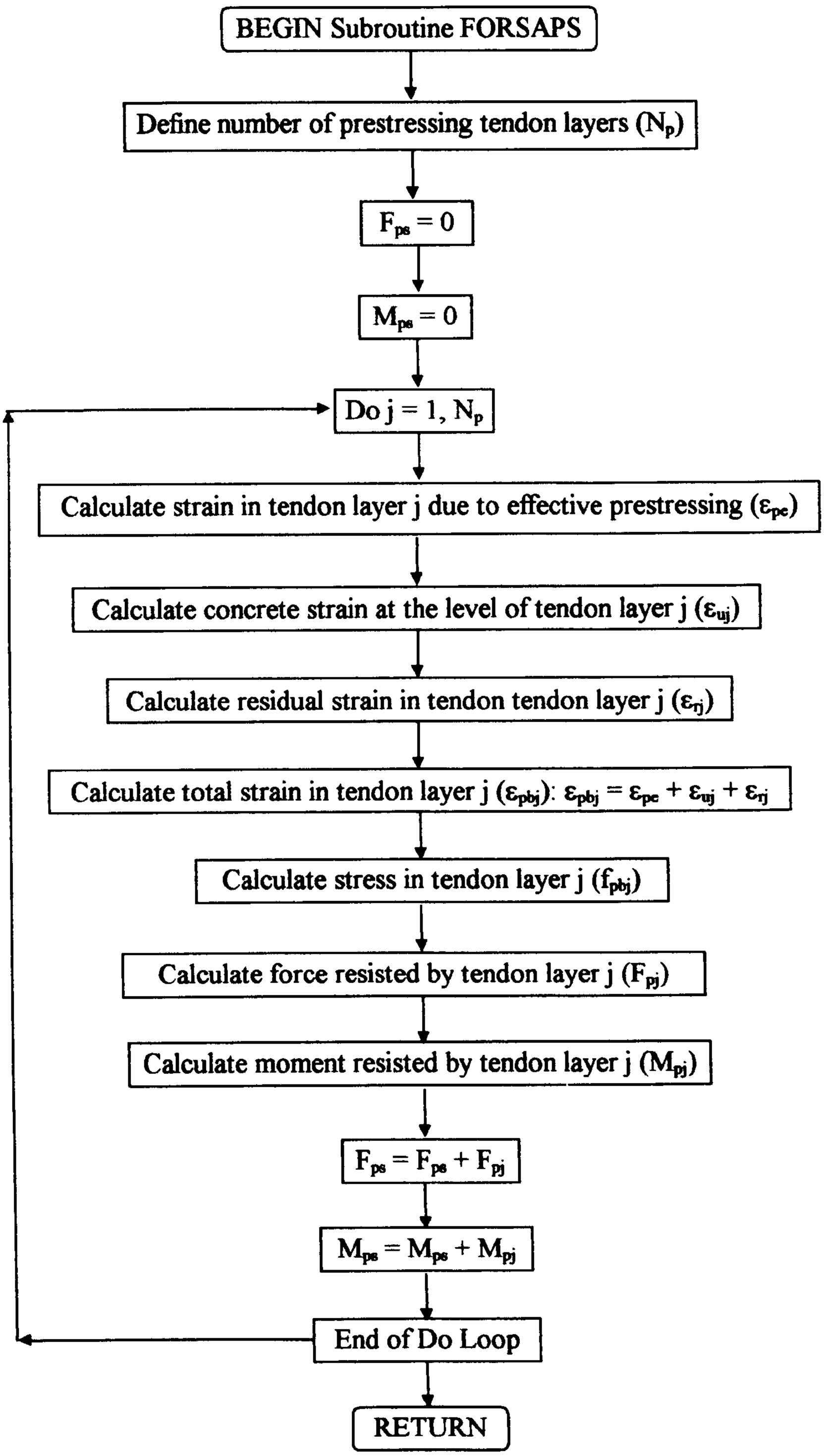

Fig. (4.19): Flow chart for subroutine FORSAPS.

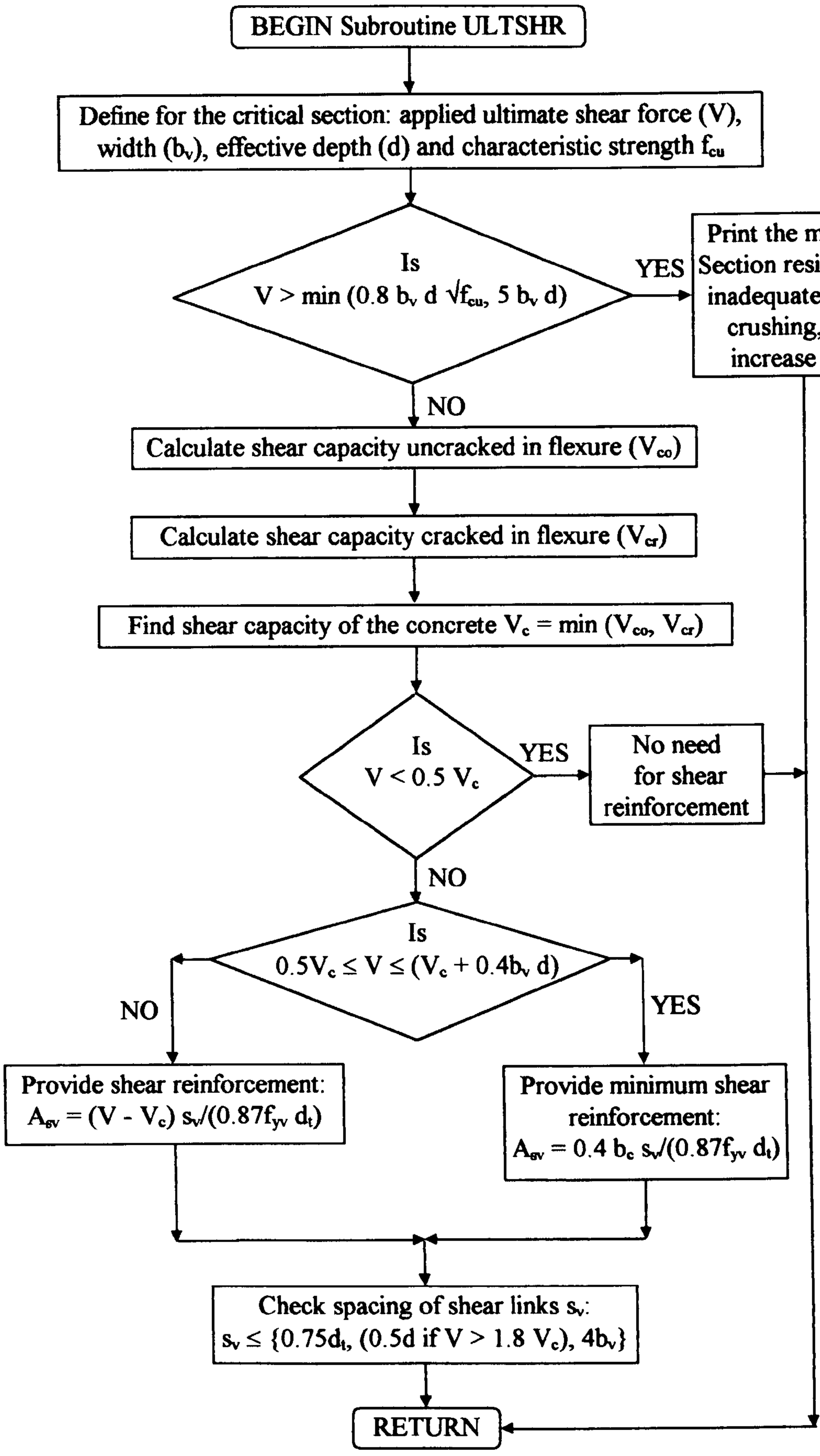

Fig. (4.20): Flow chart for subroutine ULTSHR.

CHAPTER FIVE

MATHEMATICAL MODELLING OF THE LR55 TRACK SYSTEM: ANALYTICAL SOLUTION

5.1 Introduction

One of the most practical applications of the theory of beams on elastic foundations is an analysis of a railway track system. Theoretically, a railway track system can be modelled either as a single layer or multilayer beams on elastic foundations depending on the type of support provided for the rail. For example, a conventional railway system which consists of rail, base plate or pad, transverse sleepers, ballast and subgrade, is usually treated as a single layer beam on an elastic foundation. In this case, the rail is considered as a beam while the rest of the track components are represented as one homogeneous elastic foundation. Such a model has already been considered by several researchers as presented section 2.6.1 of chapter 2.

When the rail is supported by a continuous structural element such as paved concrete slab or concrete trough as in the case of the LR55 track system, then it will be more appropriate to model the system as multilayer beams on elastic foundations. For such a case, the rail and the concrete are considered as beams having different bending rigidities while the pad and the track base are treated as elastic foundations having different moduli. Having decided upon a suitable model for the track system, then either analytical or numerical techniques can be followed to analyse the problem. In this chapter, the analytical solution for the LR55 track system modelled as multilayer beams on elastic foundations is investigated.

5.2 Basic Assumptions

The following assumptions were made for solving analytically the LR55 track system modelled as multilayer beams on elastic foundations:

1. All the materials forming the track system are homogeneous, isotropic and linear elastic.

2. The track is straight and level. This means that the effect of horizontal and vertical curvature of the track geometry is so small that it can be ignored.
3. The model can cater for vertical wheel load only. Therefore, the effect of shear resistance of the pad and the base has not been taken into consideration as it is of relevant significance in case of horizontal load applications.
4. The twisting effect of the applied load resulted from the unsymmetrical shape of the LR55 rail is not considered for sake of simplicity. This can be justified by the fact that the induced twist is small because the difference between the centroid of the rail and the concrete trough is only a small value of 4.1 mm as shown in Fig. (3.1), i.e. the eccentricity of the load is too small.
5. The soil properties underneath the track system do not vary along the length of the track.
6. The track base is firmly attached to the concrete trough. This implies that the track base is capable of resisting tension.
7. No bond failure will occur in the adhesive material forming the rail pad.
8. Downward deflection and sagging moment of the rail and concrete trough are positive. Compressive stress (pressure) on the pad and the track base are positive.

5.3 Foundations Moduli

5.3.1 Track Base Modulus

A track base modulus may be defined as the uniformly distributed line load required to cause unit deflection of the support, (Cope 1993). It depends on the following factors:

1. The modulus of subgrade reaction of the supporting soil which in turn depends on the bearing capacity and the Young's modulus of the soil. In general, the looser the soil is, the lower the value of the modulus of subgrade reaction, hence the lower the track base modulus value. Typical values for the modulus of subgrade reaction for different types of soil are available in literature, see for example (Timoshenko and Krieger 1959, Bowles 1988) which can be used as a guide to estimate the value of the track base modulus.
2. Width of the track base which is, in this case, the width of the concrete trough. A larger width of the concrete trough produces a higher value of the base modulus.

3. Number, thickness and elastic properties of the layers forming the base and subbase directly underneath the concrete trough such as ballast, sub-ballast, rigid concrete bed or asphalt pavement.

Due to the interaction of the factors mentioned above, it is not easy to specify precisely a single value for the track base modulus. It can only be calculated from field measurement of track deflection, i.e. after track construction, (Selig and Waters 1994). However, a range of values for the track base modulus, based on experience and experimental works, are available (Fastenrath 1981, Hay 1982, Esveld 1989, Cope 1993). Generally speaking, the base modulus might be taken between 5 - 10 N/mm^2 for soft track bed and between 50 - 60 N/mm^2 for stiff base.

5.3.2 Rail Pad Modulus

The rail pad modulus may be defined as the force required to cause a unit deflection of a unit length of the pad, (Cope 1993). It depends mainly on the elastic properties and the dimensions of the material forming the pad. An accurate estimate of the pad modulus should be based on experimental results. However, the approach for deriving approximately the pad modulus k_1 is by assuming the pad consists of infinite number of springs. The stiffness of each spring K_1 may be defined as, (Gent 1992):

$$K_1 = E_p A_p / h_p \qquad (5.1)$$

where

E_p = Young's modulus of the pad

A_p = contact area between the pad and the rail contributed by each spring

$= W_r L_p$

$= 165 L_p$

W_r = rail width (165 mm)

L_p = portion of pad length allocated for each hypothetical spring

h_p = thickness of the pad

Dividing both side of eq. (5.1) by L_p and substituting for the value of $A_p = 165 L_p$ into eq. (5.1) gives the rail pad modulus k_1 which is known as the force required to cause unit length of the pad unit deflection, i.e.

$$k_1 = K_1/L_p$$
$$= 165\ E_p/h_p \qquad (5.2)$$

The average thickness of the pad in the LR55 track system is 20 mm. Substituting pad thickness h_p = 20 mm into eq. (5.2), the rail pad modulus can be found for any assumed value of the pad Young's modulus as shown in Table (5.1).

5.4 Mathematical Derivation

The track system subjected to a wheel load P is considered as multilayer beams on elastic foundations as shown in Fig. (5.1). The rail is represented by a continuous beam of infinite length and bending rigidity EI_1, supported on continuous elastic foundation (rail pad) of modulus k_1 which in turn rests on a beam (concrete trough) of infinite length and bending rigidity EI_2 which is supported by another continuous elastic foundation (track base) of modulus k_2. The foundations are assumed to consist of an infinite number of independent springs of Winkler type in which the deflection of each spring is directly proportional to the pressure acting on it and the springs have lack of mutual interactions, i.e. no vertical shear transfer between the springs will take place, (Selvadurai 1979, Dulacska 1992). The base springs are assumed to equally resist both tension and compression. This implies that the supporting soil is capable for resisting tension which is physically not valid.

Consider an infinitesimal element of width dx, cut out of the track model at distance x from the point wheel load P. All the forces acting on this element are shown in Fig. (5.1). The subscripts 1 and 2 refer to forces on the upper and lower beams, i.e. the rail and the concrete trough, respectively.

Taking the equilibrium of the vertical forces acting on the upper and lower beam elements gives:

Upper beam element: $V_1 - (V_1 + dV_1) + k_1 (y_1 - y_2)\, dx = 0$ (5.3)

Lower beam element: $V_2 - (V_2 + dV_2) - k_1 (y_1 - y_2)\, dx + k_2\, y_2\, dx = 0$ (5.4)

Dividing both of eqs. (5.3) and (5.4) by dx and simplifying terms result in:

$$dV_1/dx = k_1 (y_1 - y_2) \tag{5.5}$$

$$dV_2/dx = (k_1 + k_2) y_2 - k_1 y_1 \tag{5.6}$$

Taking moment equilibrium of the forces acting on the upper and lower elements gives:

Upper beam element;

$$M_1 + (V_1 + dV_1) dx - (M_1 + dM_1) - k_1 (y_1 - y_2) dx\, dx/2 = 0 \tag{5.7}$$

Lower beam element;

$$M_2 + (V_2 + dV_2) dx - (M_2 + dM_2) + k_1 (y_1 - y_2) dx\, dx/2 - k_2 y_2 dx\, dx/2 = 0 \tag{5.8}$$

Ignoring the small terms of second order in eqs. (5.7) and (5.8) and simplifying terms gives:

$$V_1 = dM_1/dx \tag{5.9}$$

$$V_2 = dM_2/dx \tag{5.10}$$

Taking the first derivative of eqs. (5.9) and (5.10) gives:

$$dV_1/dx = d^2M_1/dx^2 \tag{5.11}$$

$$dV_2/dx = d^2M_2/dx^2 \tag{5.12}$$

Substituting eqs. (5.11) and (5.12) into eqs. (5.5) and (5.6) respectively gives:

$$d^2M_1/dx^2 = k_1 (y_1 - y_2) \tag{5.13}$$

$$d^2M_2/dx^2 = (k_1 + k_2) y_2 - k_1 y_1 \tag{5.14}$$

Assuming small deflection theory of beam is valid, the moment-curvature relationship can be expressed as, (Gere and Timoshenko 1985):

$$EI_1\, d^2y_1/dx^2 = - M_1 \tag{5.15}$$

$$EI_2\, d^2y_2/dx^2 = - M_2 \tag{5.16}$$

Taking the second derivative of eqs. (5.15) and (5.16) gives:

$$EI_1\, d^4y_1/dx^4 = - d^2M_1/dx^2 \tag{5.17}$$

$$EI_2\, d^4y_2/dx^4 = - d^2M_2/dx^2 \tag{5.18}$$

Substituting eqs. (5.17) and (5.18) into eqs. (5.13) and (5.14) respectively yields:

$$EI_1 \, d^4y_1/dx^4 = - k_1 (y_1 - y_2) \tag{5.19}$$

$$EI_2 \, d^4y_2/dx^4 = - (k_1 + k_2) y_2 + k_1 y_1 \tag{5.20}$$

The set of eqs. (5.19) and (5.20) is the governing differential equation of the track system modelled as multilayer beams on elastic foundations of infinite length and subject to a point load at the centre. It is a coupled fourth order homogeneous linear differential equation with constant coefficients.

The necessary boundary conditions required to solve the system can be set up from the fact that at $x = \pm \infty$, all the deflection, slope, bending moment and shear will diminish. In addition, at $x = 0$, the shear in the rail is half the wheel load. These can be interpreted mathematically as:

when $x = \pm \infty$

$$\text{(deflection):} \quad y_1 = y_2 = 0 \tag{5.21}$$

$$\text{(slope):} \quad dy_1/dx = dy_2/dx \tag{5.22}$$

$$\text{(moment):} \quad EI_1 \, d^2y_1/dx^2 = EI_2 \, d^2y_2/dx^2 = 0 \tag{5.23}$$

$$\text{(shear):} \quad EI_1 \, d^3y_1/dx^3 = EI_2 \, d^3y_2/dx^3 = 0 \tag{5.24}$$

and at $x = 0$

$$\text{(shear):} \quad EI_1 \, d^3y_1/dx^3 = - P/2 \tag{5.25}$$

Hetenyi (1946) presented a solution of the coupled differential equations (5.19) and (5.20), subject to the boundary conditions given by eqs. (5.21) - (5.25) for the case when the upper and lower beams have same material. In the present work, a slight modification was made to Hetenyi's solution in order to suit the case of the LR55 track system where the steel rail (upper beam) and the concrete trough (lower beam) are made of two different materials, i.e. two different Young's moduli. The solution for the track responses in terms of deflection, slope, moment and shear are as follows:

For the upper beam (rail);

$$\text{Deflection:} \quad y_1 = (P/16EI_1\beta) [D_1 A_{\lambda 1}/\lambda_1^3 - D_2 A_{\lambda 2}/\lambda_2^3] \tag{5.26}$$

$$\text{Slope:} \quad \theta_1 = (P/8EI_1\beta) [-D_1 B_{\lambda 1}/\lambda_1^2 + D_2 B_{\lambda 2}/\lambda_2^2] \tag{5.27}$$

$$\text{Moment:} \quad M_1 = (P/8\beta) [D_1 C_{\lambda 1}/\lambda_1 - D_2 C_{\lambda 2}/\lambda_2] \tag{5.28}$$

Shear: $V_1 = (P/4\beta)\,[-D_1\,D_{\lambda 1} + D_2\,D_{\lambda 2}]$ (5.29)

For the lower beam (concrete trough);

Deflection: $y_2 = (-P/16EI_2\beta)(k_1/EI_1)[A_{\lambda 1}/\lambda_1^3 - A_{\lambda 2}/\lambda_2^3]$ (5.30)

Slope: $\theta_2 = (P/8EI_2\beta)(k_1/EI_1)[B_{\lambda 1}/\lambda_1^2 - B_{\lambda 2}/\lambda_2^2]$ (5.31)

Moment: $M_2 = (-P/8\beta)(k_1/EI_1)[C_{\lambda 1}/\lambda_1 - C_{\lambda 2}/\lambda_2]$ (5.32)

Shear: $V_2 = (P/4\beta)(k_1/EI_1)[D_{\lambda 1} - D_{\lambda 2}]$ (5.33)

where

$A_{\lambda 1} = e^{-\lambda 1 x}(\cos \lambda_1 x + \sin \lambda_1 x)$ (5.34)

$A_{\lambda 2} = e^{-\lambda 2 x}(\cos \lambda_2 x + \sin \lambda_2 x)$ (5.35)

$B_{\lambda 1} = e^{-\lambda 1 x} \sin \lambda_1 x$ (5.36)

$B_{\lambda 2} = e^{-\lambda 2 x} \sin \lambda_2 x$ (5.37)

$C_{\lambda 1} = e^{-\lambda 1 x}(\cos \lambda_1 x - \sin \lambda_1 x)$ (5.38)

$C_{\lambda 2} = e^{-\lambda 2 x}(\cos \lambda_2 x - \sin \lambda_2 x)$ (5.39)

$D_{\lambda 1} = e^{-\lambda 1 x} \cos \lambda_1 x$ (5.40)

$D_{\lambda 2} = e^{-\lambda 2 x} \cos \lambda_2 x$ (5.41)

$D_1 = (k_1/EI_1) - (\alpha - \beta)$ (5.42)

$D_2 = (k_1/EI_1) - (\alpha + \beta)$ (5.43)

$\alpha = a/2$ (5.44)

$\beta = (a^2/4 - b)^{1/2}$ (5.45)

$a = k_1/EI_1 + (k_1 + k_2)/EI_2$ (5.46)

$b = (k_1/EI_1)(k_2/EI_2)$ (5.47)

$\lambda_1 = [(\alpha + \beta)/4]^{1/4}$ (5.48)

$\lambda_2 = [(\alpha - \beta)/4]^{1/4}$ (5.49)

The line force acting under the upper beam (rail), q_1, can be found as:

$q_1 = (y_1 - y_2)\,k_1$ (5.50)

Similarly, the line force acting under the lower beam (concrete trough), q_2, is:

$q_2 = y_2\,k_2$ (5.51)

To find the pressure distribution imposed on the upper foundation (rail pad), p_1, and the lower foundation (track base), p_2, we have to divide q_1 and q_2 in eqs. (5.50) and (5.51) by the rail width (W_r = 165 mm) and the concrete trough width (B) respectively, i.e.

$$p_1 = q_1/W_r$$
$$= (y_1 - y_2)\, k_1/W_r \qquad (5.52)$$
$$p_2 = q_2/B$$
$$= y_2\, k_2/B \qquad (5.53)$$

Since the analysis presented here is linear elastic, the principle of superposition is valid. Therefore, the track responses under multiple axle loads can be obtained by adding algebraically the effect of each single axle load.

It is to be noted that evaluating the slope of the deflected rail or the concrete trough at any point along the track is not of any interest from a practical point of view and therefore it will not be given further consideration.

5.4.1 Maximum Values of the Track Responses

By inspection, the maximum deflection, bending moment and shear in the rail occurs under the wheel load, i.e. by substituting for x = 0 into eqs. (5.26), (5.28) and (5.29) results in:

$$y_{1,\,max} = (P/16EI_1\beta)\,[D_1/\lambda_1^{\,3} - D_2/\lambda_2^{\,3}] \qquad (5.54)$$
$$M_{1,\,max} = (P/8\beta)\,[D_1/\lambda_1 - D_2/\lambda_2] \qquad (5.55)$$
$$V_{1,\,max} = P/2 \qquad (5.56)$$

The deflection and the bending moment in the concrete trough are also maximum under the wheel load, i.e. substituting for x = 0 into eqs. (5.30) and (5.32):

$$y_{2,\,max} = (-P/16EI_2\beta)(k_1/EI_1)[1/\lambda_1^{\,3} - 1/\lambda_2^{\,3}] \qquad (5.57)$$
$$M_{2,\,max} = (-P/8\beta)(k_1/EI_1)[1/\lambda_1 - 1/\lambda_2] \qquad (5.58)$$

If we substitute for x = 0 into eq. (5.33), we will see that the shear force in the concrete trough is zero under the wheel load application. This is because the concrete trough is

subjected to symmetrical line load about the wheel load action and the shear is always zero at the line of symmetry.

However, finding the position of maximum shear force in the concrete trough can be found by taking the first derivative of eq. (5.33) and making it equal to zero which after simplification results in:

$$\lambda_1 A_{\lambda 1} + \lambda_2 A_{\lambda 2} = 0 \tag{5.59}$$

It is clear that eq. (5.59) is highly nonlinear and of trigonometric form which cannot readily be solved analytically.

From eqs. (5.54) - (5.59) one can easily find out that the maximum deflection and bending moment both in the rail and the concrete trough and the shear force in the latter depend on the beam bending rigidities EI_1 and EI_2 and the foundation moduli k_1 and k_2 whereas the maximum shear in the rail is independent of the factors mentioned above and is always equal to half the wheel load when the track is subjected to single wheel load.

5.5 Computer Program MLBOEF

It has already been seen that the deflection, moment ...etc. of the track system were expressed by well defined mathematical expressions. However, these equations unfortunately involve a great deal of nonlinear trigonometric and exponential terms, which make the analytical solution rather tedious if it is carried out manually. Therefore, a simple computer program called MLBOEF was developed to process all the required calculations for solving analytically the LR55 track system modelled as multilayer beams on elastic foundations with speed and accuracy. The program MLBOEF was written in FORTRAN 77 for P.C. machines and its flow chart is presented in Fig. (5.2). The program was set to search for the maximum values of track responses and their locations. In addition, the program can take into account the effect of multiple axle loads with any difficulty. The computer processing time necessary for solving a typical problem of the LR55 track system by MLBOEF program has been found not to exceed a few seconds using a laptop computer having 486 DX2 microprocessor and 8 MB RAM.

5.6 Typical Example

In this example it is intended to visualise the general response of LR55 track system under the design wheel load P = 104.21 kN.

The rail moment of inertia about the x-axis is 377.328 cm^4, see Table (3.1). The Young's modulus of the rail is 200 kN/mm^2, see Table (3.2). Thus the bending rigidity of the rail EI_1 is 754.66 kN m^2 which is kept constant throughout the analysis. For an assumed concrete trough width of 400 mm and depth of 180 mm the moment of inertia about the x-axis, based on gross uncracked section is 13692.6 cm^4. Assuming the modulus of elasticity for the concrete of 20 kN/mm^2, then the bending rigidity of the concrete trough EI_2 will be 2738.52 kN m^2. The rail pad modulus k_1 is taken as 80 N/mm^2 and the assumed track base modulus k_2 is 30 N/mm^2.

The track responses in terms of deflection, bending moment and shear for both the rail and the concrete trough and the pressure on the rail pad and the track base are shown in Figs. (5.3) - (5.6). Due to symmetry only half of each graph is plotted. From these figures the following points emerge:

1. The effect of the wheel load is local and all the curves diminish very quickly (exponentially) as one moves away from the load application.
2. The maximum deflection of the rail is 3.338 mm and that of the concrete trough is 1.955 mm. At a distance of approximately 2.0 m away from the load application, an upward deflection will start to take place in the rail and the concrete trough respectively. However, the reverse maximum deflections are negligible as they are -0.103 and -0.097 mm for the rail and the concrete trough respectively. Both are occurred at a distance 2.6 m from the point load, Fig. (5.3).
3. The maximum sagging moment in the rail is 13.422 kN m and that of the concrete trough is 8.909 kN m, and occurred directly under the wheel load. There are some hogging moments in the track, but only over a short distance with a maximum value of -2.037 kN m in the rail and -3.433 kN m in the concrete trough, Fig. (5.4).
4. The maximum shear in the rail is 52.105 kN which is half the wheel load and it is at the point of load application, Fig. (5.5). The maximum shear in the concrete trough is 14.791 kN which is only 14.2% of the wheel load. This might be

attributed to the property of elastomeric pad in distributing the concentrated load over a wide range of track length. The location of the maximum shear occurs approximately at 0.5 m away from the load application, Fig. (5.5). Interestingly to note that the bending moment in the concrete trough at this location is less than half it's maximum value as shown in Fig. (5.4). This is an advantage to be taken into consideration where both the maximum shear and moment are not acting on the same section.

5. The maximum downward pressure (compressive stress) on the rail pad is 670.62 kN/m^2 and the maximum uplift pressure (tensile stress) is -9.34 kN/m^2, Fig. (5.6). Elastomers such as Series Six or KC 330 can sustain compressive stress up to 5000 kN/m^2 without failure and have tensile strength in the range of 2800 - 4000 kN/m^2 as shown in Table (3.3). This means that the stresses in the rail pad, induced by a wheel load of 104.21 kN, can be safely resisted by the pad material.
6. The maximum pressure on the track base is 146.61 kN/m^2, Fig. (5.6). Hay (1982) stated that a permissible pressure directly underneath a track system could be taken around 450 kN/m^2. Hence, the maximum pressure produced by 104.21 kN wheel load is within the permissible range.

5.7 Parametric Study

In order to investigate the sensitivity of LR55 track system responses to the main factors influencing the design of the track system, an extensive parametric study was performed using the analytical method adopted for the track system. The major parameters are the pad modulus, base modulus and axle load spacing as presented in Table (5.2).

The data which were kept constant throughout the analysis are:

1. The bending rigidity of the rail $EI_1 = 754.66$ kN m^2
2. The bending rigidity of the concrete trough $EI_2 = 2738.52$ kN m^2 as assumed in the typical example solved previously in section 5.6.
3. The magnitude of the wheel load P = 104.21 kN

The track responses of major interest are:

1. The maximum deflection of the rail and the concrete trough

2. The maximum bending moment of the rail and the concrete trough
3. The maximum shear of the rail and the concrete trough
4. The maximum pressure on the rail pad and the track base directly underneath the concrete trough

5.7.1 Effect of Pad Modulus

The effect of pad modulus on the track responses due to single wheel load of 104.21 kN is shown in Figs. (5.7) - (5.10), assuming base modulus = 30 N/mm^2. From these figures the following points emerge:

1. The maximum deflection of the rail sharply decreases as the pad modulus increases from 20 to 60 N/mm^2, then decreases gradually (from 3.655 to 3.0 mm) as the pad modulus increase to a value of 120 N/mm^2. On the other hand, the maximum deflection of the concrete trough just slightly increases (from 1.798 to 1.986 mm, i.e. by 10%) as the pad modulus increases from 20 to 120 N/mm^2, i.e. by 600%, Fig. (5.7).
2. The maximum bending moment in the rail is 17.47 kN m when the pad modulus is 20 N/mm^2, and drops gradually to a value of 12.52 kN m when the pad modulus increase to 120 N/mm^2. For the concrete trough, the bending moment varies between 6.44 and 9.58 kN m as the pad modulus increases from 20 to 120 N/mm^2, Fig. (5.8). It shows here once again that changing the pad modulus by 600% would only result in a change of maximum bending moment by no more than 30%.
3. The maximum shear force in the concrete increases from 9.34 to 16.22 kN, i.e. by 42%, as the pad modulus increases from 20 to 120 N/mm^2, i.e. by 600%, Fig. (5.9). It is interesting to note that even a maximum shear value of 16.22 kN is still about 15% of the applied wheel load of 104.21 kN. The maximum shear force in the rail remains constant at a value of 52.105 kN (i.e. half design wheel load) irrespective of the pad modulus value, Fig. (5.9). This has already been proven by eq. (5.56), see section 5.4.1.
4. The maximum pressure on the rail pad gradually increases from 487.2 to 736 kN/m^2, i.e. by 34% when the pad modulus is increased by 600%, i.e. from 20 to 120 N/mm^2. The maximum track base pressure shows insignificant change (134.5 to 149 kN/m^2, i.e., by 10%) as the pad modulus increases from 20 to 120 N/mm^2, Fig. (5.10).

5. The points discussed above reveal that over a wide range of the pad modulus, there are small changes in the track responses in terms of maximum deflection, bending moment, shear and pressure. This is because the pad modulus k_1 occurs in eqs. (5.44) - (5.49) as a fourth root. This leads to an interesting conclusion which is that any error in the assumed value of the pad modulus will introduce only a much smaller error in the magnitude of the track response values. This outcome justifies the approximate derivation of the pad modulus described previously in section 5.3.2.

5.7.2 Effect of Base Modulus

The effect of base modulus on the track responses due to single wheel load of 104.21 kN is shown in Figs. (5.11) - (5.14), assuming pad modulus = 80 N/mm^2. From these figures the following points might be observed:

1. The maximum deflections both of the rail and the concrete trough are inversely proportional to the base modulus value, starting with a sharp reduction and very soon (above base modulus 20 N/mm^2), the decrease becomes more gentle. For base modulus less than 10 N/mm^2, i.e. soft base, the maximum deflection of the track is relatively high (more than 6 and 4.7 mm for the rail and concrete respectively). However, for base modulus greater than 20 N/mm^2 the maximum deflection is not greater than 4 mm which is quite acceptable as shown in Fig. (5.11), (Sperring 1992, Cope 1993). This means a soft base of modulus less than 20 N/mm^2 should be avoided in practice in order to prevent excessive settlement of the track system.
2. As the base modulus increases from 5 to 60 N/mm^2, the maximum bending moment in the rail and the concrete trough decreases, however, the concrete moment is more sensitive to base modulus variation in comparison with the rail moment. This is because the concrete trough is directly supported by the base while the rail is distant from the base by two load absorbing layers (the pad and the concrete trough). Changing the base modulus by 300%, i.e. from 20 to 60 N/mm^2, will cause a small change in the track moment. For instance, the rail moment changes by 8%, i.e. from 13.86 to 12.812 kN m, and the concrete moment by 40%, i.e., from 10.6 to 6.47 kN m, Fig. (5.12).

3. The maximum shear force in the concrete is about 22 kN and occurs when the base is soft, i.e. base modulus ≤ 10 N/mm^2 and drops to a value of 12 kN when the base is firm. This means that the shear variation is about 45% as the base modulus changes by 300%, Fig. (5.13). The maximum shear force in the rail has a constant value of 52.105 kN for the whole range of the base modulus, Fig. (5.13). This is because the maximum shear force of the rail is independent of the base modulus as shown in eq. (5.56), see section 5.4.1.
4. The maximum pressure on the rail pad and the track base are directly proportional to the base modulus. The pad pressure gradually increases from 647.72 to 680.04 kN/m^2, i.e. by 5%, whereas the base pressure increases with higher rate from 98.4 to 168.2 kN/m^2, i.e. 40% as the base modulus increases from 5 to 60 N/mm^2, i.e. 1200%, Fig. (5.14). It is to be noted that the highest recorded values of maximum pressure of the pad (680.04 kN/m^2) and the base (168.2 kN/m^2) are still within the allowable limits as presented in section 5.6 above.
5. Similar to the point observed with the case of pad modulus effect on the track responses, one can see that large changes in the base modulus, i.e. by as much as 300%, will cause small changes in the track responses in terms of maximum deflection, bending moment, shear and pressure. This might be attributed to the fact that the base modulus k_2 occur in eqs. (5.44) - (5.49) as a fourth root. Hence, any error in the assumed value of the base modulus will result in only a much smaller error in the magnitude of the track response values. Once again, this conclusion justifies the use of an approximate assumed value of the base modulus without affecting the results appreciably.

5.7.3 Effect of Axle Load Spacing

The effect of axle load spacing on the track responses is presented in Figs. (5.15) - (5.18), assuming pad modulus = 80 N/mm^2 and base modulus = 30 N/mm^2. From these figures the following points are reported:

1. The variation in the maximum deflection of the track system changes very slightly (between 4.015 - 3.235 mm for the rail, and 2.912 - 1.858 mm for the concrete trough) for the case of two wheel loads as compared with the single wheel load case (3.338 mm for the rail, and 1.955 mm for the concrete trough). For axle load spacing around 2.0 m, the maximum deflection both in the rail and the concrete

due to two wheel loads is almost the same as the case for single wheel load, Fig. (5.15).

2. For axle load spacing up to 2.6 m, the maximum bending moments in the rail and the concrete trough are less than those for a single wheel load case. This is due to the hogging moment produced by one wheel that will counteract the effect of the sagging moment produced by the other wheel, Fig. (5.16).
3. The maximum shear in the rail is almost insensitive to the axle load spacing as it varies by only 3% for the range of axle load between 1.2 and 2.6 m. The maximum shear in the concrete shows a change of ± 14% when the axle spacing increases from 1.2 to 2.6 m as compared with single wheel load effect. For axle load spacing around 2.0 m, the maximum shear of the concrete trough due to two wheel loads is almost the same as the case for the single wheel load, Fig. (5.17).
4. The variation of the maximum pressure on the rail pad is almost insensitive (changes by no more than ± 1.5%) to the axle load spacing. On the other hand, the maximum pressure on the track base tends to decrease gradually as the axle spacing increases. At an axle load spacing around 2.0 m the maximum base pressure becomes the same as that for the single wheel load case, Fig. (5.18).
5. The effect of the multiple axle loads on the track responses seems to be almost negligible as the axle spacing exceeds 2.0 m. This is due to the fact that the variation of the deflection, bending moment, shear force and the pressure distribution are only concentrated around the region where the loads is applied and they rapidly die out away from the load application. More interestingly, at an axle load spacing around 2.0 m the maximum values of track responses are almost the same as those for the single wheel load case. Since modern rail vehicles such as the ones used on the Manchester Metrolink have smaller axle load spacing around 2.0 m, therefore, studying the behaviour of the track system under single wheel load may be considered sufficient and acceptable without sacrificing the accuracy of the result.

5.8 Summary and Conclusion

A mathematical model was developed for the LR55 track system as multilayer beams on elastic foundations. Following classical calculus method, an analytical solution was found

for the governing differential equation of the system, which is a coupled fourth order linear homogenous differential equation with constant coefficients. Accordingly, well defined mathematical expressions for the deflection, shear, bending moment and pressure distribution at any point along the track were derived. A simple computer program called MLBOEF was established to carry out the analysis with minimum required time and effort. The program is capable for finding the maximum values and locations of the track responses and the effect of multiple axle loads with high efficiency.

Several examples have been demonstrated to study the influence of important parameters such as pad and base modulus on the track behaviour under single and multiple axle loads.

Although the analytical approach may be regarded as a simple yet a powerful tool for investigating the track performance under the wheel load, it suffers from several drawbacks, namely:

1. The analytical method presumes that the track base is firmly attached to the track system. This means that nonlinearity due to track base separation (uplift) cannot be taken into account.
2. Variation of the soil properties along the track or the presence of a cavity under the track cannot be taken into consideration during the analysis.
3. The analytical method can only solve easily for the case of vertical point loads. This implies that any load combination such as vertical wheel load with horizontal braking load or with temperature effect cannot be incorporated.
4. The analytical method assumes the upper and lower beams to be continuous of infinite lengths. Actually, when the precast concrete trough units are connected together by simple joints, then hinges will exist at these connection points along the track. Such a case of track system arrangement cannot be tackled by the analytical method. Furthermore, a segment of a track system with an assumed boundary condition (fixed or simply supported) cannot be solved by the analytical method.

In order to overcome the drawbacks mentioned above a more sophisticated numerical technique should be employed such as finite element method. Such an approach will be discussed in the next chapter.

Table (5.1): Rail pad moduli corresponding to the Young's modulus.

Pad Young's modulus (E_p) (N/mm^2)	Rail pad modulus (k_1) (N/mm^2)
2.424	20
4.848	40
7.273	60
9.697	80
12.121	100
14.545	120

Table (5.2): Parameters and ranges considered in the study.

Parameter	Range
Pad modulus (N/mm^2)	20 - 120
Base modulus (N/mm^2)	5 - 60
Axle load spacing (m)	1.2 - 2.6

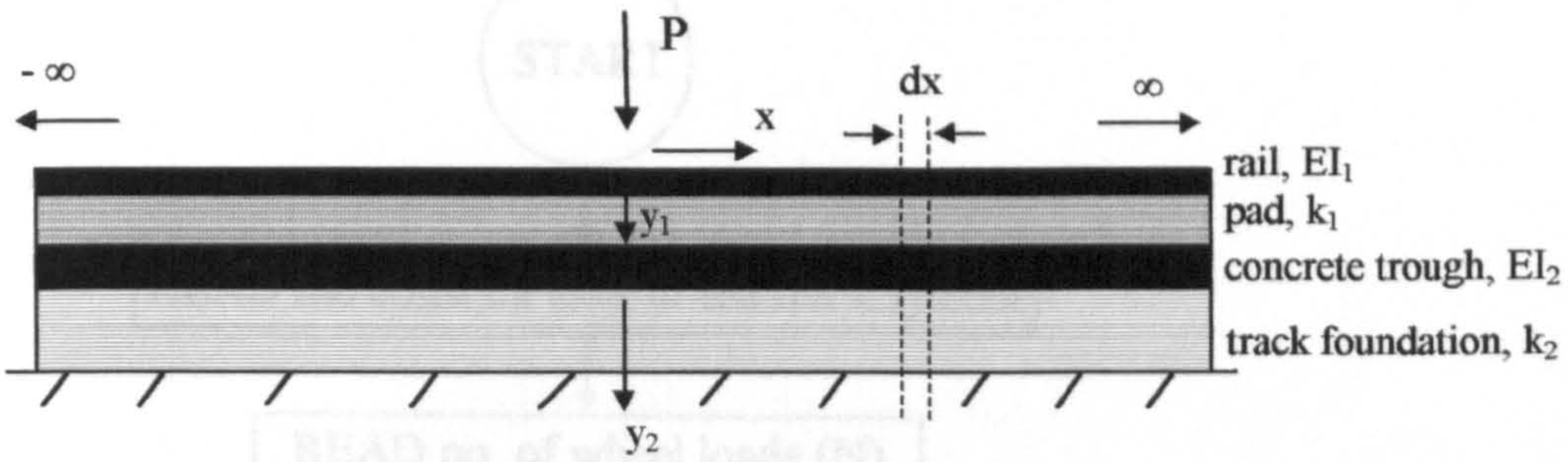

Fig. (5.1a): Longitudinal section of the LR55 track model.

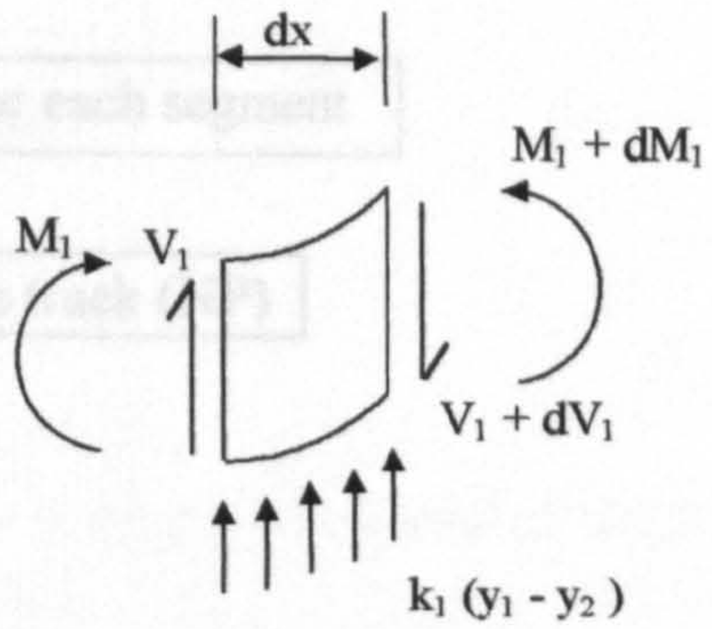

Fig. (5.1b): Infinitesimal element of the rail showing the forces acting on it.

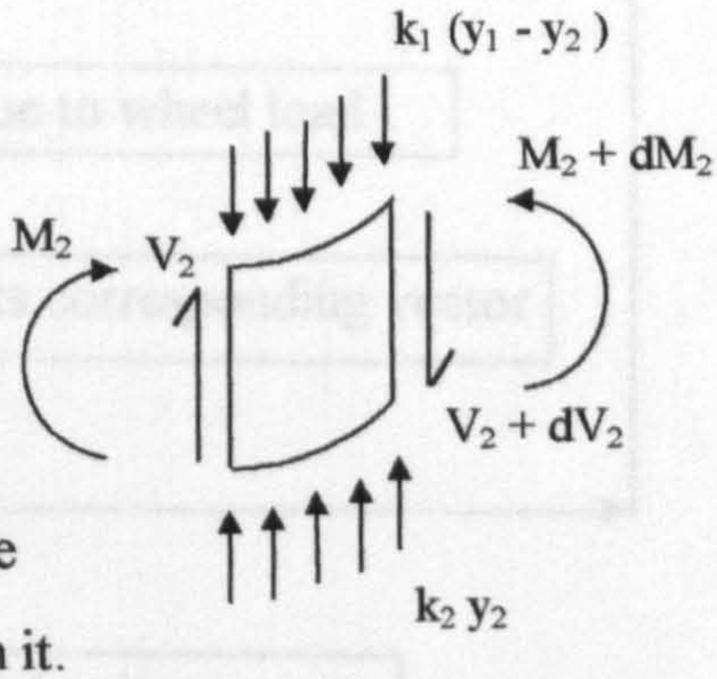

Fig. (5.1c): Infinitesimal element of the concrete trough showing the forces acting on it.

Fig. (5.1): Analytical solution of the mathematical model for the LR55 track system as multilayer beams on elastic foundations.

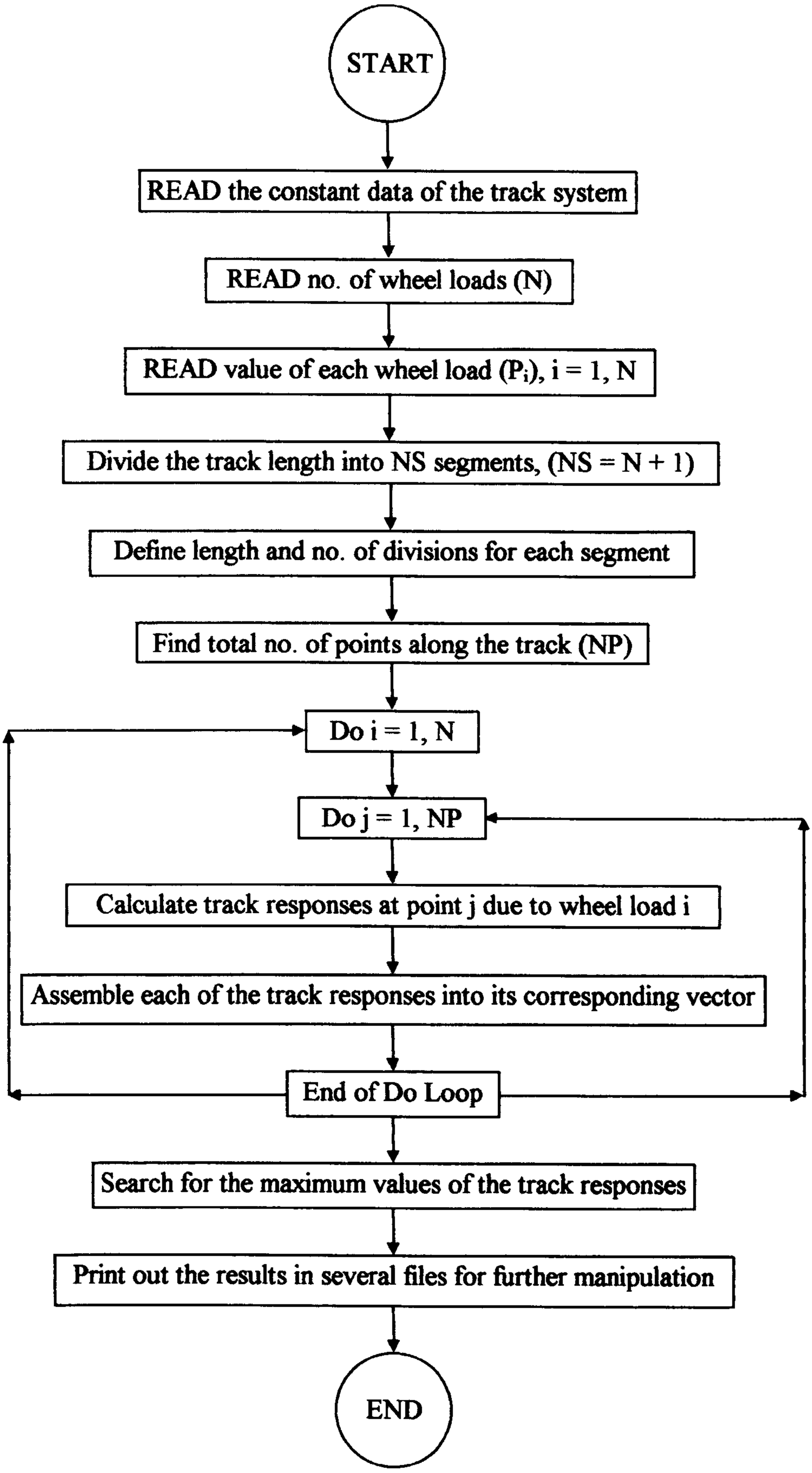

Fig. (5.2): Flow chart for the computer program MLBOEF.

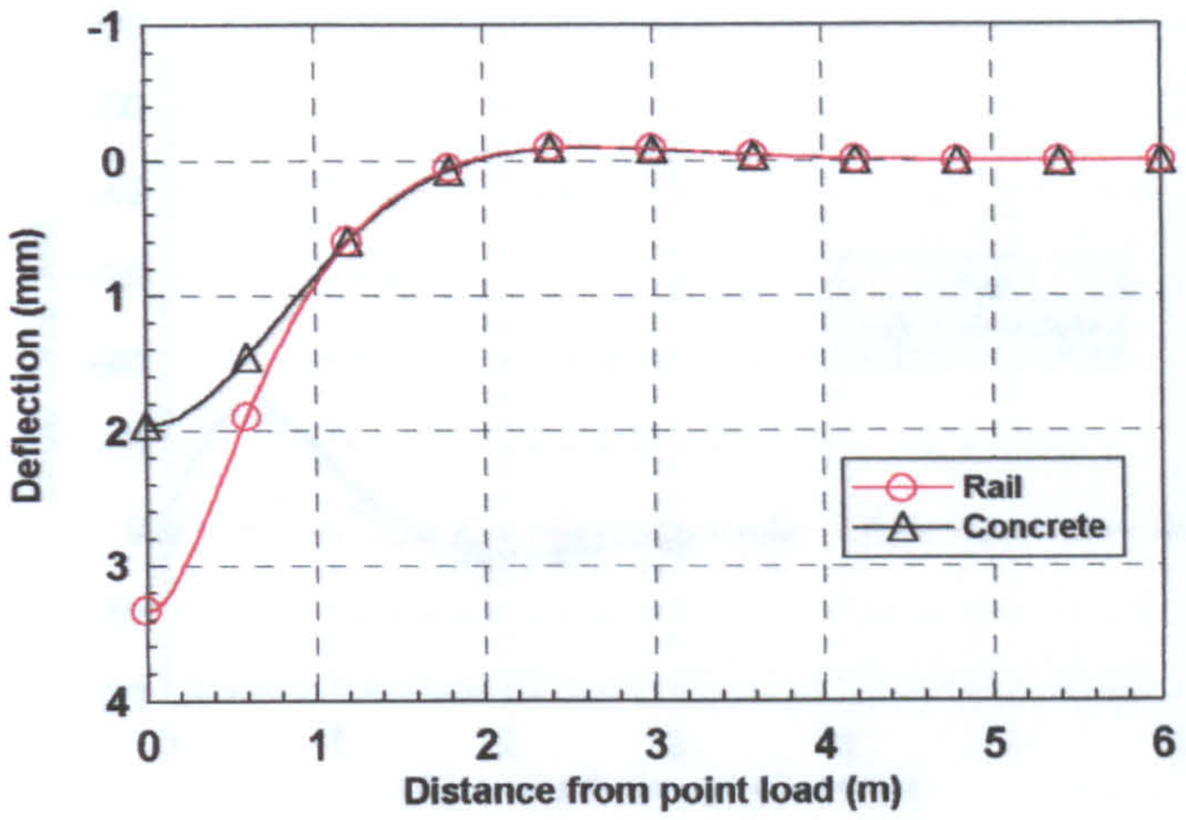

Fig. (5.3): Deflection of the track system due to single wheel load of 104.21 kN.

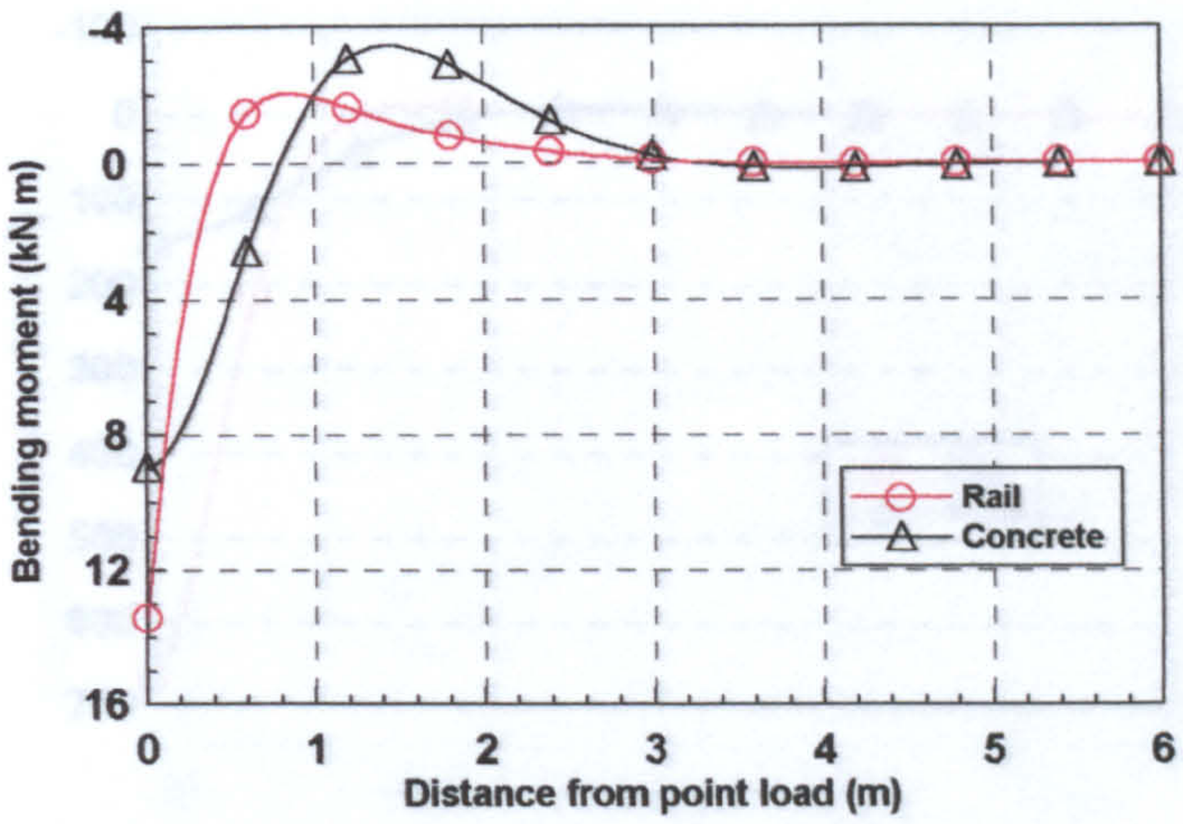

Fig. (5.4): Bending moment of the track system due to single wheel load of 104.21 kN.

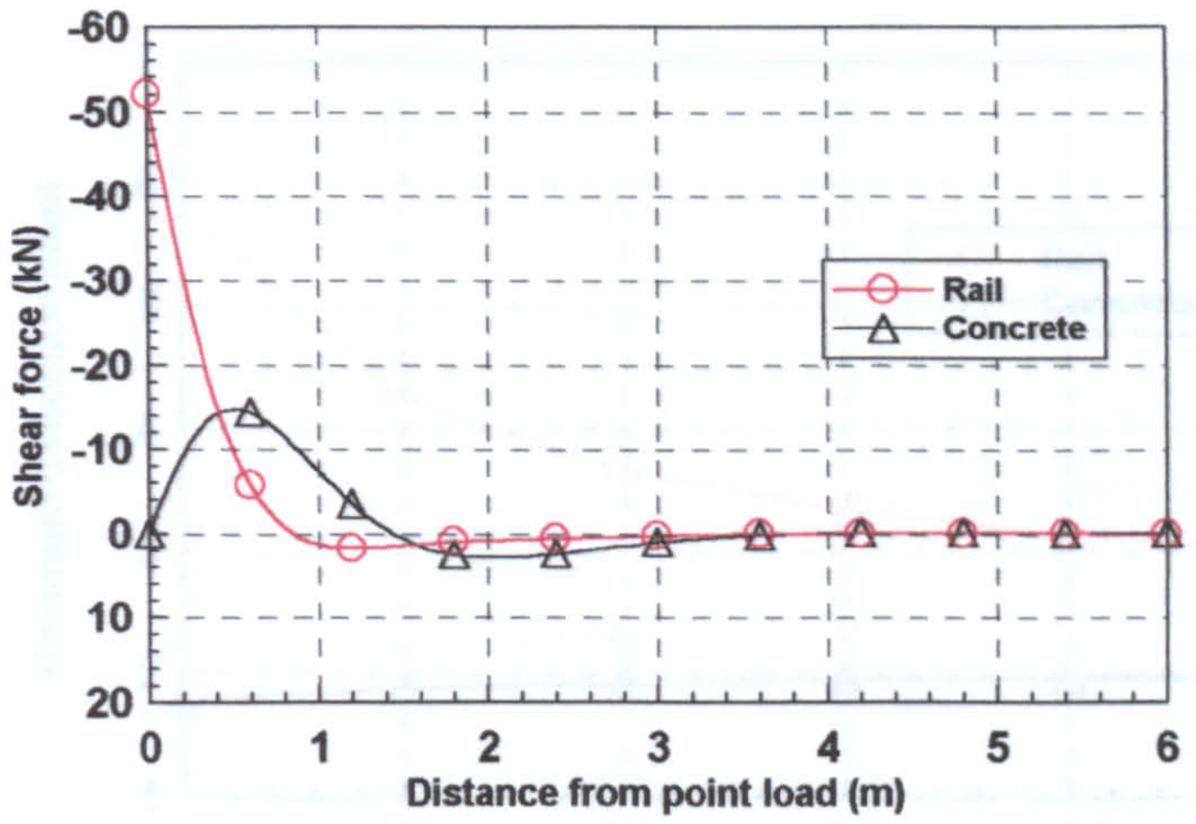

Fig. (5.5): Shear force of the track system due to single wheel load of 104.21 kN.

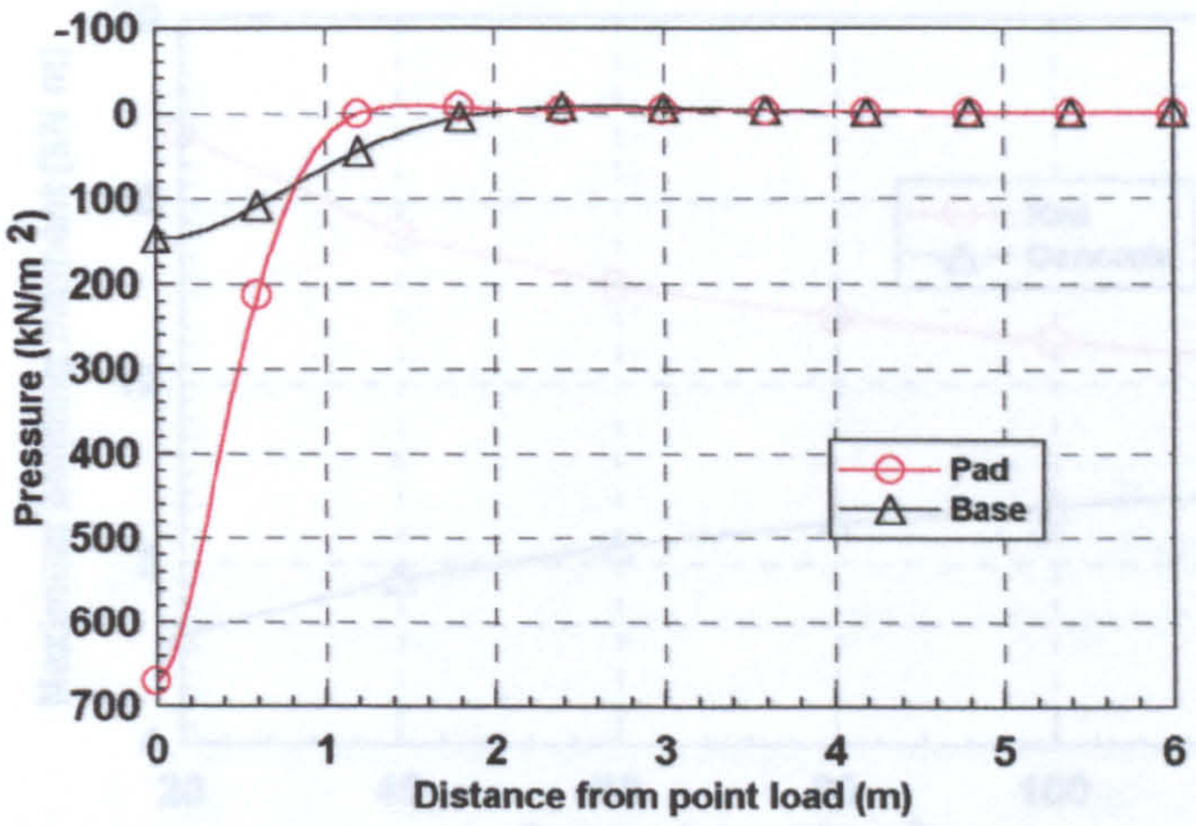

Fig. (5.6): Pressure distribution of the track system due to single wheel load of 104.21 kN.

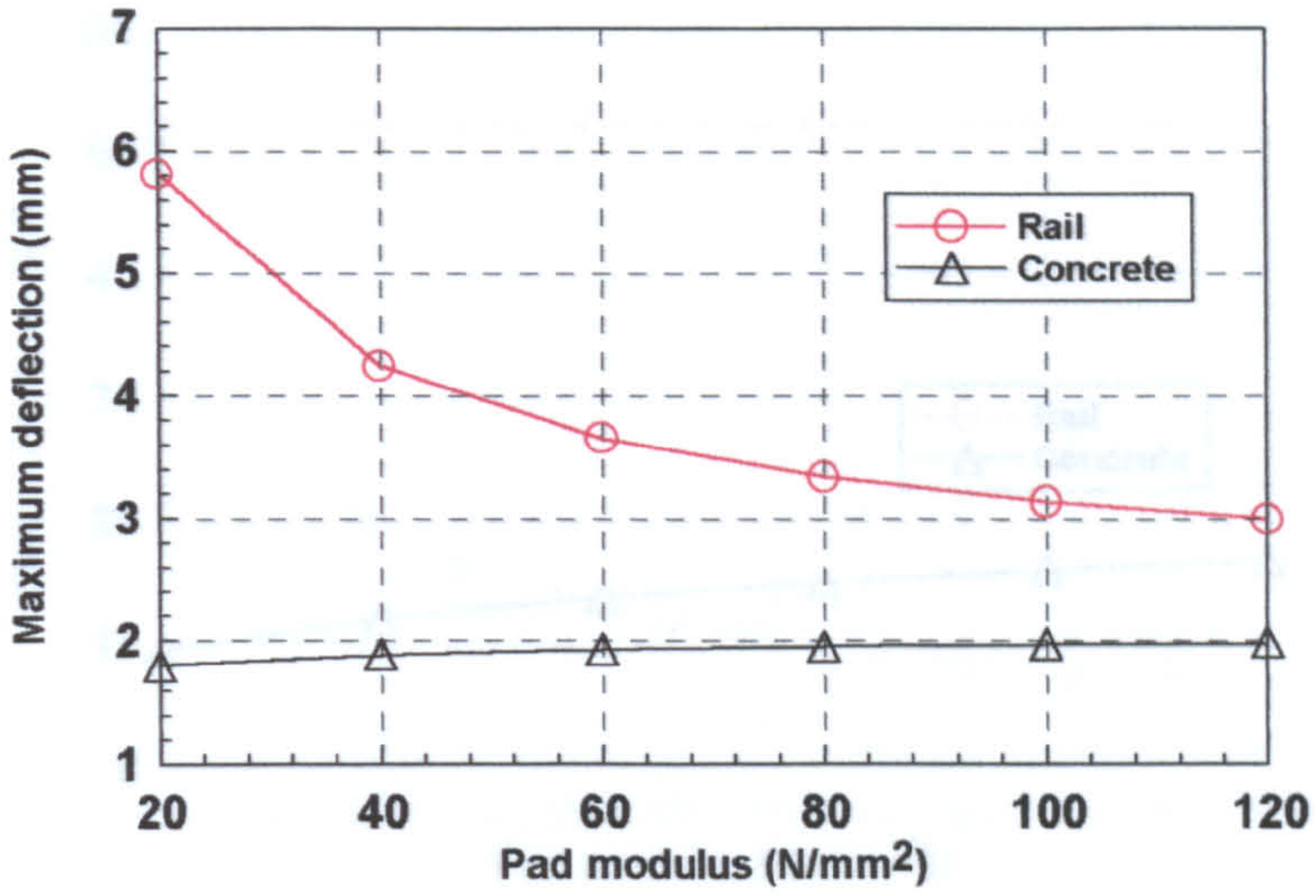

Fig. (5.7): Effect of pad modulus on the maximum deflection.

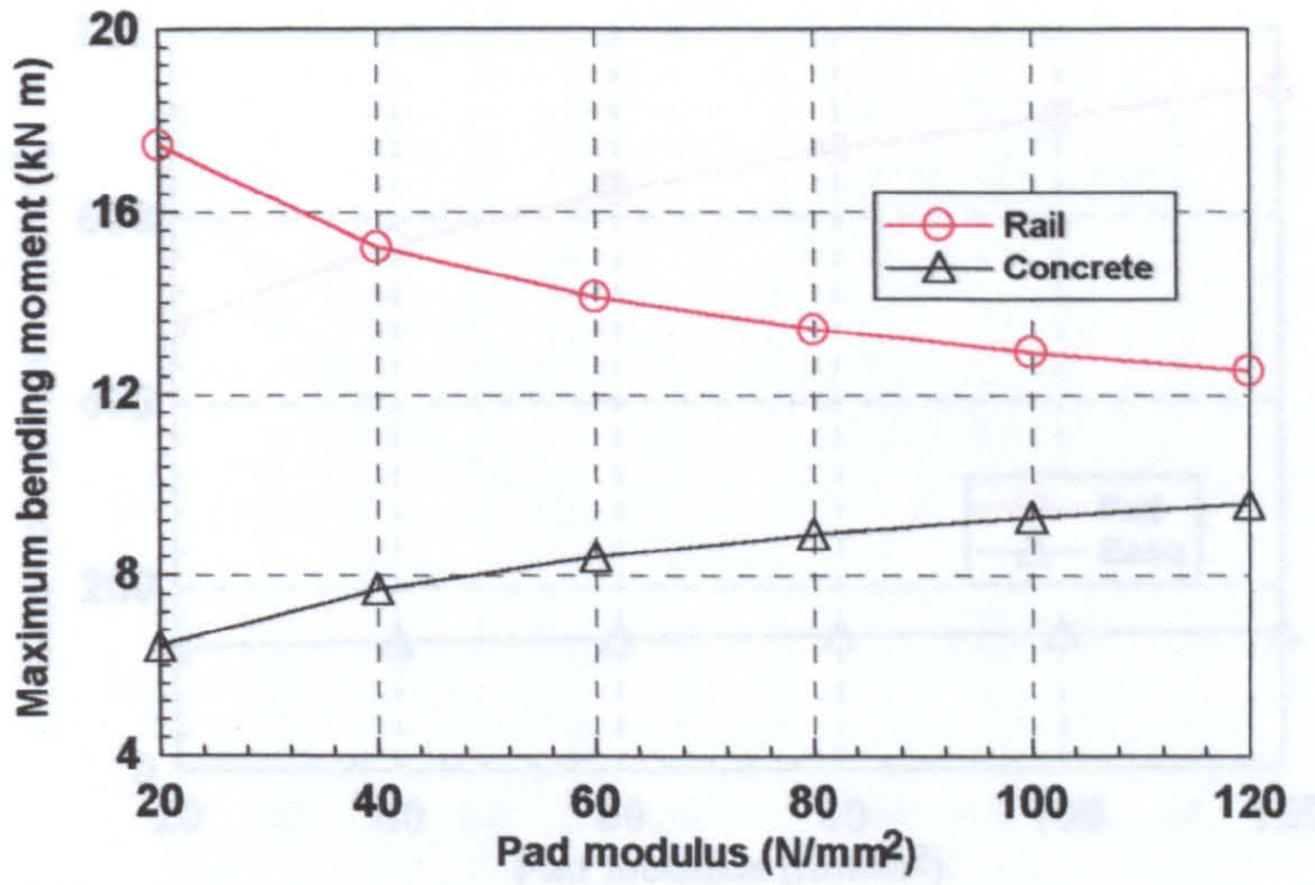

Fig. (5.8): Effect of pad modulus on the maximum bending moment.

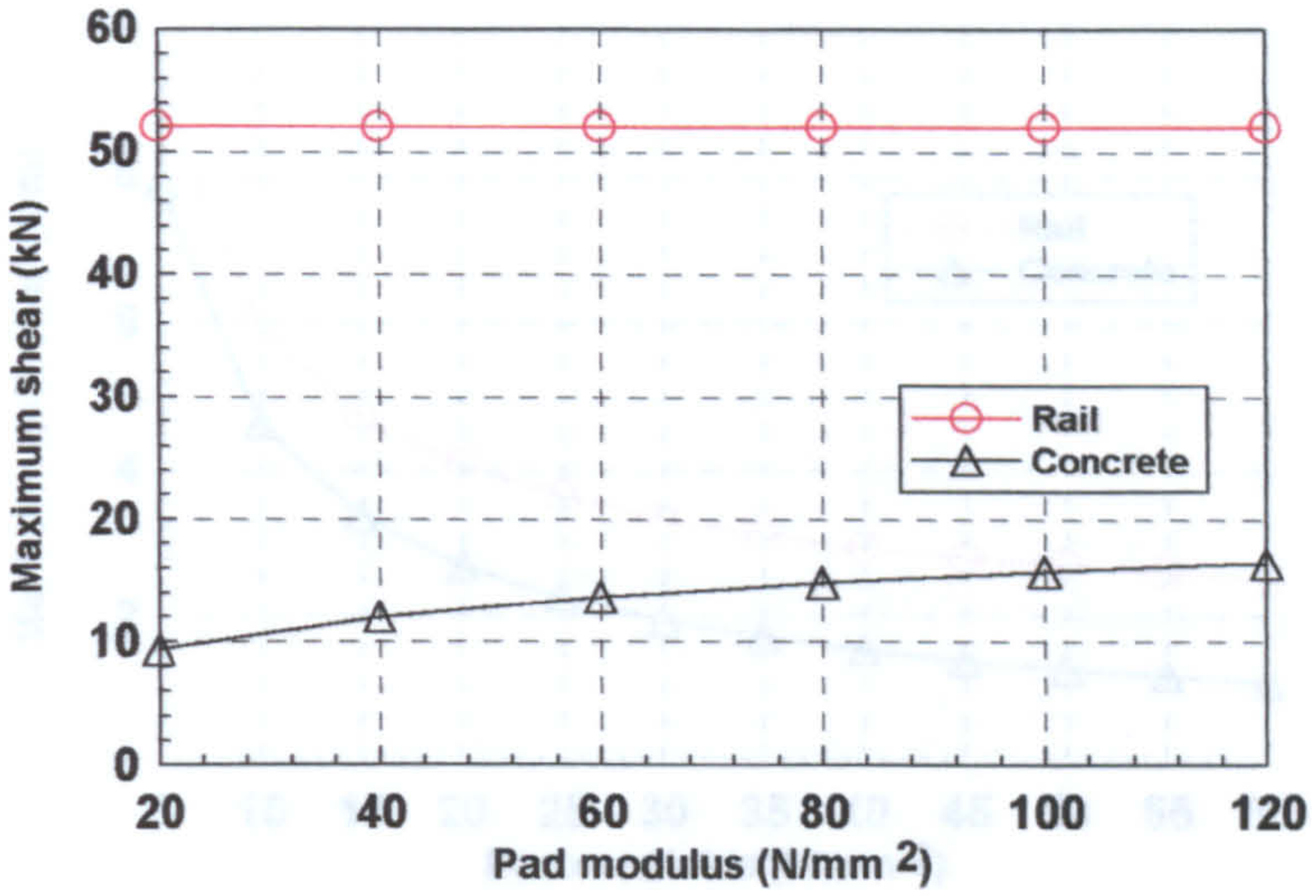

Fig. (5.9): Effect of pad modulus on the maximum shear force.

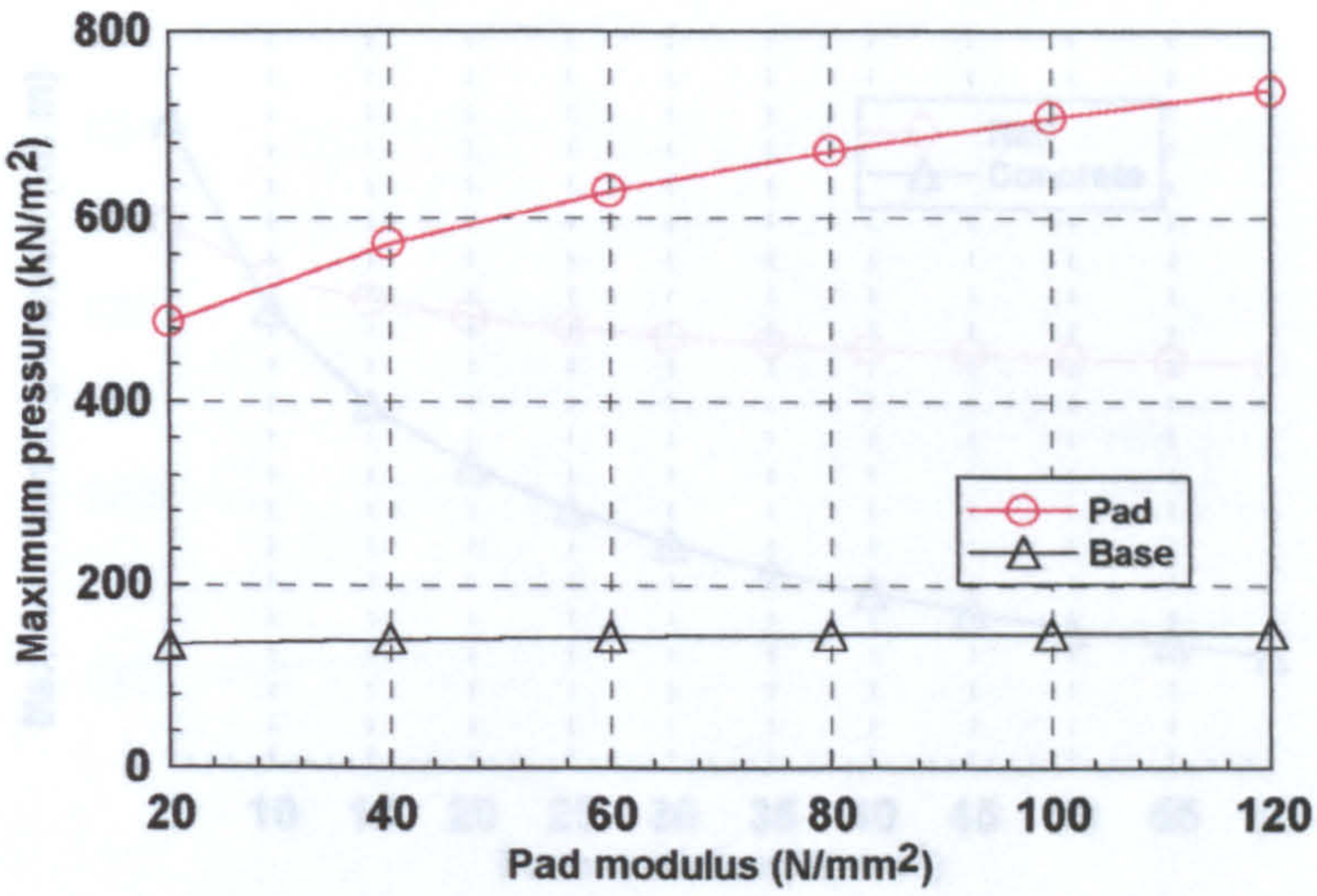

Fig. (5.10): Effect of pad modulus on the maximum pressure.

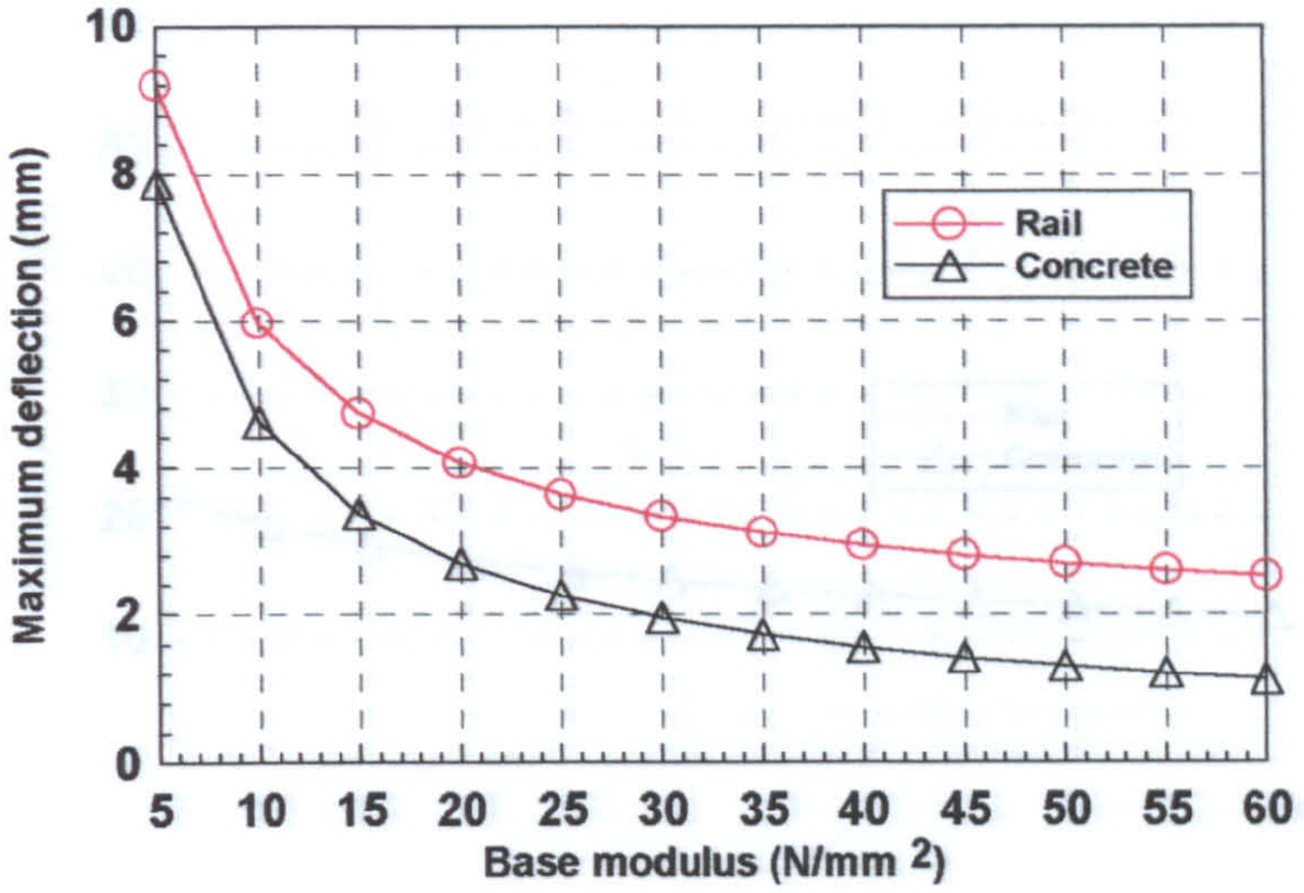

Fig. (5.11): Effect of base modulus on the maximum deflection.

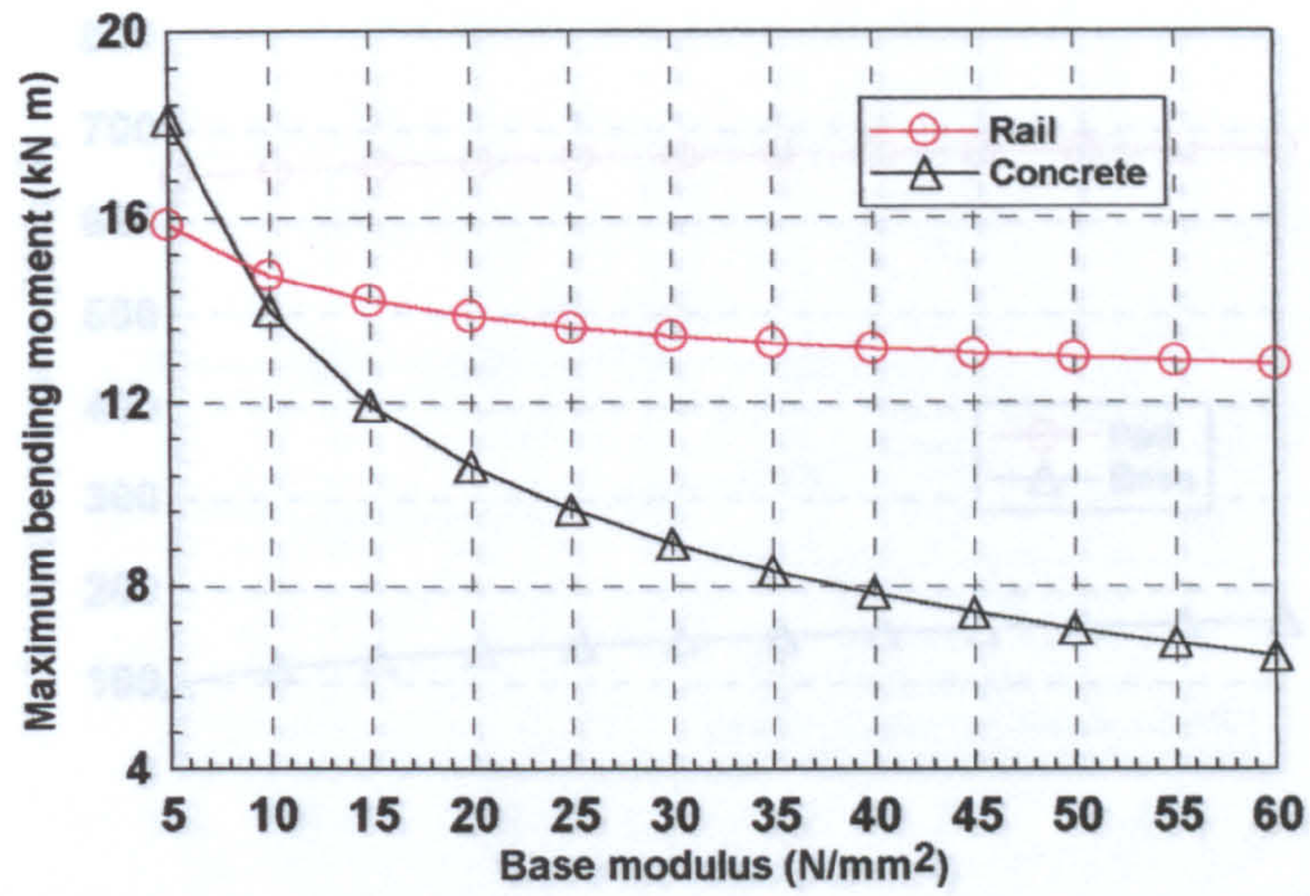

Fig. (5.12): Effect of base modulus on the maximum bending moment.

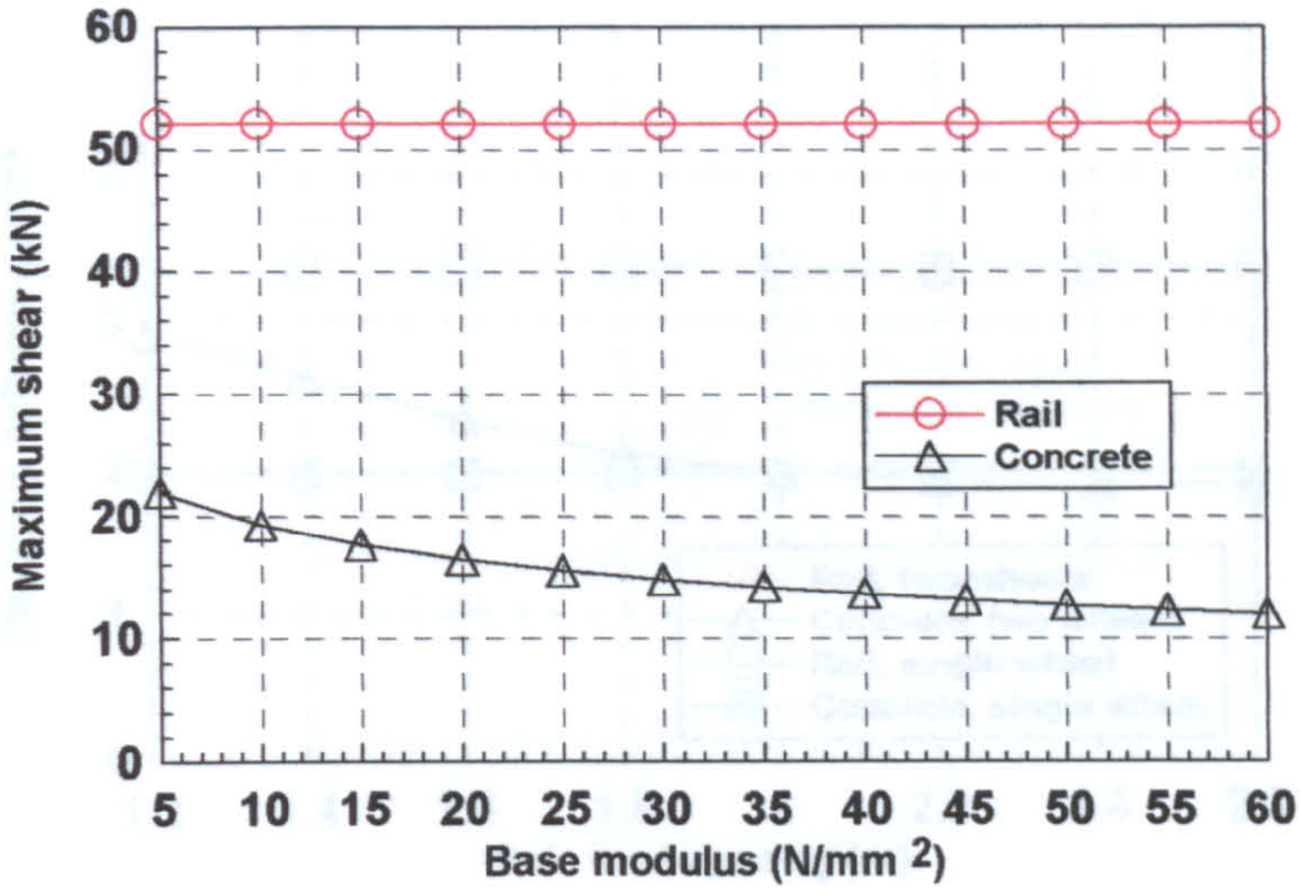

Fig. (5.13): Effect of base modulus on the maximum shear force.

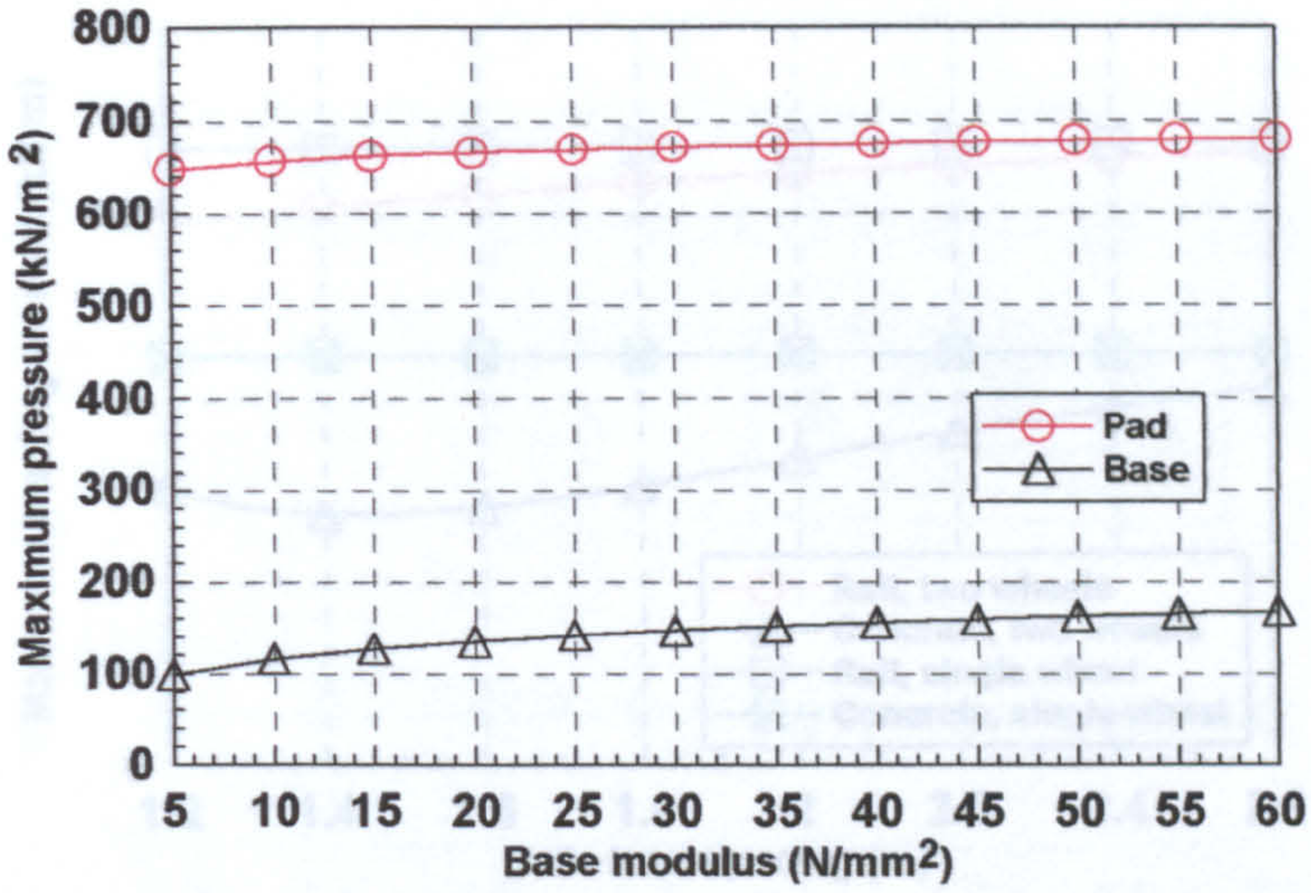

Fig. (5.14): Effect of base modulus on the maximum pressure.

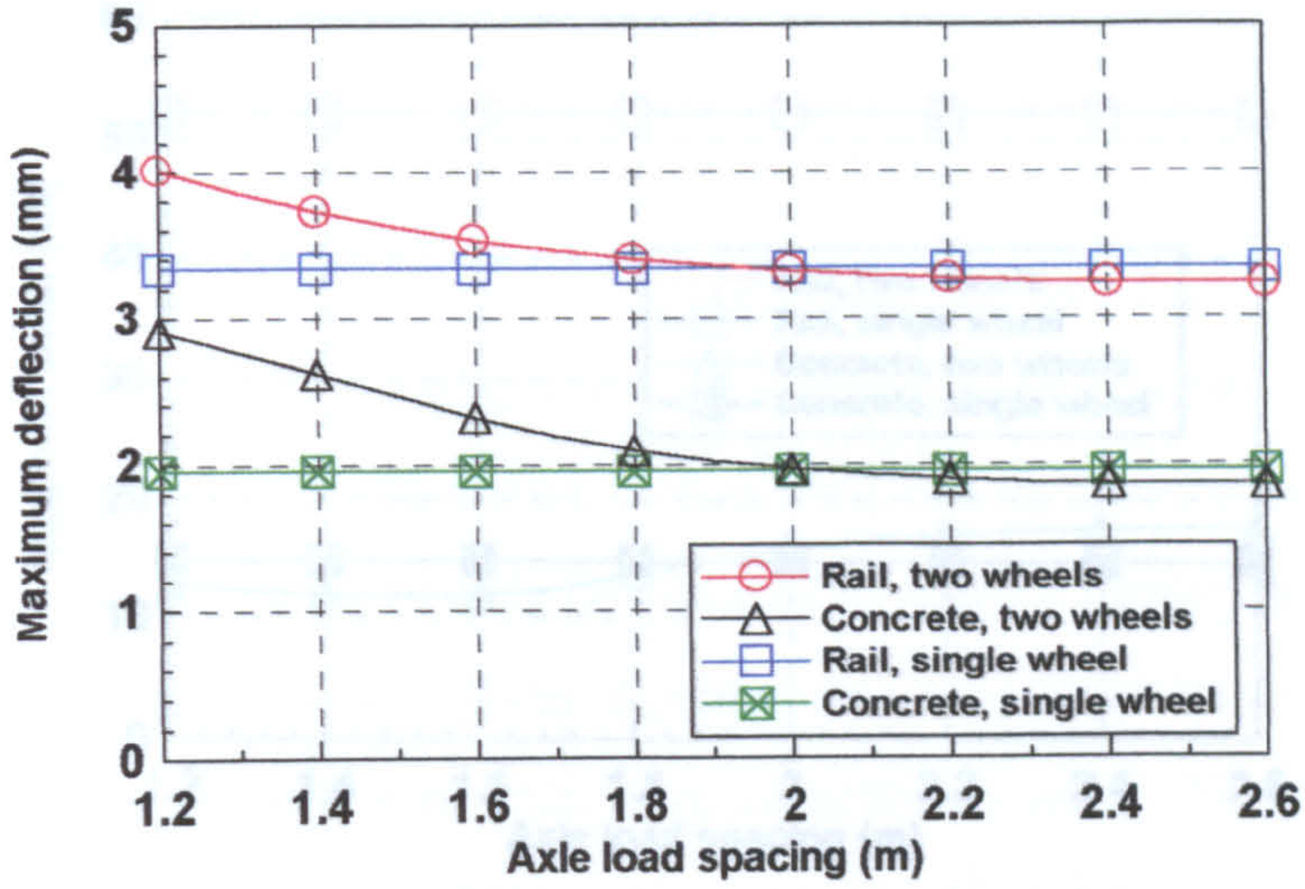

Fig. (5.15): Effect of axle load spacing on the maximum deflection.

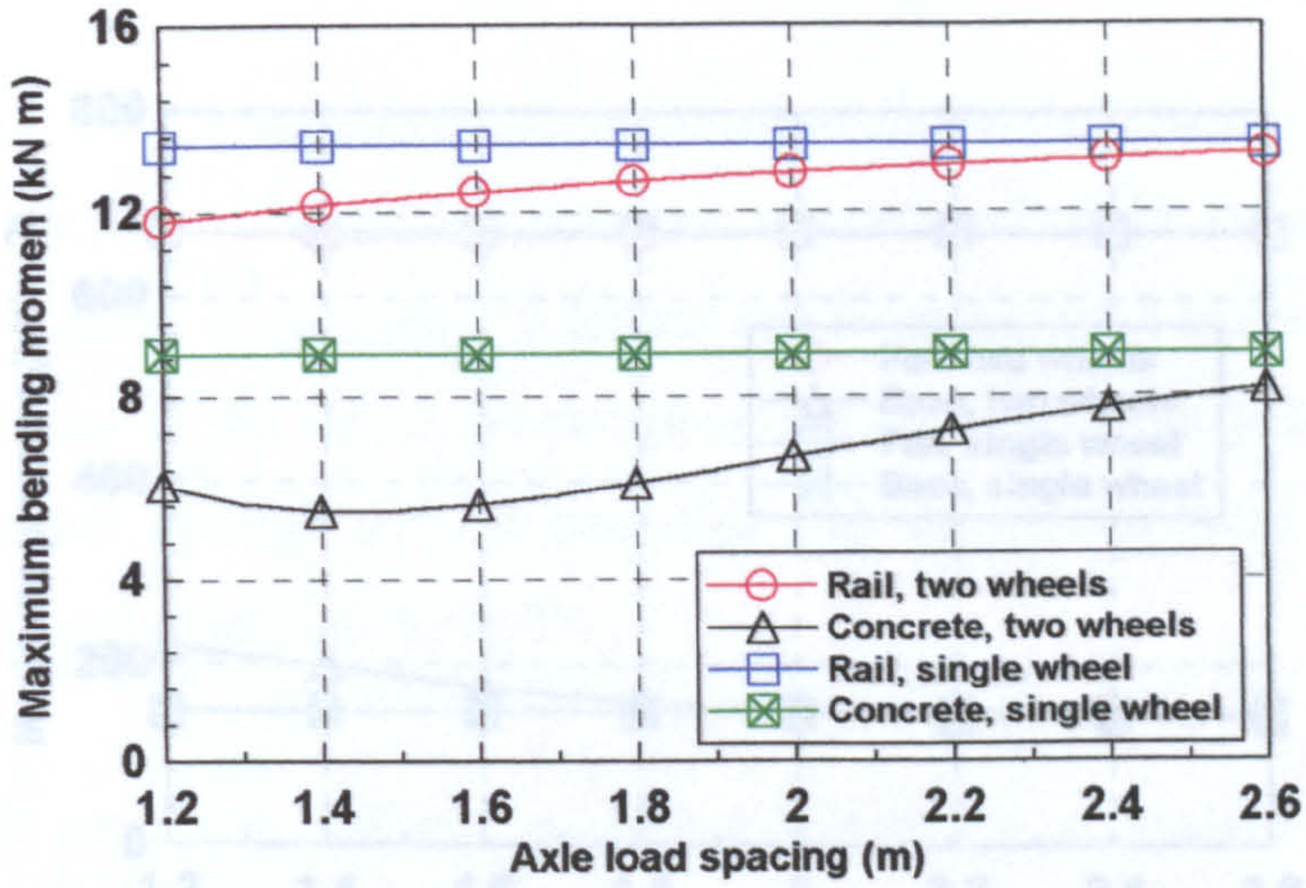

Fig. (5.16): Effect of axle load spacing on the maximum bending moment.

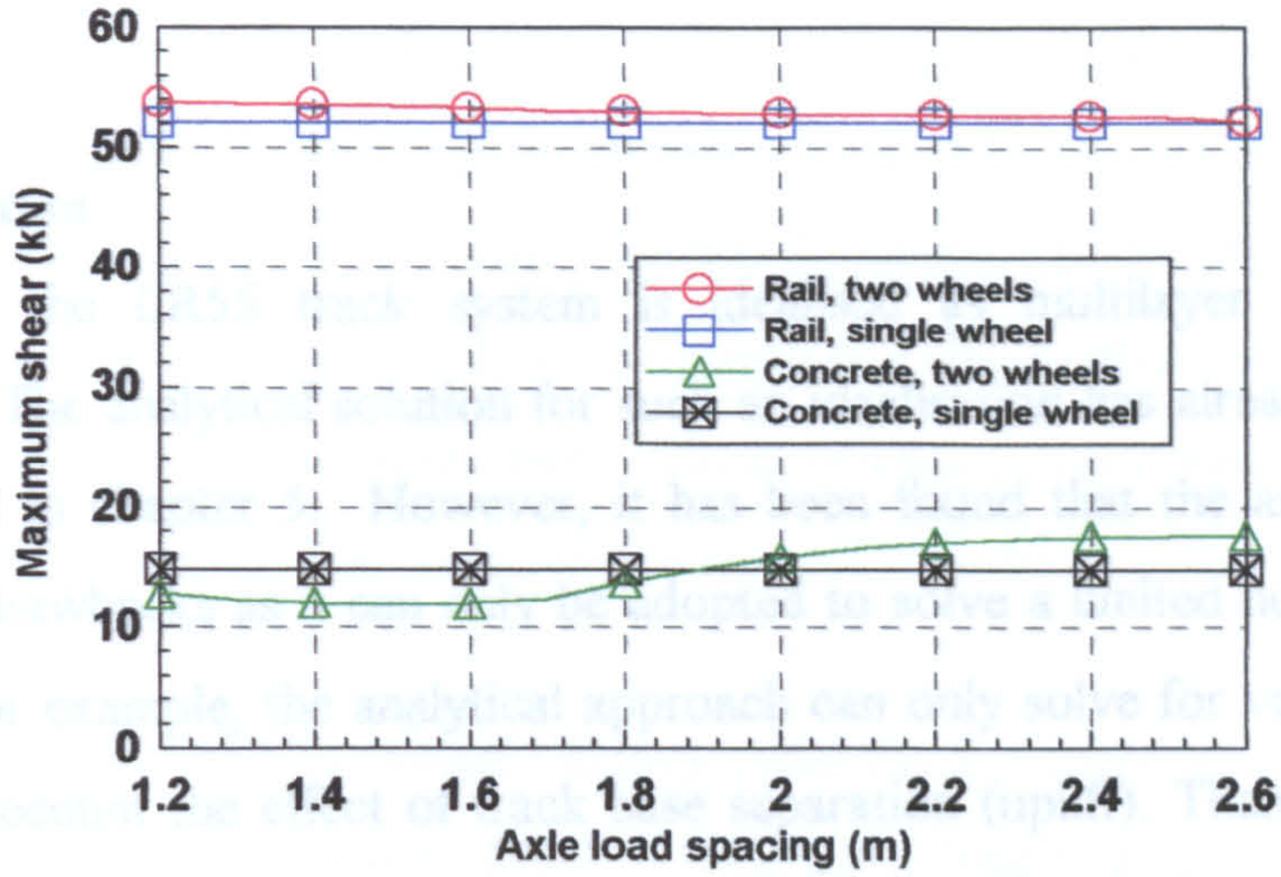

Fig. (5.17): Effect of axle load spacing on the maximum shear force.

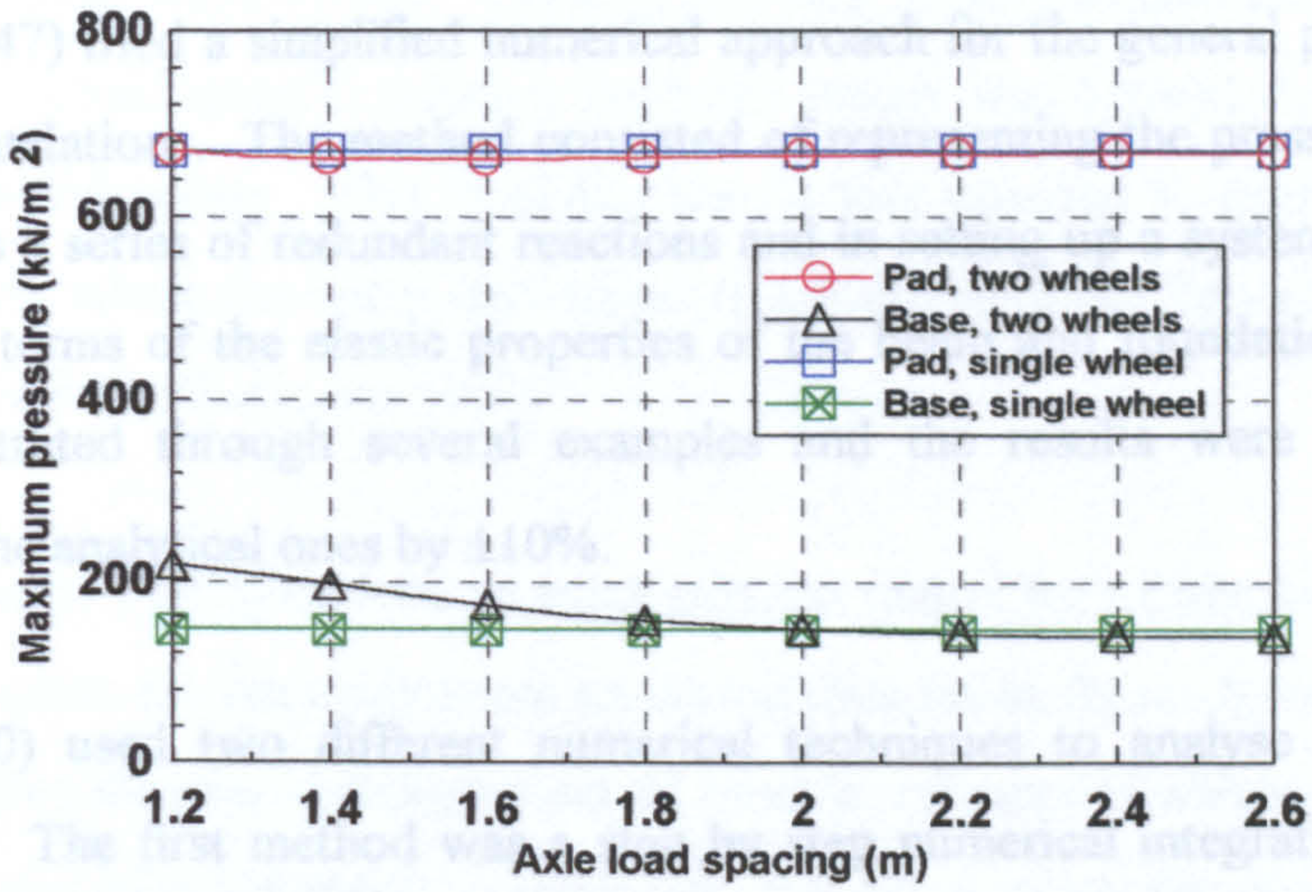

Fig. (5.18): Effect of axle load spacing on the maximum pressure.

CHAPTER SIX

MATHEMATICAL MODELLING OF THE LR55 TRACK SYSTEM: NUMERICAL SOLUTION

6.1 Introduction

Theoretically, the LR55 track system is idealised as multilayer beams on elastic foundations. The analytical solution for such an idealisation has already been explained and presented in chapter 5. However, it has been found that the analytical approach suffers from drawbacks as it can only be adopted to solve a limited number of the track problems. For example, the analytical approach can only solve for vertical loads and it cannot take account the effect of track base separation (uplift). Therefore, a numerical technique is required to solve the system for more general cases.

6.2 Review of Previous Work

Numerical approaches for the solution of beams on elastic foundations have been investigated by several researchers. Some of these prominent and studies are presented below.

Liventon (1947) tried a simplified numerical approach for the general problem of beams on elastic foundations. The method consisted of representing the pressure of the elastic foundation as a series of redundant reactions and in setting up a system of simultaneous equations in terms of the elastic properties of the beam and foundation. This method was demonstrated through several examples and the results were shown to be as accurate as the analytical ones by ±10%.

Malter (1960) used two different numerical techniques to analyse beams on elastic foundations. The first method was a step by step numerical integration process. The second was a finite difference method in which a series of simultaneous equations were solved. Both methods were proved to be general and converged rapidly, though the finite difference seemed to be less time consuming. Various examples were solved and

compared with other approximate as well as analytical methods showing satisfactory results.

Miranda and Nair (1966) followed the method of initial parameters to solve the problem of beam on elastic foundation. In this method, the differential equation of the system was expressed by four special functions that are associated with the deflection, slope, moment and shear. Such a derivation resulted in substantial simplification of boundary value problem. Later, Ting (1982) further extended this method of solution to include elastic end restraints that characterised various boundary conditions of finite beams on elastic foundations.

Harrison (1973) adopted the initial value method for the analysis of finite beam on an elastic foundation, which allowed for non-uniform beam cross-section, non-uniform foundation modulus and any type of loading. Al-Khaiat (1979) followed a similar approach of the initial value problem to develop approximate equations which easily predicted the response of the beams on elastic foundations in terms of deflection, bending moment and shear for various boundary and loading conditions. The effect of axial load was also incorporated in his derivation.

A stiffness approach FEM has been used as a numerical tool for the analysis of beams on elastic foundations since 1960's. Cheung and Nag (1966) treated the foundation as an isotropic elastic half space in which a flexibility matrix was derived due to step loads at appropriate nodal points. The flexibility matrix was inverted to obtain the foundation stiffness matrix where the latter was added to the conventional beam stiffness matrix to set up the element stiffness matrix.

Ting and Mockry (1985) derived an exact stiffness matrix for a finite beam element on an elastic foundation. Unlike other beam on elastic foundation finite elements, the degree of accuracy of this element is independent of element refinement which gives it a superior advantage over other elements. However, the expressions for the element stiffness matrix coefficients were mathematically quite complicated as they involved polynomial and hyperbolic terms.

Bowles (1988) formulated the stiffness matrix for a beam on an elastic foundation by combining a conventional beam element with discrete soil springs attached to the ends of the beam element. The main advantage of this formulation lies in its simplicity and the element is available in any standard finite element package. The only drawback of such a formulation is that the accuracy of the results is highly dependent on the number of elements for the discretised structure. However, such a limitation is no longer a problem with the advent of sophisticated computers with high memory and speed at relatively low cost.

Aydogan (1995) presented an exact formulation of stiffness matrix for a beam element with shear effect on an elastic foundation. He concluded that the shear effect becomes significant for a foundation with very high subgrade modulus (e.g. greater than 480 N/mm^2), and for a beam with small span to depth ratio (e.g. less than 3).

All the above mentioned studies dealt with the numerical solutions for a single layer beam on an elastic foundation. However, the LR55 track system is mathematically modelled as multilayer beams on elastic foundations as described in chapter 5. Therefore, a numerical approach that accounts for this particular model is adopted in this chapter. The proposed numerical method and the computer program LR551D developed for this purpose are discussed in detail below.

6.3 Basic Assumptions

The following assumptions are made for solving numerically the LR55 track system modelled as multilayer beams on elastic foundations:

1. All the materials forming the track system are homogeneous, isotropic and linear elastic.
2. The track is straight and level. This means that the effect of horizontal and vertical curvature of the track geometry is so small that it can be ignored.
3. The rail pad is replaced by a series of discrete vertical and horizontal springs of the Winkler type, (Dulacska 1992, Selvadurai 1979).
4. The track base is replaced by a series of discrete vertical and horizontal springs of the Winkler type.

5. Nonlinearity due to track base separation (uplift) is taken into consideration. This is achieved by assuming the track base vertical springs are capable of resisting compression only, since the soil cannot take any tension.

6.4 Derivation of Track Element Stiffness Matrix

In the analysis of a structure by FEM, the structure is considered to be an assembly of elements connected at a finite number of points referred to as joints or nodes. Using the stiffness approach for the solution of finite element problem, the nodal displacements are assumed to be the basic unknowns. The equations of nodal equilibrium may be expressed by means of the well known stiffness matrix equation, see for example (Przemieniecki 1968, Laursen 1979, Balfour 1986):

$$[K]\ \{\delta\} = \{P\} \tag{6.1}$$

where

[K] = global stiffness matrix of the structure

{δ} = displacement vector of the structure

{P} = applied load vector on the structure

Consider the LR55 track system modelled as multilayer beams on elastic foundations. In order to solve this model by FEM, a certain length of the track is taken and subdivided into a number of elements, each of length L_e. An individual track element is assumed to consist of a rail beam element, a concrete trough beam element, pad vertical and horizontal spring elements, and track base vertical and horizontal spring elements as shown in Fig. (6.1). To the author's knowledge, the suggested track element in the present work has not been proposed previously by any other workers.

6.4.1 Rail Beam Element

The rail beam element is treated as conventional beam element with two nodes per element. Consider the rail element with nodes j and *l* as shown in Fig. (6.1). Each node has three degrees of freedom, namely horizontal displacement (u), vertical displacement (v) and rotation about z-axis (θ). Therefore the stiffness matrix of such an element has order 6 x 6. The coefficients of the stiffness matrix of such an element is well

documented in the literature, see for example (Przemieniecki 1968, Balfour 1986). For sake of convenience they are listed below:

$$[K]_1 = \begin{array}{c} \begin{matrix} u_j & v_j & \theta_j & u_l & v_l & \theta_l \end{matrix} \\ \begin{bmatrix} S_1 & 0 & 0 & -S_1 & 0 & 0 \\ & S_2 & S_3 & 0 & -S_2 & S_3 \\ & & S_4 & 0 & -S_3 & S_5 \\ & \text{Symmetry} & & S_1 & 0 & 0 \\ & & & & S_2 & -S_3 \\ & & & & & S_4 \end{bmatrix} \end{array} \begin{matrix} u_j \\ v_j \\ \theta_j \\ u_l \\ v_l \\ \theta_l \end{matrix} \qquad (6.2)$$

where

$S_1 = E_1 A_1 / L_e$

$S_2 = 12E_1 I_1 / L_e^3$

$S_3 = 6E_1 I_1 / L_e^2$

$S_4 = 4E_1 I_1 / L_e$

$S_5 = 2E_1 I_1 / L_e$

A_1 = cross-sectional area of the rail section

I_1 = moment of inertia of the rail section

E_1 = Young's modulus of the rail material

L_e = length of the track element

6.4.2 Concrete Trough Beam Element

A concrete trough element is basically similar to the rail element presented above as it can be treated as a conventional beam element. Consider a concrete trough element with nodes i and k as shown in Fig. (6.1). If it happens that nodes i and k are rigid as is the case for an interior element, then the stiffness matrix of this element is exactly same as defined by eq. (6.2), except that the properties of the concrete trough section should be used instead of the rail, i.e.

$$[K]_2 = \begin{array}{c} \begin{matrix} u_i & v_i & \theta_i & u_k & v_k & \theta_k \end{matrix} \\ \begin{bmatrix} S_1 & 0 & 0 & -S_1 & 0 & 0 \\ & S_2 & S_3 & 0 & -S_2 & S_3 \\ & & S_4 & 0 & -S_3 & S_5 \\ & \text{Symmetry} & & S_1 & 0 & 0 \\ & & & & S_2 & -S_3 \\ & & & & & S_4 \end{bmatrix} \end{array} \begin{matrix} u_i \\ v_i \\ \theta_i \\ u_k \\ v_k \\ \theta_k \end{matrix} \qquad (6.3)$$

where

$S_1 = E_2 A_2 / L_e$

$S_2 = 12E_2 I_2 / L_e^3$

$S_3 = 6E_2 I_2 / L_e^2$

$S_4 = 4E_2 I_2 / L_e$

$S_5 = 2E_2 I_2 / L_e$

A_2 = cross-sectional area of the concrete trough section

I_2 = moment of inertia of the concrete trough section

E_2 = Young's modulus of the concrete

The concrete trough precast units are linked together along the track in practice by simple construction joints (hinges). This implies that such joints cannot take any moment, i.e. have no rotational stiffnesses. If it happens that a concrete trough element with its left end is any of these simple joints, i.e. node i is a hinge as shown in Fig. (6.1), then the stiffness matrix of such an element will be, (Balfour 1986):

$$[K]_2 = \begin{array}{c} \begin{matrix} u_i & v_i & \theta_i & u_k & v_k & \theta_k \end{matrix} \\ \begin{bmatrix} S_1 & 0 & 0 & -S_1 & 0 & 0 \\ & S_2 & 0 & 0 & -S_2 & S_3 \\ & & 0 & 0 & 0 & 0 \\ & \text{Symmetry} & & S_1 & 0 & 0 \\ & & & & S_2 & -S_3 \\ & & & & & S_4 \end{bmatrix} \end{array} \begin{matrix} u_i \\ v_i \\ \theta_i \\ u_k \\ v_k \\ \theta_k \end{matrix} \qquad (6.4)$$

where

$$S_1 = E_2 A_2 / L_e$$

$$S_2 = 3E_2 I_2 / L_e^3$$

$$S_3 = 3E_2 I_2 / L_e^2$$

$$S_4 = 3E_2 I_2 / L_e$$

Similarly, when the right end of the concrete trough element is one of these simple joints, i.e. node k is a hinge, see Fig. (6.1), then the stiffness matrix will be, (Balfour 1986):

$$[K]_2 = \begin{array}{c} \begin{matrix} u_i & v_i & \theta_i & u_k & v_k & \theta_k \end{matrix} \\ \begin{bmatrix} S_1 & 0 & 0 & -S_1 & 0 & 0 \\ & S_2 & S_3 & 0 & -S_2 & 0 \\ & & S_4 & 0 & -S_3 & 0 \\ & \text{Symmetry} & & S_1 & 0 & 0 \\ & & & & S_2 & 0 \\ & & & & & 0 \end{bmatrix} \end{array} \begin{matrix} u_i \\ v_i \\ \theta_i \\ u_k \\ v_k \\ \theta_k \end{matrix} \qquad (6.5)$$

where

$$S_1 = E_2 A_2 / L_e$$

$$S_2 = 3E_2 I_2 / L_e^3$$

$$S_3 = 3E_2 I_2 / L_e^2$$

$$S_4 = 3E_2 I_2 / L_e$$

6.4.3 Pad Vertical Spring Element

The vertical resistance of the pad is represented by a number of discrete vertical springs connected to the ends of the concrete and rail elements, for instance nodes i and j as shown in Fig. (6.1). Each spring has one degree of freedom per node which is the axial displacement. The stiffness of each spring K_{1v} may be defined as, (Gent 1992):

$$K_{1v} = E_p A_p / h_p \tag{6.6}$$

where

E_p = Young's modulus of the pad

A_p = contact area between the pad and the rail contributed by each spring

$= W_r L_e$

W_r = rail width

h_p = thickness of the pad

Since the two ends of the pad vertical spring element are free to displace then the stiffness matrix of such an element has order 2 x 2. Furthermore, as each spring is shared between two adjacent track elements, half spring stiffness has to be taken into consideration for an individual track element. Accordingly, the stiffness matrix of the pad vertical spring element will be:

$$[K]_{1v} = 0.5K_{1v} \begin{array}{c} \\ v_i \\ v_j \end{array} \begin{array}{c} \begin{array}{cc} v_i & v_j \end{array} \\ \begin{bmatrix} 1 & -1 \\ -1 & 1 \end{bmatrix} \end{array} \tag{6.7}$$

6.4.4 Pad Horizontal Spring Element

The horizontal resistance of the pad is represented by a number of discrete horizontal springs connected to the ends of the concrete and rail elements as shown in Fig. (6.1). Each spring has one degree of freedom per node which is the axial displacement. The stiffness of each spring K_{1h} may be defined as, (Gent 1992):

$$K_{1h} = G_p A_p / h_p \tag{6.8}$$

where

G_p = Shear modulus of the pad

Since the two ends of the pad vertical spring element are free to displace then the stiffness matrix of such an element has order 2 x 2. Furthermore, as each spring is shared between two adjacent track elements, half spring stiffness has to be taken into consideration for an individual track element. Accordingly, the stiffness matrix of the pad horizontal spring element will be:

$$[K]_{1h} = 0.5K_{1h} \begin{matrix} \\ u_i \\ u_j \end{matrix} \begin{matrix} \begin{matrix} u_i & u_j \end{matrix} \\ \begin{bmatrix} 1 & -1 \\ -1 & 1 \end{bmatrix} \end{matrix} \tag{6.9}$$

6.4.5 Track Base Vertical Spring Element

The vertical resistance of the track base is represented by a number of discrete vertical springs of a Winkler type. Each spring has one degree of freedom which is the axial displacement of the node. The stiffness of each spring K_{2v} is simply:

$$K_{2v} = k_2 L_e \tag{6.10}$$

where

k_2 = track base modulus

As one end of each base spring element is free to displace while the other is fixed to the ground, the stiffness matrix of this element has order 1 x 1, i.e. a single numeric value. Again, as each spring is shared between two adjacent track elements, half spring stiffness defined by eq. (6.10) has to be taken into consideration for an individual track element.

6.4.6 Track Base Horizontal Spring Element

The horizontal restraint provided by the track base can be characterised by a friction-slip (shear stress-relative displacement) relationship between the soffit of the concrete trough

and the supporting layers of the track formation. The slope of the friction-slip curve is termed as the modulus of horizontal reaction k_{sh}, (Uzan et al 1978). A suggested value of k_{sh} for a concrete foundation on a base of granular material (such as road base or ballast) is 0.15 N/mm^2/mm, (Lau et al 1994).

Similar to the track base vertical springs, the horizontal resistance of the base can be represented by a number of discrete horizontal springs of a Winkler type. Each spring has one degree of freedom which is the axial displacement of the node. The stiffness of each spring can be defined as, (Lau et al 1994):

$$K_{2h} = k_{sh} A_b \tag{6.11}$$

where

k_{sh} = modulus of horizontal (shear) reaction of the base

A_b = area of the base contributed by each spring

$= B L_e$

B = total width of the concrete trough section

As one end of each base spring element is free to displace while the other is fixed to the ground, the stiffness matrix of this element has order 1 x 1, i.e. a single numeric value. Again, as each spring is shared between two adjacent track elements, half spring stiffness defined by eq. (6.11) has to be taken into consideration for an individual track element.

6.4.7 Assemblage of Stiffness Matrices

Once the stiffness matrices for each component of a track element are established, they can be assembled in a single matrix to represent the stiffness matrix of an individual track element.

The stiffness matrix for an interior track element where all the four nodes i, j, k and *l* are rigid, may be set up by assembling the stiffness matrices defined by eqs. (6.2), (6.3), (6.7), (6.9), (6.10) and (6.11), see Fig. (6.2).

Similarly, the stiffness matrix for a track element with node i hinged can be formed by combining eqs. (6.2), (6.4), (6.7), (6.9), (6.10) and (6.11) as shown in Fig. (6.3).

In a similar manner, the assemblage of eqs. (6.2), (6.5), (6.7), (6.9), (6.10) and (6.11) will produce the stiffness matrix for a track element with node k hinged, see Fig. (6.4).

6.5 Load Vector

The load vector {P} defined in eq. (6.1) represents a set of point loads applied at the nodes of the discretised mesh for the structural system. The types of load that are incorporated in the one dimensional finite element model for the LR55 track system adopted in the present work, are summarised in the following sections.

6.5.1 Wheel Loads

Wheel loads could be vertical due to self weight of the train and/or horizontal due to traction or braking of the train vehicles. These loads are assumed to act as concentrated loads at any nodal points of the discretised mesh of the track system.

6.5.2 Track Self Weight

Track self weight refers to the weight of the rail and the concrete trough per unit length of the track system. These loads are assumed to act as uniformly distributed loads. In FEM, a uniformly distributed load acting on an element should be replaced by equivalent joint loads by using the concept of fixed end forces. This concept is presented in most structural analysis textbooks, see for example (Przemieniecki 1968, Balfour, 1986).

For a beam element with both ends rigid, the fixed ends forces due to a uniformly distributed load w, can be written as, (Balfour 1986):

$$V_L = V_R = wL/2 \tag{6.12}$$

$$M_L = -M_R = wL^2/12 \tag{6.13}$$

where

V_L = Shear force at the left end of the element

V_R = Shear force at the right end of the element

M_L = Bending moment at the left end of the element

M_R = Bending moment at the right end of the element

For a beam element with the left end hinged, the fixed end forces due to a uniformly distributed load w, can be written as, (Balfour 1986):

$$V_L = 3wL/8 \tag{6.14}$$

$$V_R = 5wL/8 \tag{6.15}$$

$$M_L = 0 \tag{6.16}$$

$$M_R = wL^2/8 \tag{6.17}$$

For a beam element with the right end hinged, the fixed end forces due to a uniformly distributed load w, can be written as, (Balfour 1986):

$$V_L = 5wL/8 \tag{6.18}$$

$$V_R = 3wL/8 \tag{6.19}$$

$$M_L = wL^2/8 \tag{6.20}$$

$$M_R = 0 \tag{6.21}$$

The equivalent nodal point forces are the negative of the fixed end forces expressed in eqs. (6.12) - (6.21).

6.5.3 Thermal Forces

Thermal forces can affect all types of structures including track systems as a result of temperature variations and displacement restraints (i.e. restriction on free movement). The fixed ends forces due to a uniform change of temperature in an element can be given as, (Balfour 1986):

$$N_L = \alpha_t \Delta T E A \tag{6.22}$$

$$N_R = -\alpha_t \Delta T E A \tag{6.23}$$

where

N_L = axial force at the left end of the element

N_R = axial force at the right end of the element

α_t = coefficient of thermal expansion of the material forming the element

ΔT = change in temperature, increase in temperature is positive

E = Young's modulus of the material forming the element

A = cross-sectional area of the element

The equivalent nodal point forces are equal to the opposite of the fixed end forces defined by eqs. (6.22) and (6.23), (Balfour 1986).

6.6 Characteristics of Program LR551D

A special purpose one dimensional finite element computer program called "LR551D" was developed to solve the LR55 track system modelled as multilayer beams on elastic foundations. The program LR551D was written in FORTRAN 77 for P.C. machines and its flow chart is presented in Fig. (6.5). The main characteristics of LR551D are:

1. A special subroutine called GEMESH was set up to perform an automatic mesh generation for the track system under consideration in order to minimise the required input data.
2. Nonlinear analysis due to loss of contact between the concrete trough and the track base, i.e. track base separation can be performed. This is achieved by an iterative procedure through checking at each iteration, the vertical displacement of every track base spring to see whether it is in tension or compression and its stiffness adjusted accordingly. For instance, if it happens that a certain spring has an upward displacement, then it will be under tension. As the supporting base (ballast or soil) cannot take any tension then zero stiffness will be assigned to that specific spring. At the end of each iteration, if some springs are adjusted, then the structure should be re-analysed after modifying the structural stiffness matrix and successive iterations will be repeated. The iteration is terminated when there is no change in the state of all track base springs for two consecutive iterations, see Fig. (6.5). After solving several trial problems, the procedure seems to be computationally inexpensive as it was found to converge with four to five iterations in most of the cases.
3. A constant or variable track base modulus along the track can be specified. This is achieved by dividing the track length into segments (could be up to 10 segments) and assigning a constant value of base modulus for each segment. Such a feature of the LR551D program is very useful to predict the behaviour of the track system when it is expected to have high variation or sudden change of base properties (e.g. a patch of soft base) along the track system. Moreover, the presence of a cavity of a certain length directly underneath the applied wheel load can be easily

represented with this feature by assigning a very small value (e.g. 0.0001 N/mm^2) for the base modulus along the cavity length. In fact, one of the cases worth investigating at the design stage of the track system is to assume the track bridging over a cavity of certain length. Such a case is most likely to occur in real life, for example the collapse of a sewer pipe laying directly underneath the track system.

4. Elements with one end being hinged (pinned connection) were incorporated in the program. This is quite useful in modelling the simple construction joints at the ends of concrete trough units when they are linked together along the track system in practice.
5. The system of simultaneous linear equations defined by eq. (6.1) was solved using a subroutine called SOLVE. This subroutine is based on the direct Gauss elimination method for a banded symmetric matrix which has the advantage of reducing appreciably the required computer processing time for solution, (Mosley and Spencer 1984, Balfour 1995).
6. The program was set up to run as a batch mode where the input data is read from a text edited file. Whereas the output results are printed in tabulated forms and stored in various text edited files for further manipulation such graphic purposes.
7. A special subroutine called MAXIM was coded to find the minimum and maximum values of track responses in each component of the track system (rail, concrete trough, pad and base). This will greatly assist in a quick search and check for critical sections of the track elements.

6.7 Applications

Various examples of the LR55 track system were selected and analysed using the numerical approach of the one dimensional FEM and LR551D program discussed above for a number of specific reasons. First, to ensure the validity of the LR551D program through comparing the results with those obtained by MLBOEF program (analytical solution presented in chapter 5) and with the commercially available finite element packages ANSYS and ABAQUS. Second, to investigate the behaviour of the LR55 track system under more practical boundary and loading conditions which otherwise could not be addressed by the analytical method discussed in chapter 5.

Throughout all the examples demonstrated, the cross sectional area of the rail A_1 is 67.155 cm^2 and moment of inertia I_1 is 377.328 cm^4, see Table (3.1). For an assumed concrete trough width of 380 mm and depth of 180 mm, the area of the concrete trough A_2 is 519.85 cm^2 and moment of inertia I_2 is 12654.2 cm^4. The applied vertical wheel load is 104.21 kN. The track base modulus was taken as 25 N/mm^2 and the Young's modulus of the pad was assumed 9.6969 N/mm^2, i.e. pad modulus k_1 is 80 N/mm^2, see Table (5.1).

6.7.1 Example 1: Effect of Track Length

In practice the LR55 track system will be laid as a continuously welded rail supported by a series of 6 m long precast concrete trough units, connected together by simple joints along the track. This means that the track system is theoretically of infinite length. On the other hand, a finite length of the track can only be considered in the numerical analysis by FEM due to restriction of the computer memory size and processing time. Thus, the main objective of this example is to find out the suitable length of the track system required for finite element analysis so as to give similar responses of an infinite structure.

Track lengths of 6, 12 and 18 m subjected to a vertical wheel load of 104.21 kN at the midspan were analysed. These lengths are chosen as multiples of 6 since the standard length of each concrete trough unit is 6 m. Due to symmetry, half the structure was considered and subdivided into a number of small track elements of 0.1 m length each. Such a discretisation results in a total number of nodes of 62, 122 and 182 for the 6, 12, and 18 m track length respectively.

Three assumptions were made in this example. Firstly, the analysis is linear, i.e. no track base separation. Secondly, the self weight of the track system (weight of the rail and concrete trough) is not included. Thirdly, the concrete trough is continuous over the whole length of the track system, i.e. there are no simple construction joints (hinges) at 6 m intervals as is practically the case. These assumptions were deliberately chosen in order to relate the results with the analytical solution (MLBOEF program) presented in chapter 5 for a track of infinite length.

The deflection and bending moment of the rail and concrete trough are presented in Figs. (6.6) - (6.9). For sake of comparison, the results obtained from the analytical solution are also depicted on the same graphs. The following points can be observed:

1. The maximum values of the deflection and bending moment for the three cases of track lengths are very close to those obtained analytically as they only vary by as much as 0.5%.
2. The overall shapes of the deflection and bending moment curves for a 6 m track length are slightly different from those of the analytical one. Thus, the solution of 6 m track length can be practically (e.g. for experimental purposes) regarded to have a similar response to an infinite length. However, for theoretical purposes, tracks longer than 6 m should be considered in order to have more accurate results.
3. The deflected shape and the bending moment for 12 and 18 m track lengths can be seen to agree excellently with those obtained analytically. For instance, the maximum difference is no more than 0.004 mm in case of deflection and 0.1 kN m in case of bending moment. Such negligible differences may be attributed to the fact the analytical model assumes an infinite length of the track system whereas a certain length of the track has to be considered in the case of numerical method which is governed by the computer memory size and the processing time. In addition, numerical error due to finite element discretisation of the track system might also be responsible for the negligible differences between the numerical and analytical techniques.
4. The size of the problem for 18 m track length (182 nodes) is larger than that for 12 m track length (122 nodes). Nevertheless, no improvement in the results are noticed for the 18 m length in comparison to 12 m length. This implies that the analysis of 18 m track length (case 3) is unnecessary, hence it may be discarded. Consequently, it can be concluded that a 12 m track length analysis is quite sufficient to give a similar response as an infinite length. Thus, all the following examples will only consider 12 m length of the track. It is worthwhile to mention that for the 12 m length problem, the total number of unknowns to be solved is 356 and the semi-band width of the global stiffness matrix is 9, i.e. the size of the global stiffness matrix for the structural system is 356 x 9. The computer processing time required to solve this problem by LR551D program is less than a minute using a laptop computer having 486 DX2 microprocessor and 8 MB RAM.

5. The matching of the numerical results with the analytical ones gives confidence in the validity of the computer program LR551D developed in the present work.

6.7.2 Example 2: Comparison of LR551D, ANSYS and ABAQUS Programs

A 12 m length of the LR55 track system, subjected to a single vertical wheel load of 104.21 kN at the midspan, was analysed using LR551D program. The analysis was linear, i.e. no track base separation. The self weight of the track system was not included. The concrete trough was assumed to be continuous over the whole length of the track system. The results are compared with those obtained from two different commercial finite element programs ANSYS and ABAQUS.

The deflection and the bending moment of the rail and concrete trough at selected points along the track are presented in Table (6.1) and (6.2). The results of the analytical solution (MLBOEF program) for infinite track are also shown in the tables for sake of comparison. It is obvious that the results obtained by the computer program LR551D developed in the present work are exactly matching with those of the commercial packages ANSYS and ABAQUS. Meanwhile, there is an excellent agreement between the results of the numerical approach (LR551D program) and the analytical one (MLBOEF) presented in chapter 5. The insignificant differences between the numerical and analytical results have already been justified in example 1 above. This example clearly demonstrates the validity of LR551D program and its correctness.

This example apparently shows that the LR551D program (numerical solution) as well as the MLBOEF program (analytical solution) or the standard finite element packages ANSYS and ABAQUS can all be equally employed to solve the LR55 track system. However, the LR551D program has special characteristics as explained previously in section 6.6, which makes it superior to the MLBOEF, ANSYS or ABAQUS in the context of treating efficiently a wide range of practical problems related to the LR55 track system.

6.7.3 Example 3: Effect of Track Self Weight and Base Separation

A 12 m length of the track system subjected to a vertical wheel load of 104.21 kN was analysed. Four cases were investigated as follows:

Case 1: Self weight included and linear analysis (no track base separation)

Case 2: Self weight included and nonlinear analysis (track base separation)

Case 3: Self weight excluded and linear analysis (no track base separation)

Case 4: Self weight excluded and nonlinear analysis (track base separation)

The results obtained for the four cases are represented graphically in Figs. (6.10) to (6.15) from which one can see that:

1. The effect of self weight on the maximum values of the deflection, bending moment and pressure distribution is almost negligible. This is due to the fact that the weight of the track system is so small compared to the applied wheel load (rail weight = 0.527 kN/m, concrete trough weight = 1.248 kN/m, whereas wheel load = 104.21 kN). In addition to that, the self weight is uniformly distributed over the whole length, while the wheel load is concentrated at one point.
2. Case 4 seems to give a relatively higher rebound deflection away from the wheel load position as compared to cases 1, 2 and 3, see Figs. (6.10) and (6.11). Such a thing happens because once the track system starts to deflect upward there is no holding force which pulls down the structure to its neutral position away from the wheel load application. This is physically not possible because it is the self weight of the track which is responsible for precompressing the track and counteracting the uplift occurred. Therefore, it is very important to include the self weight of the track, though it is very small compared to the wheel load, whenever nonlinear analysis due to track base separation is to be taken into consideration. In fact, as converting the self weight of track elements into equivalent point loads applied on the nodes are carried out automatically by LR551D program without appreciably affecting the computer processing time, it will be wiser and more precise to always include the self weight no matter how small it may be.
3. Case 4 produces rather an incorrect bending moment diagram for the concrete trough as it does not match with the other cases 1, 2 and 3, see Fig. (6.13). This is due to the same reason explained in point 2 above, i.e. the self weight is excluded while nonlinear analysis due to track base separation is performed.
4. The results for cases 2 and 3 are almost identical along the track which means including the self weight while permitting track base separation (case 2) gives similar results to the case of excluding the self weight and not allowing track base

separation (case 3). This leads to an interesting conclusion in which the assumption made that the soil can take tension during the analytical solution of the track system (see assumption 6 in chapter 5), though physically not valid, still gives acceptable results. Otherwise the solution of the differential equations established for the analytical model (eqs. (5.19) and (5.20)) becomes very complicated.

5. The rail bending moment and pad vertical pressure are almost insensitive to nonlinear analysis due to track base separation, Fig. (6.12) and (6.14).
6. Case 2 gives a more realistic base pressure in comparison to those resulted from cases 1, 3 and 4. This is because, firstly, there is no negative pressure on the base as it is the situation with cases 1 and 3. Second, there is some positive pressure, though very small, at a distance between 3.6 and 6 m away from the point load whereas case 4 shows zero pressure all the way through beyond 1.7 m from the point load, Fig. (6.15).

6.7.4 Example 4: Effect of Wheel Load Position

As mentioned earlier, the concrete trough is treated as a series of precast units linked together by simple construction joints (hinges). The objective of this example is to discuss the effect of wheel load position with respect to these joints. By inspection, two cases are critical, thus worth investigating. They are, see Fig. (6.16):

Case 1: wheel load at the centre of the concrete trough precast unit, i.e. at distance 3.0 m from the construction joint (hinge).

Case 2: wheel load at the edge of the concrete trough unit, i.e. directly above the construction joints (hinge).

The self weight of the track is included and track base separation is taken into consideration. The results of analysing a 12 m track length are presented in Figs. (6.17) - (6.20) from which the following points can be reported:

1. Case 2 gives higher maximum deflection for the rail and concrete trough than those corresponding to case 1. This is due to the fact that the track is more flexible at the construction joints since the latter has no rotational stiffness, i.e. one degree of freedom is released. Therefore, once the wheel load immediately passes over that hinge, the latter will experience higher deflection than it would otherwise being rigid, Figs. (6.17) and (6.18).

2. Case 2 seems to be responsible for producing both the maximum positive and negative bending moment in the rail, which are 15.576 and -2.684 kN m respectively. In other word, case 1 is not critical for the rail, Fig. (6.19).
3. The maximum bending moment in the concrete trough due to case 1 is sagging (positive) which has a value of 9.313 kN m, and occurs at the centre of the concrete trough unit, i.e. at distance 3 m from the construction joint. Whereas, the maximum bending moment in the concrete trough resulting from case 2, is hogging (negative) which has a value of -4.237 kN m and takes place at distance round 1.3 m from the construction joint, Fig. (6.20). This implies that the position of the critical sections of the concrete trough depends on the position of the wheel load as the latter crosses over the concrete trough unit from one end to the other. Therefore, these two cases have to be taken into account during the design of the concrete trough as will be explained in the following chapter.

6.7.5 Example 5: Effect of Soft Base Patch Underneath the Wheel Load

In practice, there is always a variation of the track base properties along the whole length of the track system. Accordingly, it is not uncommon to expect a certain part of the base whose properties differs significantly from the rest. Therefore, the main objective of this example is to investigate the effect of a soft base patch on the track responses. A range of length between 0 and 1 m was assumed for the soft base patch, and located symmetrically underneath the wheel load at the centre of the concrete trough unit. The track base modulus was assumed to be 25 N/mm^2 for the whole length of the track except for the soft patch which has an assumed modulus of 5 N/mm^2. This corresponds to the extreme case of soft track base in actual reality, (Cope 1993).

The results of the analysis are presented in Figs. (6.21) - (6.22) from which the following points are extracted:

1. The maximum deflection of the rail and concrete trough almost linearly increases as the length of the soft base patch increases. However, the existence of a soft base underneath the wheel load seems to have more influence on the concrete deflection than that of the rail. For example, when the track base is uniform, i.e. soft patch length = 0, the maximum deflection of the rail and the concrete is 3.748 and 2.368 mm respectively. The presence of 1.0 m length of a soft patch will

increase the rail maximum deflection to 5.354 mm (by 42.8%) while that of the concrete to 4.055 mm (by 71.2%), see Fig. (6.21).

2. The maximum bending moment of rail and the concrete trough also shows an almost linear relationship versus the length of the soft base patch, but with a considerably higher rate of change for the concrete as compared to the rail. For instance, the maximum bending moment of the rail is 13.592 kN m for zero soft patch length, and this value is increased to 15.265 kN m (by 12.3%) as the soft base patch becomes 1 m long. Whereas, the maximum bending moment of the concrete trough is increased from 9.313 kN m to 16.461 kN m (by 76.7%) as the soft base patch increases from 0 to 1 m long, see Fig (6.22).
3. The reason for the concrete being more sensitive than the rail due to the existence of a soft patch as shown in points 1 and 2 above, can be argued in the following. The concrete trough is directly supported by the base while the rail is separated from the base by two load absorbing structural elements, the pad and the concrete trough. Therefore, it is logical that any change in the track base property will directly and more appreciably affect the concrete response than that of the rail. Such a logical outcome obtained from this example supports qualitatively the correctness of the LR551D program developed in the present work.
4. The problem of a base with a nonuniform property dealt with in this example has evidently demonstrated the power and efficiency of the one dimensional FEM for the track system (presented in this chapter) in comparison to the analytical approach (discussed in chapter 5), where the base can only be assumed uniform. In a similar manner, the effect of a cavity underneath the wheel load can be easily investigated using LR551D program as will be shown in the following chapter.

6.8 Summary and Conclusion

A one dimensional FEM was followed to solve the LR55 track system modelled as multilayer beams on elastic foundations. A computer program called LR551D was developed for this purpose. Its correctness was validated through comparing the examples solved with the MLBOEF program (analytical solution) and commercial finite element packages ANSYS and ABAQUS.

The LR551D program was found superior to the analytical approach MLBOEF, ANASYS or ABAQUS. This is because the LR551D has special characteristics by which a wide range of the track problems can be tackled more efficiently. For example, a track system under different boundary conditions and load combinations can be easily involved in the problem. Concrete trough with construction joints at the ends is accounted for. Nonlinearity due to track uplift can be taken into account. Variation of the base modulus along the track system and existence of a soft patch or cavity underneath the wheel load can be taken into consideration during the analysis without any difficulty.

The examples demonstrated in this chapter gives us a better insight toward the most critical load cases governing the design and checking of the LR55 track components (rail, concrete trough, pad and base). These will be considered in detail in the following chapter.

Table (6.1): Comparison for the deflection of the rail and concrete obtained numerically by LR551D with those analytically and other commercial FE softwares.

Distance from wheel load (m)	Rail deflection (mm)			Concrete deflection (mm)		
	Numerical		Analytical	Numerical		Analytical
	LR551D	ANSYS & ABAQUS	MLBOEF	LR551D	ANSYS & ABAQUS	MLBOEF
0	3.662	3.662	3.662	2.289	2.289	2.289
0.1	3.582	3.582	3.582	2.270	2.270	2.270
0.2	3.382	3.382	3.382	2.217	2.217	2.217
0.4	2.799	2.799	2.799	2.017	2.017	2.017
0.5	2.479	2.479	2.479	1.879	1.879	1.879
0.6	2.164	2.164	2.164	1.725	1.725	1.725
0.8	1.592	1.592	1.592	1.390	1.390	1.390
1	1.120	1.120	1.120	1.051	1.051	1.051
1.2	0.749	0.749	0.749	0.741	0.741	0.741
1.4	0.466	0.466	0.466	0.478	0.478	0.478
1.6	0.256	0.256	0.256	0.270	0.270	0.270
1.8	0.105	0.105	0.105	0.115	0.115	0.115
2	0.001	0.001	0.000	0.008	0.008	0.008
2.2	-0.065	-0.065	-0.065	-0.059	-0.059	-0.059
2.4	-0.102	-0.102	-0.102	-0.096	-0.096	-0.096
2.6	-0.117	-0.117	-0.117	-0.110	-0.110	-0.111
2.8	-0.116	-0.116	-0.116	-0.110	-0.110	-0.110
3.0	-0.106	-0.106	-0.106	-0.100	-0.100	-0.100
4.0	-0.027	-0.027	-0.027	-0.025	-0.025	-0.025
5.0	0.001	0.001	0.004	0.001	0.001	0.004
6.0	0.000	0.000	0.004	0.000	0.000	0.003

Table (6.2): Comparison for the moment of the rail and concrete obtained numerically by LR551D with those analytically and other commercial FE softwares.

Distance from wheel load (m)	Rail moment (kN m)			Concrete moment (kN m)		
	Numerical		Analytical	Numerical		Analytical
	LR551D	ANSYS & ABAQUS	MLBOEF	LR551D	ANSYS & ABAQUS	MLBOEF
0	13.587	13.587	13.679	9.297	9.297	9.253
0.1	8.926	8.926	9.014	9.034	9.034	8.994
0.2	5.314	5.314	5.392	8.289	8.289	8.258
0.4	0.736	0.736	0.788	5.795	5.795	5.785
0.5	-0.535	-0.535	-0.495	4.300	4.300	4.299
0.6	-1.327	-1.327	-1.298	2.796	2.796	2.821
0.8	-1.963	-1.963	-1.949	0.093	0.093	0.109
1	-1.931	-1.931	-1.927	-1.888	-1.888	-1.871
1.2	-1.666	-1.666	-1.665	-3.050	-3.050	-3.035
1.4	-1.369	-1.369	-1.370	-3.499	-3.499	-3.488
1.6	-1.108	-1.108	-1.109	-3.430	-3.430	-3.424
1.8	-0.892	-0.892	-0.893	-3.044	-3.044	-3.041
2	-0.709	-0.709	-0.710	-2.506	-2.506	-2.506
2.2	-0.550	-0.550	-0.550	-1.935	-1.935	-1.936
2.4	-0.408	-0.408	-0.409	-1.403	-1.403	-1.404
2.6	-0.285	-0.285	-0.286	-0.947	-0.947	-0.949
2.8	-0.182	-0.182	-0.183	-0.580	-0.580	-0.583
3.0	-0.100	-0.100	-0.100	-0.303	-0.303	-0.305
4.0	0.053	0.053	0.051	0.161	0.161	0.160
5.0	0.022	0.022	0.022	0.069	0.069	0.068
6.0	-0.014	-0.014	0.000	-0.043	-0.043	0.001

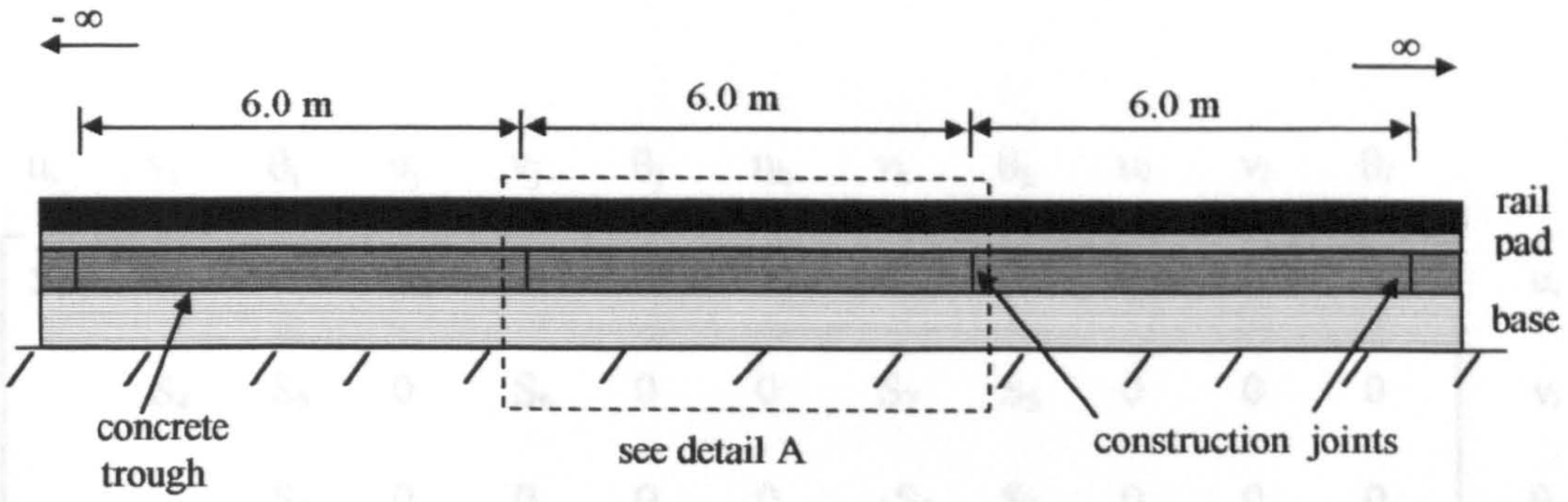

Fig. (6.1a): LR55 track system modelled as multilayer beams on elastic foundations.

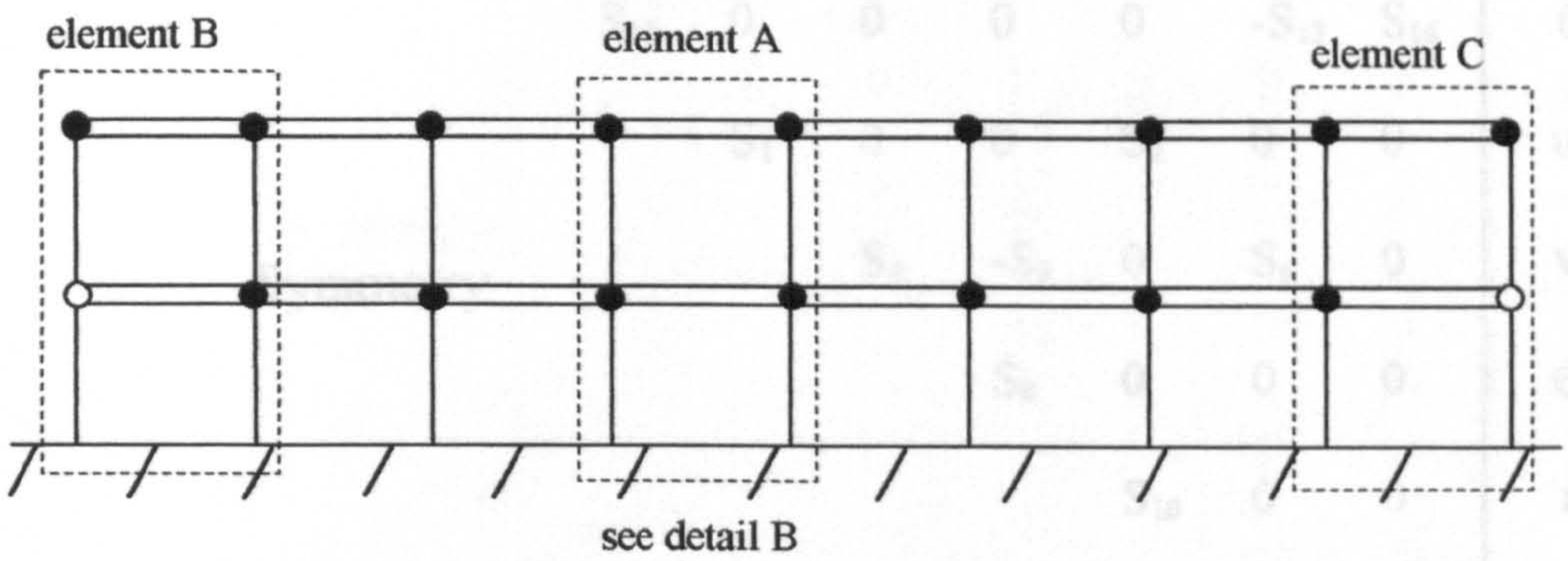

Fig. (6.1b): Detail A, finite element discretisation for a segment length of the LR55 track system.

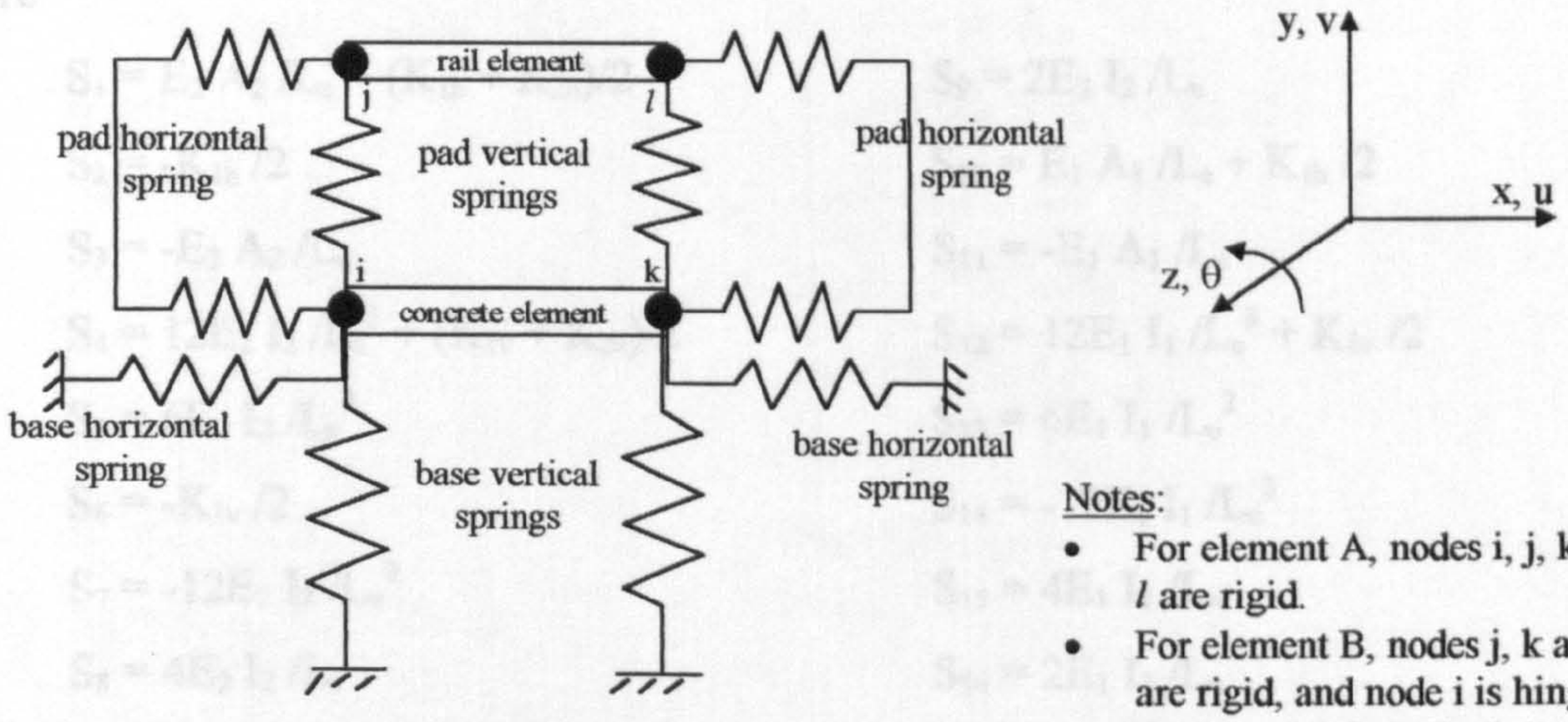

Fig. (6.1b): Detail B, typical track element.

Notes:

- For element A, nodes i, j, k and *l* are rigid.
- For element B, nodes j, k and *l* are rigid, and node i is hinged.
- For element C, nodes i, j and *l* are rigid, and node k is hinged.

Fig. (6.1): One dimensional finite element idealisation for the LR55 track system.

u_i	v_i	θ_i	u_j	v_j	θ_j	u_k	v_k	θ_k	u_l	v_l	θ_l	
S_1	0	0	S_2	0	0	S_3	0	0	0	0	0	u_i
	S_4	S_5	0	S_6	0	0	S_7	S_5	0	0	0	v_i
		S_8	0	0	0	0	$-S_5$	S_9	0	0	0	θ_i
			S_{10}	0	0	0	0	0	S_{11}	0	0	u_j
				S_{12}	S_{13}	0	0	0	0	S_{14}	S_{13}	v_j
					S_{15}	0	0	0	0	$-S_{13}$	S_{16}	θ_j
						S_1	0	0	S_2	0	0	u_k
Symmetry							S_4	$-S_5$	0	S_6	0	v_k
								S_8	0	0	0	θ_k
									S_{10}	0	0	u_l
										S_{12}	$-S_{13}$	v_l
											S_{15}	θ_l

where:

$S_1 = E_2 A_2 / L_e + (K_{1h} + K_{2h})/2$

$S_2 = -K_{1h} /2$

$S_3 = -E_2 A_2 / L_e$

$S_4 = 12E_2 I_2 / L_e^3 + (K_{1v} + K_{2v})/2$

$S_5 = 6E_2 I_2 / L_e^2$

$S_6 = -K_{1v} /2$

$S_7 = -12E_2 I_2 / L_e^3$

$S_8 = 4E_2 I_2 / L_e$

$S_9 = 2E_2 I_2 / L_e$

$S_{10} = E_1 A_1 / L_e + K_{1h} /2$

$S_{11} = -E_1 A_1 / L_e$

$S_{12} = 12E_1 I_1 / L_e^3 + K_{1v} /2$

$S_{13} = 6E_1 I_1 / L_e^2$

$S_{14} = -12E_1 I_1 / L_e^3$

$S_{15} = 4E_1 I_1 / L_e$

$S_{16} = 2E_1 I_1 / L_e$

Fig. (6.2): Stiffness matrix for a track element with four nodes i, j, k and *l* rigid, as an assembly of rail, concrete trough, pad and base stiffness matrices.

u_i	V_i	θ_i	u_j	v_j	θ_j	u_k	v_k	θ_k	u_l	v_l	θ_l	
S_1	0	0	S_2	0	0	S_3	0	0	0	0	0	u_i
	S_4	0	0	S_5	0	0	S_6	S_7	0	0	0	v_i
		0	0	0	0	0	0	0	0	0	0	θ_i
			S_8	0	0	0	0	0	S_9	0	0	u_j
			S_{10}	S_{11}	0	0	0	0	S_{12}	S_{11}		v_j
				S_{13}	0	0	0	0	$-S_{11}$	S_{14}		θ_j
					S_1	0	0	S_2	0	0		u_k
						S_4	S_6	0	S_5	0		v_k
							S_{15}	0	0	0		θ_k
								S_8	0	0		u_l
									S_{10}	S_{11}		v_l
									S_{13}			θ_l

Symmetry

where:

$S_1 = E_2 A_2 / L_e + (K_{1h} + K_{2h})/2$

$S_2 = -K_{1h} /2$

$S_3 = -E_2 A_2 / L_e$

$S_4 = 3E_2 I_2 / L_e^3 + (K_{1v} + K_{2v})/2$

$S_5 = -K_{1v} /2$

$S_6 = -3E_2 I_2 / L_e^3$

$S_7 = 3E_2 I_2 / L_e^2$

$S_8 = E_1 A_1 / L_e + K_{1h} /2$

$S_9 = -E_1 A_1 / L_e$

$S_{10} = 12E_1 I_1 / L_e^3 + K_{1v} /2$

$S_{11} = 6E_1 I_1 / L_e^2$

$S_{12} = -12E_1 I_1 / L_e^3$

$S_{13} = 4E_1 I_1 / L_e$

$S_{14} = 2E_1 I_1 / L_e$

$S_{15} = 3E_2 I_2 / L_e$

Fig. (6.3): Stiffness matrix for a track element with nodes j, k and *l* rigid and node i hinged, as an assembly of rail, concrete trough, pad and base stiffness matrices.

u_i	v_i	θ_i	u_j	v_j	θ_j	u_k	v_k	θ_k	u_l	v_l	θ_l	
S_1	0	0	S_2	0	0	S_3	0	0	0	0	0	u_i
	S_4	S_5	0	S_6	0	0	S_7	0	0	0	0	v_i
		S_8	0	0	0	0	$-S_5$	0	0	0	0	θ_i
			S_9	0	0	0	0	0	S_{10}	0	0	u_j
				S_{11}	S_{12}	0	0	0	0	S_{13}	S_{12}	v_j
					S_{14}	0	0	0	0	$-S_{12}$	S_{15}	θ_j
						S_1	0	0	S_2	0	0	u_k
							S_4	0	0	S_6	0	v_k
								0	0	0	0	θ_k
									S_9	0	0	u_l
										S_{11}	$-S_{12}$	v_l
											S_{14}	θ_l

Symmetry

where:

$S_1 = E_2 A_2 / L_e + (K_{1h} + K_{2h})/2$

$S_2 = -K_{1h} /2$

$S_3 = -E_2 A_2 / L_e$

$S_4 = 3E_2 I_2 / L_e^3 + (K_{1v} + K_{2v})/2$

$S_5 = 3E_2 I_2 / L_e^2$

$S_6 = -K_{1v} /2$

$S_7 = -3E_2 I_2 / L_e^3$

$S_8 = 3E_2 I_2 / L_e$

$S_9 = E_1 A_1 / L_e + K_{1h} /2$

$S_{10} = -E_1 A_1 / L_e$

$S_{11} = 12E_1 I_1 / L_e^3 + K_{1v} /2$

$S_{12} = 6E_1 I_1 / L_e^2$

$S_{13} = -12E_1 I_1 / L_e^3$

$S_{14} = 4E_1 I_1 / L_e$

$S_{15} = 2E_1 I_1 / L_e$

Fig. (6.4): Stiffness matrix for a track element with nodes i, j and *l* rigid and node k hinged, as an assembly of rail, concrete trough, pad and base stiffness matrices.

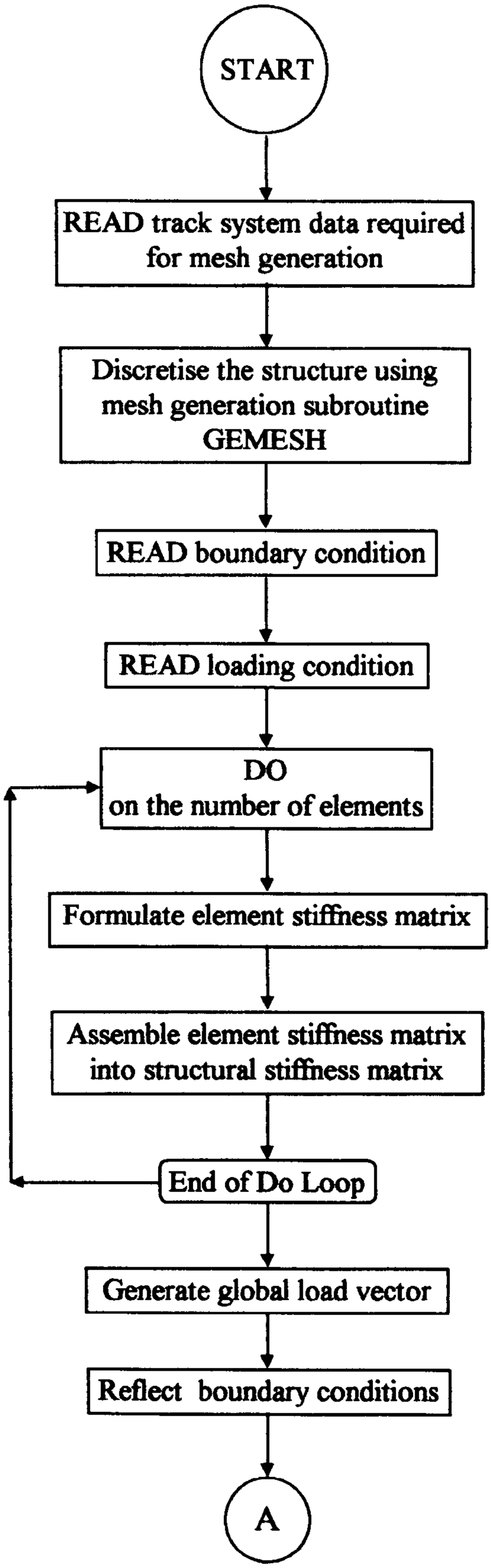

Fig. (6.5): Flow chart for the computer program LR551D.

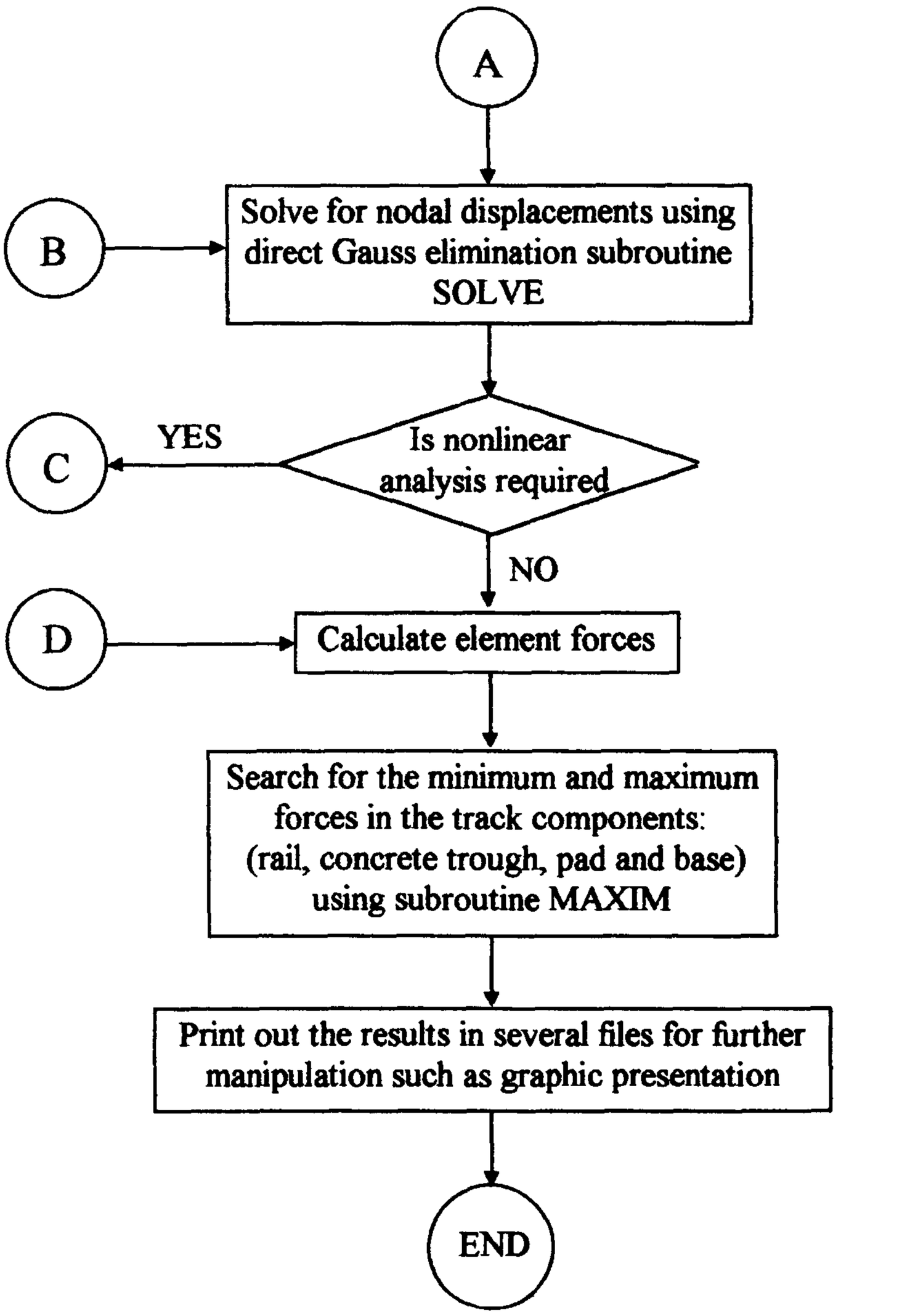
A
B
Solve for nodal displacements using direct Gauss elimination subroutine SOLVE
YES
C
Is nonlinear analysis required
NO
D
Calculate element forces
Search for the minimum and maximum forces in the track components: (rail, concrete trough, pad and base) using subroutine MAXIM
Print out the results in several files for further manipulation such as graphic presentation
END

Fig. (6.5): Cont.

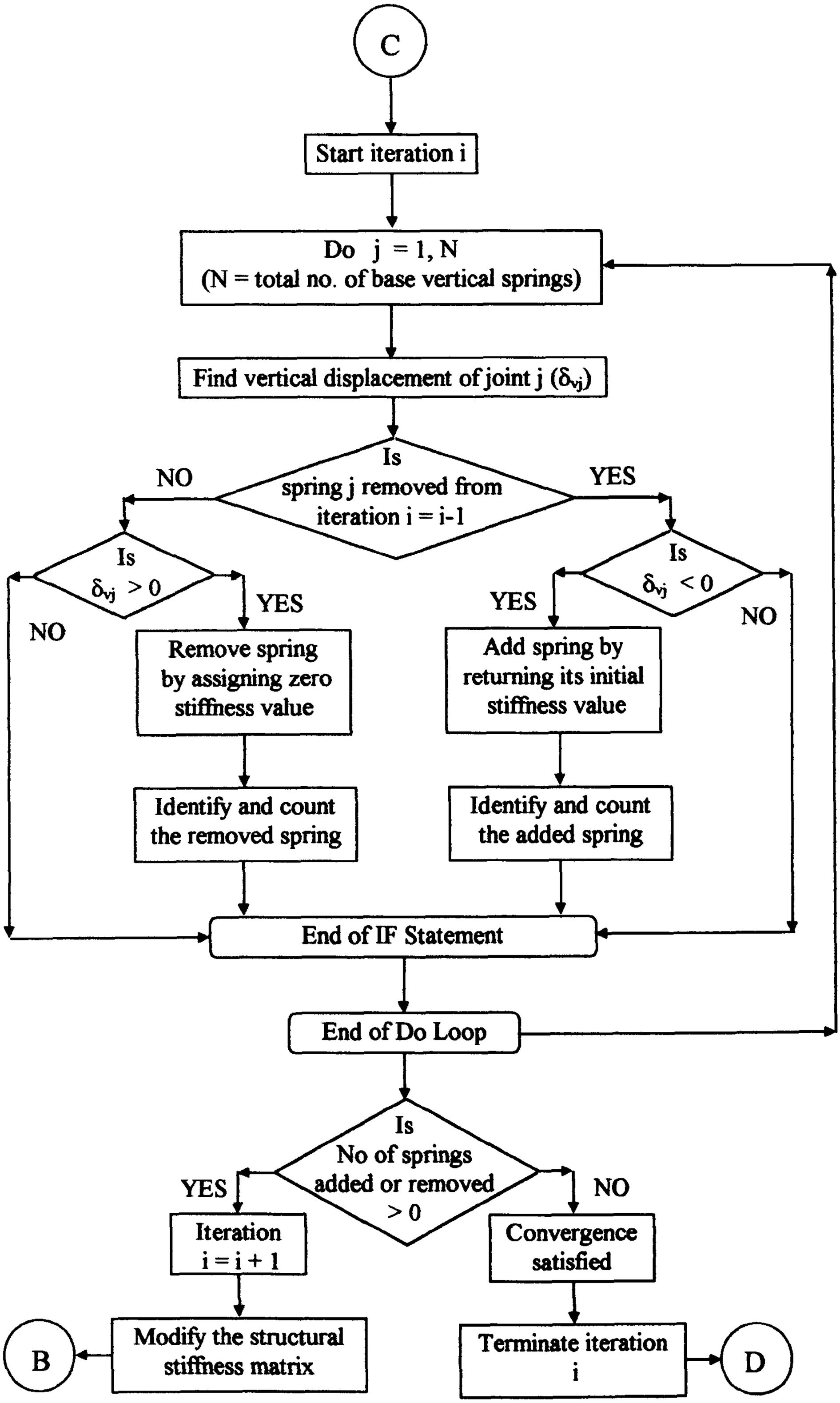
C
Start iteration i
Do j = 1, N
(N = total no. of base vertical springs)
Find vertical displacement of joint j (δ_{vj})
Is
spring j removed from
iteration i = i-1
NO
YES
Is
δ_{vj} > 0
NO
YES
Remove spring
by assigning zero
stiffness value
Identify and count
the removed spring
Is
δ_{vj} < 0
YES
NO
Add spring by
returning its initial
stiffness value
Identify and count
the added spring
End of IF Statement
End of Do Loop
Is
No of springs
added or removed
> 0
YES
NO
Iteration
i = i + 1
Modify the structural
stiffness matrix
B
Convergence
satisfied
Terminate iteration
i
D

Fig. (6.5): Cont.

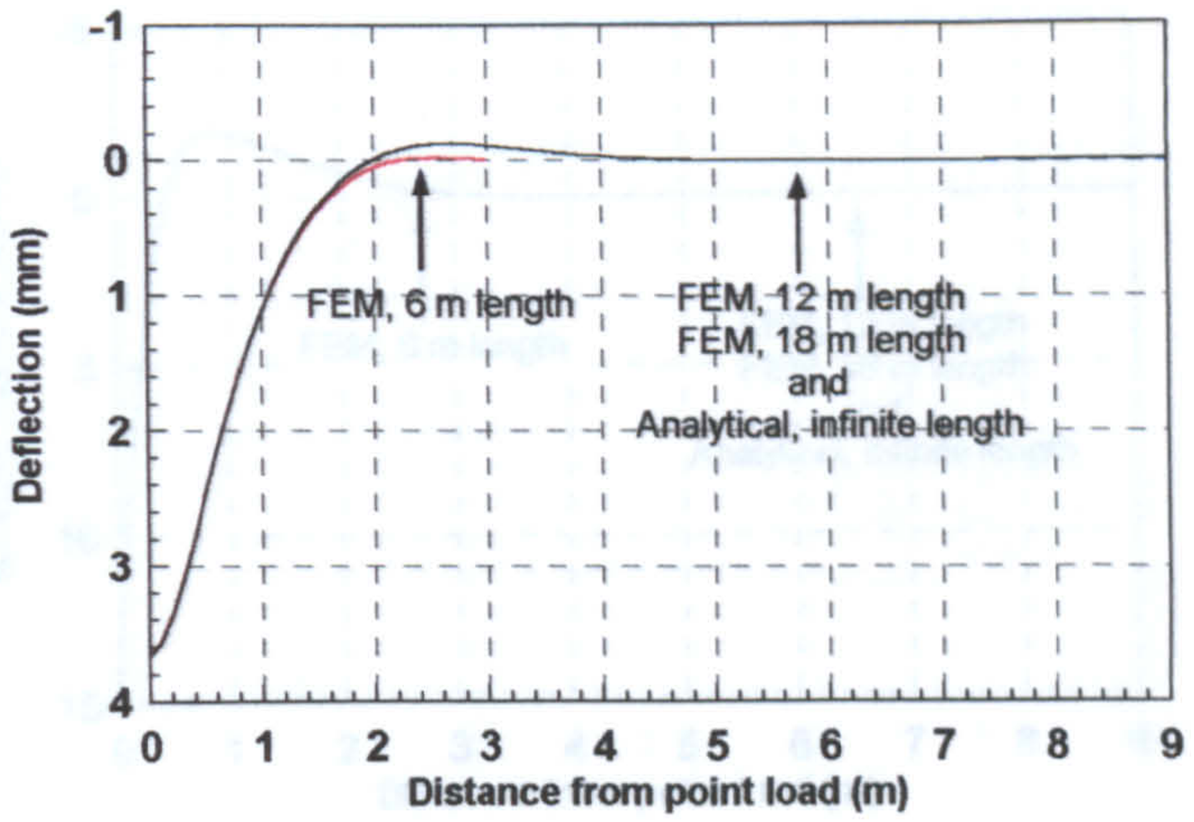

Fig. (6.6): Comparison of the rail deflection for various track lengths.

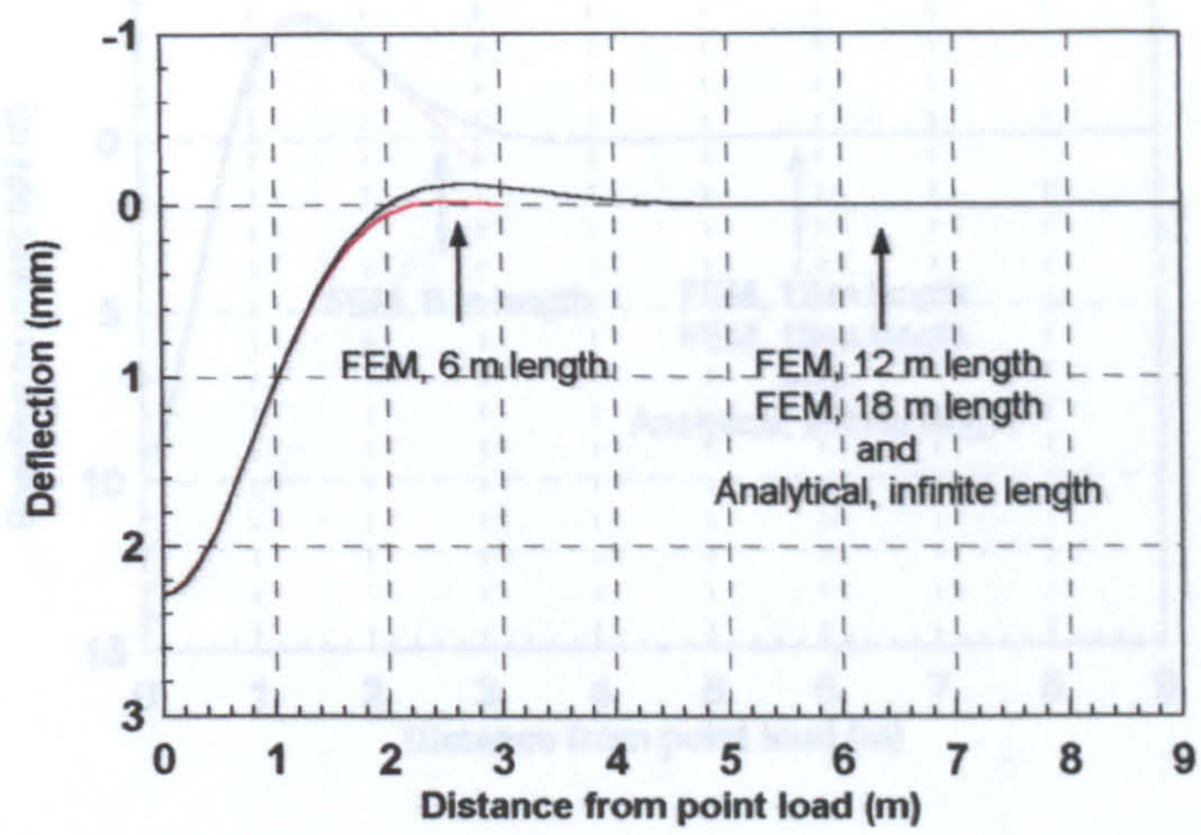

Fig. (6.7): Comparison of the concrete trough deflection for various track lengths.

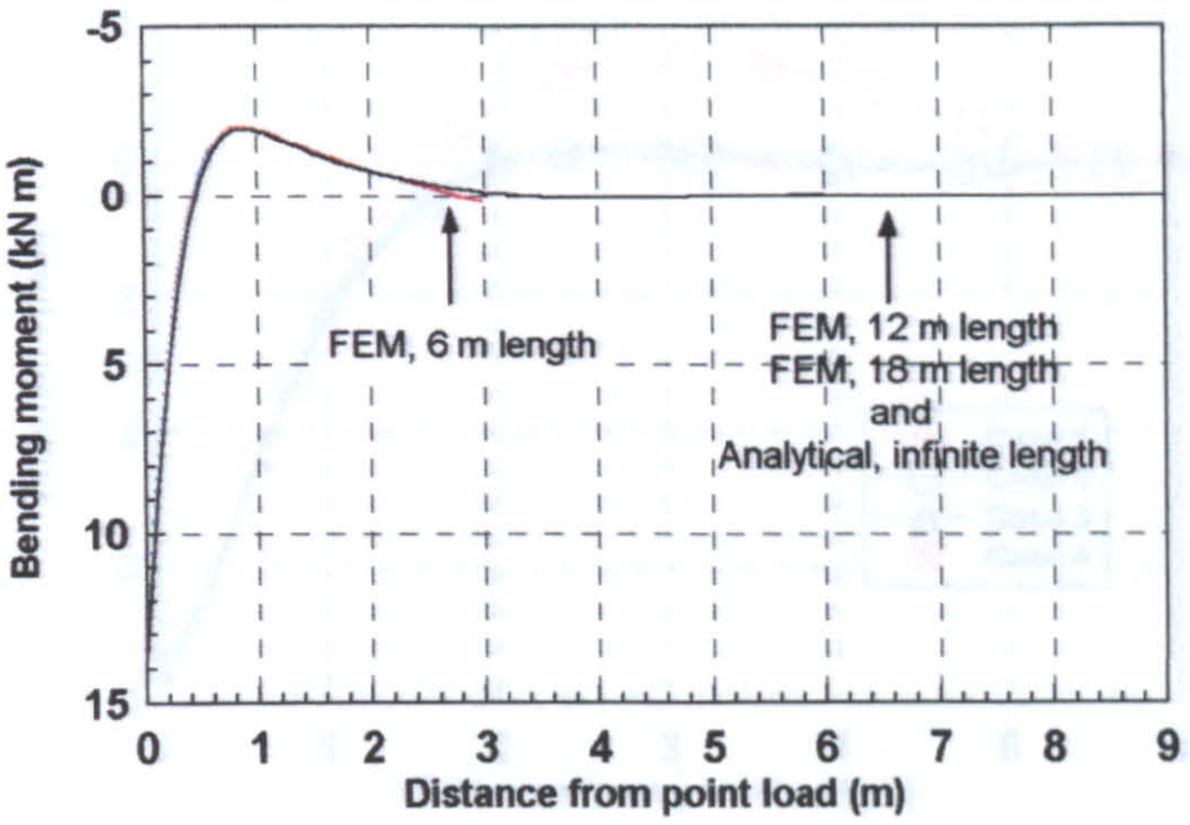

Fig. (6.8): Comparison of the rail bending moment for various track lengths.

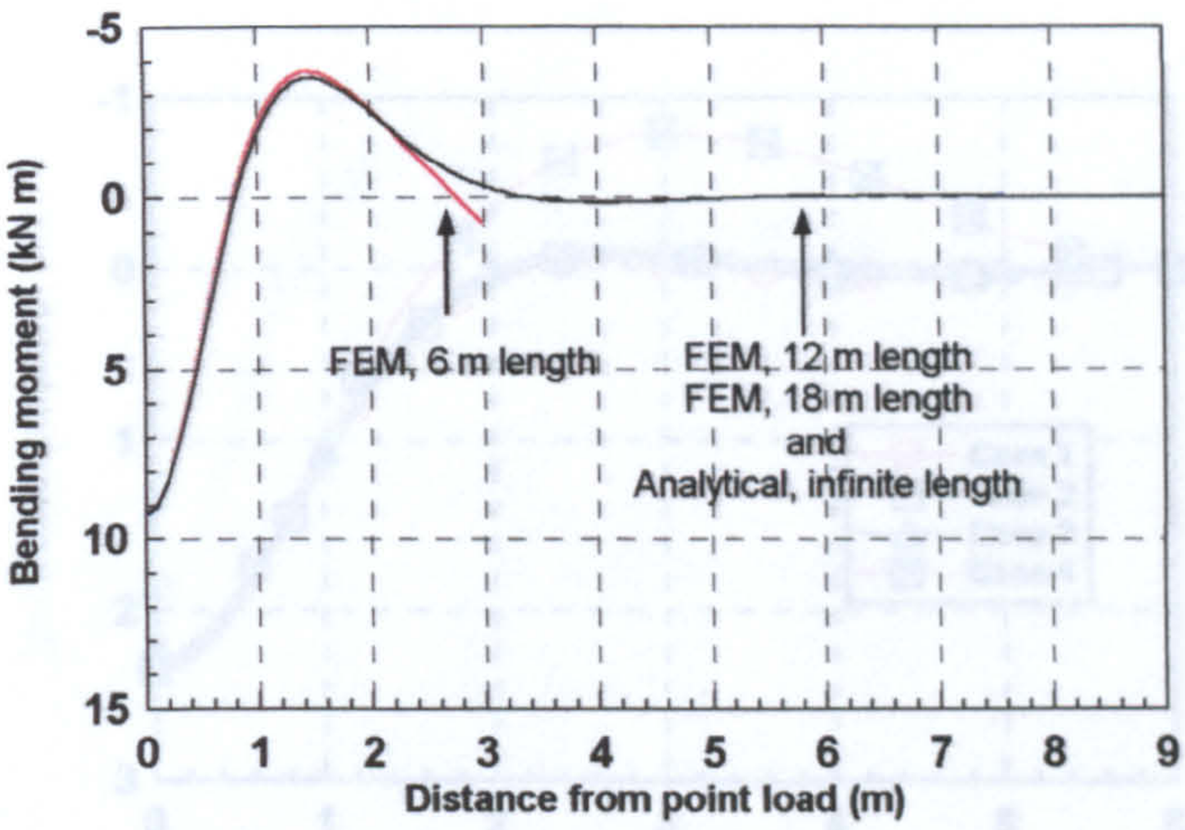

Fig. (6.9): Comparison of the concrete trough bending moment for various track lengths.

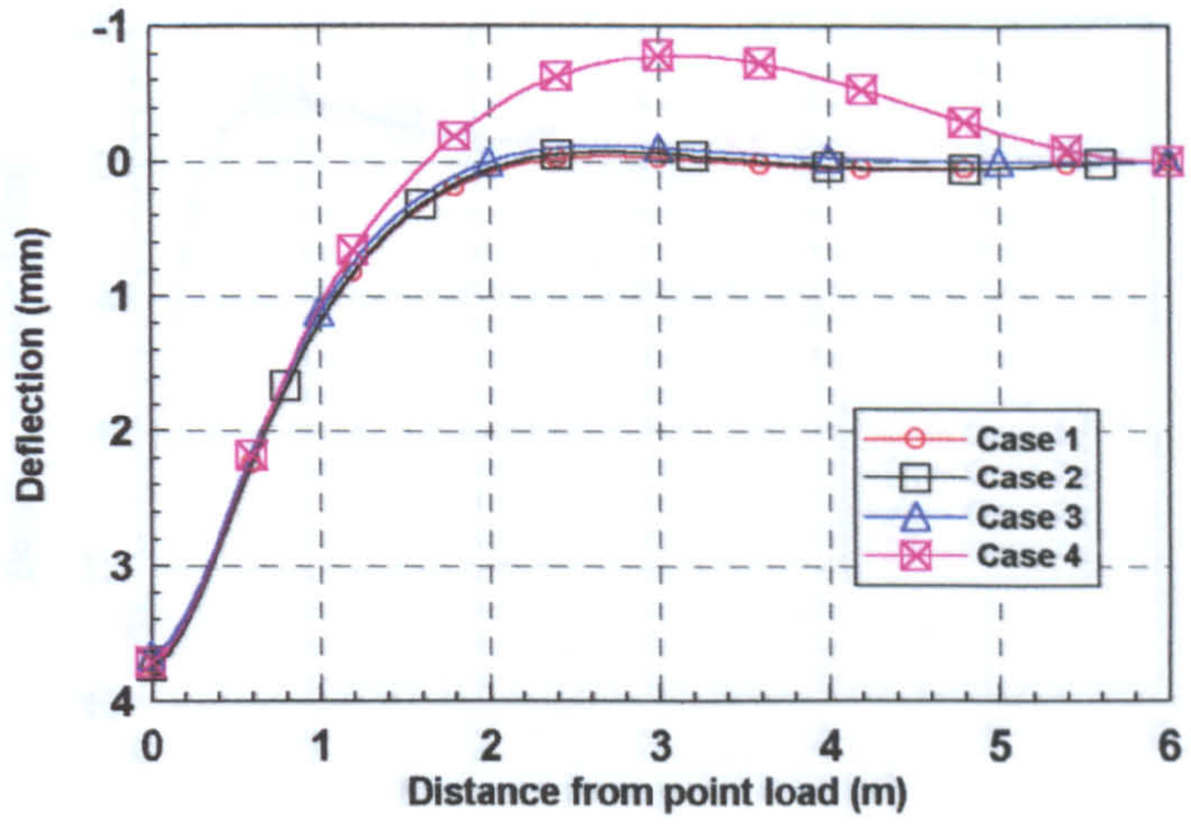

Fig. (6.10): Effect of track self weight and base separation on the rail deflection.

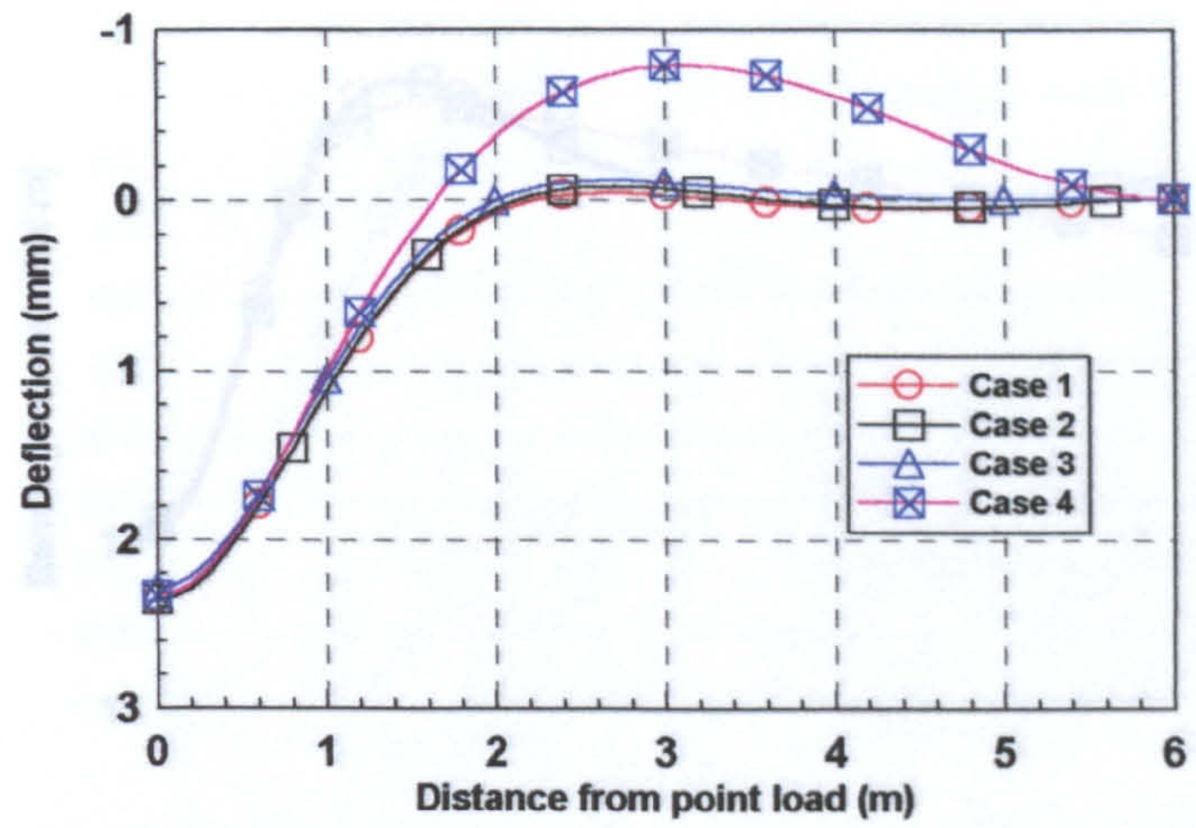

Fig. (6.11): Effect of track self weight and base separation on the concrete trough deflection.

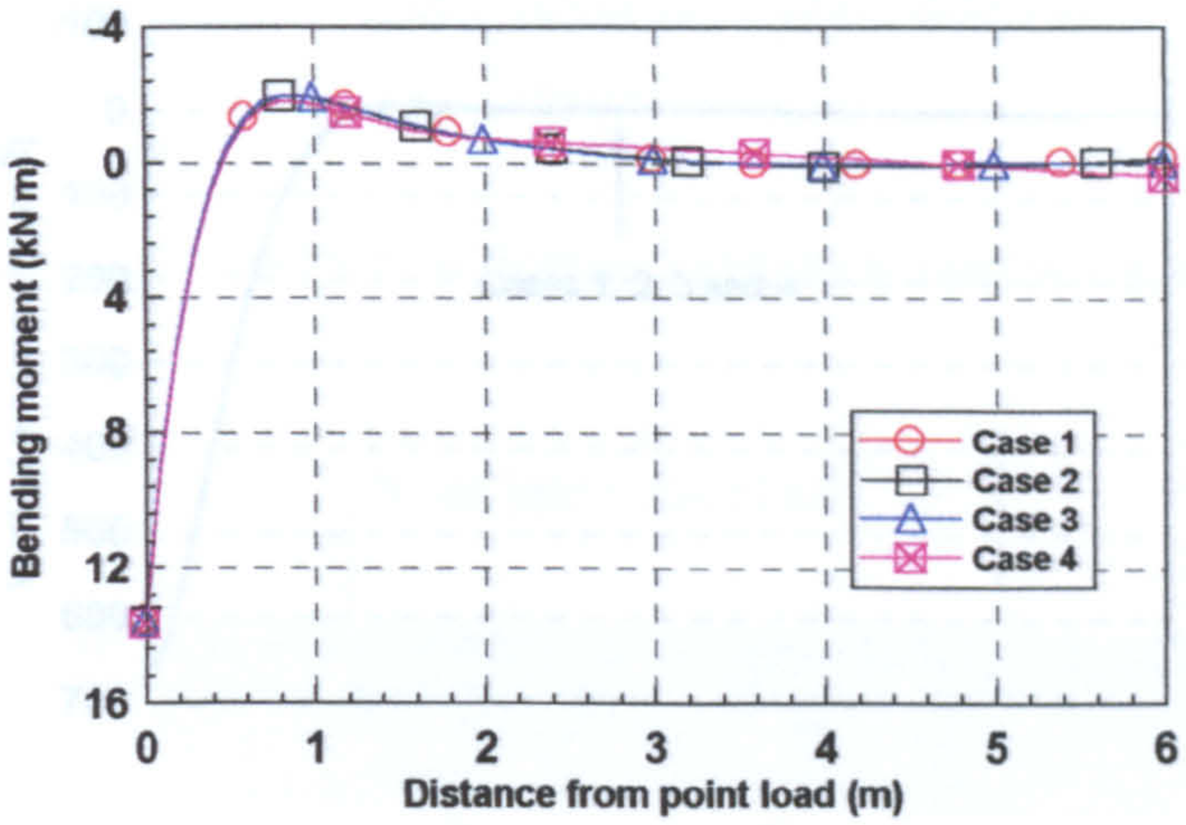

Fig. (6.12): Effect of track self weight and base separation on the rail moment.

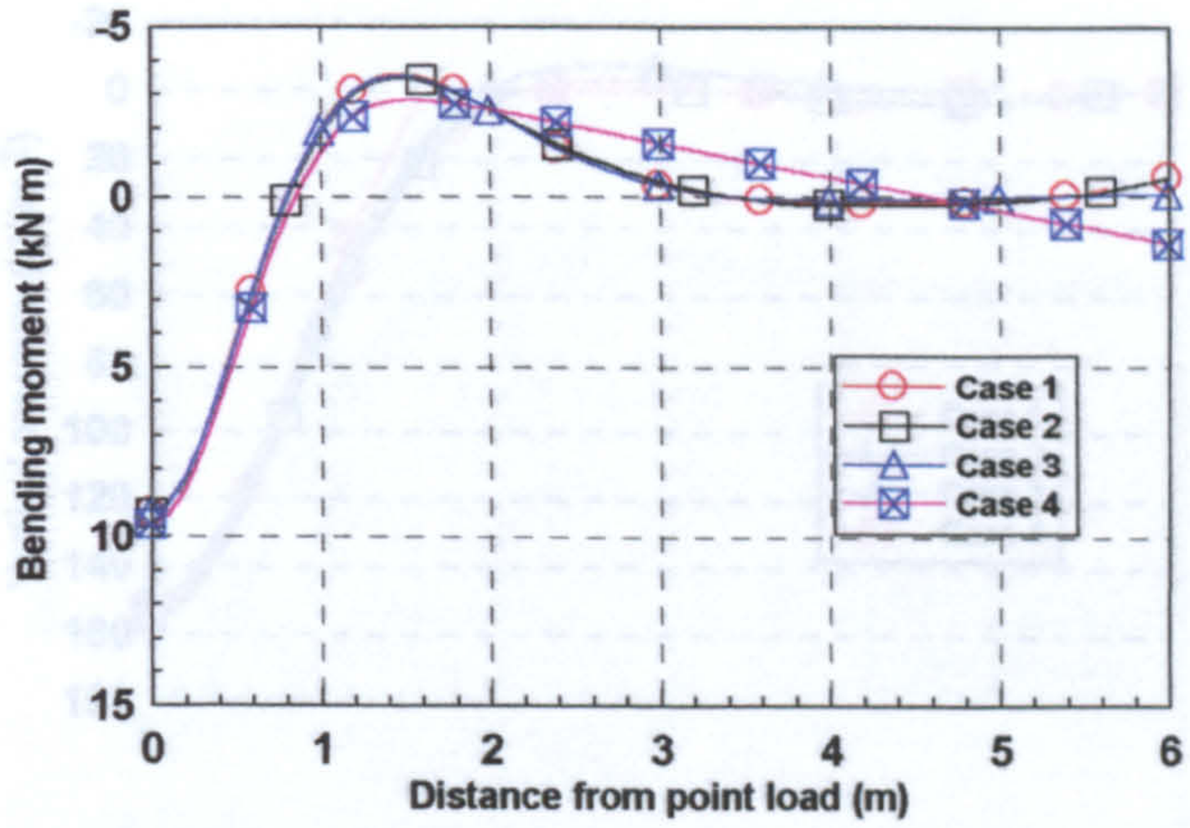

Fig. (6.13): Effect of track self weight and base separation on the concrete trough bending moment.

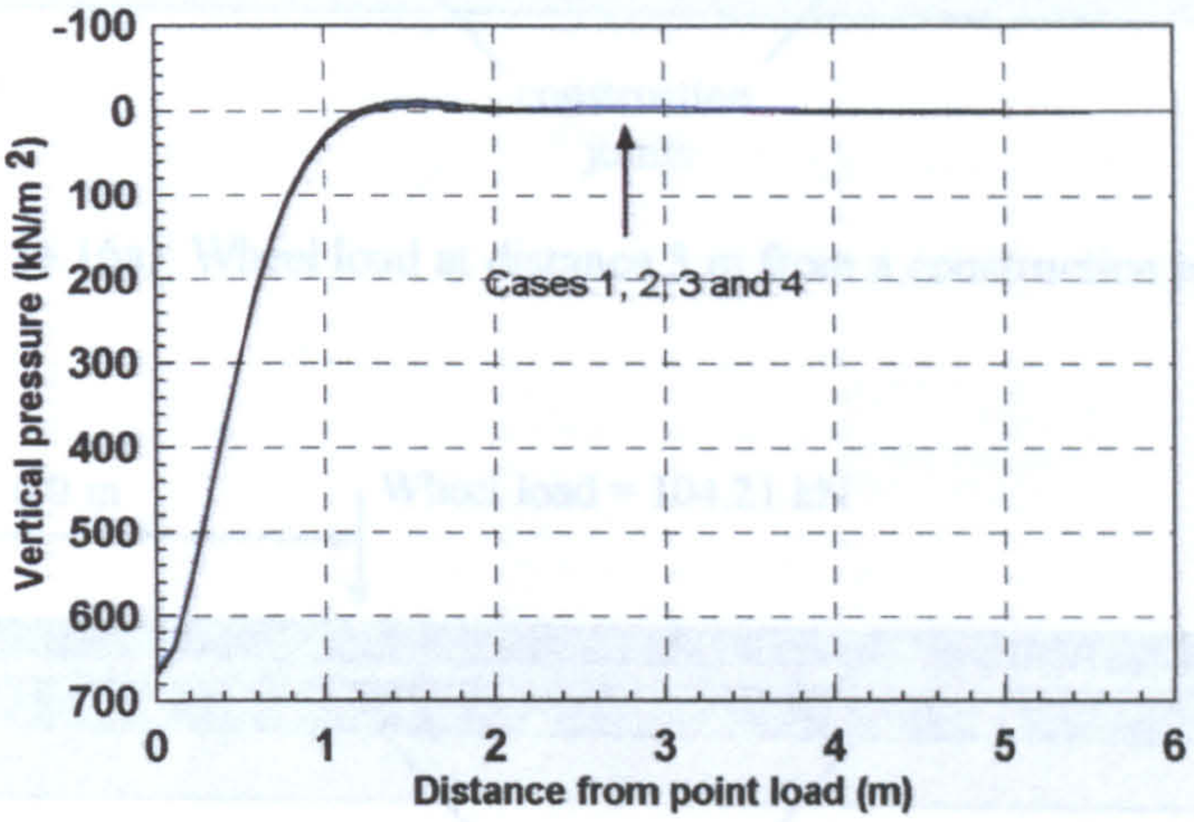

Fig. (6.14): Effect of track self weight and base separation on the pad pressure.

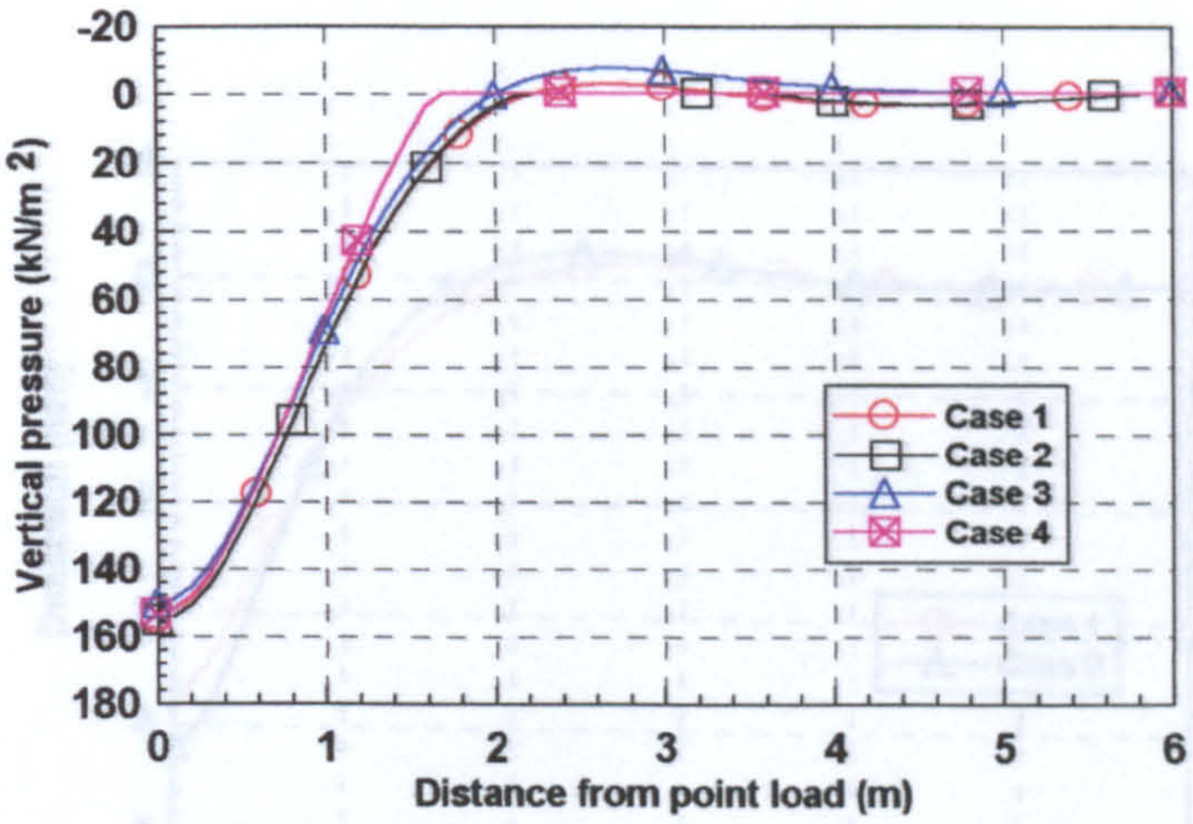

Fig. (6.15): Effect of track self weight and base separation on the base pressure.

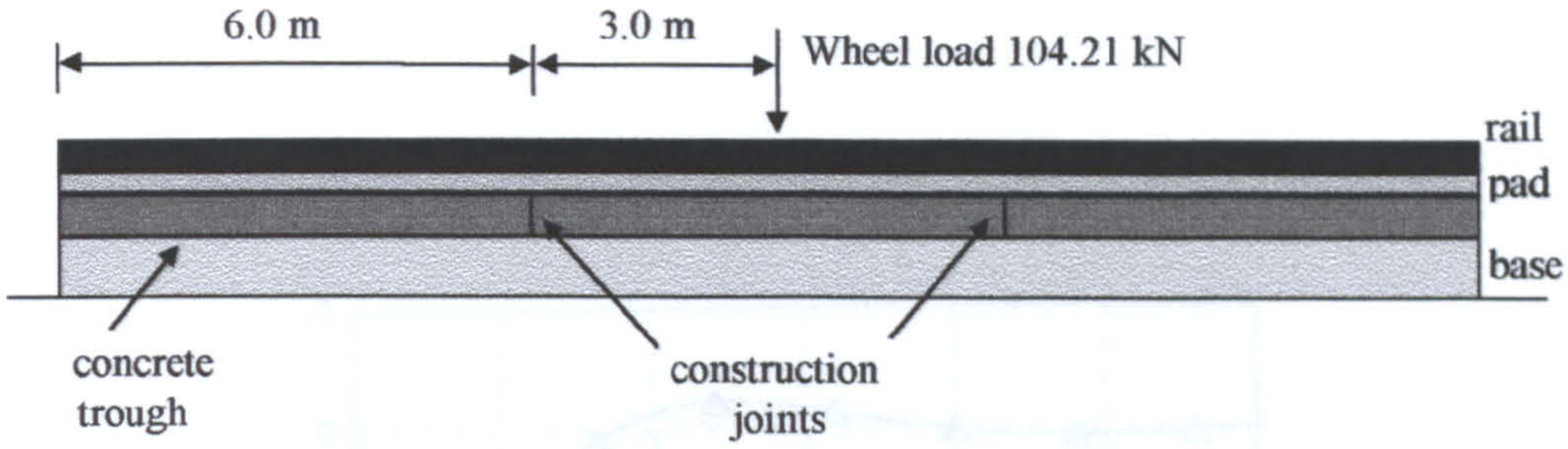

Fig. (6.16a): Wheel load at distance 3 m from a construction joint.

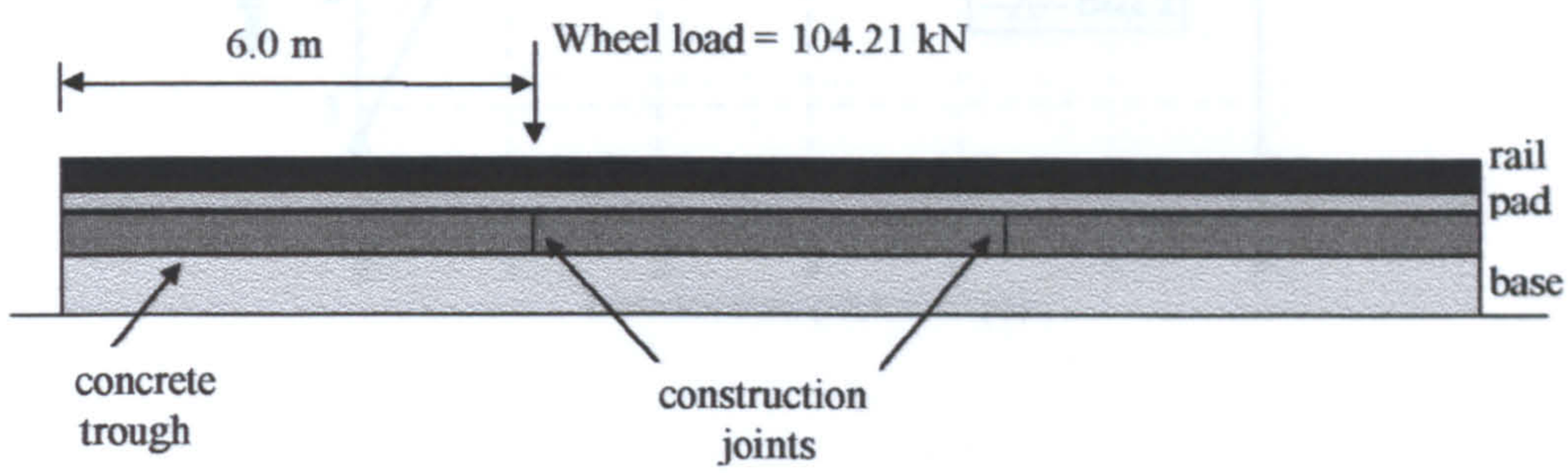

Fig. (6.16b): Wheel load directly above a construction joint.

Fig. (6.16): Wheel load position with respect to the concrete trough construction joints.

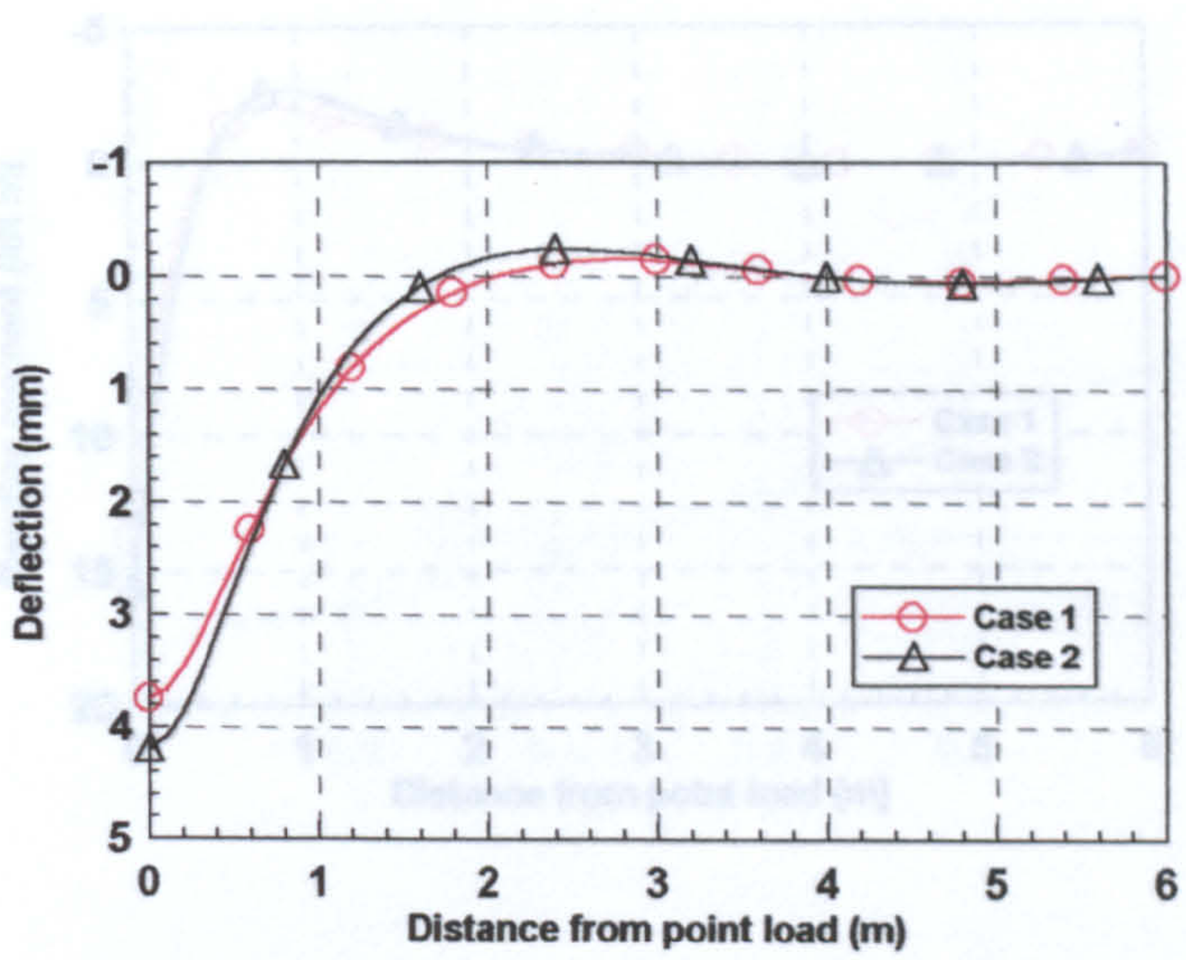

Fig. (6.17): Effect of wheel load position on the rail deflection.

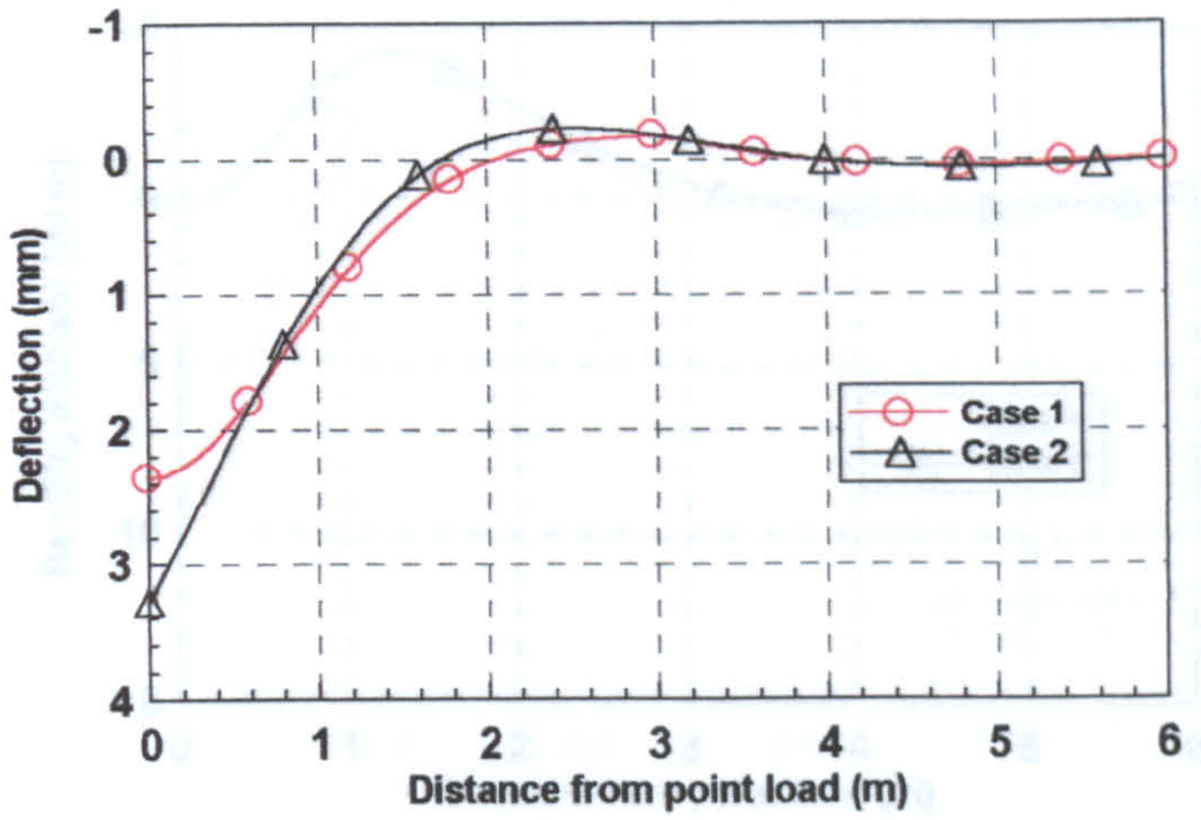

Fig. (6.18): Effect of wheel load position on the concrete trough deflection.

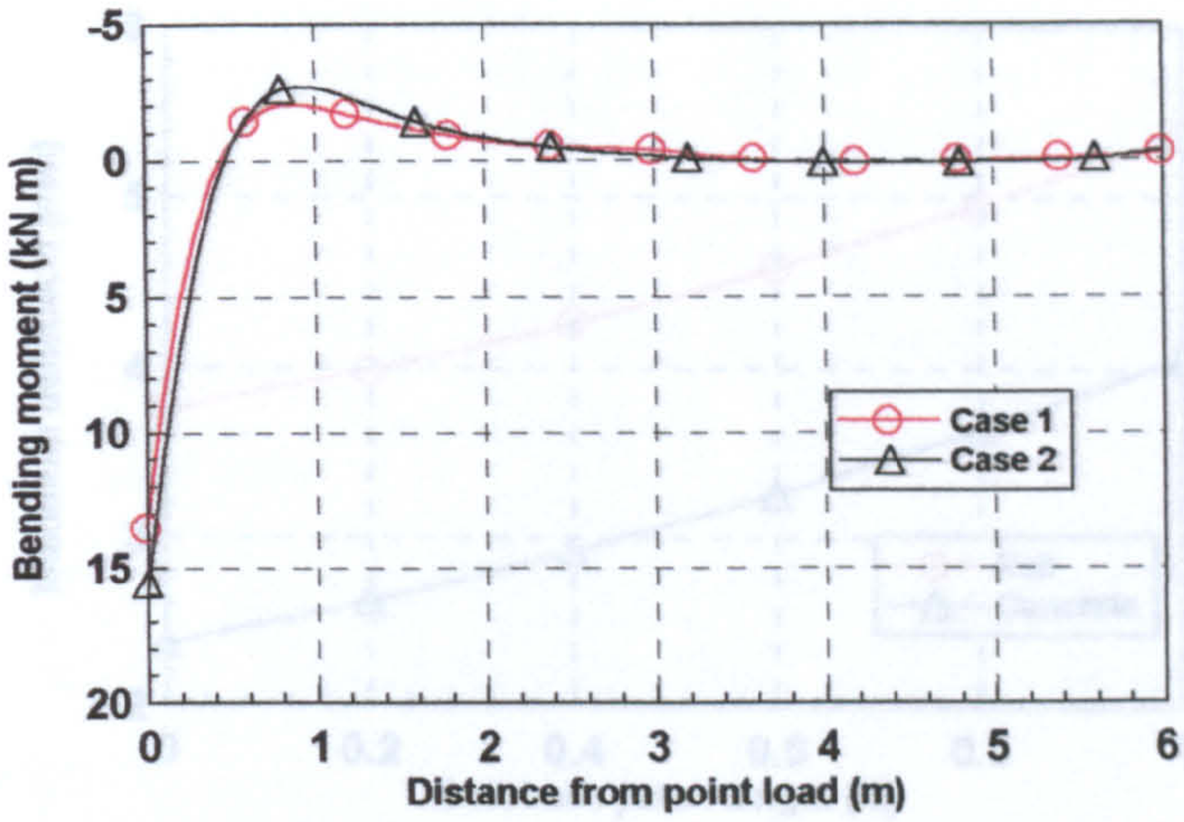

Fig. (6.19): Effect of wheel load position on the rail bending moment.

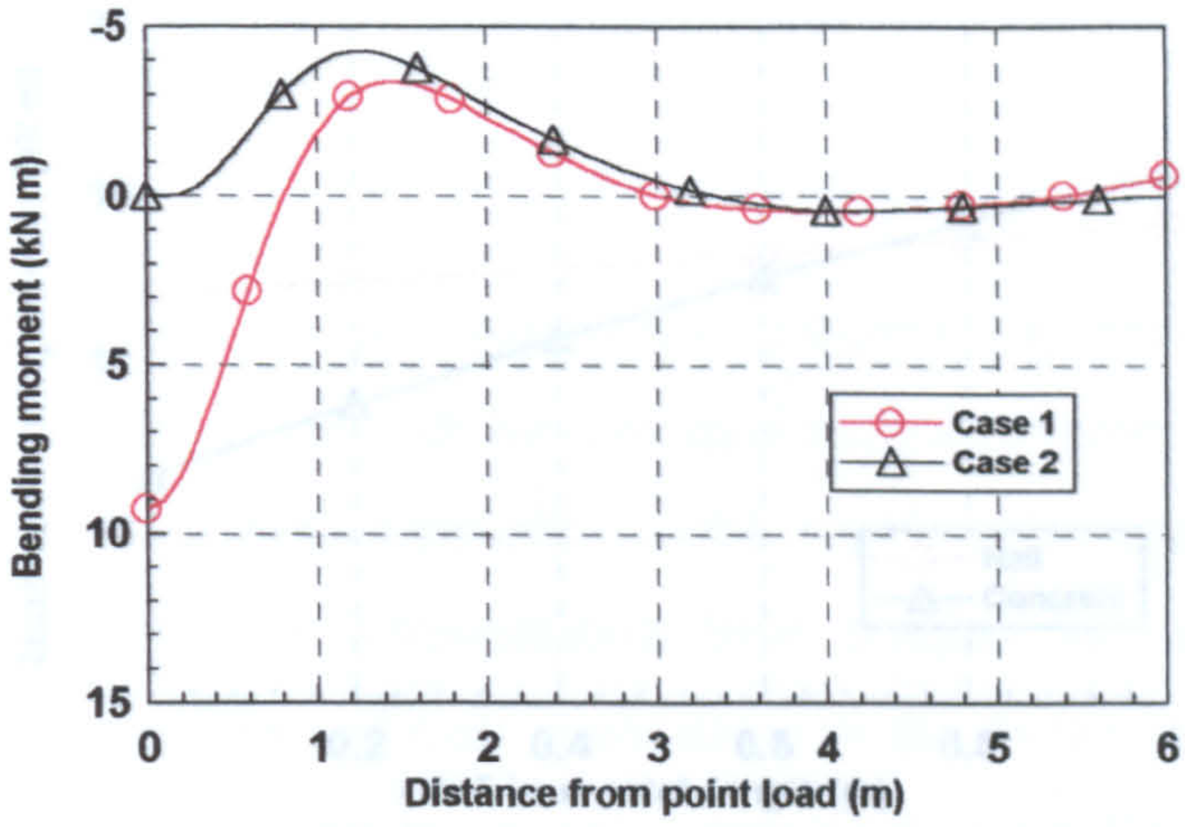

Fig. (6.20): Effect of wheel load position on the concrete trough bending moment.

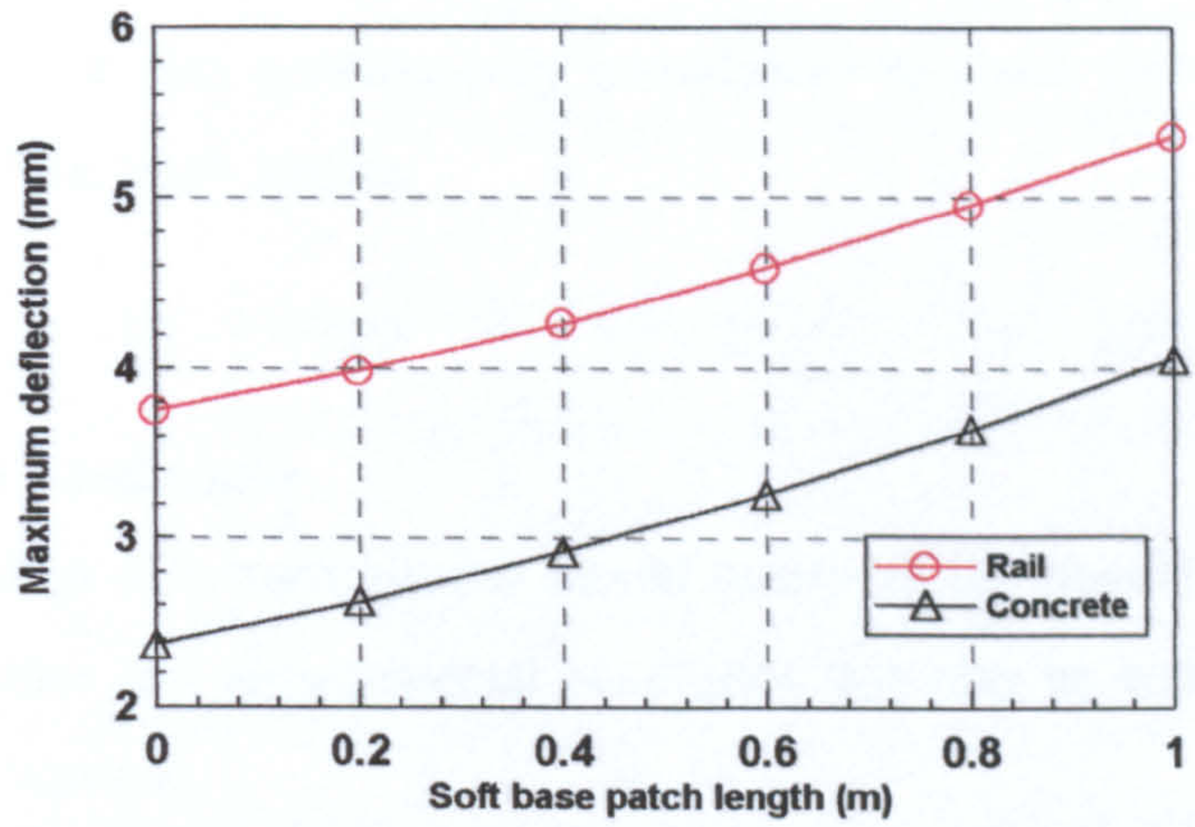

Fig. (6.21): Effect of soft base patch underneath the wheel load on the maximum deflection of the track system.

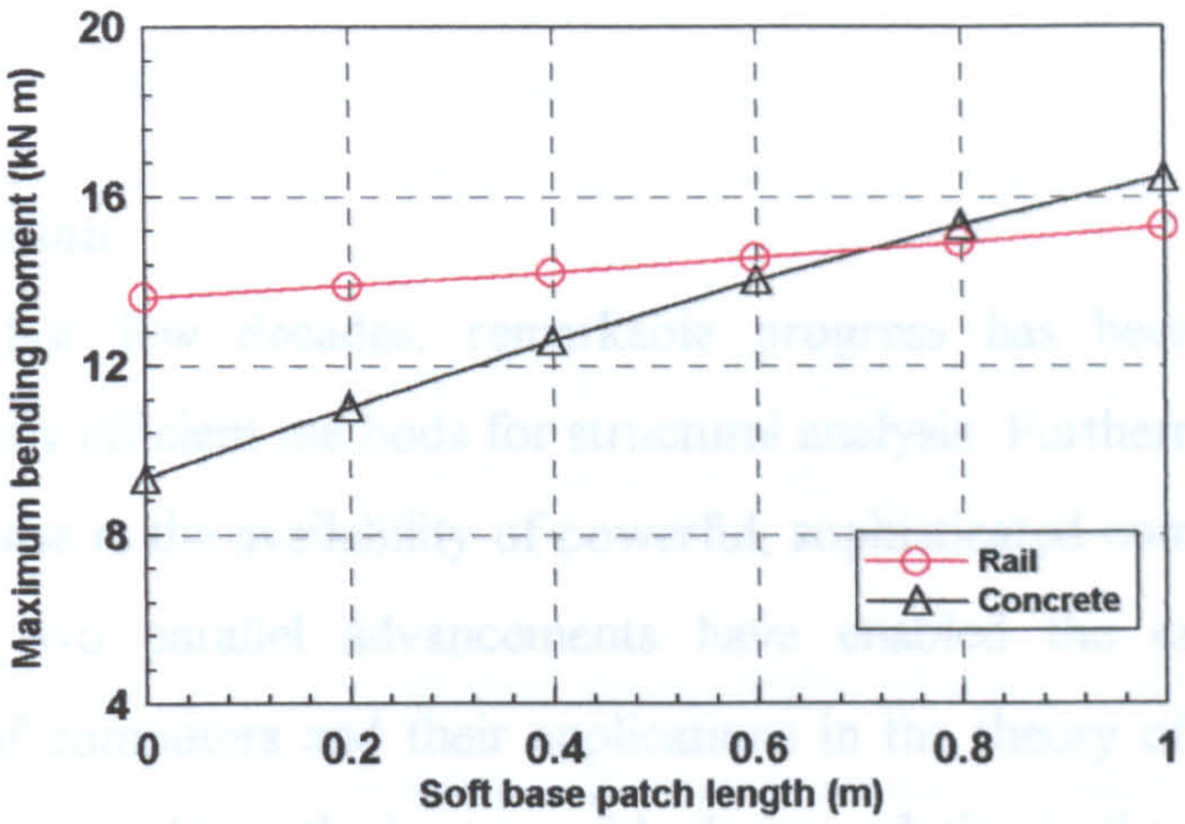

Fig. (6.22): Effect of soft base patch underneath the wheel load on the maximum bending moment of the track system.

CHAPTER SEVEN
THEORETICAL DESIGN OF THE LR55 TRACK SYSTEM

7.1 Introduction

During the last few decades, remarkable progress has been made in developing computationally efficient methods for structural analysis. Furthermore, there has recently been an increase in the availability of powerful, sophisticated computers at relatively low cost. These two parallel advancements have enabled the engineers to utilise the capabilities of computers and their applications in the theory of structural analysis and design in order to achieve the best possible design solution in the shortest time.

The LR551D program, as described in chapter 6, is a computer-based model to predict the behaviour of the track system under various loading and boundary conditions and to find the critical values of track responses that govern the design of its components. In this chapter, the concrete trough section is designed using a nonlinear optimisation technique. A purpose built computer program called OPTIM that acts interactively with LR551D program, is set up to perform the whole design optimisation process. The rail, pad and base are also systematically investigated to check their adequacies during the service life of the track system.

7.2 Critical Load Cases

A robust design of a track system should satisfy all the possible load cases due to the passing vehicles and environmental conditions that may be expected during the whole period of its service.

As a result of thorough analysis for the LR55 track system carried out in the previous chapters, three principal load cases have been found worth considering for the design of the LR55 track system as a street running transit system. They are:

1. Existence of a 1.0 m long cavity underneath the wheel load of 104.21 kN to simulate the case of a foundation subsidence due to a sudden collapse of 1.0 m diameter sewer pipe in the underlying surfaces, see Fig. (7.1).
2. Existence of a soft base patch underneath the wheel load of 104.21 kN to resemble the case of weakness in the track base, see Fig. (7.2).
3. Combined effect of wheel load (vertical), traction load (horizontal) and temperature variation, see Fig. (7.3). The traction load is taken as 40 kN by assuming a conservative coefficient of friction and adhesion of about 0.38 between the rail and the wheel load of 104.21 kN, (Cope 1993).

For each of those main critical load cases, eight possible combinations of wheel load position and foundation moduli were taken into account as follows:

1. Two positions of the wheel load. One at distance 3.0 m from a construction joint (i.e. at the centre of a concrete trough unit of 6 m length); and another directly above a construction joint. This will reflect the effect of moving load along the track system.
2. Two values of base modulus which are 25 and 45 N/mm^2. This will cover a practical wide range of track base stiffness in the vertical direction.
3. Two values of pad modulus which are 80 and 120 N/mm^2. This range will inherently take into account the change of the elastomeric pad material due to stress state condition within the pad and temperature effect on the pad.

Additionally, if the temperature rise and fall of the track system are considered, then there will be a resultant of 16 possibilities to be studied for load case 3.

The methodology adopted in the present work is first to design an optimum concrete trough section for load case 1; second to check the optimum section against load cases 2 and 3. Having decided upon a final optimum cross section for the concrete trough that satisfies all the three load cases, the LR55 rail, pad and the base are routinely examined under the same load cases. Following such a strategy will considerably reduce the size of the optimisation problem, as well as the limits for the maximum length of soft base patch and temperature variation can be accurately specified for safe performance of the LR55 track system as will be shown later.

7.3 Basic Definition of Structural Optimisation

The structural optimisation problem can be stated as, (Lund 1974, Rao 1978):

Find the set of (n) design variables,

$$\{x\} = (x_1, x_2, \ldots\ldots, x_n)$$

which minimises the objective function given by,

$$Z = f(\{x\}) = f(x_1, x_2, \ldots x_n) \tag{7.1}$$

subject to (m) behavioural (implicit) constraints,

$$g_j(\{x\}) = g_j(x_1, x_2, \ldots., x_n) \leq 0, \qquad j = 1, 2, \ldots., m \tag{7.2}$$

and (n) side (explicit) constraints,

$$\{L\} \leq \{x\} \leq \{U\} \tag{7.3}$$

where

$\{L\}$ = lower limit vector of the design variable point $\{x\}$

$\{U\}$ = upper limit vector of the design variable point $\{x\}$

In a structural optimisation problem, the design variables $\{x\}$ may be either continuous e.g. member dimensions and joint coordiantes, or discrete e.g. number of prestressing tendons in a concrete section and area of a standard steel section.

The objective function Z defined by eq. (7.1) is a scalar quantity of the design variables and represents the most important single property of the structural system such as the weight, cost or other measures of performance. The objective function (Z) is said to be linear when all the design variables have unit power and independent of each other, otherwise it is claimed to be nonlinear, (Himmelblau 1972, Rao 1978).

The constraints are, in general, restrictions to be satisfied in order for the design to be acceptable. The behavioural (implicit) constraints $g_j(\{x\})$ given by the inequality (7.2) are typically formed by actual responses of the structure to meet the requirements of stiffness, strength, stability ...etc. In most cases, they cannot be stated as explicit (direct) functions of the design variables, hence the name implicit constraints. Similar to the objective function, the behavioural constraints $g_j(\{x\})$ might be either linear or nonlinear. This largely depends on the method of analysis and assumption made to simplify the problem. In general, for most problems based on elastic theory, the constraints $g_j(\{x\})$

are normally nonlinear while those based on plastic theory, can be set in linear forms, (Moe 1974, Lund 1974, Vanderplaats 1982, Levy and Lev 1987).

The side (explicit) constraints expressed by inequality (7.3) are prescribed limitations (lower and upper quantities) imposed directly on the design variables. They represent some sort of physical constraints due to manufacturing, architectural purposes, functional requirements, ...etc. They are typically given by formulae presented in the design specifications such as minimum thickness of concrete slab, maximum amount of reinforcing steel in a concrete column, ...etc.

If the objective function and all the constraints are linear, then the optimisation problem is considered as linear, otherwise, it turns out to be nonlinear. In the real world, there are few structural optimisation problems which are entirely linear whereas the vast majority of the problems are nonlinear in nature.

7.4 Mathematical Solution of Structural Optimisation Problem

Structural optimisation problems may conveniently be solved using various mathematical techniques. Analytical methods, employing the theory of classical calculus or variational calculus, might be pursued to solve only simple and relatively small structural problems provided that the objective and constraint functions can be represented in well-defined mathematical expressions. In these analytical approaches, the optimum design is theoretically found exactly through the solution of a system of equations defining the conditions for optimality, (Moe 1974, Iyengar and Gupta 1981).

Numerical methods for solving structural optimisation problems are inevitably needed when the analytical approaches become either cumbersome or not applicable at all. Mathematical programming methods have been extensively utilised as efficient numerical tools for handling optimisation problems since the 1940's. At that time the term "programming" was synonymous with "planning" and was not used to describe the development of computer code. The advent and rapid growth of high resolution computers has recently stimulated further research on new methods. Consequently, numerous optimisation techniques have emerged that are based on the various branches

of mathematical programming such as linear programming, nonlinear programming, integer and mixed integer programming. In these numerical methods, a near-optimal design is sought in an iterative manner. An initial guess is used as a starting point for a systematic search for an increasingly better design. The search is terminated when certain criteria are satisfied which ensure that the current design is sufficiently close to the true optimum, (Dixon 1972, Rao 1978, Feiring 1986).

If the structural optimisation problem is linear, it may be appropriately solved using the linear programming algorithm known as the Simplex method of Dantzig, (Williams 1969, Thompson 1971, Srinath 1983).

Nonlinear problems could be tackled approximately by a sequence of linear programming problems. This is achieved by replacing the nonlinear objective and constraints functions by the first order term of their Taylor series expansion at a given initial point and thereby obtaining a corresponding linear programming problem. The solution of this linear programming problem is then used in place of the assumed initial point, yielding a sequence of linear programming problems, hence the name sequential linear programming, (Majid 1974, Rao 1978).

On the other hand, several optimisation algorithms have been devised that treat the objective function and the constraints in their basic nonlinear forms and as a result can provide greater generality and flexibility. Some examples of these methods are the direct search method of Rosenbrock, Complex method of Box, steepest decent methods, penalty function methods. Due to space limit, it is not possible to present a full explanation of all these methods. For further details, one may consult any text book of optimisation, (Dixon 1972, Himmelblau 1972, Majid 1974, Rao 1978, Kirsch 1981, Arora 1989).

It should be emphasised that none of the optimisation techniques developed so far are superior under all conditions since the practical applications have demonstrated that their efficiencies depend widely on the type of problem. Those which have a reasonable evidence, reliability, guarantee and faster rate of convergence are obviously preferred in structural optimisation, (Lund 1974, Arora 1989).

The Complex method of Box (1965) was adopted in this work to find the optimum design of the prestressed concrete trough due to the following reasons, (Box 1965, Rao 1978, Bunday 1984):

1. The Complex method has already been successfully applied in solving various structural optimisation problems and proved to converge rather rapidly, see for example (Lipson and Gwin 1977, Haque 1985).
2. The Complex method operates in design space for most structural problems where it is highly nonlinear; may be nonconvex and very irregular; and may contain discontinuities.
3. The Complex method does not require the time consuming partial derivatives (gradients) of the objective function and the constraints, which are necessary in many other nonlinear optimisation methods.
4. The method has a high probability of locating a global optimum due to the random search for feasible points.

7.5 Literature Survey of Structural Optimisation

The field of structural optimisation has been pursued quite vigorously by many researchers for the last few decades. As a result, substantial literature has been published and it is almost impossible to present a complete survey. Only those papers that deal with the optimisation of concrete structures are discussed below due to their relevancy to the present work.

Kirsch (1973) investigated the optimum design problem of prestressed concrete plates, formulated as a nonlinear programming model. The thickness of the plate, prestressing force and tendon configuration were taken as the design variables, while the structural material properties, plate shape, number of tendons and external loads were given as design parameters. The objective function was the cost of the material, set in terms of the plate thickness and the applied prestressing force. Only the stress constraints at selected points were considered. After certain simplifications, the entire optimisation problem was arranged in linear form and solved for the minimal plate thickness or minimal prestressing force using the Simplex algorithm.

Friel (1974) solved analytically the problem of optimum singly reinforced concrete rectangular sections using Lagrange multiplier procedure, (Rao 1978). A closed form equation was derived for the optimum ratio of steel to concrete. The objective function was the cost of the beam per unit length that comprised the cost of concrete, steel and formwork plus the cost of increasing the building height in order to provide space for the beam. A single constraint function was specified which was the ultimate moment requirement of the American Concrete Institute Building Code, (ACI 318-71 1971). Following a similar approach to Friel's work, Chou (1977) derived formulae for the optimum steel ratio and the optimum effective depth of reinforced concrete T-section including rectangular or slab sections as a special case. The problem was selected again to satisfy the requirements of the American Concrete Institute Building Code ACI 318-71 for the ultimate moment capacity.

Thakkar and Rao (1974) found an optimum solution for prestressed concrete pipes using the Simplex algorithm. The objective function was the cost of materials only. The other cost parameters of mortar cover, secondary reinforcement, labour and laying were assumed constant through out the problem. Three design variables were assigned: thickness of the pipe, number of longitudinal prestressing steel wires and number of circumferential prestressing steel wires per unit length of pipe. The constraints were derived from the safe behaviour at various loading stages specified by the Indian Standards Code of Practice for Prestressed Concrete Structures, (IS:784 1970, IS:1343 1960).

Andam and Knapton (1980) managed to find the optimum cost of a family of precast concrete portal framed buildings using nonlinear programming via the Rosenbrock algorithm, (Himmelblau 1972). The cost factors including fabrication, haulage, foundation, cladding and erection were studied. The specified design variables were the span length of the structure, number of spans, frame spacing and roof pitch height. The behavioural constraints were identified to satisfy the strength and stiffness requirements. The side constraints were set to satisfy the cost and client requirements such as building area and height to eave.

Naaman (1982) proposed an optimisation procedure for the design of prestressed concrete tension member to satisfy the requirements of ultimate strength, maximum allowable compressive stress, reinforcement, deflection and safety against cracking according to American Concrete Institute Building Code, (ACI 318-77, 1977). Using an acceptable design approximation, both the objective function and constraints were formulated as linear functions of two design variables namely the areas of concrete section and the prestressing steel. Thus, the problem was solved by a linear programming technique in which the objective function was to minimise the cost and/or the weight of the structural member.

Cohn and MacRae (1984) presented a procedure for the optimal design of simply supported concrete beams under distributed or concentrated loads using a nonlinear programming technique. This approach could handle reinforced concrete, full prestressed concrete and partial prestressed concrete beams of any cross section. The design variables for each section included the cross-sectional dimensions, amount of prestressing and non-prestressing steel. The imposed design constraints were taken to satisfy the requirements of the Canadian Code of Practice, (CSA/NBC 1977) with regard to the serviceability and ultimate limit states, limitation on steel reinforcements, ductility and minimum construction steel. The objective function represented the cost per unit length and could easily be adapted to design for minimum weight, minimum reinforcement or minimum prestress.

7.6 Optimal Design of the Concrete Trough Section

7.6.1 Design Variables

Consider a prestressed concrete trough section with the geometrical configuration shown in Fig. (7.4). The main factors that affect the optimum design of the section are the width (b_1) and depth (d_1) dimensions, number of prestressing tendon layers, eccentricity of each layer, number of tendons per each layer and the material properties of both the concrete and prestressing steel. To simplify the optimisation process, some of the mentioned factors could be taken as basic design variables, while others as design parameters where they are given pre-assigned constant values based on engineering judgement as discussed below.

The dimensions b_1 and d_1 were treated as basic design variables. They may acquire any continuous values, and then at the final design stage, will be rounded to the nearest practical integer figures. It should be emphasised that the other dimensions of the concrete trough section (b_2, b_3, b_4, b_5, d_2 and d_3) are fixed by the shape of the rail.

The concrete trough experiences sagging and hogging moment during its service life as shown in previous chapters 5 and 6. So, it is preferable to group the tendons in two layers, one placed near the bottom surface and the other near the top surface in order to achieve the greatest ultimate moment strength with a minimum prestressing force, (Goble and Lapay 1971, Naaman 1976). This, in turn, implies that the tendon layers eccentricities can only be varied within a narrow range. Therefore, it is more judicious to treat tendon layers and eccentricities as design parameters.

The number of tendons per each layer was taken as design parameters where each case was investigated separately. Otherwise the optimisation problem should be handled using mixed integer programming methods because there would be discrete variables (number of tendons) along with the continuous variables (b_1 and d_1 dimensions). However, such methods have proven to be too complicated, and inefficient in terms of computational time, (Lund 1974). The jacking force was assumed a constant value of 70% the characteristic strength of the tendon (f_{pu}) as recommended by BS8110 (1985).

The concrete compressive strength at transfer (f_{ci}) was taken as 30 N/mm^2 which is the minimum recommended value for a prestressed concrete structure as per BS8110 (1985). The concrete compressive strength at service (f_{cu}) was taken as 50 N/mm^2 since any higher strength concrete is rarely used, (Taylor 1992, Cope 1993). This is because higher strength concrete is too expensive. To give an example according to a recent quotation provided by Ready Mixed Concrete Limited, the cost of concrete per m^3 for grade 50, (i.e. f_{cu} = 50 N/mm^2) is £54 and that for grade 60 is £140. Such a sharp increase in the price is due to the indispensable need for using special chemical additives within the concrete mix to achieve the target strength above 50 N/mm^2 as well as a more strict quality control is required for producing higher strength concrete.

As a summary, the optimisation problem of the concrete trough has two design variables b_1 and d_1 which are, for convenience, will be termed as x_1 and x_2 respectively, while the prestressing steel areas and eccentricities and material properties are treated as design parameters.

7.6.2 Objective Function

As stated previously the objective function may be expressed in terms of weight or cost of the structural system. Weight objective function is quite common since it is the most easily quantified measure of merit. Cost is of a wider practical importance, but, it is not always possible to obtain sufficient data to define accurately the cost function since it involves several parameters that are changeable with time and vary from country to country. As far as a track system is concerned, setting a cost function is even more complicated as the total optimum cost depends on two main factors: the initial cost of track construction; and the maintenance cost. It is the second factor which is more important as it ensures safe, smooth and comfortable running of the train vehicles. Hence it forms a high percentage of the total cost of the track during its service life. This is why the ultimate objective in the design of a track system is to have ideally a maintenance free cost. In any case, maintenance cost study is beyond the scope of the present research. Accordingly, the objective function (Z) studied in the present work is to minimise the area of the concrete trough (A_c) (which implies minimum weight), i.e.:

$$Z = A_c \tag{7.4}$$

The area of the concrete trough is calculated by the subroutine SECT described in chapter 3. It should be noted that the objective function (Z) is nonlinear since the area (A_c) contains a product multiplication of the design variables ($x_1 = b_1$ and $x_2 = d_1$). The following derivation proves this statement, see Fig. (7.4):

$$\begin{aligned} A_c &= B\,D - d_2\,(b_3 + b_5)/2 - d_3\,[(2b_2 + b_3) + (2b_4 + b_3)]/2 \\ &= (2x_1 + 2b_2 + b_3)(x_2 + d_2 + d_3) - d_2\,(b_3 + b_5)/2 \\ &\quad - d_3\,(b_2 + b_3 + b_4) \qquad (7.5) \\ &= 2x_1x_2 + 2(d_2 + d_3)x_1 + (2b_2 + b_3)x_2 + (2b_2 + b_3)(d_2 + d_3) \\ &\quad - d_2\,(b_3 + b_5)/2 - d_3\,(b_2 + b_3 + b_4) \qquad (7.6) \end{aligned}$$

In mathematical terminology, the area (A_c) defined by eq. (7.6) is a nonlinear polynomial since it contains the product term (x_1x_2). Hence, the objective function Z is nonlinear which can be written in a general short form as:

$$Z = f(x_1, x_2) = f(\{x\}) \tag{7.7}$$

One can easily see that the objective function defined by eq. (7.7) resembles the one given by eq. (7.1).

Beside searching for the minimum area, the cost of producing 1 m long of the optimum concrete trough section was also investigated in order to envisage what sort of relationship does exist between the minimum area and the production cost. Based on the data supplied by Tarmac Precast Concrete Limited (a partner in the LR55 track project), the cost per metre length may be expressed in terms of concrete material, formwork, prestressing tendons and shear reinforcement as follows:

$$\text{Cost per metre length} = C_c A_c + C_f A_f + C_{ps} w_s A_{ps} + C_{sv} w_s V_{sv} \tag{7.8}$$

where

C_c = unit cost of concrete material. For concrete grade 50,

= £55 per m^3

C_c = unit cost of formwork,

= £50 per m^2

C_{ps} = unit cost of prestressing tendons,

= £600 per tonne

C_{sv} = unit cost of shear reinforcement,

= £600 per tonne

A_f = surface area of the formwork per metre length of the concrete trough

A_{ps} = area of the prestressing tendon

V_{sv} = volume of shear reinforcement per metre length

w_s = unit weight of steel,

= 7.857 tonne/m^3

Concerning the formwork, in practice the concrete trough is casted in an inverted way, i.e. upside-down as shown in Fig. (7.5) for a number of specific reasons. First, to achieve the necessary accurate dimensions of the inner faces in order to accommodate precisely

the shape of the LR55 rail. Second, to have a better rough bottom surface of the section which will enhance the frictional resistance of the track system with respect to the base. In such circumstances, the surface area of the formwork per metre length of the concrete trough (A_f) may be determined as, see Fig. (7.5):

$$A_f = 2D + 2b_1 + 2b_4 + b_5 + 2[d_3^2 + (b_2 - b_4)^2]^{1/2} + 2[d_2^2 + \{(b_3 - b_5)/2\}^2]^{1/2} \quad (7.9)$$

It must be emphasised that cost estimate for the concrete trough unit covered in the present study should not be taken for tendering purposes because the final cost will depend on other factors which are not included in eq. (7.8) such as handling, transportation, storage, overheads, ...etc.

7.6.3 Design Constraints

7.6.3.1 Behavioural (Implicit) Constraints

A feasible design of the prestressed concrete trough should satisfy the requirements of serviceability (transfer and service) and ultimate limit states which have already explained thoroughly in chapter 4.

At serviceability limit state, the behavioural (implicit) constraints may be defined either in terms of stresses or forces (moments). If they are expressed in terms of stresses, then 8 limitations have to be satisfied which are 4 at transfer (tensile and compressive stresses at both top and bottom fibres) and a similar 4 at service. On the other hand, if the constraints are set in terms of forces (moment of resistance) then only 4 restrictions have to be met which are sagging and hogging moments at transfer and service, see section 4.5 in chapter 4. Consequently, it is more advantageous to consider the moment constraints as this will reduce the number of constraints by half, hence giving rise to more efficient optimisation problem in terms of processing time. These constraints are:

- Transfer

  sagging: $(M_{t+})_{app} - (M_{t+})_{pro} \leq 0$ (7.10)

  hogging: $|(M_{t-})_{app}| - |(M_{t-})_{pro}| \leq 0$ (7.11)

- Service

  sagging: $(M_{s+})_{app} - (M_{s+})_{pro} \leq 0$ (7.12)

  hogging: $|(M_{s-})_{app}| - |(M_{s-})_{pro}| \leq 0$ (7.13)

where

$(M_{t+})_{app}$ = applied positive (sagging) moment at transfer as given by eq. (4.4), see section 4.5.3, chapter 4.

$(M_{t-})_{app}$ = applied negative (hogging) moment at transfer as given by eq. (4.7), see section 4.5.3, chapter 4.

$(M_{s+})_{app}$ = applied positive (sagging) moment at service, to be obtained by LR551D program for load case 1 explained in section 7.2.

$(M_{s-})_{app}$ = applied negative (hogging) moment at service, to be obtained by LR551D program for load case 1 explained in section 7.2.

$(M_{t+})_{pro}$ = provided positive (sagging) moment at transfer as given by eq. (4.15), see section 4.5.6, chapter 4.

$(M_{t-})_{pro}$ = provided negative (hogging) moment at transfer as given by eq. (4.18), see section 4.5.6, chapter 4.

$(M_{s+})_{pro}$ = provided positive (sagging) moment at service as given by eq. (4.21), see section 4.5.6, chapter 4.

$(M_{s-})_{pro}$ = provided negative (hogging) moment at service as given by eq. (4.24), see section 4.5.6, chapter 4.

At ultimate limit state, the concrete trough should have a sufficient factor of safety against failure. For a light rail sleeper (type EF29S) a factor of safety of 1.6 over the working load is recommended, (Taylor 1992). As the LR55 track system is meant for light rail transit, same factor of safety may be adopted for the prestressed concrete trough. Therefore, the flexural constraints for the ultimate limit state can be written as:

sagging: $$1.6\,(M_{s+})_{app} - (M_{u+})_{pro} \leq 0 \qquad (7.14)$$

hogging: $$1.6\,|(M_{s-})_{app}| - |(M_{u-})_{pro}| \leq 0 \qquad (7.15)$$

where

$(M_{u+})_{pro}$ = provided positive (sagging) moment at ultimate to be calculated numerically as explained in section 4.6, chapter 4.

$(M_{u-})_{pro}$ = provided positive (hogging) moment at ultimate to be calculated numerically as explained in section 4.6, chapter 4.

The shear constraints at ultimate limit state may be expressed as:

$$1.6\,(V_s)_{app} - V_{per} \leq 0 \qquad (7.16)$$

where

$(V_s)_{app}$ = applied shear force at service, to be obtained by LR551D program for load case 1 explained in section 7.2.

V_{per} = maximum permitted shear force by the concrete trough section necessary to prevent web crushing which is, (see section 4.7.3):

$= \min (0.8\ b_v\ d\ \sqrt{f_{cu}}\ ,\ 5\ b_v\ d)$

It is well known that the internal forces (moments and shear) are nonlinear functions of the cross-sectional properties of the concrete trough (area and moment of inertia) which in turn are nonlinear functions of the design variables ($x_1 = b_1$ and $x_2 = d_1$). Therefore, the behavioural constraints defined by the 7 inequalities (7.10) - (7.16) are highly nonlinear functions in terms of x_1 and x_2, which can be written alternatively in a general compact form as:

$$g_j (x_1, x_2) \leq 0 \qquad j = 1, 2, \ldots 7 \qquad (7.17)$$

One can easily find the similarity between inequality (7.17) and (7.2).

It is worthwhile to mention that the deflection constraint was not included for the following reasons:

1. It was shown through the examples demonstrated previously that the deflection of the track system is within the acceptable limits for a wide range of pad and base moduli.
2. The deflection constraint was found to marginally affect the optimum flexural design of prestressed concrete beams, (Lounis and Cohn 1993).
3. According to the personal communication between the author and Dr. H. Taylor (Technical director of Tarmac Precast Concrete Limited), the latter emphasised that even a deflection of 10 mm is acceptable as far as the stresses in the section are within the permissible limits. This implies that deflection constraint hardly influences the optimum design of the prestressed concrete trough section.

Thus, the deflections both at transfer and service of the concrete trough were left to be checked at the final stage of the design process.

7.6.3.2 Side (Explicit) Constraints

The lower limits of the design variables, width ($x_1 = b_1$) and depth ($x_2 = d_1$) cannot be taken less than 75 mm owing to reasons of practicality that involve providing enough space within the concrete trough shape to accommodate the prestressing tendons and shear links arrangements as well as offering sufficient amount of concrete cover to protect the steel against corrosion.

The upper limits of the design variables ($x_1 = b_1$) and ($x_2 = d_1$) can theoretically take very large values. For instance, the dimension ($x_1 = b_1$) may be chosen such that the total width of the concrete trough will be around 1432 mm which represents the rail gauge, (Esveld 1989, Cope 1993). As for the dimension ($x_2 = d_1$), there is no theoretical upper bound. However, for sake of an efficient optimisation process, it is preferable to reduce the range between the lower and upper limits, i.e. assigning smaller values for the upper limits. Therefore, based on engineering inspection, the upper limits of x_1 and x_2 were selected as 140 mm and 195 mm respectively which correspond to a total width (B) of 500 mm and depth (D) of 300 mm. As a result, the side constraints for the design variables (x_1) and (x_2) can be expressed as:

$$\{L\} \leq \{x\} \leq \{U\} \tag{7.18}$$

where

$$\{L\} = (75, 75)$$

$$\{U\} = (140, 195)$$

$$\{x\} = (x_1, x_2)$$

It is quite obvious that the side constraints given by inequalities (7.18) is similar to that defined by inequality (7.3).

7.6.4 Optimisation Procedure

The nonlinear optimisation problem of the prestressed concrete trough section was tackled using the Complex method (Box 1965) for reasons mentioned previously in section 7.4. The main steps of the optimisation procedure are briefly illustrated in the following:

1. Specify an initial feasible point $\{x\}_1$. In other words the initial point should satisfy all the constraints given by inequalities (7.17) and (7.18).

2. Generate randomly a set of additional (k-1) points in such a way that the side (explicit) constraints defined by inequality (7.18) are automatically satisfied. The set of k points (vertices) forms a geometric figure called a "Complex". Box (1965) recommended the value of k = 2n (where n is the total number of design variables. For this particular problem n = 2) because it was found from a parametric study that a smaller Complex has a tendency to collapse prematurely. The (k-1) points are found by the use of random numbers lying in the interval (0, 1) as:

$$x_{i,j} = L_j + r_{i,j} (U_j - L_j) \qquad (7.19)$$

where

$x_{i,j}$ = jth component of point $\{x\}_i$

L_j = jth component of the lower limit vector $\{L\}$

U_j = jth component of the upper limit vector $\{U\}$

$r_{i,j}$ = a random number in the range 0 to 1 . It is generated by using an intrinsic function built within the computer language.

i = 2, 3, ... k

j = 1, 2, ... n

3. Move any of the (k-1) points, that do not satisfy the behavioural (implicit) constraints given by inequality (7.17), halfway towards the centroid of those already accepted points ($\{x\}_c$). This may be expressed mathematically as:

$$\{x\}_i \text{ (new)} = (\{x\}_i + \{x\}_c)/2 \qquad (7.20)$$

where

$$\{x\}_c = \left(\sum_{e=1}^{i-1} \{x\}_e\right) /(i - 1) \qquad (7.21)$$

If the trial point $\{x\}_i$ found by eq. (7.20) is still not feasible, the process of moving halfway towards the centroid $\{x\}_c$ is continued again and again until all the behavioural constraints are satisfied. If the number of trials for finding the feasible points exceeds a specified limit (ξ_1) without any success, then a different initial point $\{x\}_1$ has to be selected, and the solution restarted as a fresh problem. By processing in this way, one will ultimately be able to find the required feasible points $\{x\}_1, \{x\}_2, ..., \{x\}_k$ which form the vertices of the Complex.

4. Evaluate the objective function $Z = f(\{x\})$ defined by eq. (7.7) at each of these k points (vertices).
5. Order these k points according to the magnitude of the corresponding function values and record the lowest (best) objective function value.
6. Define the point with highest (worst) function value ($\{x\}_h$) and form the centroid ($\{x\}_o$) of the other (k-1) points as:

$$\{x\}_o = \left(\sum_{\substack{j=1 \\ j \neq h}}^{k-1} \{x\}_j\right) /(k - 1) \qquad (7.22)$$

7. Replace the point $\{x\}_h$ with a new point $\{x\}_r$ by reflecting it on the centroid $\{x\}_o$ along a line joining $\{x\}_h$ and $\{x\}_o$ points as:

$$\{x\}_r = (1 + \alpha)\ \{x\}_o - \alpha\ \{x\}_h \qquad (7.23)$$

where

α = reflection factor. Box (1965) suggested,

= 1.3

8. Test the reflected point $\{x\}_r$ for feasibility as follows:

a. If the lower limit (L_j) is violated, then move the point $\{x\}_r$ inside the boundary of the violated side constraint (L_j), i.e.

$$x_{r,j} = L_j + 10^{-6} \qquad (7.24)$$

b. If the upper limit (U_j) is violated, then move the point $\{x\}_r$ inside the boundary of the violated side constraint (U_j), i.e.

$$x_{r,j} = U_j - 10^{-6} \qquad (7.25)$$

where

$x_{r,j}$ = jth component of point $\{x\}_r$

c. If any of the behavioural constraints $g_j(\{x\})$ are violated, then move the point $\{x\}_r$ halfway in towards the centroid, i.e.

$$\{x\}_r \text{ (new)} = (\{x\}_r + \{x\}_o)/2 \qquad (7.26)$$

As long as the point $\{x\}_r$ is modified according to either eq. (7.24), (7.25) or (7.26), checking for feasibility has to be tried again, i.e. repeating step 8 until a feasible point can be obtained. However, if the number of trial reflections exceeds

a predetermined limit (ξ_2), with or without any success, the procedure will be automatically terminated because the Complex seems to be either flattened against one of its boundaries (side constraints) or collapsed into its centroid. In such a case the current point $\{x\}_r$ does not guarantee an optimum solution.

9. Find the objective function $f(\{x\}_r)$ at this new trial point $\{x\}_r$ and compare it with the highest (worst) objective function value $f(\{x\}_k)$ (which corresponds to point $\{x\}_k$ since the function values have been ordered) as follows:

   a. If $f(\{x\}_r) \geq f(\{x\}_k)$, then move the point $\{x\}_r$ half way towards the centroid $\{x\}_o$, i.e.:

   $$\{x\}_r \text{ (new)} = (\{x\}_r + \{x\}_o)/2 \qquad (7.27)$$

   and then return to step 8

   b. If $f(\{x\}_r) < f(\{x\}_k)$ then replace the point $\{x\}_r$ by $\{x\}_k$ and reorder the points and objective function values of the Complex.

10. Test the convergence of the problem by calculating the variance (s) of k function values and the maximum distance (d_m) between two points of the Complex. The variance (s) is required to see how the feasible points are scattered with respected to their centroid. It may be determined as, (Bunday 1984):

$$s = \{\sum_{e=1}^{k} [f(\{x\}_e)]^2 - [\sum_{e=1}^{k} f(\{x\}_e)]^2 / k\} / k \qquad (7.28)$$

The requirement for maximum distance (d_m) gives an indication of how the size of the Complex shrinks. It can be found as, (Bunday 1984):

$$d_m = \max \{[\sum_{e=1}^{n} (x_{i,e} - x_{j,e})^2]^{1/2}\} \qquad (7.29)$$

where

$i = 1, 2, \ldots, k-1$

$j = i+1, i+2, \ldots, k$

If the quantities (s) and (d_m) are smaller than prescribed small parameters ξ_3 and ξ_4 respectively (these parameters depend on the nature of the design variables and objective function), one may assume convergence of the problem and hence the

optimum solution is deemed to be achieved. Otherwise return to step 6 and repeat the process.

11. Record the optimum point $\{x\}_1$ and the minimum objective function $Z = f(\{x\}_1)$ since the function values have been ordered, and terminate the problem.

7.6.5 Characteristics of Program OPTIM

A purpose built design optimisation program named as "OPTIM" was established to find the minimum area of the perstressed concrete trough section. The program OPTIM was coded in FORTRAN 77 for P.C. machines and its flow chart is shown in Fig. (7.6). The main characteristics of OPTIM program are:

1. The cross-sectional properties of the concrete trough (area, elastic section modulus, moment of inertia, ...etc.) for any defined values of the design variables ($x_1 = b_1$) and ($x_2 = d_1$) are calculated by calling the subroutine SECT. This subroutine was explained in detail in chapter 3.
2. Subroutine PRESTR presented in chapter 4, is used to determine the provided (resistant) moment and shear of the concrete trough section at serviceability and ultimate limit states for any set of design variables ($x_1 = b_1$) and ($x_2 = d_1$) during the optimisation process.
3. The applied moments and shear force are given as input data to the program OPTIM. These forces are obtained by analysing the track system using the LR551D program for an assumed trial section of the concrete trough subjected to load case 1 explained in section 7.2. This means that the two programs OPTIM and LR551D are manually interacted which can be justified as follows. It is found that when the two programs LR551D and OPTIM are linked together, the resulting program becomes too large for the memory of the available P.C. machine. More interestingly, the manual interaction approach has not shown to be tedious as only very few (in most cases no more than 2) interactive attempts are required between the LR551D and OPTIM programs so as to find the optimum solution.
4. Subroutine CONSTRN was set to calculate the behavioural constraints defined by inequality (7.17) and to check the feasibility of the design variables versus the implicit and explicit constraints during the optimisation process. If it is wanted, for any reason, to have a different set of constraint functions, OPTIM program can still

be used provided that the subroutine CONSTRN is amended accordingly to suit the new constraints.

5. The stopping and convergence criteria (ξ_1, ξ_2, ξ_3 and ξ_4) mentioned earlier are found to be dependent on the nature of the problem namely: number and dimensional units of the design variables; objective function; number of the implicit constraints; side constraints and the assumed starting initial point. After several trials, the following values are suitable to be assigned for these parameters in the OPTIM program:

   $\xi_1 = 100$, $\xi_2 = 200$, $\xi_3 = 0.1$ and $\xi_4 = 0.1$

6. The program is run as a batch job where all the input data are read from a text edited file, while the necessary output results are printed into another text edited file.

7.6.6 Solution of the Problem

The solution of the design optimisation problem for the concrete trough section can be started by assuming the following data:

1. Concrete compressive strength at transfer $f_{ci} = 30$ N/mm^2.
2. Concrete compressive strength at service $f_{cu} = 50$ N/mm^2.
3. Prestressing tendon of 7-wire strand having diameter $\phi = 9.3$ mm, as requested by Tarmac Precast Concrete Limited because of their prestressing factory standards. The nominal area of this particular tendon = 52 mm^2, and the characteristic strength $f_{pu} = 1770$ N/mm^2 as per BS5896 (1980). It is to be noted that any other prestressing steel can be equally considered within the OPTIM program without affecting its generality.
4. The prestressing jacking force = 0.7 f_{pu}.
5. Number of tendons at the bottom layer = 6 which gives a total area of prestressing steel at this level = 52 x 6 = 312 mm^2. The number of tendons at the top layer = 2, one in each web of the concrete trough, i.e. total area of prestressing steel at this level = 52 x 2 = 104 mm^2.
6. The concrete cover measured from the extreme bottom fibre to the centroid of the bottom tendon layer = 40 mm. Similarly, the concrete cover measured from the extreme top fibre to the centroid of the top tendon layer = 40 mm. These covers

will indirectly define the eccentricities of the tendon layers with respect to the centroid of the concrete trough section.

7. Shear link diameter = 6 mm and its characteristic strength $f_{yv} = 250$ N/mm^2.

Twenty different initial design variables (b_1) and (d_1) were chosen arbitrarily to start the optimisation process in order to ensure obtaining the global optimum solution rather than the local optimum. The OPTIM program was used to search for the dimensions ($x_1 = b_1$) and ($x_2 = d_1$) that minimise the area of the concrete trough section. The results are presented in Table (7.1).

It can be seen that all the different initial points except the last two leads to almost the same optimum values, $b_1 \cong 84.5$ mm and $d_1 \cong 75.0$ mm) which might be confidently claimed as the global minimum point. Alternatively, the last two points may be regarded as local optima and hence may be ignored. Such an observation demonstrates the fact that the Complex method has a high probability of locating a global optimum due to the randomly generated feasible points. Rounding the figures to the nearest digit, the optimum dimensions for b_1 and d_1 can be assumed as 85 and 75 mm respectively, which correspond to a total width B = 390 mm and depth D = 180 mm.

It may also be noted that some cases of starting initial points cause the problem to converge after over 100 objective function (Z) evaluations (the latter was taken as a measure for rate of convergence). In other cases, the optimum solution was achieved in less than 50 objective function evaluations. This reveals that there is no ideal means of guessing the initial point, but instead, it is a mere trial and error experiment. However, the average number of function evaluations can be said to be around 70 for most cases, see Table (7.1). It is worthwhile to mention that even for the case with highest number of function evaluations (case 4), the computing time required to solve the problem on P.C. machine with 486 microprocessor is less than 1 minute.

Having found the optimum width and depth of the concrete trough section, the LR551D program was used again to calculate the applied moment and shear forces for this section because the initial forces were based on a different assumed section. The results are presented in Table (7.2) and compared with the provided (resistant) moment and shear

forces. It is see that all the moments and shear forces at serviceability and ultimate limit states are satisfied except the hogging moment at service where there is only a marginal discrepancy of 2.62% (compare the provided moment = -10.78 kN m with the applied one = -11.07 kN m). Such a difference might be judged as practically insignificant and hence can be reasonably accepted. Interestingly, it is found that when the cover for the bottom tendon layer is increased from 40 to 41 mm (i.e. by 1 mm), the provided hogging moment at service becomes -11.09 kN m (which is now satisfactory), and at the same time the other resistant forces are slightly altered, but remain within acceptable limits. In the author's opinion, there is no practical difference between 40 and 41 mm concrete cover as it would be within manufacturing tolerance. However, just to be on the safe side, the concrete trough (with bottom tendon layer cover = 41 mm) will be considered the right one. It is to be noted that in Table 7.2, case 1 (40/40) means the bottom and top tendon layer have 40 mm cover; case 2 (41/40) means the bottom tendon layer has 41 mm cover while the top one has 40 mm cover.

The second critical (near active) constraint was found to be the ultimate sagging moment (compare applied sagging moment of 33.9 kN m with the provided one of 34.33 kN m). This means that the optimum concrete trough section has two stringent constraints which are the hogging moment at service and the sagging moment at ultimate.

It can be seen that the moment constraints at transfer are not critical at all as the applied moments are much smaller than the provided ones due to the small effect of the concrete self weight compared to the design wheel load. This leads to an interesting conclusion that the initial compressive strength of the concrete (f_{ci}) need not be taken higher than 30 N/mm^2.

It was found that minimum shear reinforcement using links of 6 mm diameter at spacing of 100 mm centre to centre is sufficient. This can be justified as the applied shear force V_u = 62.02 kN is less than actual shear capacity of the concrete section V_c = 74.56 kN but greater than $0.5V_c = 0.5 \times 74.56 = 31.01$ kN as explained in section 4.7.3, chapter 4.

7.6.6.1 Effect of Number of Prestressing Tendons

As mentioned previously that the number of prestressing tendons is treated as a design parameter. It is intended to investigate the effect of number of prestressing tendons, i.e. prestressing steel area, on the optimum cross-sectional area of the concrete trough. Three different cases were selected as follows:

Case 1: using 8-ϕ 9.3 mm diameter of 7-wire strand tendons, (6 tendons at the bottom layer and 2 at the top layer), i.e. total area of prestressing steel = 416 mm^2.

Case 2: using 7-ϕ 9.3 mm diameter of 7-wire strand tendons, (5 tendons at the bottom layer and 2 at the top layer), i.e. total area of prestressing steel = 364 mm^2.

Case 3: using 6-ϕ 9.3 mm diameter of 7-wire strand tendons, (4 tendons at the bottom layer and 2 at the top layer), i.e. total area of prestressing steel = 312 mm^2.

Case 1 has already been solved in section 7.6.6 and the optimum section is found to be B x D = 390 x 180 mm. Following exactly the same systematic procedure as for case 1, the optimum concrete trough section for case 2 is shown to be B x D = 370 x 195 mm, and that corresponding to case 3 is B x D = 370 x 205 mm. The main characteristics and cost for the three different alternative optimum sections are listed in Table (7.3) from which the following points can be extracted:

1. Case 1 has the lowest cross sectional area of the three optimum concrete trough sections (compare 53578 mm^2 versus 55735 and 59435 mm^2). At the same time, section 1 seems to be the least expensive in terms of production cost per metre length of the concrete trough unit, (compare £53.79 versus £53.99 and £54.84), although it has the largest amount of prestressing steel area. This finding leads to an interesting conclusion that the design of concrete trough for minimum area also yields the minimum cost of producing 1 m long of the concrete trough element.
2. As the area is directly proportional to the weight, case 1 gives the least weight among the three optimum sections (compare 129 kg/m versus 134 and 143 kg/m). This implies concrete trough section of B x D = 390 x 180 mm is relatively easier to handle which is an advantage to be considered during lifting and transporting process.
3. Case 1 has the shallowest depth among the three optimum sections, (compare 180 mm versus 195 and 205 mm) which entails least depth of excavation. This is one of

the most important design aspects of the LR55 track system where the depth of the foundation is desired to be as minimum as possible.

4. Case 1 has the widest breadth among the three sections (compare 390 mm versus 370 mm). This has the advantage of producing better pressure distribution on the track base due to greater contact area between the concrete trough and the supporting base.
5. Case 1 necessitates the least volume of excavation (compare 70200 mm^3 versus 72150 and 75850 mm^3). The smallest volume also inherently implies least storage space required to occupy the same number of concrete trough units. This consequently has an advantage of saving some extra costs incurred from excavation and storage.
6. Owing to the points 1-5 mentioned above, concrete trough section of B x D = 390 x 180 mm may be nominated as the best among the three alternative optimum sections being investigated. Therefore, it is highly recommended as a viable design for the LR55 track system.
7. A lateral conclusion is that the total cost of the concrete trough unit is largely dominated by the cost of formwork as the latter shares, on average, around 88%, while the concrete material 6%, prestressing steel 3% and shear reinforcement 3%, see Table (7.3). This means that the total production cost of the concrete trough might be appreciably reduced if it is possible to cut down the cost of the formwork. It is to be emphasised that these figures are only related to the UK standards of manufacturing prestressed elements. In some other countries such as developing countries where the prestressing technology is very expensive and the steel is not locally available, but the workmanship is relatively cheap, it is most likely to expect a completely different answer concerning the production cost and its governing factors.

7.6.6.2 Checking the Concrete Trough against Load Case 2

It is required to check the adequacy of the optimum concrete trough section (B x D = 390 x 180 mm) against load case 2 where a soft base patch exists underneath the wheel load. This soft patch was assumed to have a modulus of 5 N/mm^2, which represents the extreme case of soft track base (see section 5.3, chapter 5), and a range of length between 1.4 and 2.2 m. The LR55 track system was analysed by running the LR551D

program for each of these lengths taking into account the eight possible combination of wheel load position and foundation moduli as discussed earlier in section 7.2. The results are presented in Table (7.4). It is found that the applied maximum sagging moments are due to the case where the wheel load is at distance 3.0 m from the construction joint. However, the applied critical hogging moments correspond to the case where the wheel load is directly above the construction joint. These critical values of applied moments occur when the base and pad moduli are 45 and 120 N/mm^2 respectively. The provided (resistant) hogging and sagging moments of the concrete trough were obtained by using TROUGH program (a program which determines all the characteristics of a prestressed concrete section for specified dimensions and applied design forces, as explained in section 4.9, chapter 4). The results are shown on the same Table (7.4) for sake of comparison and ease of locating the maximum permitted length of a soft base patch that the track system can sustain safely without failure.

Referring to Table (7.4), it can be seen that the critical length of the soft base patch is round 1.8 m where the applied hogging moment (-11.05 kN m) is just below the provided one (-11.07 kN m) which is satisfactory. It is interesting to note that the sagging moment is not critical for the whole range of soft patch length and there is a margin of safety of (25.19 / 20.49 = 1.22) at the length of 1.8 m for the soft base patch.

As a concluding remark from this investigation, the track system can safely resist the design wheel load of 104.21 kN when it passes over a soft patch of 1.8 m long, an incident which might occur in practice as a result of weakness in the track base due to any reason.

7.6.6.3 Checking the Concrete Trough against Load Case 3

It is required to check the optimum concrete trough section against load case 3 where the combined effect of vertical wheel load of 104.21 kN, horizontal traction load of 40 kN and temperature change was considered simultaneously. A range of temperature variation between ±20 and ±30 °C is examined in order to find the maximum temperature change that the concrete trough can withstand before any allowable stresses are violated. It should be emphasised that the temperature variation was assumed uniform across the whole depth of the track system which is on the safe side. In fact, the actual temperature

distribution within the LR55 track components is nonuniform and might only be determined to a certain degree of accuracy by following the theories of heat transfer for solid bodies, a subject which is beyond the scope of the present work. The coefficient of thermal expansion for the rail steel material is 12 x 10^{-6} per °C (as given in Table 3.2), and that of the concrete is 10 x 10^{-6} per °C, (Macleod 1990).

Using the LR551D program, the track system was analysed for each case of wheel load position, temperature change, and base and pad moduli to search for the critical sections where maximum axial forces (compression or tension) exist together with maximum bending moments (sagging or hogging). The results are presented in Table (7.5) where a positive axial force/stress means compression and a positive bending moment means sagging.

By employing the TROUGH program, the extreme bottom and top fibre stresses of the concrete trough were calculated at the critical sections and compared with the permissible values. For concrete characteristic strength f_{cu} = 50 N/mm^2, the allowable stresses at service are, (see Table (4.1), chapter 4):

allowable compressive stress (f_{cs}) $= 0.48\ f_{cu}$

$= 0.48 \times 50$

$= 24$ N/mm^2

allowable tensile stress (f_{ts}) $= -0.64\ (f_{cu})^{0.5}$

$= -0.64 \times (50)^{0.5}$

$= -4.525$ N/mm^2

It is shown that when the temperature drops by 25 °C, the tensile stress at top fibre reaches a value of -4.455 N/mm^2 which is very close to the allowable limit of -4.525 N/mm^2 (the difference is only 0.07 N/mm^2). As the temperature falls by 30 °C, the tensile stress at top fibre (-5.455 N/mm^2) becomes unacceptable as it exceeds the permissible value of -4.525 N/mm^2. For a temperature rise by up to +30 °C, the top and bottom stresses remain within the admissible limits. This is because any temperature increase creates compressive stresses across the concrete section which will cancel out the effect of tensile stresses due to bending, but will add to bending compressive stresses. The resultant will be large compressive stress and little or no tensile stress within the concrete

section. However, this is not problematic because concrete material is reputed for its relatively high compressive strength compared to tension (e.g. its allowable compressive stress is 24 N/mm^2 and the tensile stress is -4.525 N/mm^2).

As a conclusion, the recommended maximum temperature variation that the concrete trough may sustain, can be safely stated between -25 and +25 °C. It should be noted that the expected temperature change for the LR55 track system is practically smaller than the range ±25 °C. This is because both the rail and the concrete trough are not fully exposed to the direct ambient atmosphere as is the case for conventional rail system. For instance, over 50% of the rail surface area and 80% that of the concrete trough are sealed and surrounded by thermally stable materials (elastomeric pad, pavement wearing surface and base course materials).

7.7 Checking the LR55 Rail

Once the optimum design of the prestressed concrete trough is fulfilled, it is a straightforward procedure to check the behaviour of the LR55 rail subject to the same load cases discussed in section 7.2. The maximum axial and bending forces at the critical rail sections are obtained from the analysis of the LR55 track system using LR551D program for each of these possible load cases and presented in Table (7.6).

The stresses (σ_z) in the rail due to a bending moment (M_x) can be calculated using the flexural formula for an unsymmetrical section given by eq. (3.1), see section (3.3), i.e.

$$(\sigma_z)_{bending} = M_x (yI_y - x I_{xy}) / (I_y I_x - I_{xy}^2) \qquad (7.30)$$

Based on mechanics of materials, the direct stress due to axial force is simply the force (N) divided by area (A), (Benham and Warnock 1976), i.e.

$$(\sigma_z)_{direct} = N/A \qquad (7.31)$$

Owing to the principle of superposition for elastic structures, the resultant stress at any fibre of the rail section due to the combined effect of axial force and bending moment is the algebraic sum of the stresses defined by eqs. (7.30) and (7.31), i.e.:

$$\sigma_z = N/A + M_x (yI_y - x I_{xy}) / (I_y I_x - I_{xy}^2) \quad (7.32)$$

Referring to section 3.3, the required constant data of the LR55 rail for finding the maximum stresses in the rail according eq. (7.32) are:

$A = 67155.5\ mm^2$

$I_x = 377.328 \times 10^4\ mm^4$

$I_y = 834.634 \times 10^4\ mm^4$

$(I_y I_x - I_{xy}^2) = 313020.913 \times 10^8\ mm^8$

The x coordinate of the critical top fibre = 47.641 mm

The y coordinate of the critical top fibre = 37.143 mm

For the critical top fibre, $(yI_y - x I_{xy}) = 3.30828 \times 10^8\ mm^5$

The x coordinate of the critical bottom fibre = -27.296 mm

The y coordinate of the critical bottom fibre = -41.841 mm

For the critical bottom fibre, $(yI_y - x I_{xy}) = -3.61148 \times 10^8\ mm^5$

The calculated stresses at the critical bottom and top fibres of the rail are presented in Table (7.6). It is found that the maximum tensile stress experienced by the rail is 278.169 N/mm^2 which corresponds to load case 1 as shown in Table (7.6). This figure is well below the yield stress of 467 N/mm^2 for normal grade rail steel used for the LR55 rail, see Table (3.2).

In order to investigate the buckling of the rail due to a compressive stress of 254.816 N/mm^2 (see Table 7.6), the unsupported buckling length of the rail has to be specified. The critical buckling stress (σ_{cri}) of the rail acting as a strut can be determined as, (Gere and Timoshenko 1985):

$$\sigma_{cri} = \pi^2 E / (L_{eff}/r_{min})^2 \quad (7.33)$$

where

E = Young's modulus of the material. For steel rail, (see Table (3.2), chapter 3):

$= 200\ 000\ N/mm^2$

L_{eff} = effective length (unsupported length) of the member

r_{min} = minimum radius of gyration. From Table (3.1),

$= 23.6$ mm

By making $\sigma_{cri} = 254.816$ N/mm^2 and substituting the values of E and r_{min} into eq. (7.33) and then solving for L_{eff} gives

$$L_{eff} = 2077.1 \text{ mm, say } 2.0 \text{ m}$$

This means that only when about 2.0 m length of the rail is completely separated from the pad and becomes fully unrestrained over this length, then buckling might occur. However, by engineering judgement such a thing is almost impossible to happen because the rail is continuously supported by the concrete trough and fixed in position by the elastomeric pad which has an excellent adhesion characteristics proven by field trials. The bonding of the pad to the rail and concrete trough has experienced vigorous tests under extreme environmental conditions (high and low temperature and submersed under 10 mm of water, as discussed in section 3.3.2, chapter 3), yet no sign of debonding was witnessed, (Sika 1990, ALH 1992 and 1996, Lesley and Al-Nageim 1996). In practice, the chance of having bond failure of pad is primarily and most probably due to poor quality of workmanship during installation, (i.e. construction mistake) when the surfaces of the rail and concrete trough are not properly cleaned and dusted before injecting the elastomeric pad.

As a conclusion, the buckling resistance of the rail seems to be ensured under such a high compressive stress of 254.816 N/mm^2.

7.8 Checking the Deflection of the Track System

For reasons mentioned earlier, checking the deflection of the track system had been left until the concrete trough was designed. It is required to examine the deflection of the optimum concrete trough section B x D = 390 x 180 mm at transfer and service as well as the deflection of the LR55 rail at service.

Using the TROUGH program, the camber due to prestressing at transfer is found to be 0.425 mm upward. There is no specified limit on camber by BS 8110 (1985). However, it is good practice to have a small value of camber. This is because excessive camber will create difficulties in setting the vertical alignment of the concrete trough units along the track system. Tarmac Precast Concrete Limited suggests that the camber should

preferably be less than 1 mm for the 6 m long concrete trough unit). Accordingly, the camber of 0.425 mm for the optimum concrete trough section seems to be acceptable as it is too small to cause any practical problems.

Using the LR551D program, the maximum recorded downward deflections of the LR55 rail and concrete trough at service are found to be 4.185 and 3.328 mm respectively. This occurs when the wheel load is directly above the construction joint (the end of a concrete trough unit). It is also seen that the maximum upward deflection of the rail is 0.223 mm and that of the concrete trough is 0.224 mm which corresponds to the same loading and boundary condition mentioned above.

These figures are less than the maximum permissible track deflection of 4.0 - 5.0 mm according to British practice (Sperring 1992, Cope 1993) or 6.4 mm according to American practice (Tayabji 1976).

7.9 Checking the Base and Pad

Finally, it is required to check the behaviour of base and pad when the track system is subjected to the load cases mentioned in section 7.2. Using the LR551D program, the maximum values of the track base pressure and pad compressive, tensile and shear stresses were determined for each of these load cases. The results are shown in Table (7.7).

It can be seen that the maximum pressure on the base is 372.90 kN/m^2 which corresponds to load case 1. The recommended permissible pressure directly underneath the track system is round 450 kN/m^2, (Hay 1982, FIP 1987), which is well above the critical recorded pressure of 372.9 kN/m^2 experienced by the track base.

The maximum compressive stress in the pad is 0.692 N/mm^2 which is very small compared to the capacity of pad in taking compression up to 3.2 N/mm^2 without failure, as shown in Table (3.3) of chapter 3. Similarly, the maximum tensile stress in the pad is 0.298 which is less than the lower bound of the pad tensile strength of 2.8 N/mm^2 as given by Table (3.3). The shear stress in the pad due to load case 3 is a small value of

0.114 N/mm^2 which is less than 1.372 N/mm^2 shear strength of the pad at elevated temperature of 60 °C, (Mohammad 1997).

7.10 Summary and Conclusion

An optimum design for the prestressed concrete trough section was determined using OPTIM program based on a nonlinear optimisation algorithm of the Complex method. It was found that the minimum area of the concrete trough section also results in a minimum cost of producing 1 m length of the concrete trough unit. The total width of the section (B) is 390 mm and depth (D) is 180 mm. The section is provided with 6-ϕ 9.3 mm diameter of 7-wire strand tendons at the bottom and similar 2 tendons at the top, and shear links of 6 mm diameter at 100 mm centre to centre as shown in Fig. (7.7). The optimum concrete section was designed to satisfy the serviceability and ultimate limit states as per BS 8110 (1985) and Tarmac Precast Concrete Limited requirements for the most severe load cases of 1.0 m long cavity, 1.8 m length of soft base patch and temperature variation of ±25 °C that are expected during the life period of the track system service. The performances of the LR55 rail, elastomeric pad and track base were routinely examined and found to be satisfactory under the same critical load cases.

Table (7.1): Results of the optimum design problem of the concrete trough, starting with 20 different initial design points.

Case No.	Initial b_1 (mm)	Initial d_1 (mm)	Optim. b_1 (mm)	Optim. d_1 (mm)	Optim. Area A_c (mm^2)	No. of Funct. Z Evaluations
1	135	190	84.47	75.00	53593.5	81
2	110	165	84.47	75.00	53593.5	34
3	130	130	84.47	75.00	53593.5	38
4	130	185	84.46	75.01	53593.8	113
5	115	115	84.46	75.01	53593.8	111
6	105	105	84.45	75.02	53593.9	70
7	110	110	84.44	75.03	53594.1	74
8	135	135	84.44	75.03	53594.1	59
9	105	125	84.44	75.03	53594.1	87
10	95	135	84.44	75.03	53594.1	71
11	125	180	84.43	75.04	53594.3	75
12	100	155	84.43	75.04	53594.3	85
13	120	175	84.43	75.04	53594.3	89
14	110	180	84.43	75.04	53594.3	75
15	120	120	84.43	75.04	53594.3	71
16	125	110	84.42	75.05	53594.4	64
17	100	100	84.41	75.07	53595.3	67
18	105	160	84.40	75.07	53595.5	59
19	140	140	82.82	76.65	53636.8*	60
20	130	170	79.31	80.35	53762.5*	65

* means the point seems to be local mimimum, hence discarded.

Table (7.2): Moment and shear force Characteristics of the concrete trough section (390 x 180).

Item Description	Section Resistance		Applied Moment and Shear Forces
	Case 1 40/40	Case 2 41/40	
1. Serviceability limit state			
1.1 Transfer:			
Sagging moment, M_{t+}, (kN m)	13.13	12.76	1.45
Hogging moment, M_{t-}, (kN m)	-4.48	- 4.85	-0.103
1.2 Service:			
Sagging moment, M_{s+}, (kN m)	25.50	25.19	21.19
Hogging moment, M_{s-}, (kN m)	-10.78	-11.09	-11.07
2. Ultimate limit state			
2.1 Moment:			
Sagging, M_{u+}, (kN m)	34.75	34.33	33.9
Hogging, M_{u-}, (kN m)	-21.52	-21.75	17.71
2.2 Shear:			
Maximum permitted, V_{per}, (kN)	97.75	97.11	62.02
Capacity of concrete, V_c, (kN)	74.56	73.57	62.02

Table (7.3): Comparison of three different optimum concrete trough sections.

Item Description	Section 1 390 x 180, 8-ϕ 9.3 mm strands	Section 2 370 x 195, 7-ϕ 9.3 mm strands	Section 3 370 x 205, 6-ϕ 9.3 mm strands
I. Section Characteristics			
1. Width dimension, b_1, (mm)	85	75	75
2. Depth dimension, d_1 (mm)	75	90	100
3. Total width, B, (mm)	390	370	370
4. Total depth, D, (mm)	180	195	205
5. No. of tendons in the bottom layer	6	5	4
6. No. of tendons in the top layer	2	2	2
7. Area of concrete (mm^2)	53785	55735	59435
8. Surface area of formwork (mm^2)	937409	947409	967409
9. Area of prestressing steel (mm^2)	416	364	312
10. Weight of prestressing steel per metre length (kg)	3.268	2.860	2.451
11. Spacing of shear link R6 (mm)	100	110	120
12. Weight of shear reinforcement per metre length (kg)	3.330	3.068	2.886
13. Volume of excavation (mm^3)	70200	72150	75850
14. Weight of concrete trough per metre length (kg)	129	134	143
II. Production cost per metre length			
1. Cost of concrete material (£)	2.96	3.06	3.27
2. Cost of formwork (£)	46.87	47.37	48.37
3. Cost of prestressing steel (£)	1.96	1.72	1.47
4. Cost of shear reinforcement (£)	2.00	1.84	1.73
5. Total cost of producing 1 metre long of the concrete trough (£)	53.79	53.99	54.84

Table (7.4): Comparison of the applied and provided moments of the concrete trough for various length of soft base patch, (load case 2).

Wheel Load Position	Base/Pad Modulus (N/mm^2)	Soft Base Patch Length (m)	Applied Moment (kN m)	Provided Moment (kN m)
I. at the centre to produce maximum sagging moment	45/120	1.4	18.80	25.19
		1.6	19.76	25.19
		1.8	20.49	25.19
		2.0	21.05	25.19
		2.2	21.38	25.19
II. at the end to produce maximum hogging moment	45/120	1.4	-10.07	-11.07
		1.6	-10.61	-11.07
		1.8	-11.05*	-11.07
		2.0	-11.33**	-11.07
		2.2	-11.42**	-11.07

* means the applied moment is just below the provided one, hence the case is acceptable.

** means the applied moment is greater than the provided one, hence the case is not acceptable.

Table (7.5): Concrete trough stresses due combined wheel (vertical) load 104.21 kN, traction (horizontal) load 40 kN and temperature variation of ±20, ±25 or ±30 °C.

Wheel Load Position	Base/Pad Modulus (N/mm^2)	Temp. Variation (°C)	Axial Load (kN)	Bending Moment (kN m)	Btm. Fibre Stress (N/mm^2)	Top Fibre Stress (N/mm^2)
at the centre	25/80	±20	±215.16	10.19	8.283 0.282	16.206 8.206
at the end	25/120	±20	±215.69	-4.63	16.890 8.869	4.565 -3.455
at the centre	25/80	±25	±268.96	10.19	9.283 -0.718	17.206 7.205
at the end	25/120	±25	±269.47	-4.63	17.889 7.869	5.565 -4.455*
at the centre	25/80	±30	±322.73	10.19	10.283 -1.718	18.206 6.206
at the end	25/120	±30	±323.26	-4.63	18.890 6.860	6.565 -5.455**

* means the stress due to applied forces is just below the permissible one.
** means the stress due to applied forces exceeds the permissible one.

Table (7.6): Maximum stresses in the rail for the three possible load cases.

Load Case No.	Axial Load (kN)	Bending Moment (kN m)	Btm. Fibre Stress (N/mm^2)	Top Fibre Stress (N/mm^2)
1. Load case 1: 1.0 m long cavity under the wheel load	0	24.11	-278.169	254.816
2. Load case 2: 1.8 m long soft base patch under the wheel load	0	16.25	-187.48	171.745
3. Load case 3: combined effect of vertical wheel load (104.21 kN), horizontal traction load (40 kN) and temperature variation (±25 °C)	±422.85	15.55	-116.443 -242.375	227.310 101.378

Table (7.7): Base pressure and pad stresses for the three possible load cases.

Load Case No.	Base Pressure (kN/m^2)	Pad stresses (N/mm^2) Compression	Tension	Shear
1. Load case 1: 1.0 m long cavity under the wheel load	372.90	0.674	0.298	0
2. Load case 2: 1.8 m long soft base patch under the wheel load	267.01	0.692	0.155	0
3. Load case 3: combined effect of vertical wheel load (104.21 kN), horizontal traction load (40 kN) and temperature variation (±25 °C)	209.74	0.521	0.014	0.114

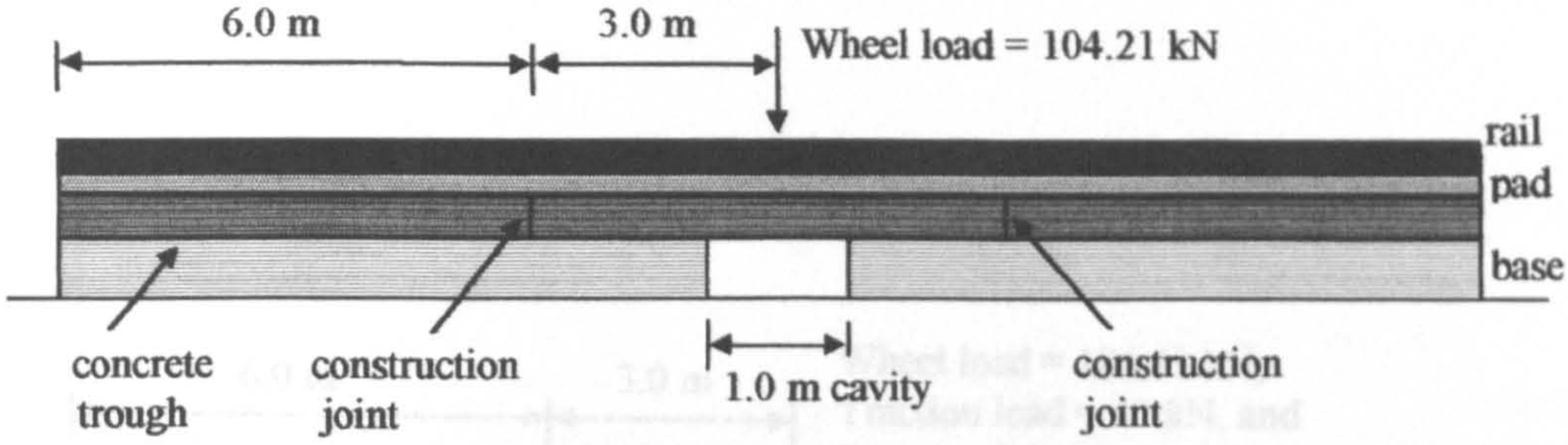

Fig. (7.1a): Wheel load at distance 3 m from a construction joint.

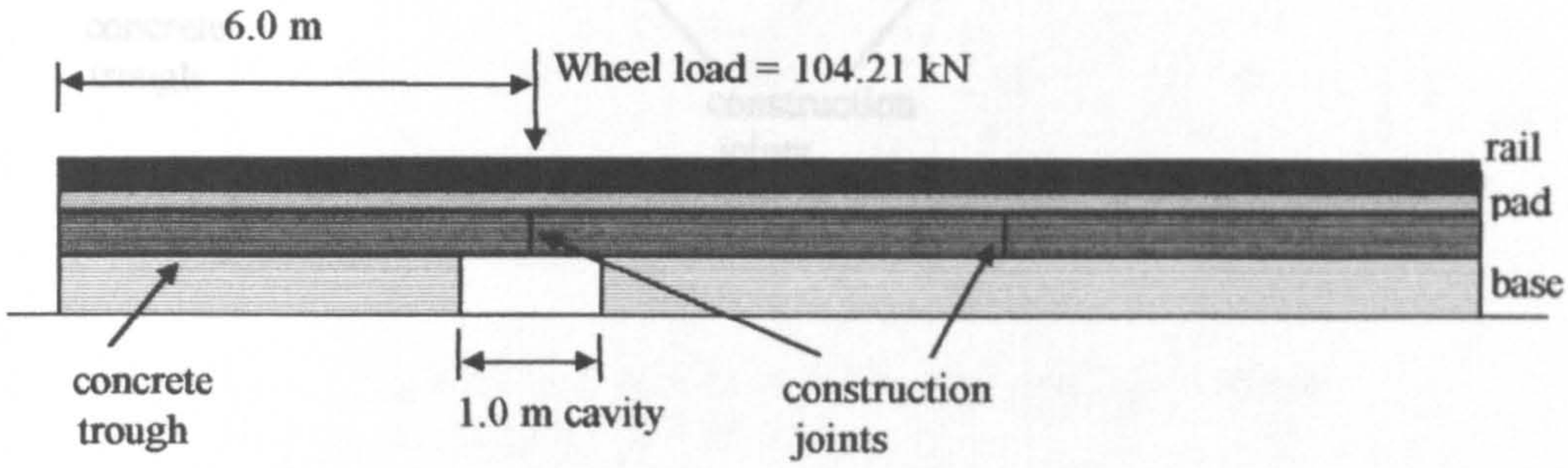

Fig. (7.1b): Wheel load directly above a construction joint.

Fig. (7.1): Load case 1, existence of 1.0 m long cavity underneath the wheel load.

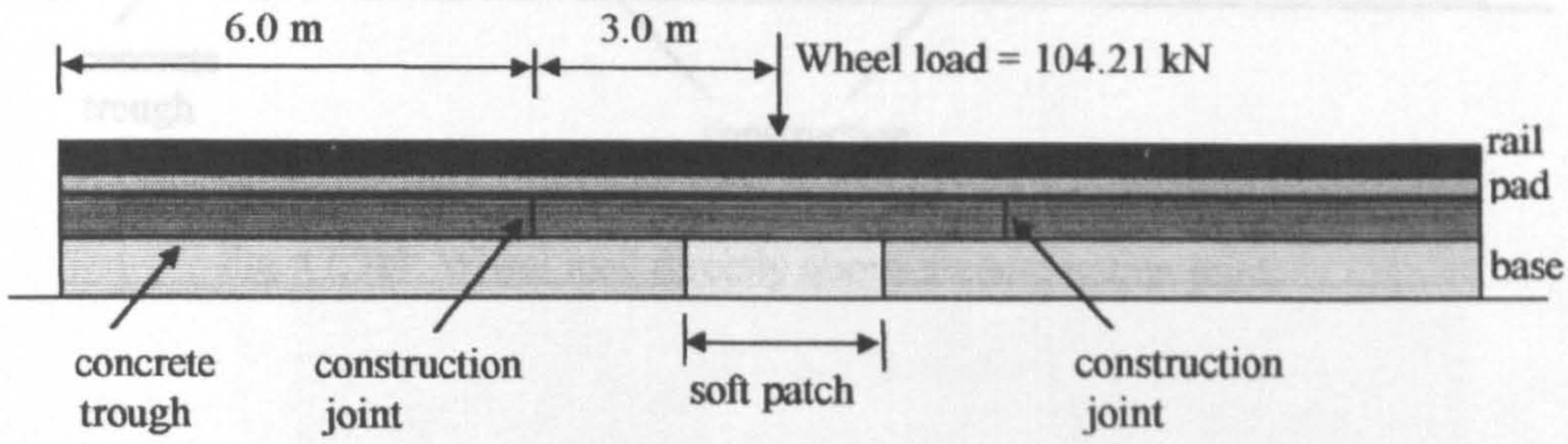

Fig. (7.2a): Wheel load at distance 3 m from a construction joint.

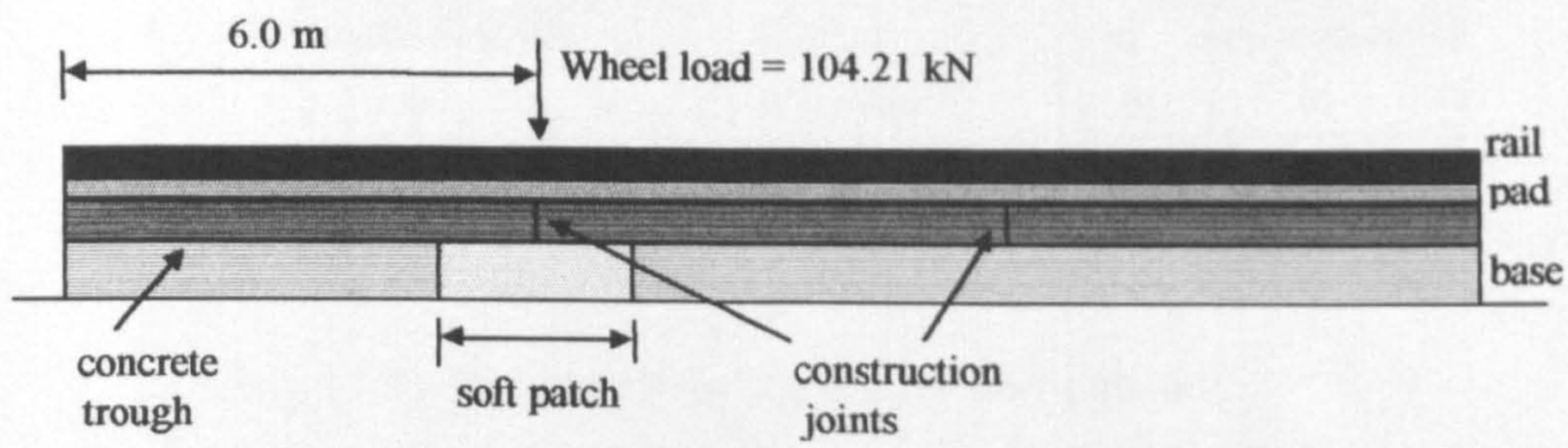

Fig. (7.2b): Wheel load directly above a construction joint.

Fig. (7.2): Load case 2, existence of soft base patch underneath the wheel load.

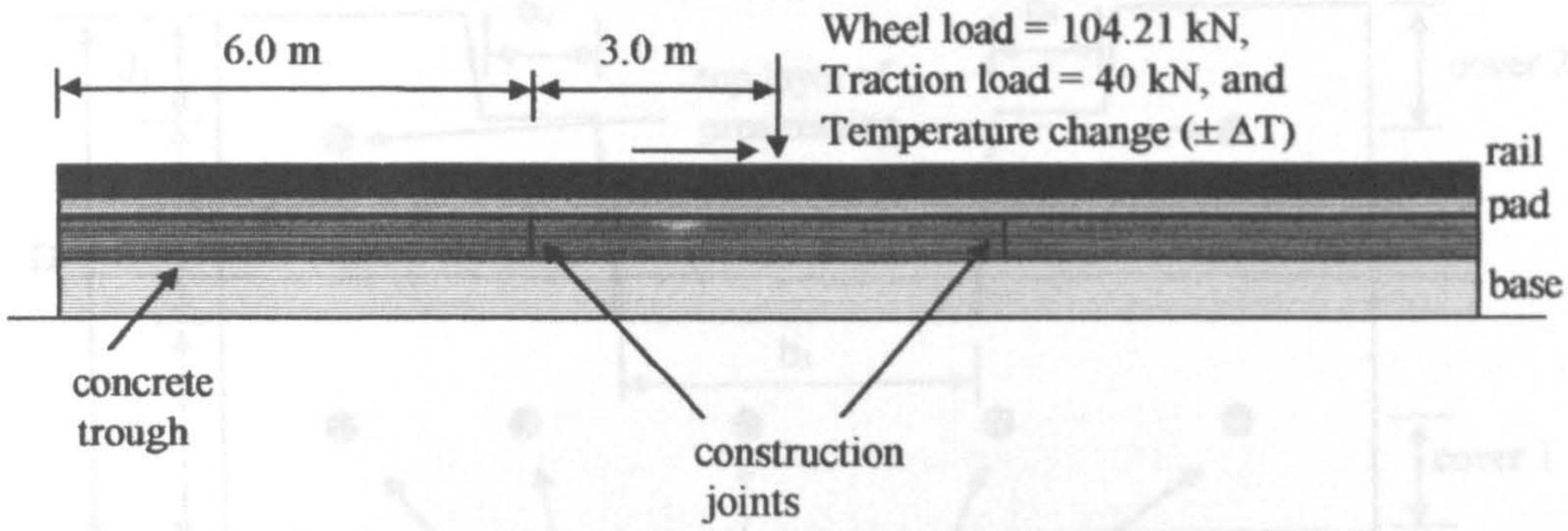

Fig. (7.3a): Wheel load at distance 3 m from a construction joint.

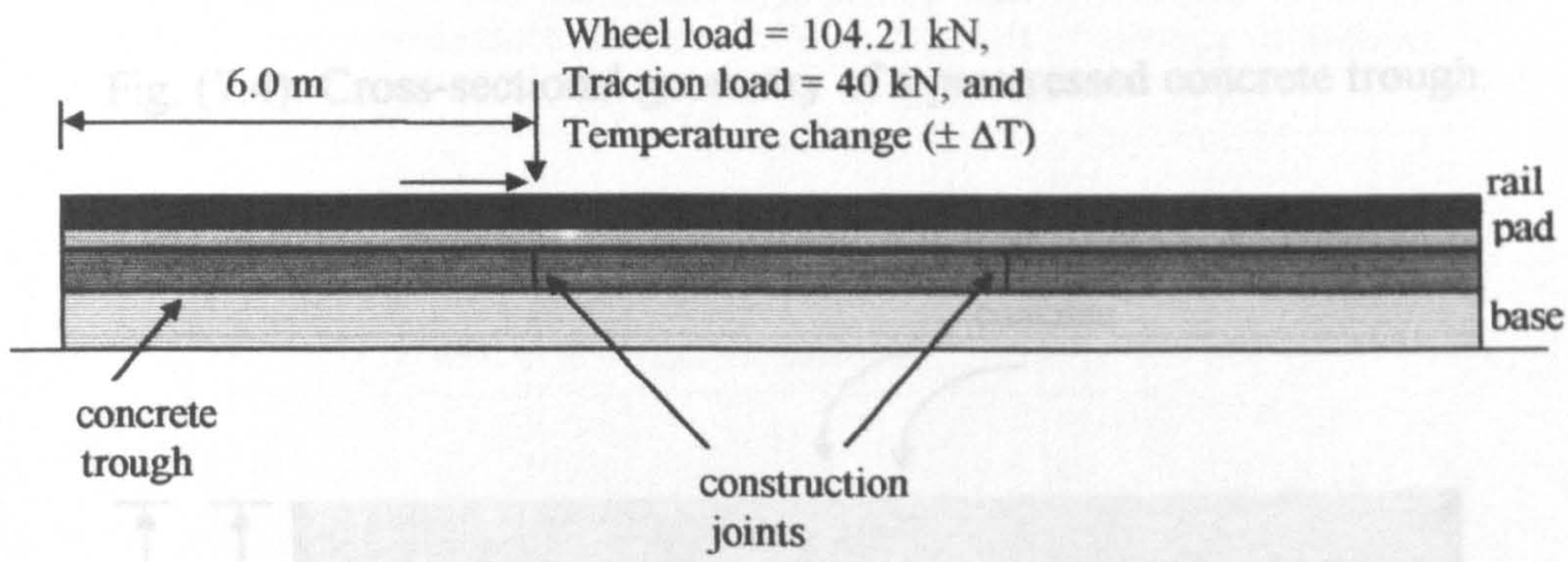

Fig. (7.3b): Wheel load directly above a construction joint.

Fig. (7.3): Load case 3, combined effect of vertical wheel load, horizontal traction load and temperature variation.

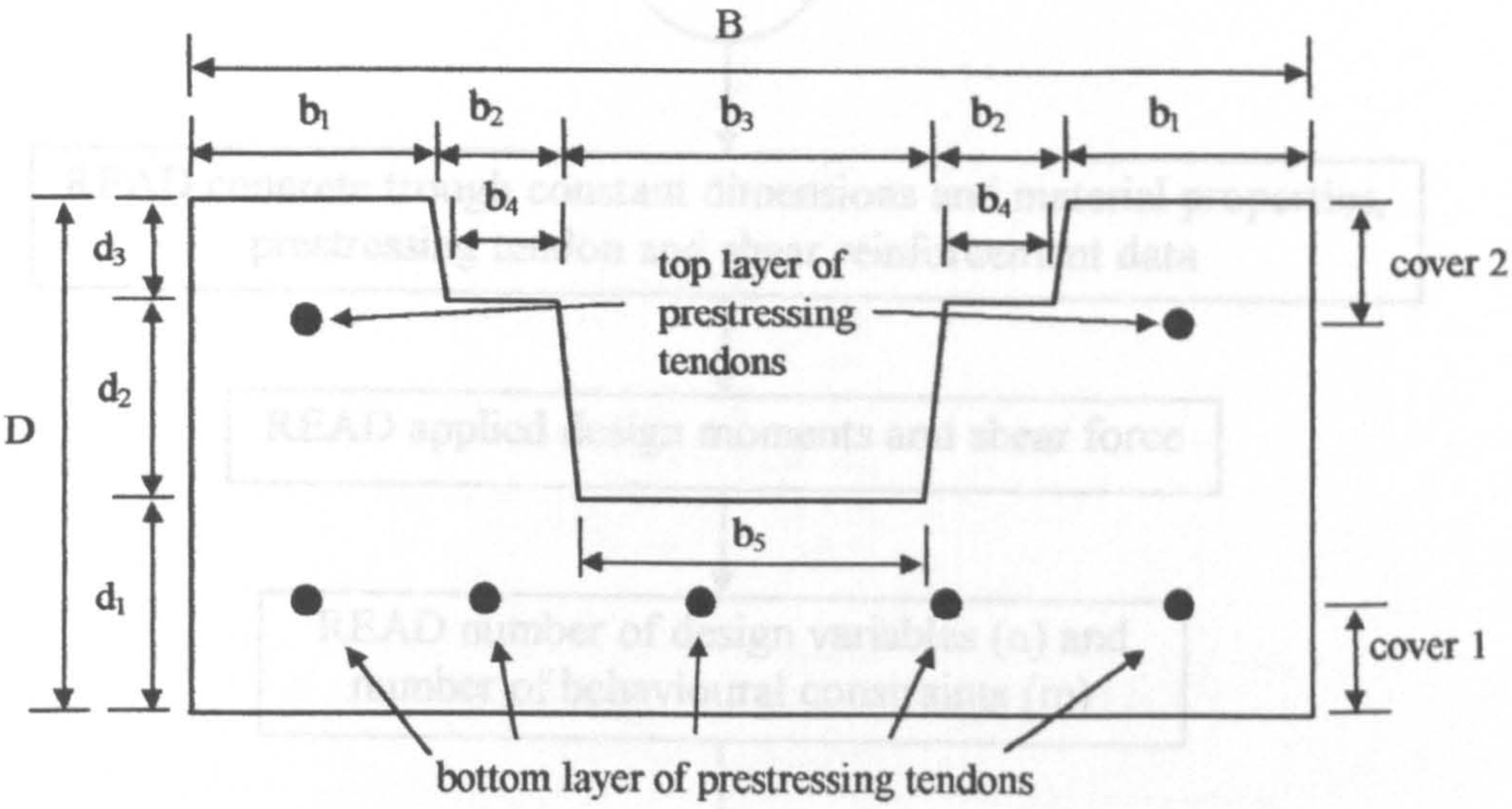

$b_1 = x_1$, $b_2 = 43$ mm, $b_3 = 134$ mm, $b_4 = 38$ mm, $b_5 = 120$ mm
$d_1 = x_2$, $d_2 = 70$ mm, $d_3 = 35$ mm

Fig. (7.4): Cross-sectional geometry of a prestressed concrete trough.

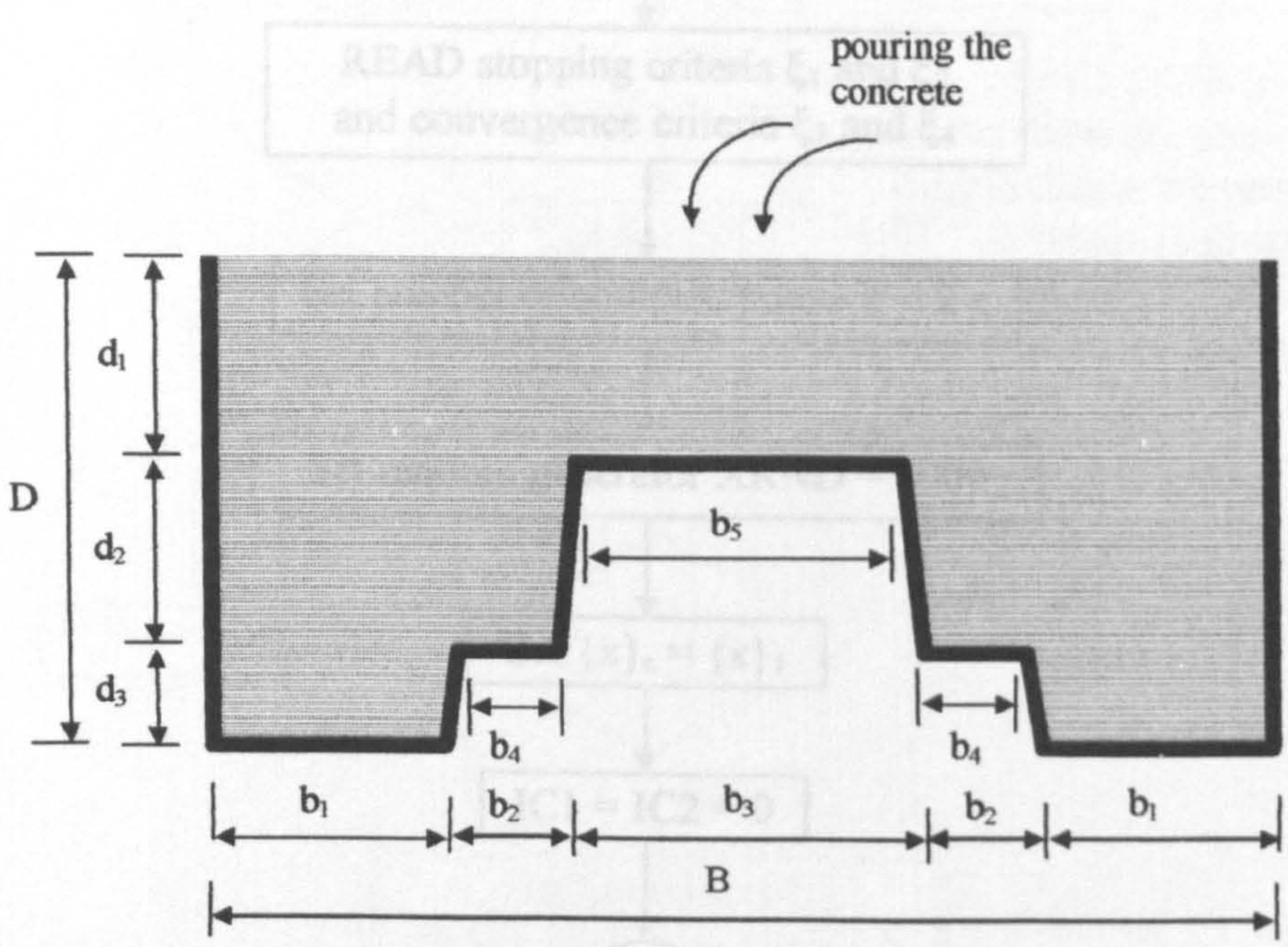

Fig. (7.5): Formwork for the concrete trough unit.

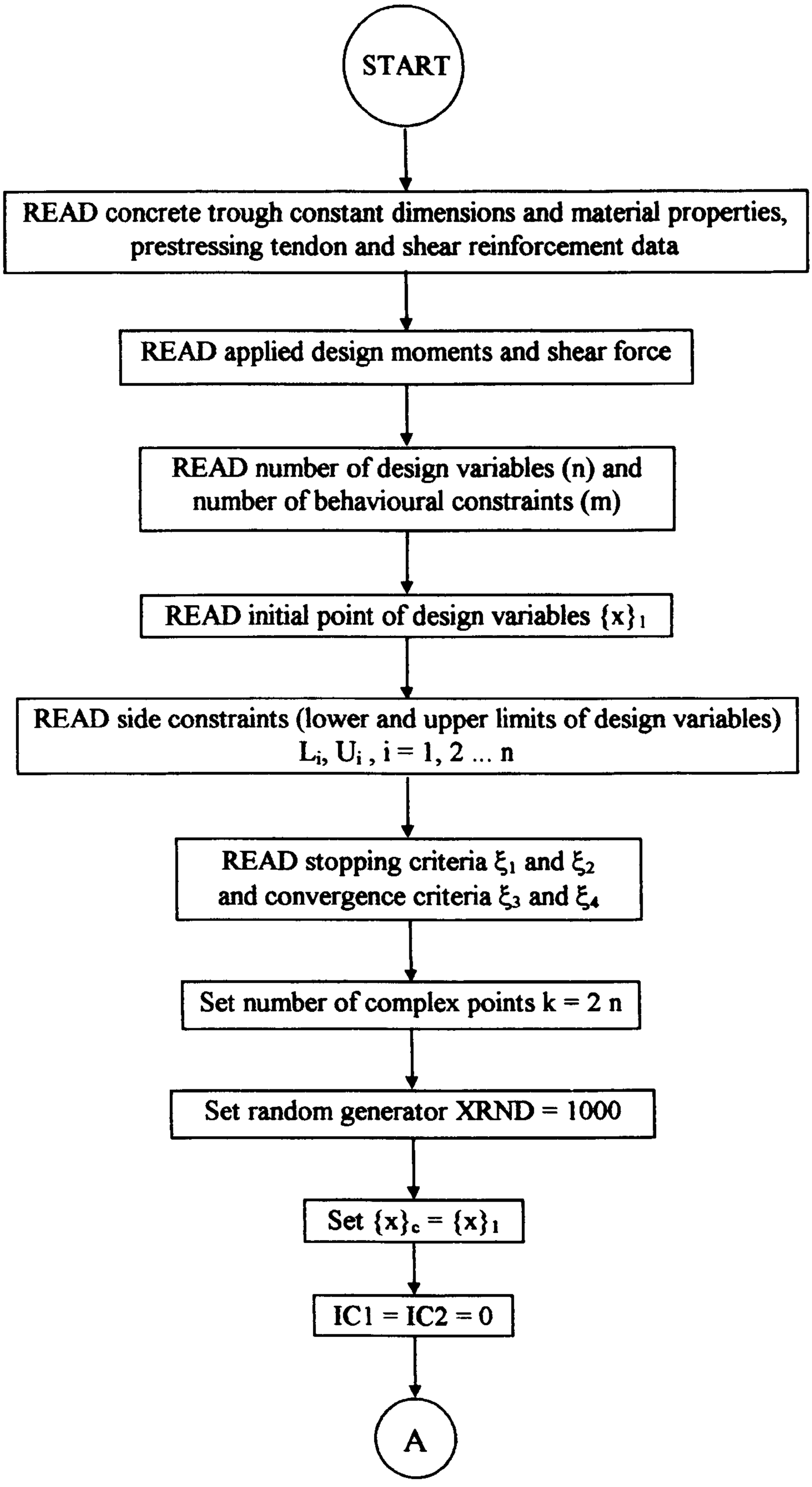

Fig. (7.6): Flow chart for the computer program OPTIM.

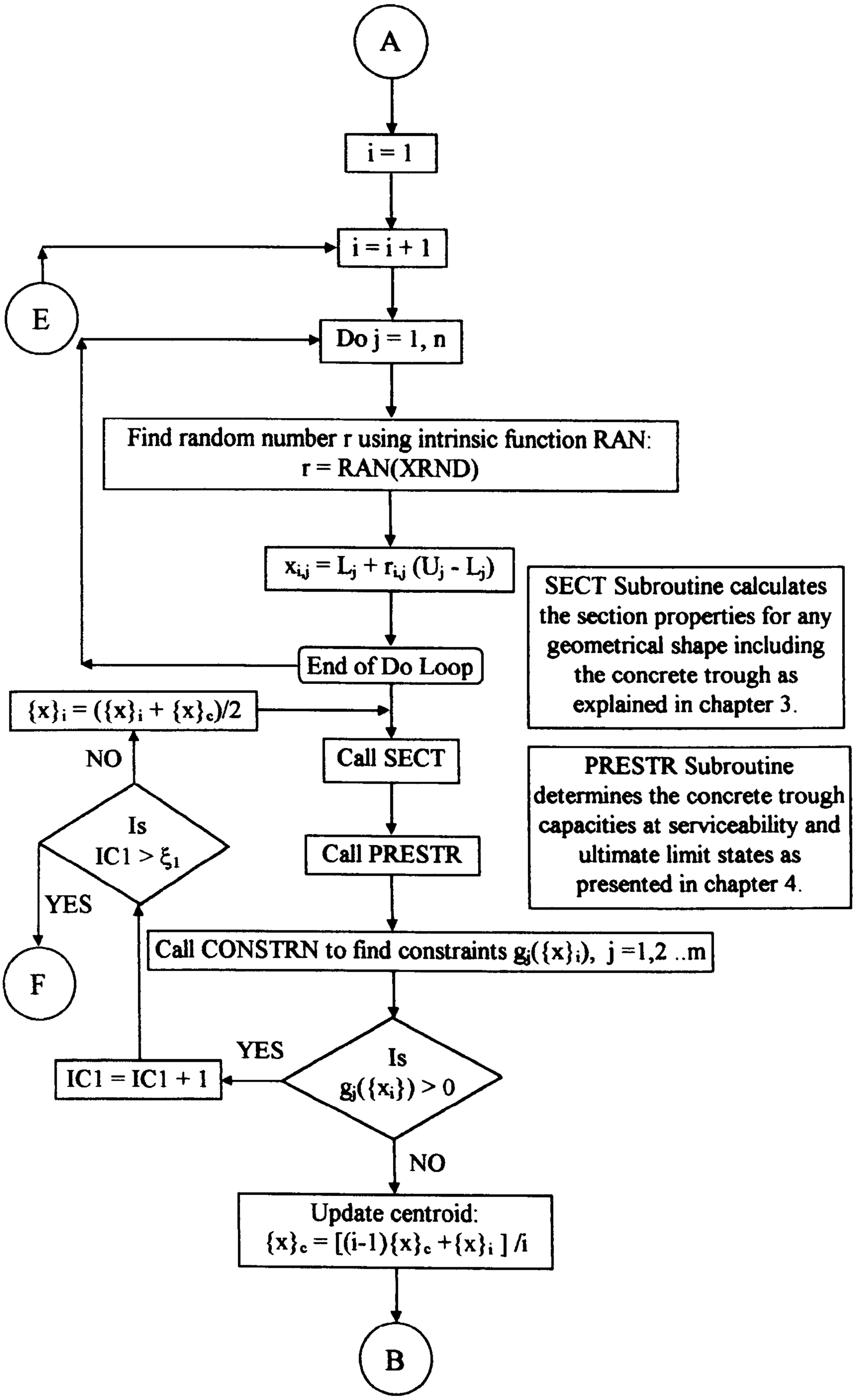
A
i = 1
i = i + 1
E
Do j = 1, n
Find random number r using intrinsic function RAN:
r = RAN(XRND)
$x_{i,j} = L_j + r_{i,j} (U_j - L_j)$
End of Do Loop
$\{x\}_i = (\{x\}_i + \{x\}_c)/2$
NO
Is
IC1 > ξ_1
YES
F
IC1 = IC1 + 1
YES
Is
$g_j(\{x_i\}) > 0$
NO
Call SECT
Call PRESTR
Call CONSTRN to find constraints $g_j(\{x\}_i)$, j =1,2 ..m
Update centroid:
$\{x\}_c = [(i-1)\{x\}_c + \{x\}_i] /i$
B
SECT Subroutine calculates the section properties for any geometrical shape including the concrete trough as explained in chapter 3.
PRESTR Subroutine determines the concrete trough capacities at serviceability and ultimate limit states as presented in chapter 4.

Fig. (7.6): Cont.

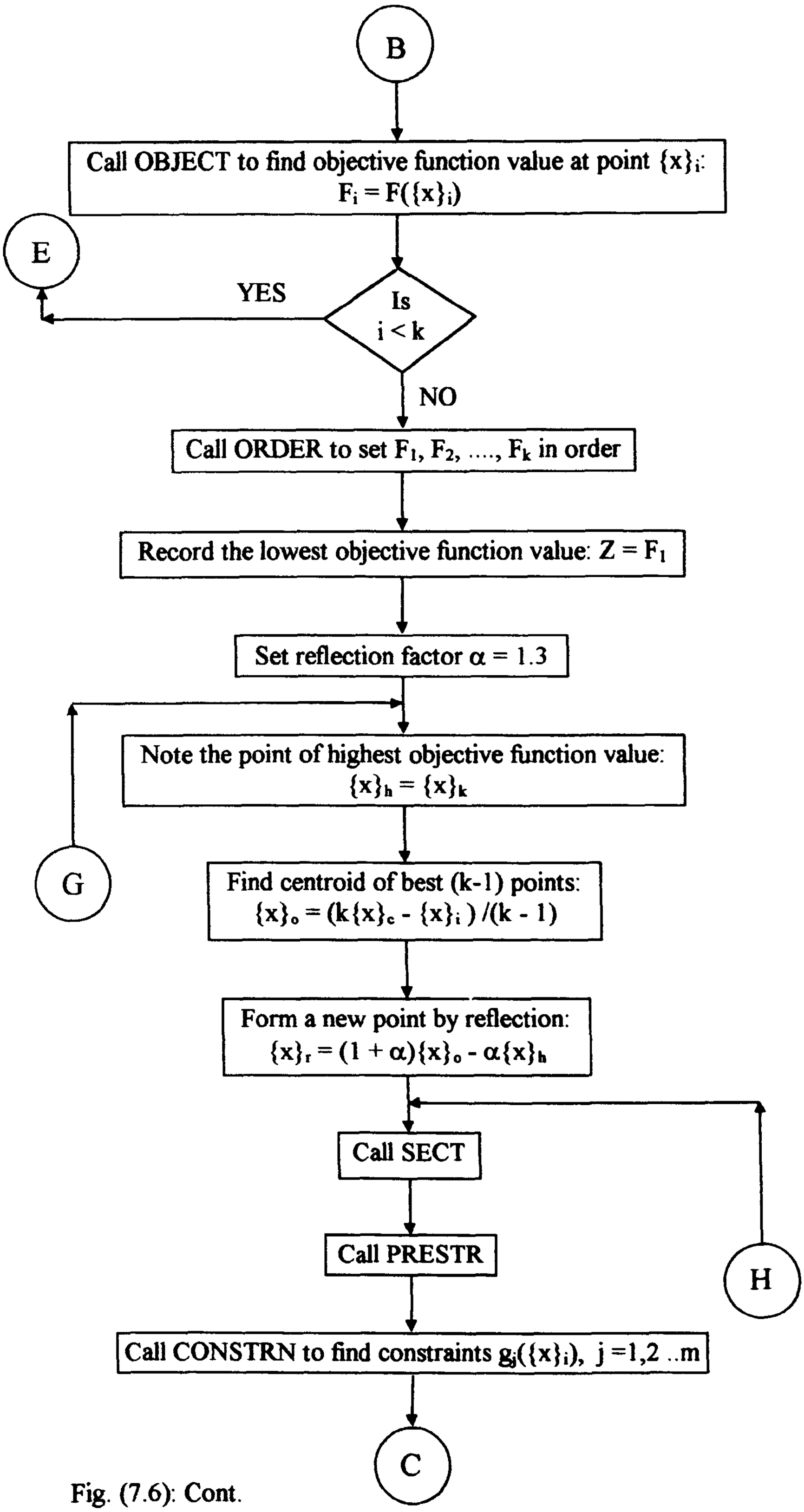
B
Call OBJECT to find objective function value at point {x}i:
Fi = F({x}i)
E
YES
Is
i < k
NO
Call ORDER to set F1, F2, ..., Fk in order
Record the lowest objective function value: Z = F1
Set reflection factor α = 1.3
Note the point of highest objective function value:
{x}h = {x}k
G
Find centroid of best (k-1) points:
{x}o = (k{x}c - {x}i) /(k - 1)
Form a new point by reflection:
{x}r = (1 + α){x}o - α{x}h
Call SECT
Call PRESTR
H
Call CONSTRN to find constraints gj({x}i), j =1,2 ..m
C

Fig. (7.6): Cont.

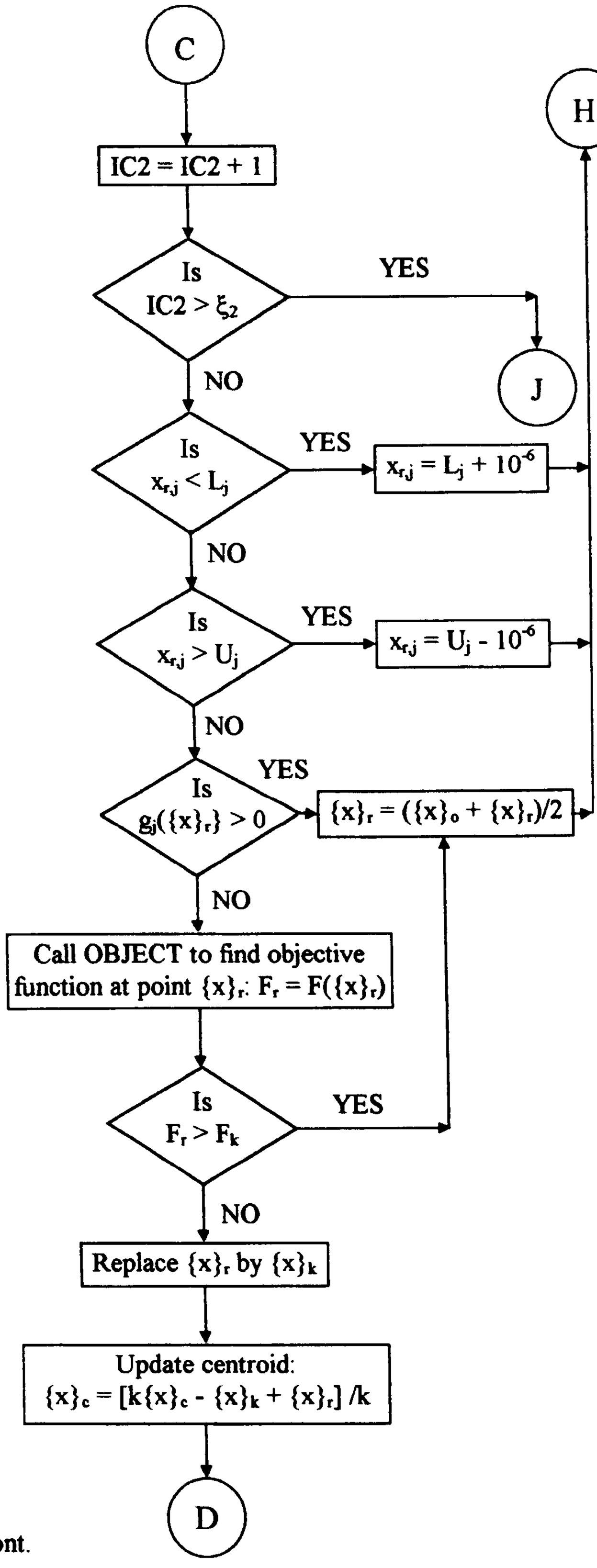
C
IC2 = IC2 + 1
Is
IC2 > ξ2
YES
NO
H
J
Is
xr,j < Lj
YES
xr,j = Lj + 10-6
NO
Is
xr,j > Uj
YES
xr,j = Uj - 10-6
NO
Is
gj({x}r} > 0
YES
{x}r = ({x}o + {x}r)/2
NO
Call OBJECT to find objective function at point {x}r: Fr = F({x}r)
Is
Fr > Fk
YES
NO
Replace {x}r by {x}k
Update centroid:
{x}c = [k{x}c - {x}k + {x}r] /k
D

Fig. (7.6): Cont.

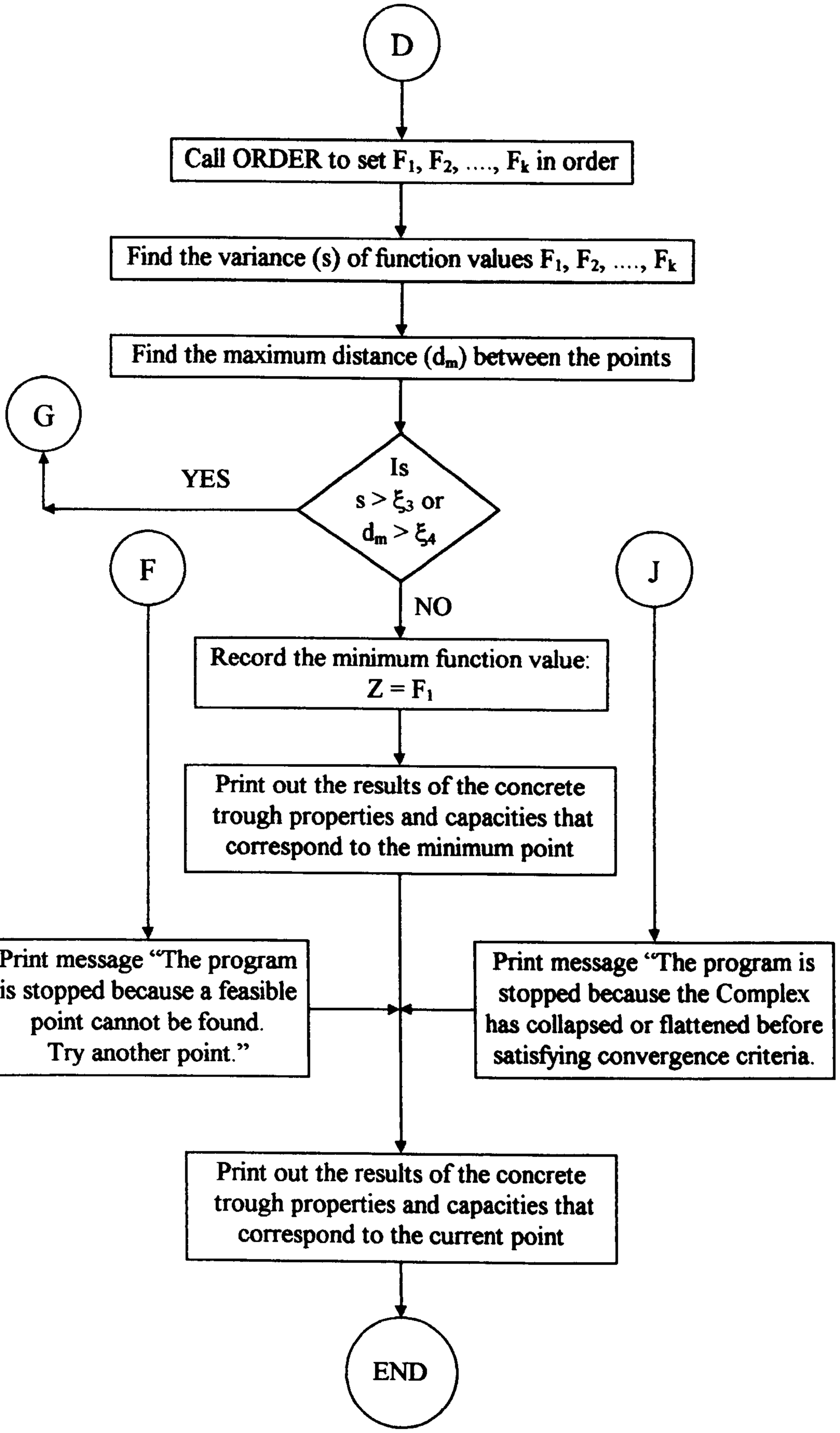
D
Call ORDER to set $F_1, F_2, ..., F_k$ in order
Find the variance (s) of function values $F_1, F_2, ..., F_k$
Find the maximum distance (d_m) between the points
G
YES
Is
$s > \xi_3$ or
$d_m > \xi_4$
F
J
NO
Record the minimum function value:
$Z = F_1$
Print out the results of the concrete trough properties and capacities that correspond to the minimum point
Print message "The program is stopped because a feasible point cannot be found. Try another point."
Print message "The program is stopped because the Complex has collapsed or flattened before satisfying convergence criteria.
Print out the results of the concrete trough properties and capacities that correspond to the current point
END

Fig. (7.6): Cont.

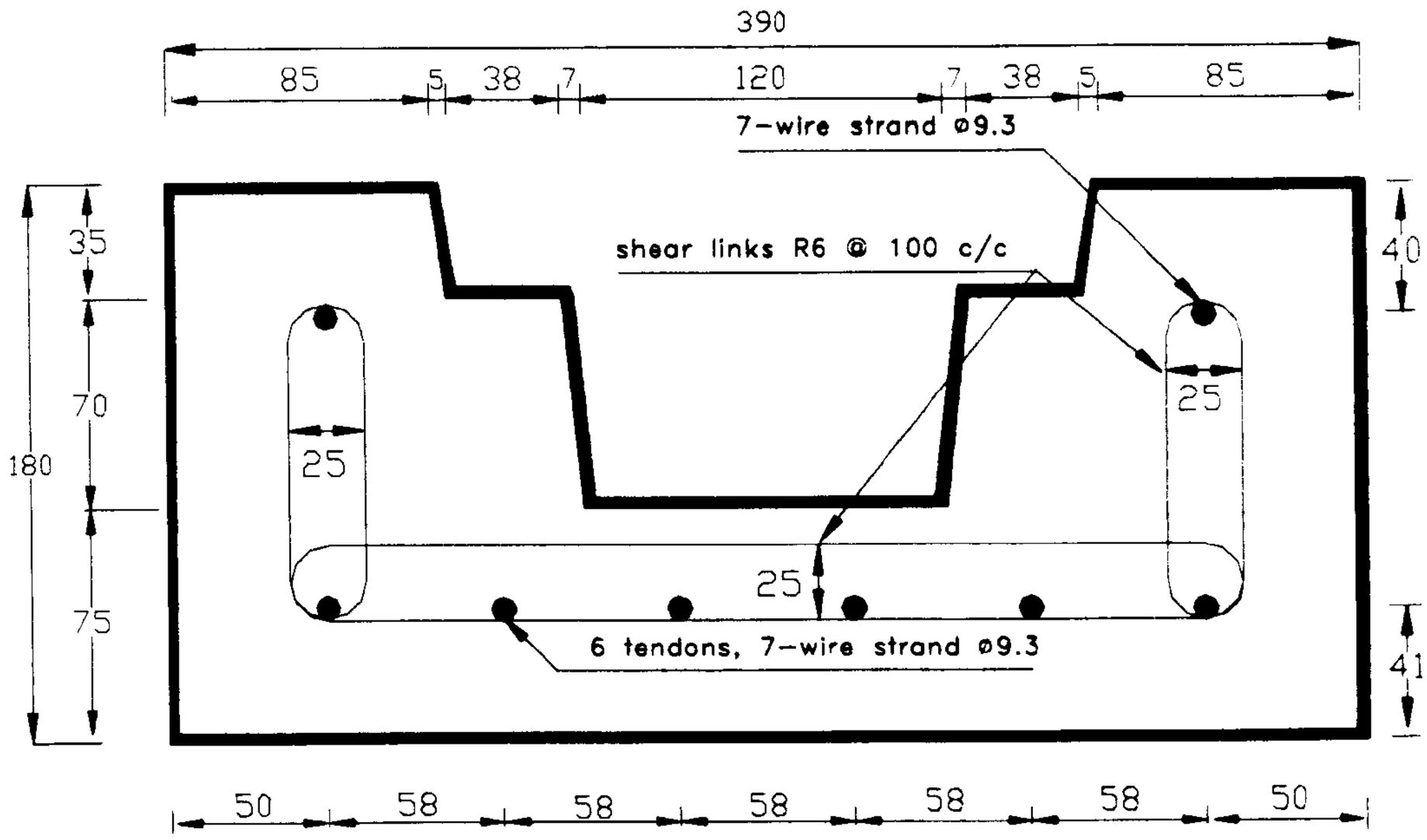

Notes

1. Concrete compressive strength at transfer (f_{ci}) = 30 N/mm^2
2. Concrete compressive strength at service (f_{cu}) = 50 N/mm^2
3. Characteristic strength of prestressing tendon, 7-wire strand, (f_{pu}) = 1770 N/mm^2
4. Initial prestressing (jacking force) = 0.7 f_{pu}

Fig. (7.7): Optimum prestressed concrete trough section.

CHAPTER EIGHT
EXPERIMENTAL WORK

8.1 Introduction

Physical models play an important role in structural engineering design, research and education. They are widely used in the design of unconventional structures, such as track systems and offshore rigs, and also conventional structures exposed to complicated loading and environmental effects such as multi-storey buildings subjected to earthquakes. A structural model may be defined as any physical representation of a structure or portion of a structure which is to be tested, (Sabnis et al 1983). It is often built to a reduced scale in comparison with full size structure for practical convenience and economy. However, the interpretation of test results could only be made after applying laws of similitude and dimensional similarity between the structural prototype and model to extrapolate the model test results for assessing the prototype capacity and response. But, unfortunately a proper scientific basis has not yet been established for modelling all the governing aspects of structural system behaviour. This means the current available similitude theories are inherent and liable to a certain degree of error because of size effect, i.e. change in indicated unit strength or stiffness due to change in specimen size, (Chana 1984). Furthermore, scaling of some important parameters of a concrete test model cannot be practically guaranteed such as aggregate size or bar diameter. For instance, if a concrete prototype is provided with prestressed strands of 9.3 mm diameter, then with model scale of 1:2 there is no commercially available corresponding strand size, or else, only prestressing wires could be used instead. Similarly, if the maximum aggregate size of a concrete prototype is 10 mm, then with model scale of 1:10, only sand can be used as a replacement. On the other hand, the results obtained from full-scale model test can be directly interpreted. Thus the problem of similarity is circumvented and eventually any related approximations could be avoided. Furthermore, testing a full-scale model helps in a better understanding of how a completed structure behaves in use. Owing to these factors, it was decided in the present work to carry out full-scale tests on a 6 m long LR55 track model.

In practice, the LR55 track system is supported by the layers of an existing street pavement which are surfacing, road base, subbase and subgrade. However, it is not feasible due to space and time restrictions to accommodate the same cross-sectional profile of a pavement in terms of layers thicknesses and material types for conducting indoor experiments on a 6 m long LR55 track model in the structural laboratory of Liverpool John Moores University. Therefore, a representative track foundation has to be devised provided that it can be easily constructed and dismantled within a reasonable short period of time. Accordingly, it was suggested to build a timber box, filled with sand to a certain depth and lay the track model onto it. The whole arrangement of the sand box was based on a relatively rigid concrete floor slab. The question raised was what depth of sand was sufficient to represent the actual track foundation in terms of stiffness and capacity? To answer this question, preliminary plate-load tests were necessarily required before doing any further tests on the track model as will be explained in the following sections.

8.2 Plate-load Tests

A plate-load test involves the replacement of the proposed foundation by a small square steel plate usually of size 300 - 750 mm, placed in position on the surface of the soil to be examined. A load is applied in increments until failure, and deflections (settlements) of the soil at the interface with the plate are measured correspondingly. From these measurements, a plot of soil pressure (load divided by nominal contact area) versus deflection can be established. It should be expected that the recorded deflections are constant across the plate. This can be secured by increasing the rigidity of the plate through stacking a smaller plate concentric with a larger one, but in any case the deflection should be measured at more than one point across the plate and the average deflection is taken, (Bowles 1988, Smith 1990).

In the current experiment, a series of plate-load tests were performed where a range of sand depth between 400 and 800 mm were investigated. The aim of these tests was to find the optimum depth of the sand that ensure the followings: First, the foundation modulus required for testing the track model fell within the practical range, i.e. neither too soft (5 - 10 N/mm^2) nor too stiff (50 - 60 N/mm^2), (Cope 1993). In other words, it

was preferable to be between 25 and 45 N/mm^2 or as an average of 35 N/mm^2. Second, the bearing capacity of the sand box arrangement was larger than the predicted pressure on the track base lest a premature failure of the sand should happen before reaching the maximum load specified for the track model tests. The preparation of the plate-load test and discussion of the results are described below. A schematic diagram and some photos of the plate-load tests are found in Figs. (8.1) - (8.3).

8.2.1 Plate-load Test Equipment, Apparatus and Materials

- Sand

  Well graded fine river sand of effective particle size = 0.28 mm, dry density 1739 kg/m^3 and angle of internal friction = 40 °

- Two stacked plates welded together with 6 mm fillet weld

  Large plate dimensions = 390 x 390 x 20 mm

  Small plate dimensions = 370 x 370 x 20 mm

  The size of the larger plate was taken as 390 mm which is the same width as the concrete trough. The reason for welding a smaller plate to the larger one was to increase the rigidity as mentioned earlier, hence expecting uniform deflection and pressure across the plate surface.

- Timber box of 2400 mm long, 700 mm wide and 1200 high, made of plywood sheets of 25 mm thickness.
- I-sections (for packing purpose only) with total depth of 350 mm, width of 320 mm and length of 230 mm.
- Linear Variable Displacement Transducers (LVDT's)

  Type HS 25B: Displacement range 25.8 mm

  Voltage sensitivity 6.7 mV/V

  Strain sensitivity 520 x 10^{-6} /mm

  Fully active 350 ohm strain gauge bridge

  Temperature range -10 to 60 °C

  Manufactured by Welmyn Strain Measurement

- Load Cell

  Type 403 Mayes full bridge load cell (200 kN capacity)

- Hydraulic Ram

  Type RSC 506 (50 Tonne Capacity)

  Manufactured by Tangye Hydraulics

- Hydraulic Pump

  Type MH30 double speed Pump

  Hand operated

  Manufactured by Tangye Hydraulics

- Personal Computer

  Laptop

  Pentium microprocessor

  16MB RAM/500 MB hard drive

- Data Logger

  Autonomous Data Acquisition Unit (ADU),

  It has 64 channels and supports 1/4, 1/2 and full bridge arrangements

  Manufactured by ELE Intentional

- Software for the Logger

  ELE ADU Dialogue Management Software: DOS based

  1MB memory required

  Version 2.07

8.2.2 Testing Procedure

The main steps involved in the plate-load test procedure were:

1. Building a timber box with a total length of 2400 mm, width of 700 mm and height of 1200 m, made of plywood sheets 25 mm thickness.
2. Strengthening the box by timber buttresses made of 50 x 50 mm white wood.
3. Fixing the test rig up-right and cross head in place and inserting steel packing between the frame and box width.
4. Filling the box with sand in layers up to a depth of 400, 500, 600, 700 or 800 mm. The thickness of each layer was not more than 75 mm and was compacted manually using steel plate of 250 x 250 x 12 mm welded to a steel rod.
5. Levelling the top surface of the sand.

6. Identifying the locations of three points on the centre line across the width of the box with a distance of 190 mm centre to centre.
7. Making holes at these points to fit the transducers in with their spring arms making contact with the top surface of the sand.
8. Compacting carefully the disturbed sand due to burying the transducers and their connection wires to the data logger.
9. Placing the stacked plates in position such that the centre of the plates was coincidental with the middle transducer.
10. Placing one or two I-sections depending on the total depth of the sand, hydraulic ram, load cell, packing pieces and ball joints so that the arrangement was firmly inserted between the cross head and the top surface of the plate.
11. Applying the load incrementally through hydraulic pump and ram.
12. Recording the deflection and load readings automatically every 2 seconds through a computer software and data logger connected to the transducers and load cell.
13. Terminating the test when there was no significant change in load reading between several time intervals which indicated failure of the sand soil by bearing pressure.

8.2.3 Interpretation of the Test Results

Plate-load tests were completed for sand depths ranging from 400 to 800 mm. The summary of results in terms of soil pressure versus deflection are presented in Figs. (8.4) - (8.8). The actual (measured) non-smooth pressure-deflection curves are represented by idealised second order polynomials using nonlinear regression analysis of best fit, which is available within EXCEL software. From these curves the foundation modulus (k_b) for the sand soil is derived as follows:

The modulus of subgrade reaction may be defined as the pressure to deflection ratio of the soil at any point on the curve obtained from plate-load test, i.e., (Bowles 1988):

$$k_{plate} = p/\delta \qquad (8.1)$$

where

k_{plate} = modulus of subgrade reaction of the soil obtained from plate-load test

p = pressure on the soil due to applied load

δ = deflection (settlement) of the soil due to applied load

Since the soil behaviour is generally nonlinear as demonstrated by these tests, it is evident that the value of k_{plate} depends on the slope at any prescribed point on the curve.

However, the concept of a tangent or secant modulus could be equally well adopted for design purposes without affecting the accuracy of the results appreciably, (Bowles 1988). In the present experiments, the value of k_{plate} is based on the secant modulus at a deflection of 1 mm as the soil still performs linearly at this small deflection. Thence, it will be appropriately compatible with the theoretical analysis where the soil is represented by linear elastic springs. Interestingly, it can be seen from Figs. (8.4) - (8.8) that there is insignificant difference between the secant and tangent modulus which justifies the use of either.

The definition of secant modulus is the slope of the line joining the origin and the specified point on the pressure-deflection curve. Accordingly, eq. (8.1) can be rewritten as:

$$\begin{aligned} k_{plate} &= \Delta p/\Delta\delta \\ &= [p_{(\delta=1)} - p_{(\delta=0)}]/(1 - 0) \\ &= [p_{(\delta=1)} - 0]/(1 - 0) \\ &= p_{(\delta=1)} \end{aligned} \tag{8.2}$$

The foundation modulus corresponding to a full size foundation may be obtained from a small size plate-load test through following relationship, (Bowles 1988):

$$k_b = B[(L + 0.5\,B)/1.5L]\,k_{plate} \tag{8.3}$$

where

k_b = foundation modulus of the soil corresponding to full size foundation

L = length of the foundation. In case of the track model,

= 6 m

B = width of the foundation. In case of the track model,

= 0.39 m

Substituting eq. (8.2) and the values of L and B into eq. (8.3) gives,

$$k_b = (0.39)[(6 + 0.5 \times 0.39)/(1.5 \times 6]\ p_{(\delta=1)}$$
$$= 0.2685\ p_{(\delta=1)} \qquad (8.4)$$

The bearing capacity is the maximum pressure the sand soil can sustain at failure. It is simply equal to the highest recorded load during the test divided by the nominal cross-sectional area of the plate (0.39 x 0.39 m^2). Table (8.1) presents the foundation modulus obtained by eq. (8.4) and the bearing capacity for the range of sand depth between 400 and 800 mm.

It can be seen from Table (8.1) that for sand depths between 400 and 800 mm the foundation modulus ranges from about 43 to 23 N/mm^2 respectively. A sand soil having this range of foundation modulus can be classified as medium dense sand, Bowles (1988). Such a finding was also demonstrated by Tulloch (1997) who carried out a number of tests on the same sand suggested for shallow strip foundation. It can also be observed that both the modulus and bearing capacity of the sand increases as the depth decreases. For depth smaller than 400 mm, the foundation modulus tends to approach the limiting value of 50 - 60 N/mm^2 for very stiff track base. Similarly, for depth greater than 800 mm, the foundation modulus of the sand layer turns out to be too low as it reaches the limiting value of 5 - 10 N/mm^2 for very soft track base, (Cope 1993). This might be attributed to the influence of the relatively rigid concrete floor slab provided as a base for the sand box. As a conclusion, the optimum sand depth required for the tests of the track model can be judged round 500 - 600 mm as the foundation modulus lies somewhere between 38 to 32 N/mm^2 or as an average of 35 N/mm^2. Furthermore, the bearing capacity at these depths is about 430 - 400 kN/m^2. This value is well above the expected pressure of 210 - 370 kN/m^2 on the track base as observed during the theoretical analysis, see Table (7.7), chapter 7.

Consequently, it was decided to select a sand depth of 550 mm below the track model where the predicted foundation modulus will be expected round 35 N/mm^2 and the bearing pressure will be about 420 kN/m^2.

8.3 Full-scale Tests for 6 m long LR55 Track Model

Four laboratory tests on a full-scale 6 m long LR55 track model were carried out for a number of specific reasons: First, to validate the mathematical model suggested for the LR55 track system, in which the latter is treated as multilayer beams on elastic foundations, through comparing the theoretical results with the experimental ones. Second, to ensure the design safety and develop confidence in the capability performance of the LR55 track system. Third, to observe the overall behaviour of the track model subjected to loading and boundary conditions that are similar to actual situations, thus grasping a clear insight as to how the track system will respond in practice. Eventually, to serve as an extension to the theoretical study carried out in the previous chapters of this project since the full-scale testing can be viewed as an invaluable complement to the mathematical model.

The tests were static and non-destructive in nature. These were fulfilled by applying at the centre of the track model a single point load up to a pre-assigned maximum value which was estimated to be within the expected service load. The reason for deciding on non-destructive tests was to repeat several tests on the same track model under various loading and boundary conditions, hence making a firm conclusion on accuracy of results. Otherwise, multiple track models were required in order to treat the results statistically, but the expense of even a single test specimen was usually high.

The first experiment was intended to be a trial one in order to see whether the instrumentation is fixed properly, i.e. if any of the strain gauges or transducers failed or were damaged during installation, and to examine how sturdy and robust was the prepared timber box for containing the sand and track model during the tests. Besides that, the obtained results can, of course, still be used for comparison with the theoretical ones. Therefore, The specified maximum load was limited to a small value of 43.27 kN which is about 40% of the design wheel load of 102.43 kN. The maximum load for the other three tests were made roughly close to the design wheel load (as the load was generated through a manual hydraulic pump it was not possible to accurately control the required level of the load). The maximum loads were 95.48, 98.34 and 98.21 kN for tests 2, 3 and 4 respectively.

The track model was continuously supported by the sand layer during tests 1 and 2. Whereas, it was bridged over a 1 m long cavity for tests 3 and 4 to simulate a subsidence of the foundation in practice due to any reason such as the collapse of a sewer pipe underneath the track system. The cavity was symmetrically located underneath the applied load. The characteristics of these four tests are also summarised in Table (8.2). A schematic diagram for the track model and sand box is illustrated in Fig. (8.9). Locations of the strain gauges on the track model are shown in Fig. (8.10), and those of the dial gauges and transducers are presented in Figs. (8.11) and (8.12). Some photos showing various aspects of the tests are also supplied in Figs. (8.13) - (8.17). The preparation for the tests are briefly described in the following sections.

8.3.1 Test Equipment, Apparatus and Materials

- Full-scale LR55 Track Model of 6 m long

  LR55 Rail: Manufactured by Edgar Allan Engineering Ltd

  Pre-tensioned Prestressed Concrete Trough: Manufactured by Tarmac Company Precast Concrete Limited as per details shown in Fig. (7.7), see chapter 7.

  Elastomeric Pad: Manufactured by ALH Systems Limited

  The components of the track model were assembled in Tarmac Company.

- Timber box of total length of 7200 mm, width of 700 mm and height of 800 mm, made of plywood sheets of 25 mm thickness.

- Strain Gauges

  Steel: Type FLA-2-11
  Gauge length 2 mm
  Gauge width 1.5 mm
  Base dimensions 6.5 x 3 mm^2
  Nominal gauge resistance 120 ± 0.3 ohms
  Gauge factor 2.13 ± 1%
  Manufactured by Tokyo Sokki Kenkyujo Co. Ltd.

  Concrete: Type PL-60-11
  Gauge length 60 mm
  Gauge width 1 mm
  Base dimensions 74 x 8 mm^2

Nominal gauge resistance 120 ± 0.3 ohms

Gauge factor 2.13 ± 1%

Manufactured by Tokyo Sokki Kenkyujo Co. Ltd.

- Connecting Terminals

  Type TF-2SS

  Manufactured by Tokyo Sokki Kenkyujo Co. Ltd.

- Adhesives

  Cyanoacrylate (CN) type for the steel strain gauges

  Polyester filler PS type as a precoating for concrete strain gauges

  Polyester RP-2 type for fixing the concrete strain gauges

  Manufactured by Tokyo Sokki Kenkyujo Co. Ltd.

- Coating Materials

  Neoprene (N-1) type. It was used to protect the strain gauges against moisture and light mechanical damages.

- Transducers

  Type HS 5B: Displacement range 6.2 mm

  Voltage sensitivity 4.6 mV/V

  Strain sensitivity 1474 x 10^{-6} /mm

  Fully active 350 ohm strain gauge bridge

  Temperature range -10 to 60 °C

  Manufactured by Welmyn Strain Measurement

  Type HS 25B: (same as that described in section 8.2.1)

- Dial Gauges

  Batty type CL-5: Diameter 75 mm

  Displacement range 50 mm

  Reading Division 0.01 mm

  Mechanical analogue

  Manufactured by Batty Ltd

- Strain Gauge Tester

  Probe style multimetre

  Range up to 300 ohm

  Resolution 0.1 ohm

Accuracy ± 1.2%

Circuit voltage 1.3 Volt

Manufactured by ISO-TECH IDM 17

- Sand: (same as that described in section 8.2.1)
- Load Cell: (same as that described in section 8.2.1)
- Hydraulic Ram: (same as that described in section 8.2.1)
- Hydraulic Pump: (same as that described in section 8.2.1)
- Personal Computer: (same as that described in section 8.2.1)
- Data Logger: (same as that described in section 8.2.1)
- Software for the Logger: (same as that described in section 8.2.1)

8.3.2 Test Preparation

8.3.2.1 Strain Gauges Installation

The following points summarise the main steps conducted in the installation of the strain gauges before testing the track model:

1. Marking out the position where the strain gauges were to be installed (33 strain gauges for the concrete trough and 25 for the steel rail).
2. Cleaning an approximate area of 100 x 60 mm at each gauge location for the concrete gauges, finishing by using grinding discs and degreasing the cleaned area with Acetone. For the steel gauges, an area of 50 x 40 was abraded using a power file and finished by hand using carborandum paper.
3. Bonding the strain gauges and the connecting terminals to the surface using the recommended strain gauge adhesive.
4. Soldering the 3 lead cables to each gauge using flux cored 40/60 tin/lead alloy solder.
5. Checking the conformity of the installation for gauge resistance of 120 ± 2 ohm using multimetre gauge tester.
6. Applying the coating material Neoprene (N-1) type to cover whole of prepared surface to prevent moisture ingress. Allow curing for a minimum of 12 hours.
7. Fixing number indents to both ends of each lead wire.
8. Checking that leads run in such a manner as to avoid them being accidentally caught and damaged.

9. Carrying out installation conformity check with multimetre gauge tester.
10. Using gauge factor to convert the resistance change into engineering units.

8.3.2.2 Testing Procedure

The procedure for testing the full-scale track model are listed in the following points:

1. Erecting a timber box of 7200 mm long, 700 mm wide and 800 mm high, made of 25 mm thick plywood sheets.
2. Strengthening the box by steel tie rods of 10 mm diameter, timber buttresses made of 50 x 50 mm white wood, and plywood straps placed at the middle two-thirds of the box.
3. Assembling the test rig up-right and inserting steel packing between the up-right on either side of the box and the box.
4. Filling the box with the sand in layers up to a height of 550 mm. Each layer was not more than 75 mm thick and was compacted manually using steel plate of 250 x 250 x 12 mm welded to a steel rod.
5. Levelling the top surface of the sand and placing the 6 m long track model in the box.
6. Filling the box with sand up to the finished floor level (up to 730 mm height) in three layers and compacting carefully to prevent damaging the installed stain gauges and cables.
7. Strengthening the box with some additional steel tie rods near the top surface and adjusting the inside box dimension to the required width of 700 mm.
8. Fixing the cross head to the steel frame up-right.
9. Placing the hydraulic ram, load cell, packing pieces and ball joints so as to tightly inserted between the cross head and the top surface of the track model.
10. Locating 9 mechanical dial gauges and 5 transducers (LVDT's) at certain points along the track model as shown in Figs. (8.11) and (8.12) to measure the deflections of the concrete trough and steel rail.
11. The test was ready to start by applying a single point load at the centre of the track model and increased gradually up to a specified maximum limit.
12. Taking deflection, strain and load readings at each load increment. All the measurements except those of the mechanical gauges which were noted manually, were recorded automatically through a computer aided data acquisition equipment.

13. Unloading the track specimen by reducing the load again incrementally from maximum to zero value and recording the corresponding deflection and strain readings.
14. Waiting for all the stored data to be converted from electrical signals to useful engineering units and saved in an allocated file through a special software equipped within the computer system. This process had taken about 2 - 3 hours because of the huge size of the data (all the 64 channels of the data logger were fully utilised during each test).
15. The test was finished and ready to start another one.

8.3.3 Discussion of the Results

Three basic parameters were measured during each test of the track model, namely loads, displacements and strains. The recorded loads and displacements could be directly interpreted without further manipulations. However, the strain measurements were utilised to derive the moments acting on the rail and concrete trough sections along the track model using simple beam theory as described below.

The direct stress (σ) is proportional to its strain (ε) by a constant known as Young's modulus of the material (E), i.e., (Gere and Timoshenko 1985):

$$\sigma = E\,\varepsilon \tag{8.6}$$

The bending stress-moment relationship for an unsymmetrical rail section can be determined by eq. (3.1), (see section 3.3.1, chapter 3). Substituting eq. (8.6) into eq. (3.1) and solving for the moment gives,

$$M = E\,\varepsilon\,(I_y I_x - I_{xy}^2)/(yI_y - x\,I_{xy}) \tag{8.7}$$

The standard flexural formula for a symmetrical section such as the concrete trough is, (Gere and Timoshenko 1985):

$$\sigma = M\,y/I_x \tag{8.8}$$

Similarly, combining eq. (8.6) and (8.8) and solving for the moment results in:

$$M = E\,\varepsilon\,I_x/y \tag{8.9}$$

The x and y coordinates for the strain gauge with respect to the centroid of the rail and concrete trough sections are given in Tables (8.3) and (8.4) respectively. Eqs. (8.7) and (8.9) were used to calculate the bending moment of the rail and concrete trough sections from the measured strain at a specific point along the track model. The results of the four tests in terms of deflections and moments for the rail and concrete trough are shown in Figs. (8.18) - (8.33).

For each of these tests, a corresponding theoretical analysis was made using the LR551D program (explained in chapter 6) in which four cases of base and pad moduli were investigated as shown in Table (8.5). Accordingly, a set of deflection and moment curves were produced covering a range of base modulus between 25 and 45 N/mm^2 and pad modulus between 80 and 120 N/mm^2. The curves were depicted on the same Figs. (8.18) - (8.33) for sake of comparison. The following points summarises the general observations and findings extracted from these tests:

1. It was found from test 1 that concrete strain gauges no. 30 and 33 and rail strain gauges no. 56, 57 and 58 gave suspicious results. This is because they were either not properly cemented to the surfaces during installation or were damaged by accident during testing preparation. Therefore, their readings will be discarded and not given any further consideration.
2. The measured deflections of the rail and concrete trough in all tests are generally in good agreement with the theoretical ones as in most situations they lie within a narrow banded width defined by lower and upper theoretical values. For example, recorded rail deflection at distance 0.025 m from the point load is 1.226 mm in test 1 whereas the corresponding theoretical value ranges between a lower limit of 1.033 mm and an upper limit of 1.537 mm, see Fig. (8.18). Similarly, the recorded rail deflection at the same point (i.e. distance 0.025 m from the point load) in test 2 is 2.409 mm while the corresponding theoretical value fluctuates between lower and upper limits of 2.223 and 3.287 mm respectively, see Fig. (8.22). The maximum measured deflection of the concrete trough in test 2 is 1.843 mm which is bounded by a theoretical lower limit of 1.258 mm and upper limit of 2.033 mm, see Fig. (8.19). Similar findings can also be observed in tests 3 and 4 as presented in Figs. (8.26), (8.27), (8.30) and (8.31).

3. The measured bending moments of the rail excellently match with the theoretical ones as shown in Figs. (8.20), (8.24), (8.28) and (8.32). For example, the maximum recorded moments of the rail for tests 1 - 4 are 5.631, 12.443, 13.856 and 13.638 kN m respectively. Their corresponding maximum theoretical values are 5.506 kN m (i.e. -2.27% difference), 12.152 kN m (i.e. -2.39% difference), 14.134 kN m (i.e. +1.96% difference) and 14.116 kN m (i.e. +3.38% difference) for tests 1 - 4 respectively. As far as the concrete trough is concerned, there are good agreements between the measured and calculated moments. For instance, the maximum measured moment for tests 1 - 4 are 5.132, 11.407, 18.597 and 18.117 kN m respectively. The corresponding maximum theoretical values are 5.108 kN m (i.e. -0.47 % difference), 11.277 kN m (i.e. -1.15 % difference), 22.172 kN m (i.e. +16.12% difference) and 22.143 kN m (i.e. +18.18% difference) for tests 1 - 4 respectively. It should be noted that the positive percentage difference means the theoretical applied moments are overestimated which is on the safe side. By engineering judgement, a range of difference up to ±20% between the experimental and theoretical results for concrete structures is quite common and acceptable, particularly when testing an unconventional structure such as a track system and when the mathematical model predicts safer results as it is the case with the subjected investigated in the present work.
4. No sign of cracking or crashing was noticed in the concrete trough anywhere along the 6 m long track model through out all the tests. This means that the tensile and compressive stresses induced in the concrete trough due to test loads around 100 kN were within the permissible limits. Therefore, the correctness of the theoretical design for the pre-tensioned prestressed concrete trough section according to the serviceability limit states (transfer and service) requirements was firmly demonstrated. Consequently, as a factor of safety of 1.6 was assumed over the working load, (see section 7.6.3 in chapter 7), the ultimate limit state requirements for the prestressed concrete trough design were implicitly checked by these tests, though they were non-destructive. Eventually, the performance of the concrete trough as a principal supporting structure to the LR55 rail, at service and ultimate conditions, was confidently ensured both theoretically and experimentally.
5. The elastomeric pad remained firmly intact after conducting all the tests as no indication of tearing within the material or debonding at the rail or concrete inter-

face occurred. This strongly supports the excellent mechanical (tensile and shear strength) and chemical (adhesion) characteristics of the grouting polymer pad determined through rigorous tests as discussed previously in chapter 3.

6. The supporting track base of sand soil did not fail even when there was a cavity of 1 m length as the pressure on the track base was expected to be relatively high at the edge of the cavity. This observation confirms the initial estimation of sand bearing capacity obtained from plate-load tests.

7. The main reasons for the discrepancies in the results found between the physical and mathematical model of the LR55 track model might be assigned to the following factors: First, the theoretical model assumes the rail and concrete are linear, elastic, homogeneous and isotropic. In fact, such assumptions are appropriate to the steel rail, but they are less applicable to the concrete as it is practically nonlinear, anisotropic (its physical qualities depend on direction) and nonhomogeneous (it has macroscopic heterogeneous composition), (Mûller 1984). This is why there is close agreement (differences in the range of ±2.5%) between the experimental and predicted theoretical rail moments, whereas the difference is up to around 18% for the concrete moment, (see point 3 above). Second, the theoretical model represents the resistance of the pad and base by linear elastic uniaxial springs. However, the actual behaviour of these foundations depends on their material constitutive laws. For instance, the elastomeric pad is visco-elastic material which is characterised by slow and time dependent deformation under the influence of applied load, (Nagdi 1995). The behaviour of supporting track base is generally nonlinear elastic that relies on the stress state condition within the material, i.e. its response is stress-path dependent, (Tayabji and Thompson 1976, Raymond 1990). Third, due to the unsymmetrical shape of the LR55 rail which causes a difference of 4.1 mm between the centroid of the rail and the concrete trough, it is not possible to coincide the line of action of the imposed load with the centroid of the rail and concrete trough simultaneously. Thus there is always an avoidable twisting effect, though it is slight because of that small eccentricity. This induced twisting effect has not been taken into account in the theoretical model. Fourth, the whole process of experimental work normally involved various possible source of errors including inaccuracies in geometrical dimensions occurring during fabrication of the track specimen components, measuring instruments set up,

loading techniques and data recording during the tests. These errors would be accumulated and eventually leading to the variation between the experimental and theoretical results.

8.4 Summary and Conclusion

Four static and non-destructive tests were carried out on a full scale 6 m long track model, including the case of 1 m collapsed foundation simulation by applying a single point at the centre of the track model up to a pre-assigned maximum value. The track specimen consisted of a pre-tensioned prestressed concrete trough and a cast steel LR55 rail section bounded together by an elastomeric pad. The track model was mounted on a compacted sand foundation in which the latter was contained in a timber box. The whole arrangement of the sand box was set to have equivalent characteristics of an actual supporting track base that were specified through a series of plate-load tests. The instrumentation comprised of 58 electrical resistance strain gauges and 14 displacement measuring devices (9 mechanical dial gauges and 5 electrical transducers).

In general, the information gained experimentally compared well with the theoretical solution using one dimensional finite element analysis (LR551D program). The theoretical optimum design of the prestressed concrete trough section, satisfying the serviceability and ultimate limit states requirements was also demonstrated through these tests. Consequently, the mathematical model developed for the LR55 track system as multilayer beams on elastic foundations was validated. At last, this experimental work enhanced the theoretical investigation, leading to an increased understanding of the system potential performance in service.

Table (8.1): Foundation modulus and bearing capacity for various sand depths.

Sand depth (mm)	Idealised pressure-deflection equation*		k_{plate}	k_b	Bearing capacity
	$p = f(\delta)$	R^2	eq. (8.2) (kN/m^3)	eq. (8.4) (N/mm^2)	(kN/m^2)
400	$-14.421\delta^2 + 174.59\,\delta$	0.9894	160.169	43.005	519.96
500	$-13.617\delta^2 + 152.70\delta$	0.9873	139.083	37.344	430.815
600	$-10.769\delta^2 + 131.75\delta$	0.9887	120.981	32.483	400.197
700	$-11.302\delta^2 + 125.36\delta$	0.9744	114.058	30.624	334.892
800	$-8.3651\delta^2 + 93.054\delta$	0.9729	84.689	22.739	267.285

* The equations and their coefficient of correlation (R^2) are obtained by nonlinear regression analysis available within EXCEL software.

Table (8.2): Characteristics of the tests on the full-scale 6 m long track model.

Test no.	Maximum load (kN)	Support condition
1	43.27	continuously supported by the sand soil
2	95.48	continuously supported by the sand soil
3	98.34	bridged over a 1 m long cavity
4	98.21	bridged over a 1 m long cavity

Table (8.3): The x and y coordiantes of the rail strain gauges with respect to the centroid of the rail.

Strain gauge no.*	x-coordinate (mm)	y-coordinate (mm)
37, 40, 43, 46, 49, 52 and 55	-45.859	+37.160
36, 39, 42, 45, 48, 51 and 54	-10.859	+37.637
35, 38, 41, 44, 47, 50 and 53	59.141	+20.341
56, 57 and 58	+21.641	-8.862

* For strain gauge no. see Fig. (8.10)

Table (8.4): The y-coordiantes of the concrete strain gauges with respect to the centroid of the concrete trough.

Strain gauge no.	y-coordinate (mm)
1, 2, 3, ..., 27, 28	+103.574
31 and 32	+73.574
30 and 33	+13.574
29 and 34	-46.426

* For strain gauge no. see Fig. (8.10)

Table (8.5): Base and pad moduli for the cases investigated in the theoretical analysis.

Case No.	Base modulus (N/mm^2)	Pad modulus (N/mm^2)
1	25	80
2	25	120
3	45	80
4	45	120

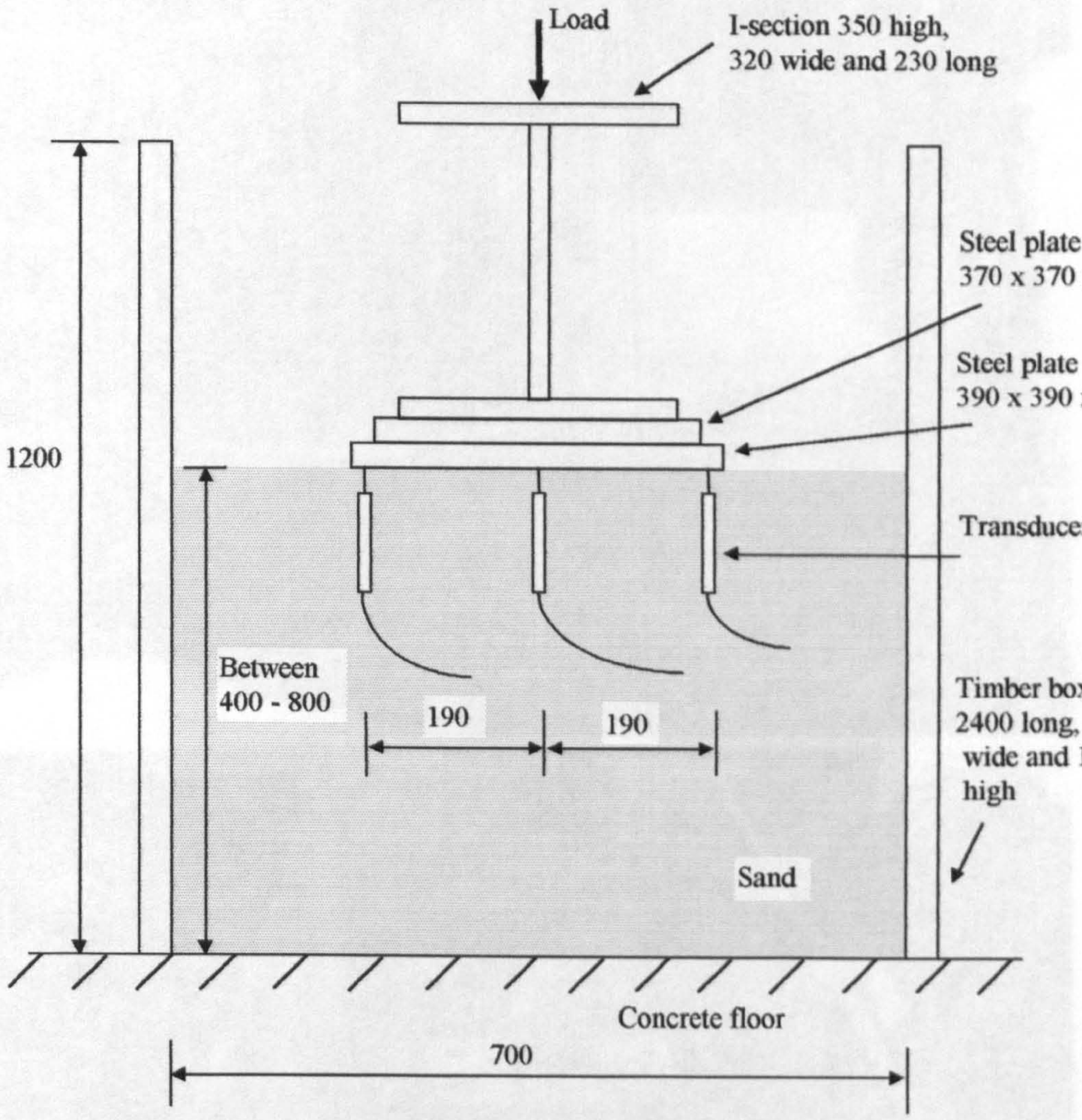

Fig. (8.1): A schematic diagram of the plate-load test.

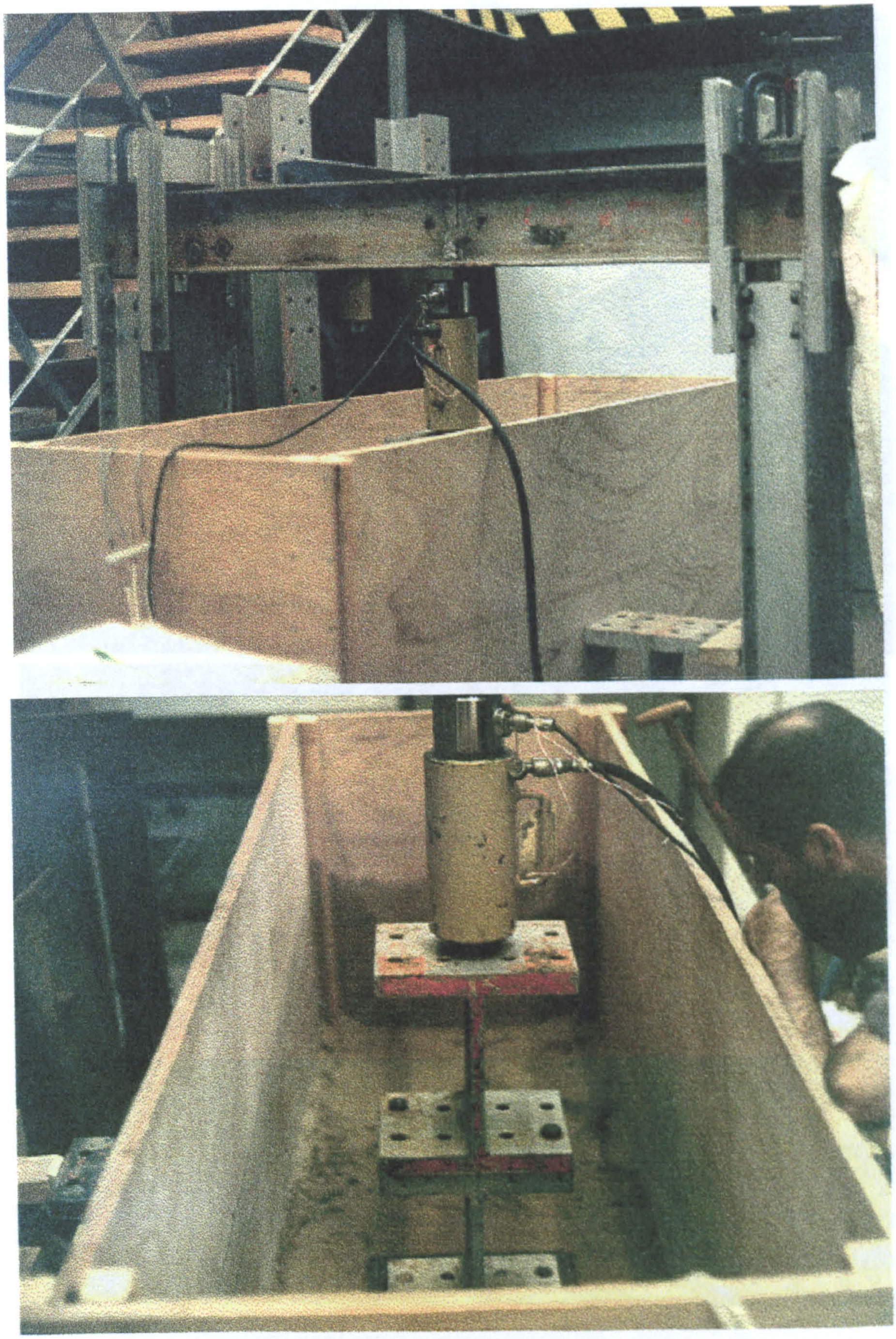

Fig. (8.2): Plate-load test showing the sand box and loading rig.

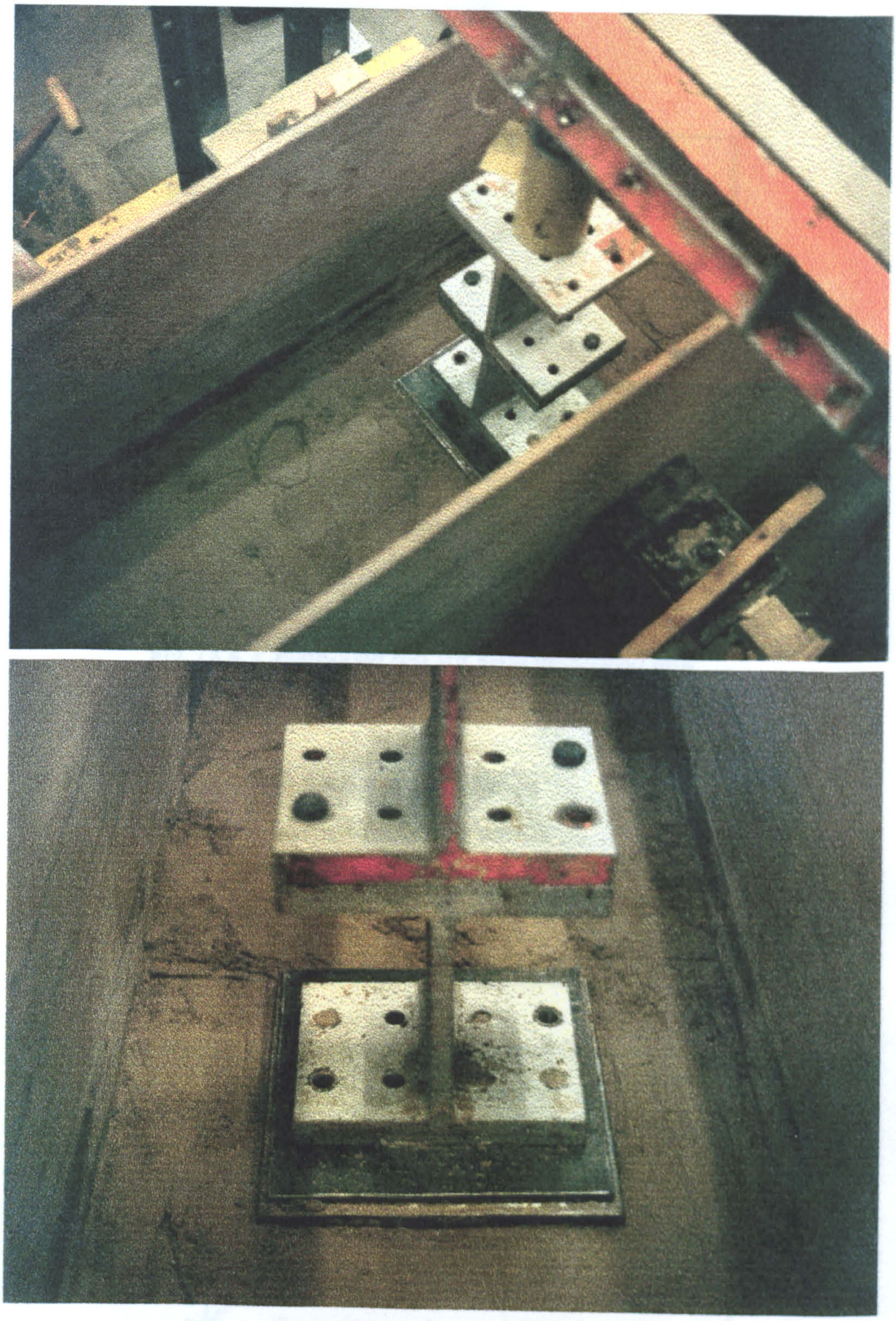

Fig. (8.3): Plate-load test showing the stacked plates and I-sections.

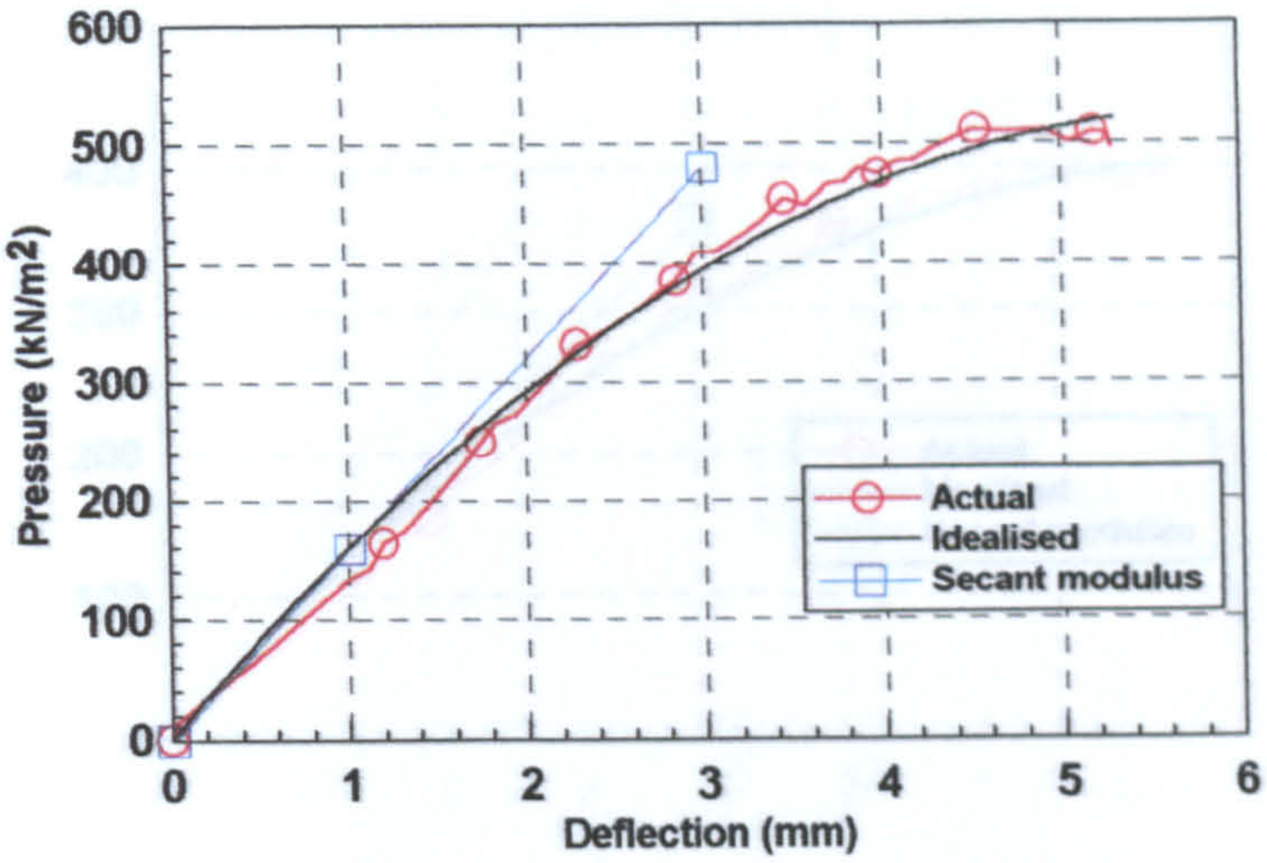

Fig. (8.4): Plate-load test for sand depth 400 mm.

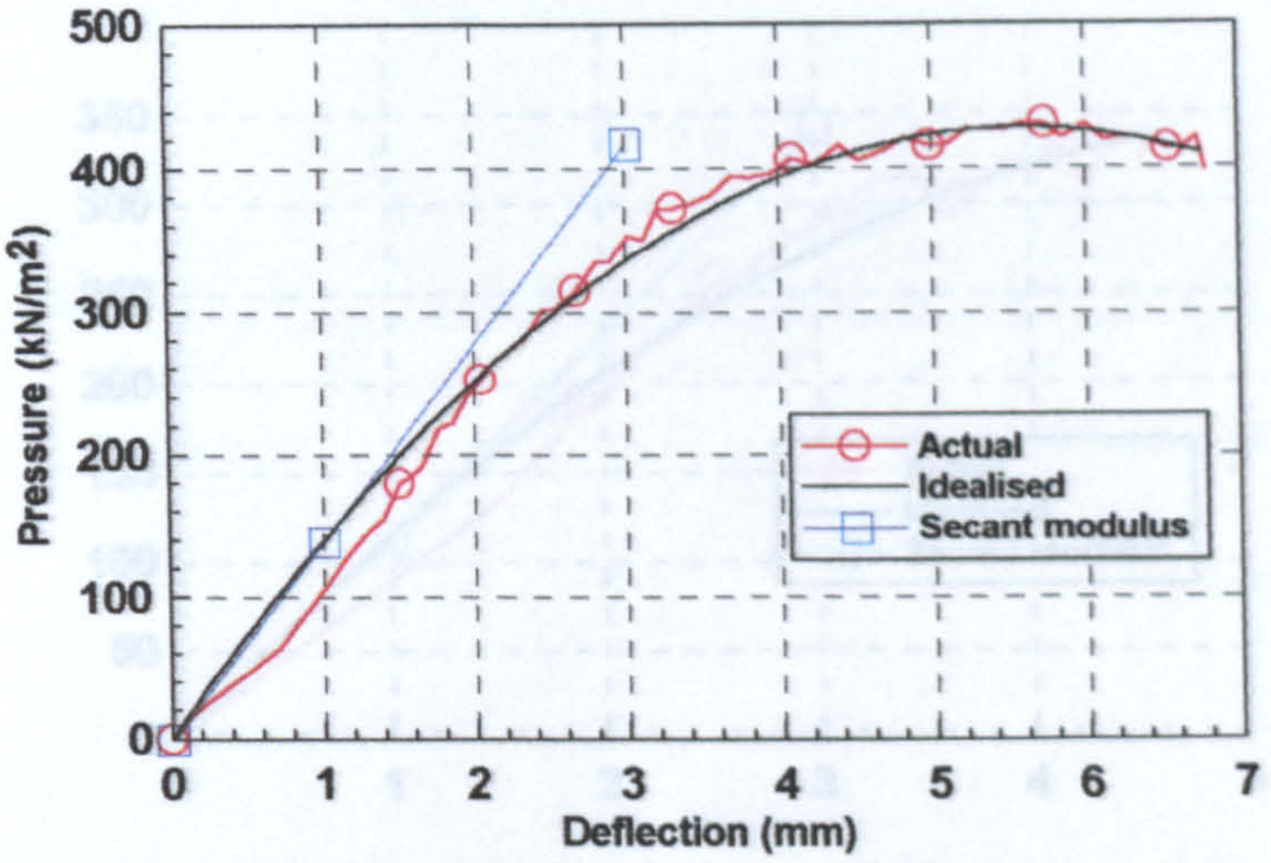

Fig. (8.5): Plate-load test for sand depth 500 mm.

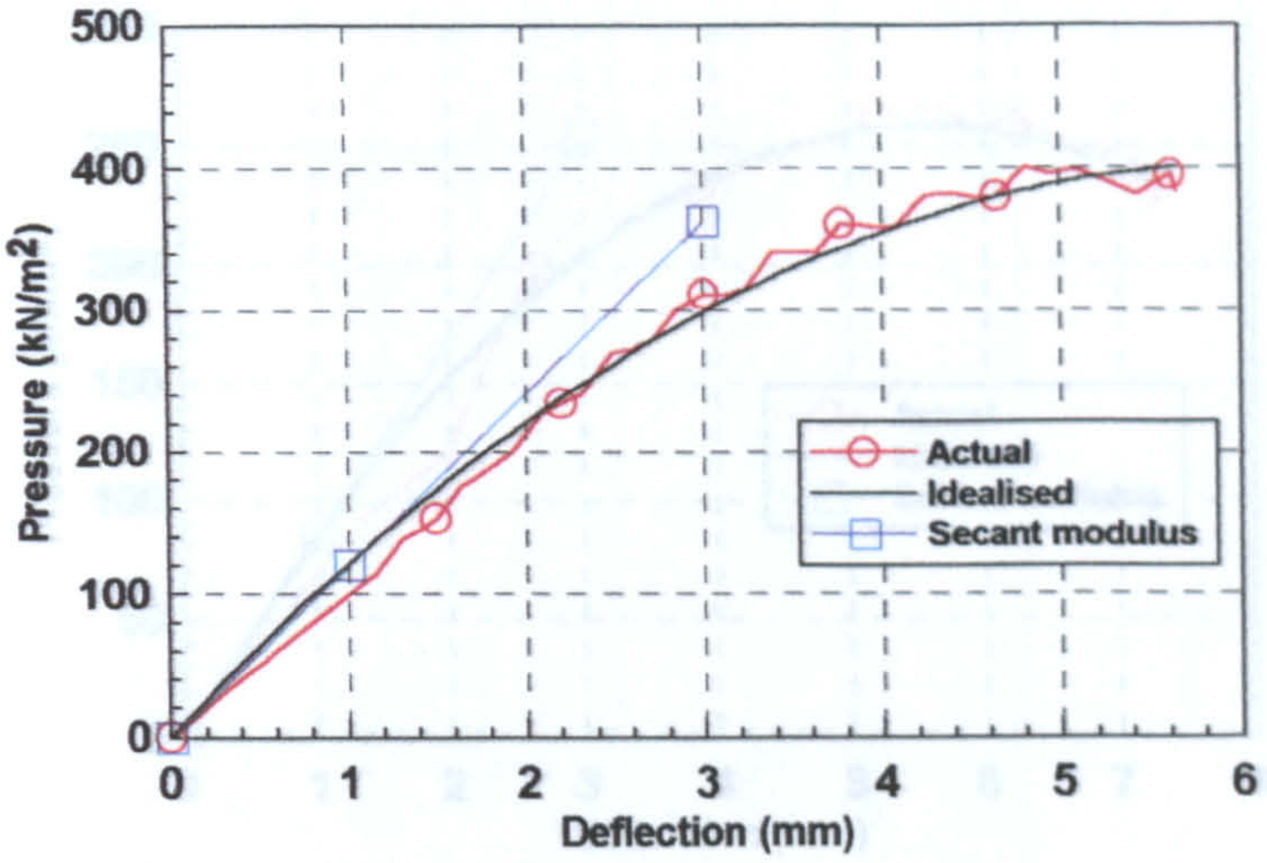

Fig. (8.6): Plate-load test for sand depth 600 mm.

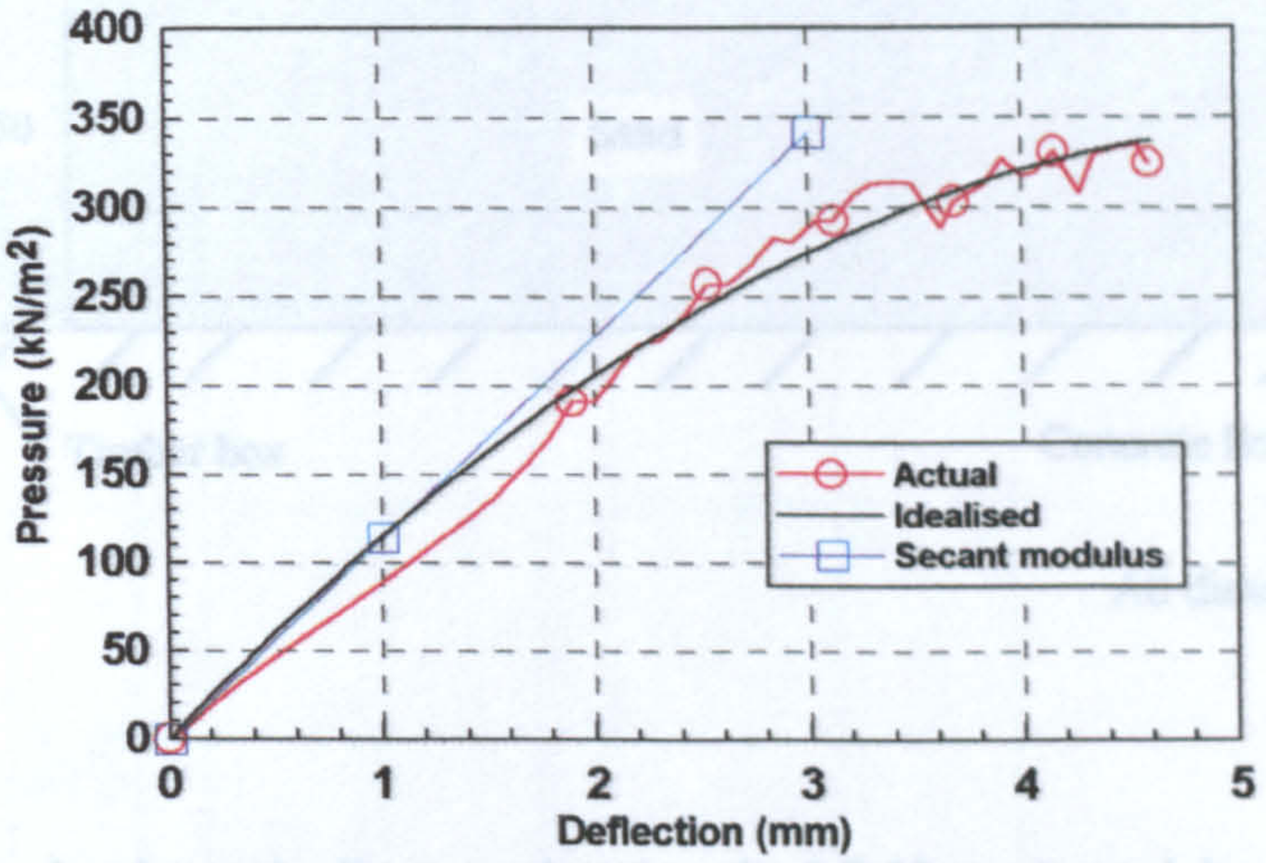

Fig. (8.7): Plate-load test for sand depth 700 mm.

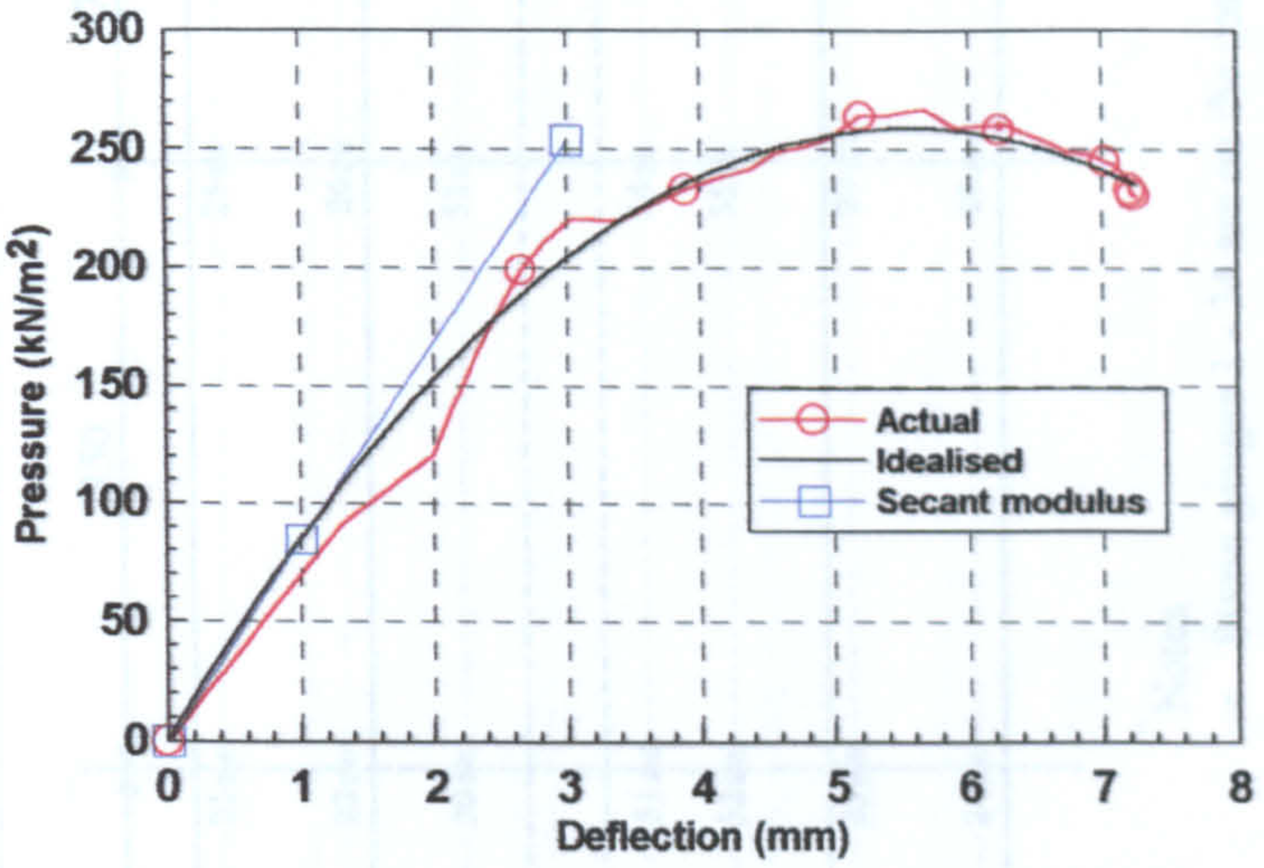

Fig. (8.8): Plate-load test for sand depth 800 mm.

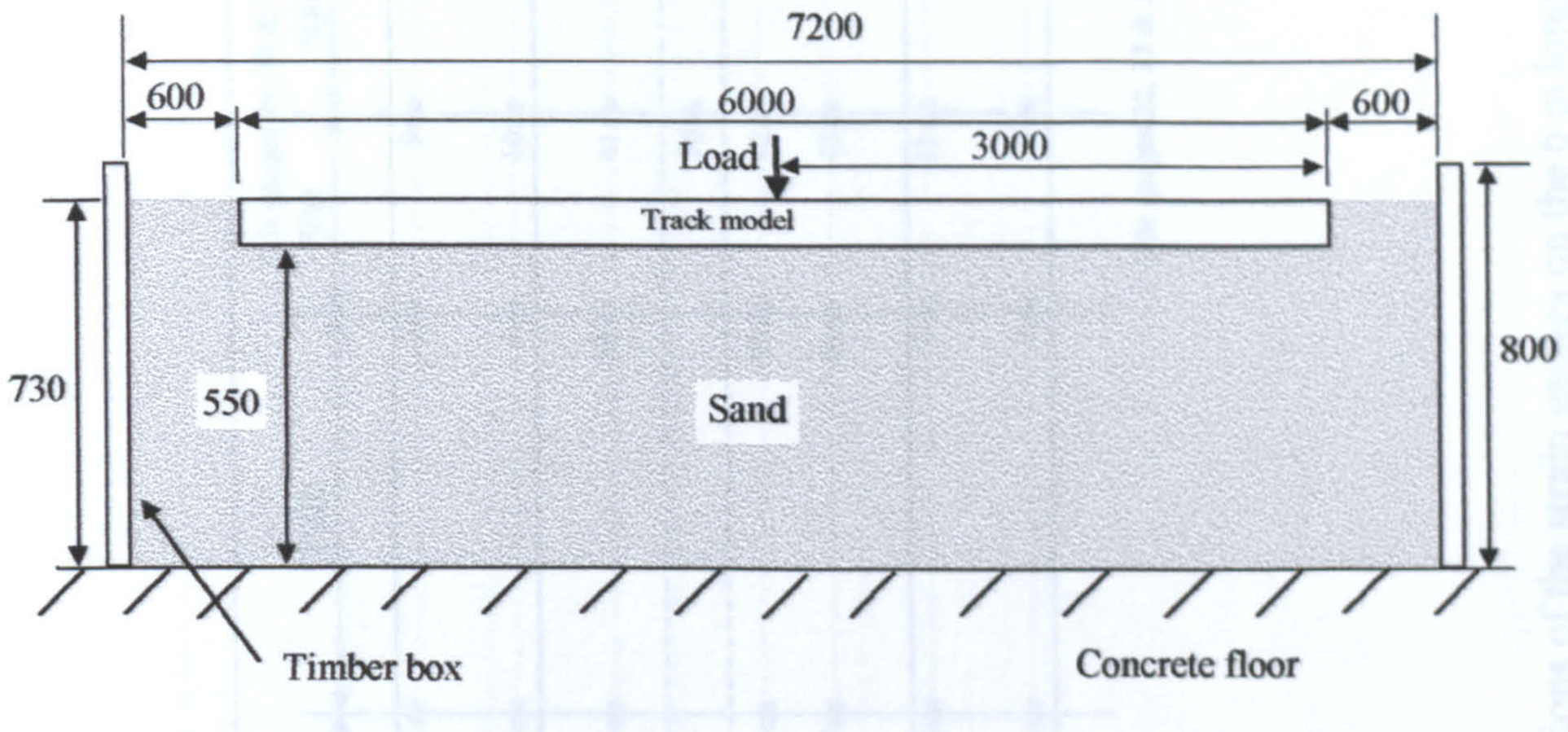

Fig. (8.9): A schematic diagram showing the LR55 track model and sand box.

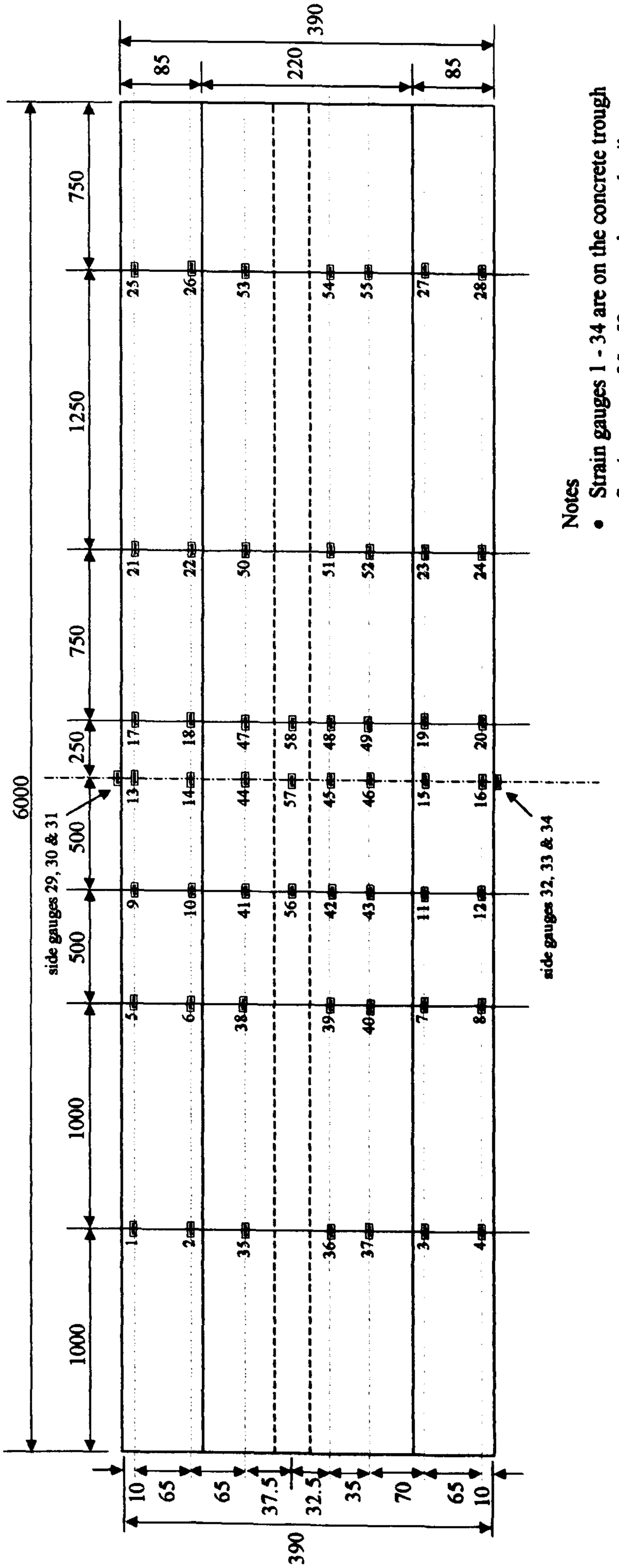

Notes

- Strain gauges 1 - 34 are on the concrete trough
- Strain gauges 35 - 58 are on the steel rail
- All dimensions are in mm

Fig. (8.10): Locations of the strain gauges on the 6 m long track model for all the tests.

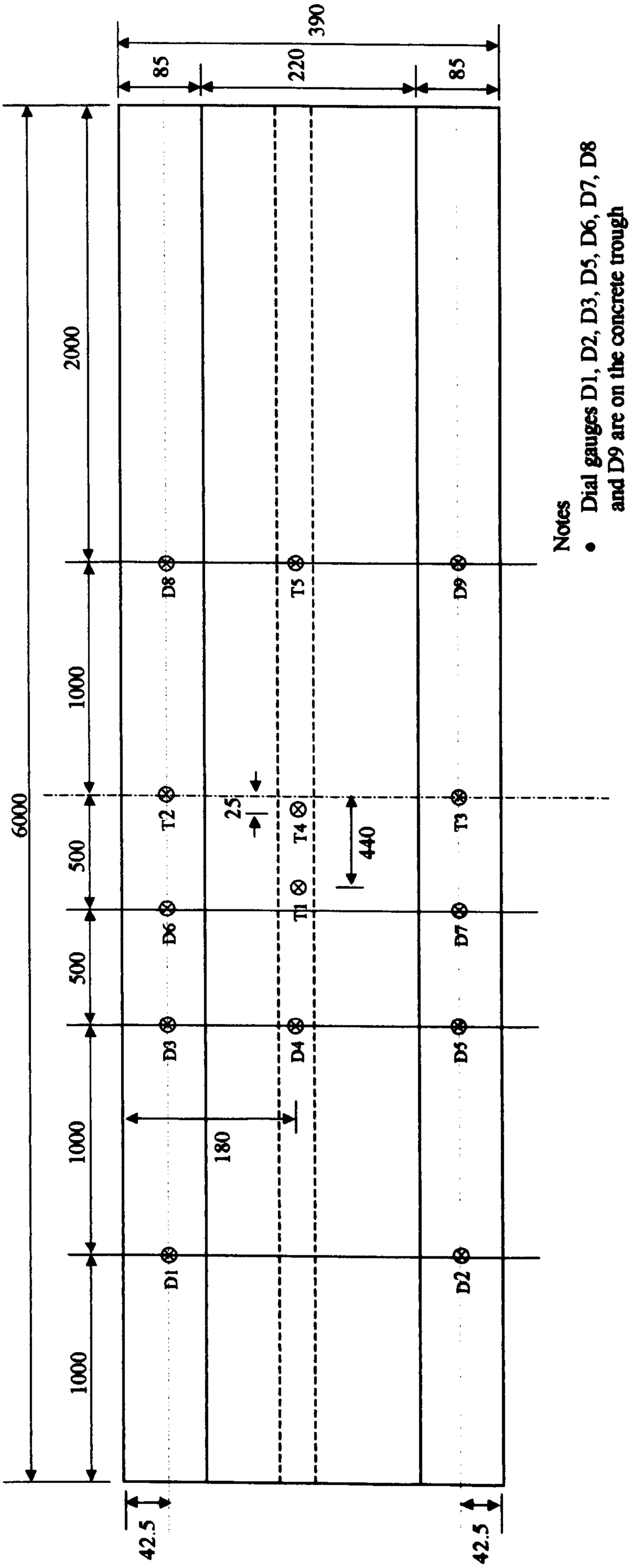

Notes

- Dial gauges D1, D2, D3, D5, D6, D7, D8 and D9 are on the concrete trough
- Dial gauge D4 is on the steel rail
- Transducers T2 and T3 are on the concrete trough
- Transducers T1, T4 and T5 are on the steel rail
- All dimensions are in mm

Fig. (8.11): Locations of the dial gauges and transducers on the 6 m long track model for tests 1 and 2.

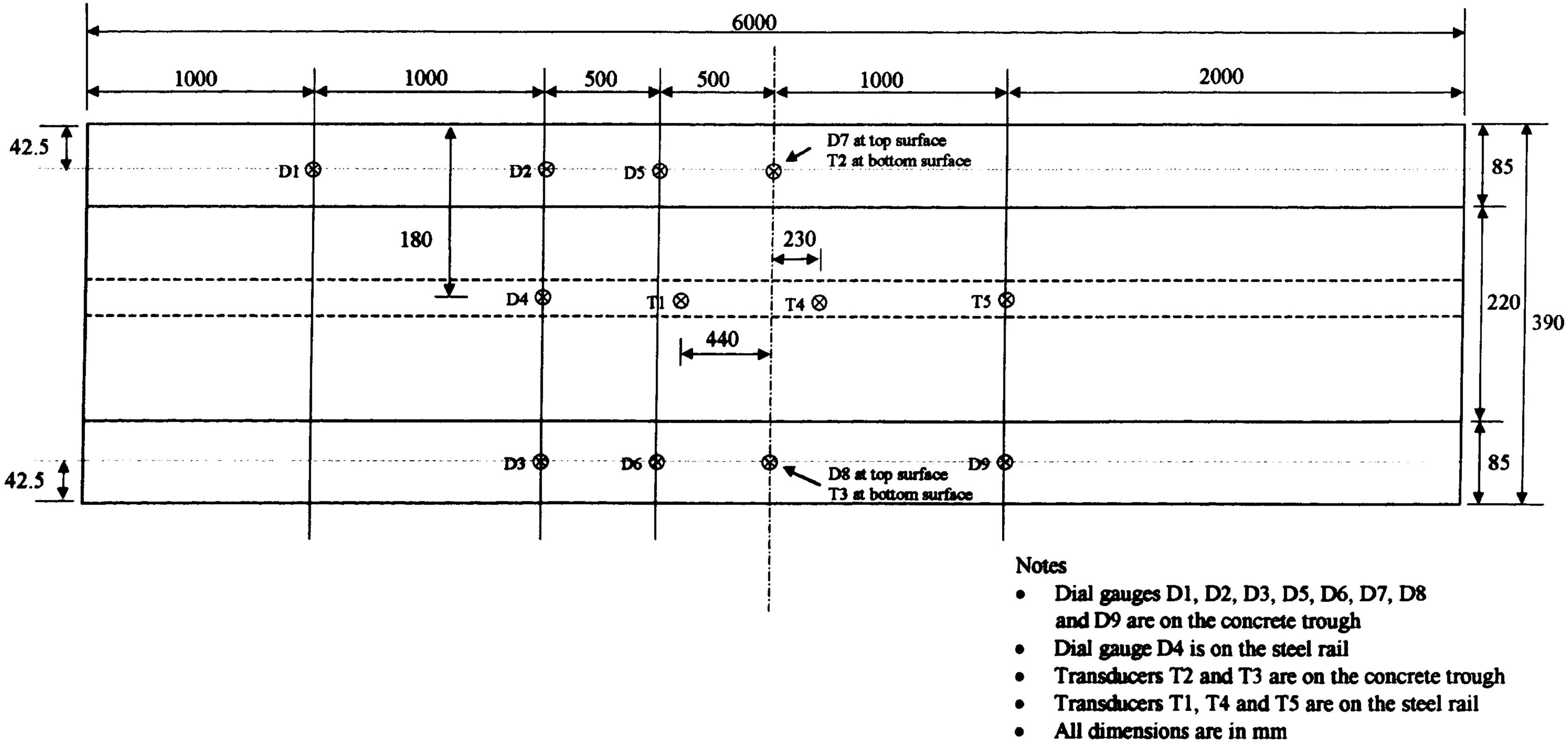

Fig. (8.12): Locations of the dial gauges and transducers on the 6 m long track model for tests 3 and 4.

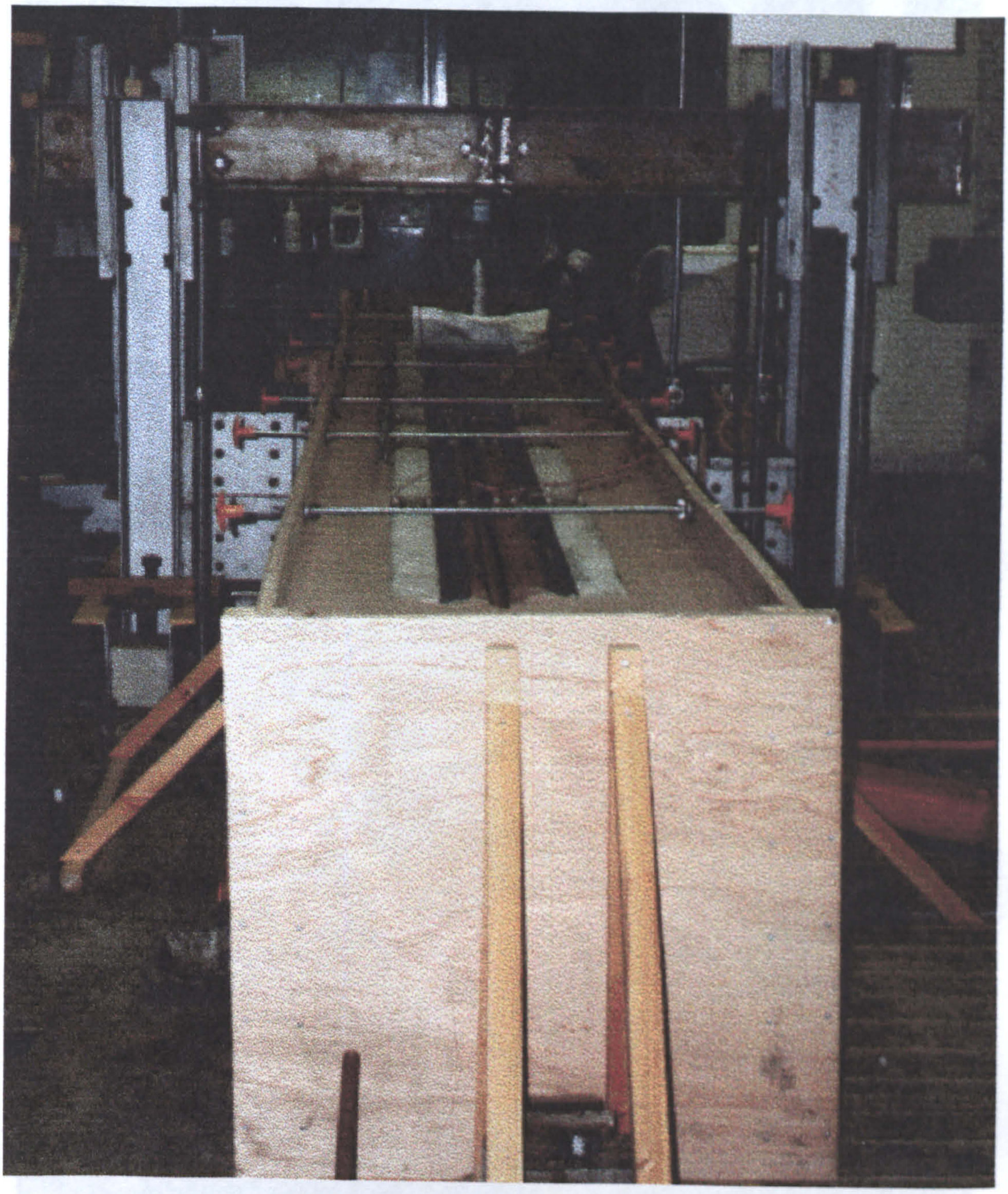

Fig. (8.13): A test rig for the full-scale 6 m long LR55 track model.

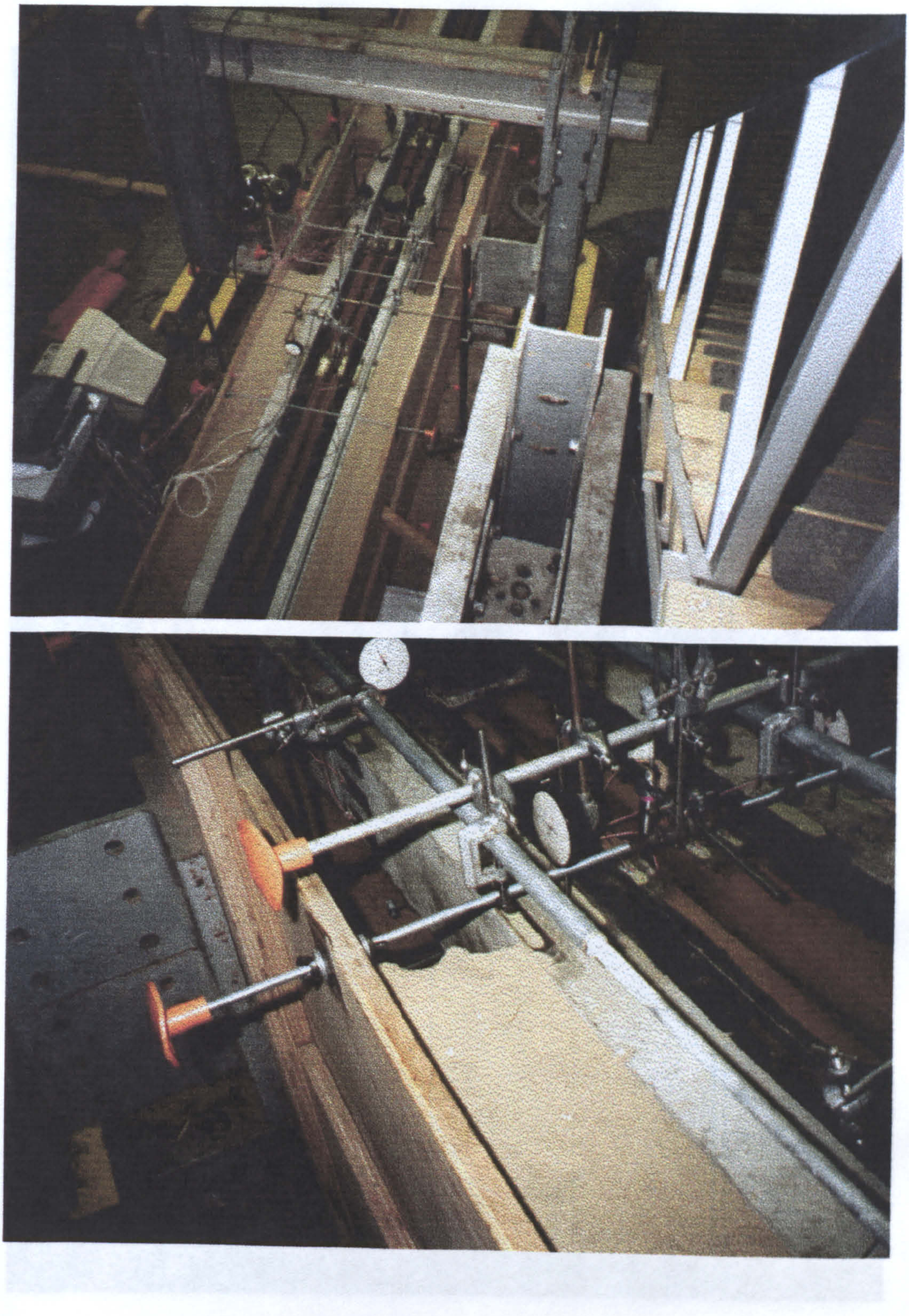

Fig. (8.14): A test for the LR55 track model with1 m long cavity underneath to simulate foundation subsidence.

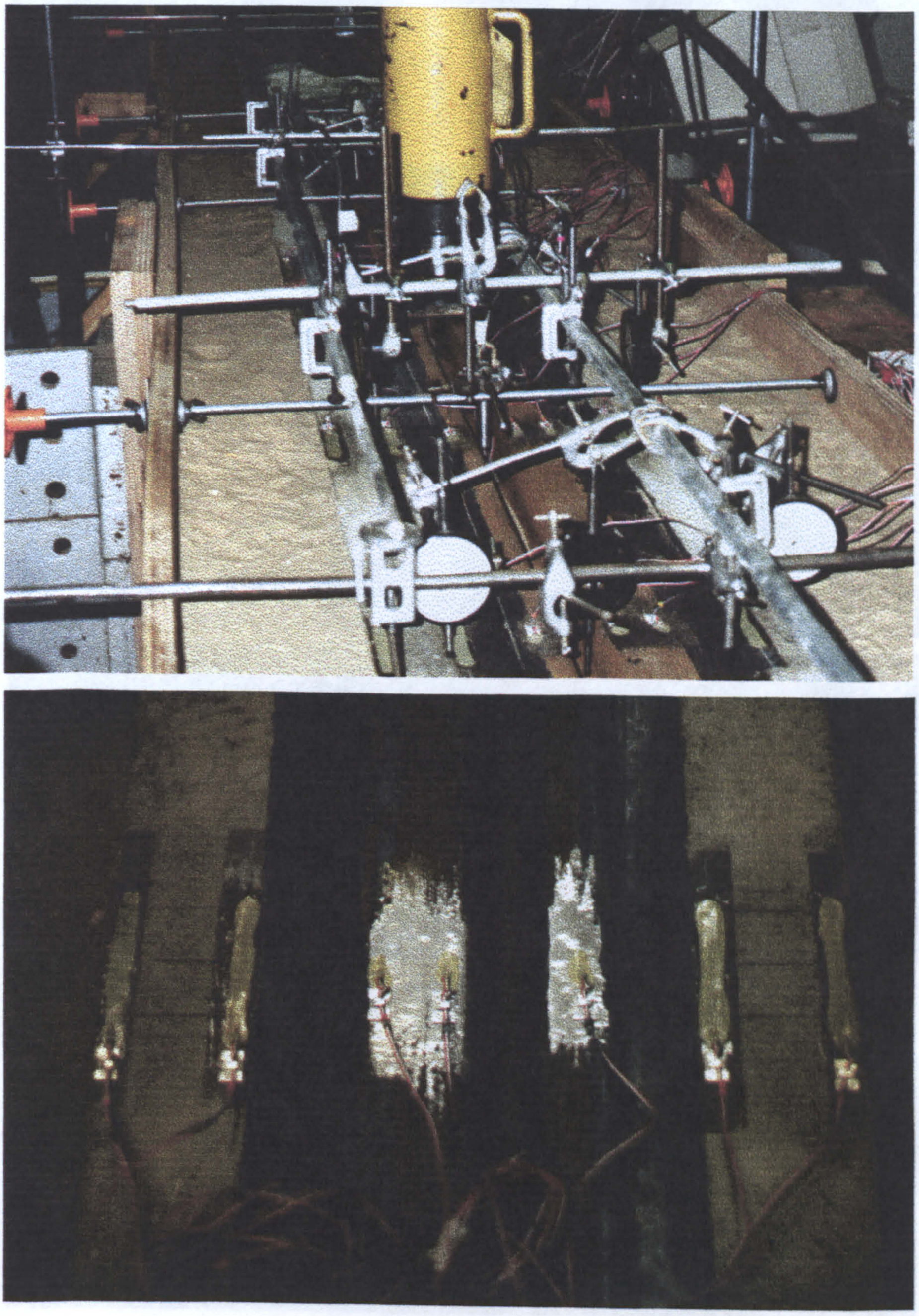

Fig. (8.15): A test for the LR55 track model showing the strain and displacement instrumentation.

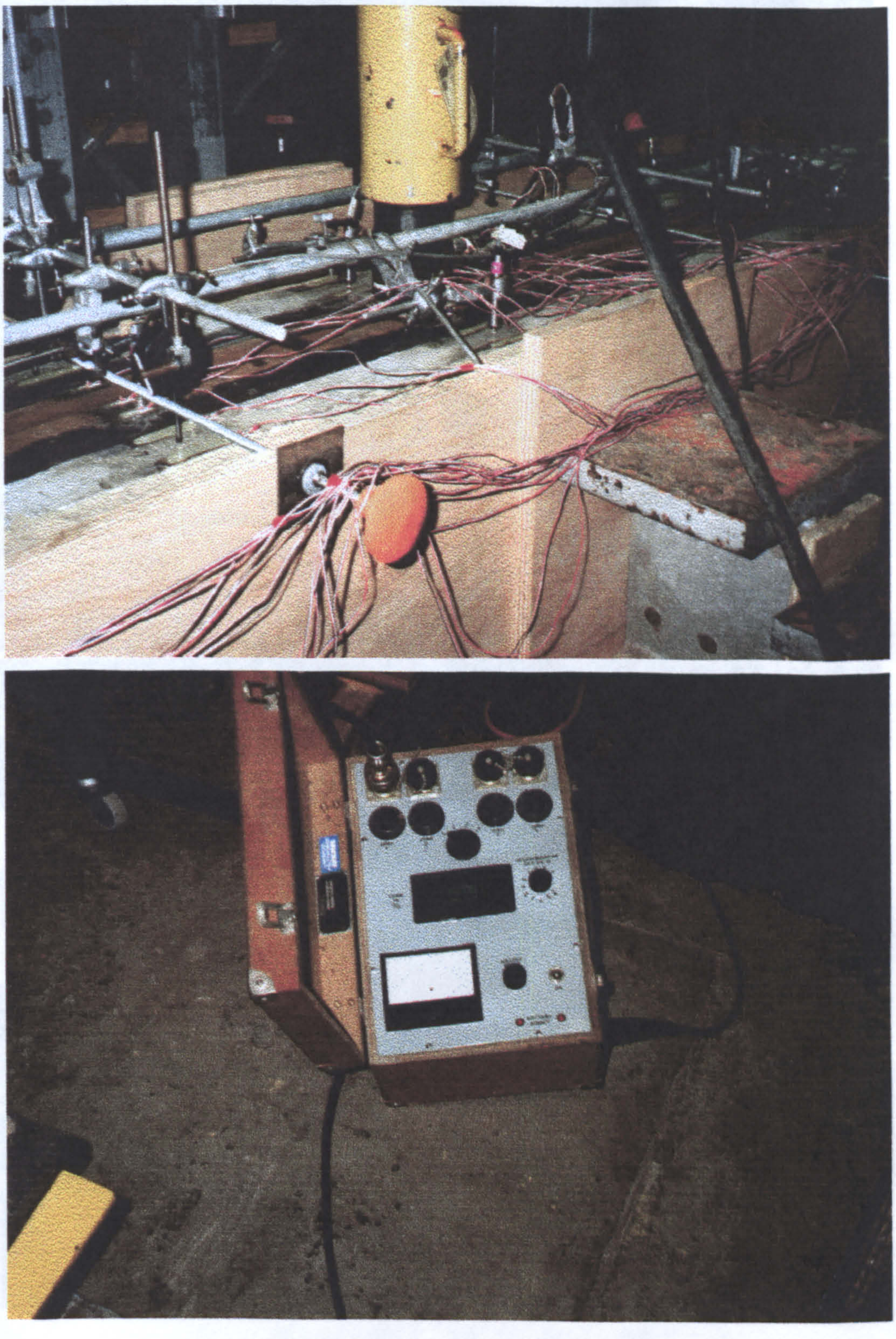

Fig. (8.16): A test for the LR55 track model showing the hydraulic ram and load reading metre.

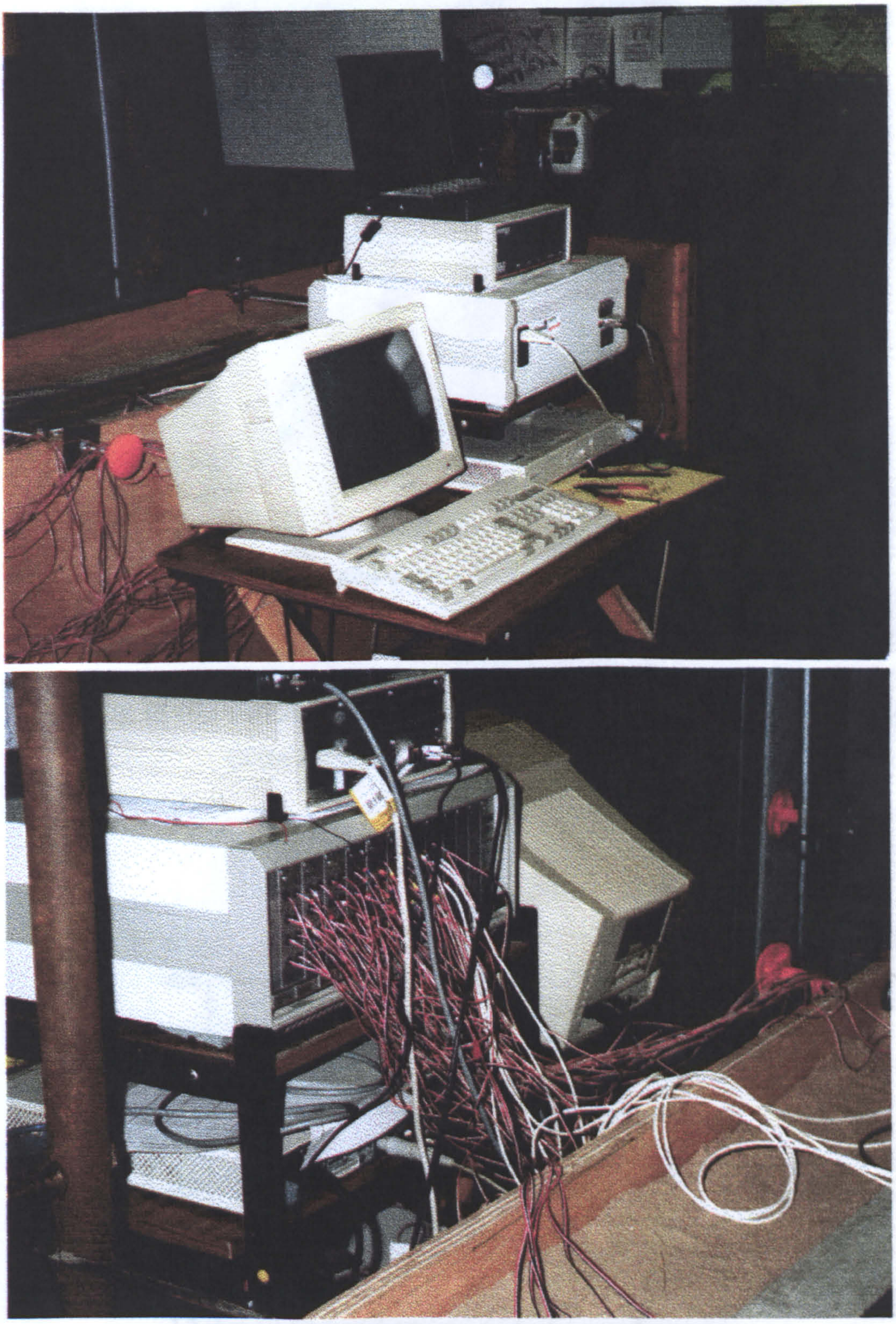

Fig. (8.17): A test for the 6 m LR55 track model showing computer aided data acquisition equipment.

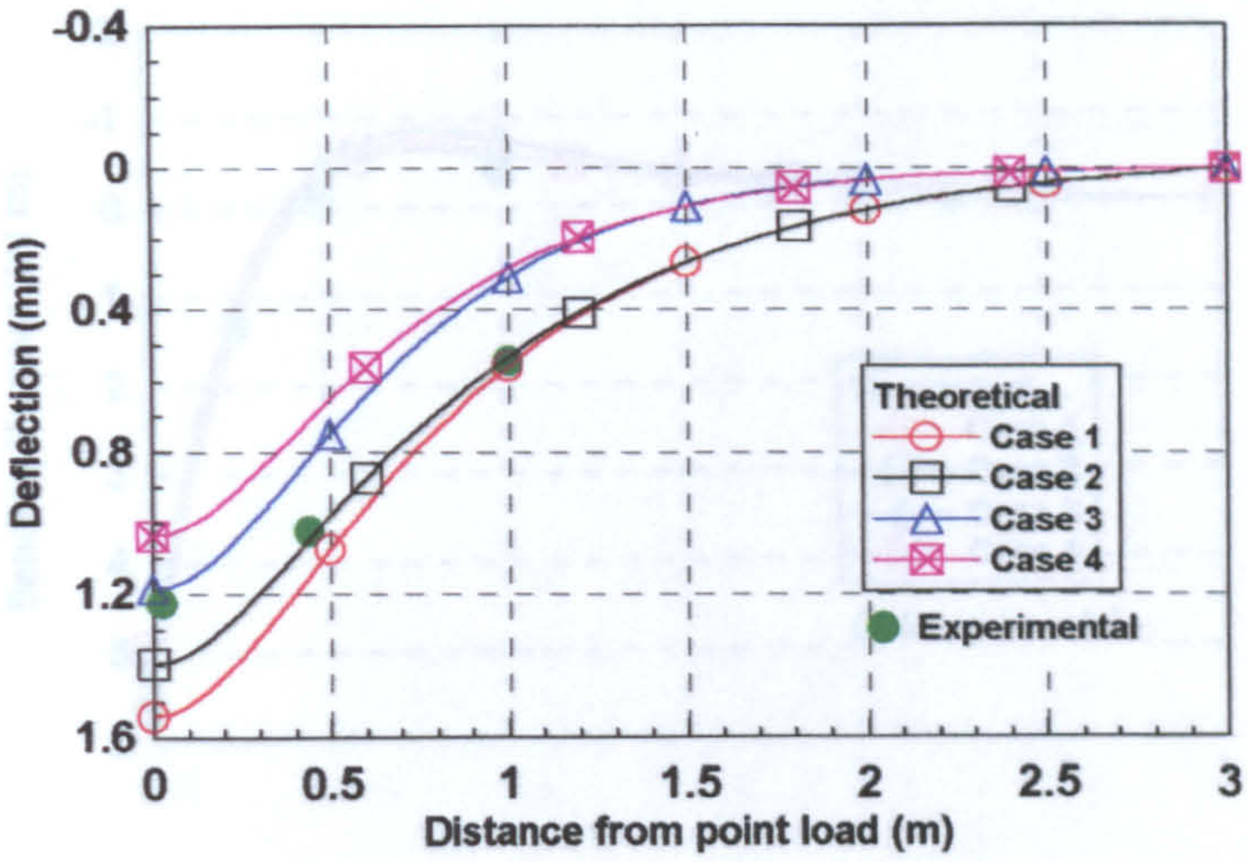

Fig. (8.18): Comparison between the experimental and theoretical deflections of the rail for test 1, (load = 43.27 kN).

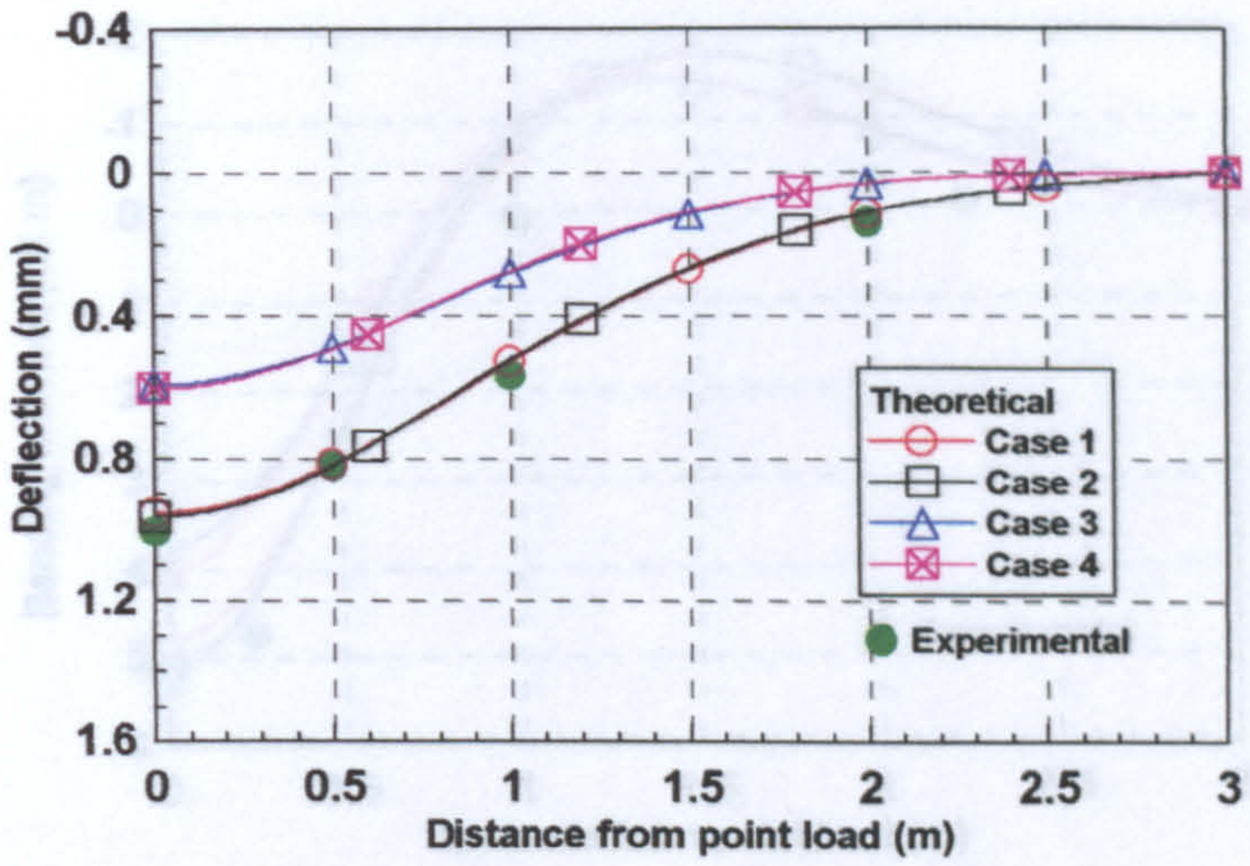

Fig. (8.19): Comparison between the experimental and theoretical deflections of the concrete trough for test 1, (load = 43.27 kN).

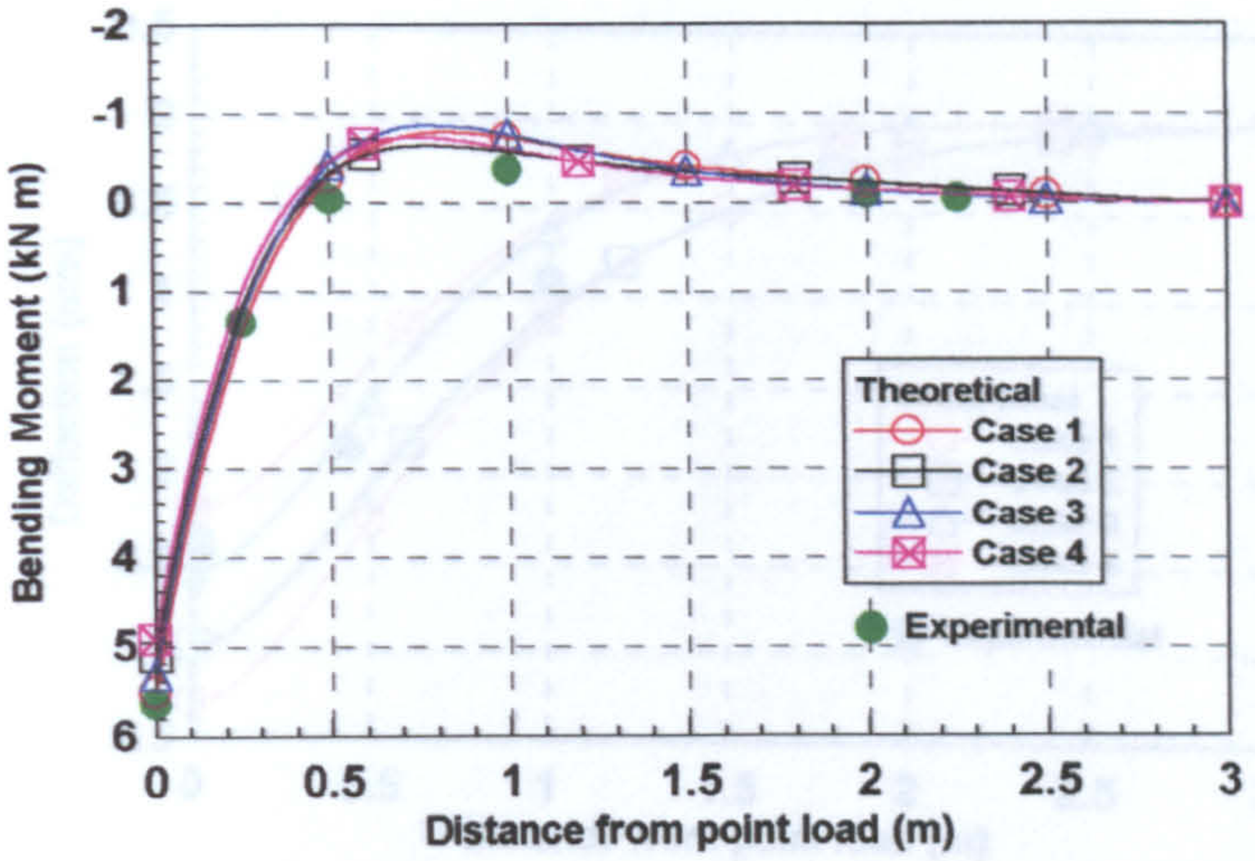

Fig. (8.20): Comparison between the experimental and theoretical bending moments of the rail for test 1, (load = 43.27 kN).

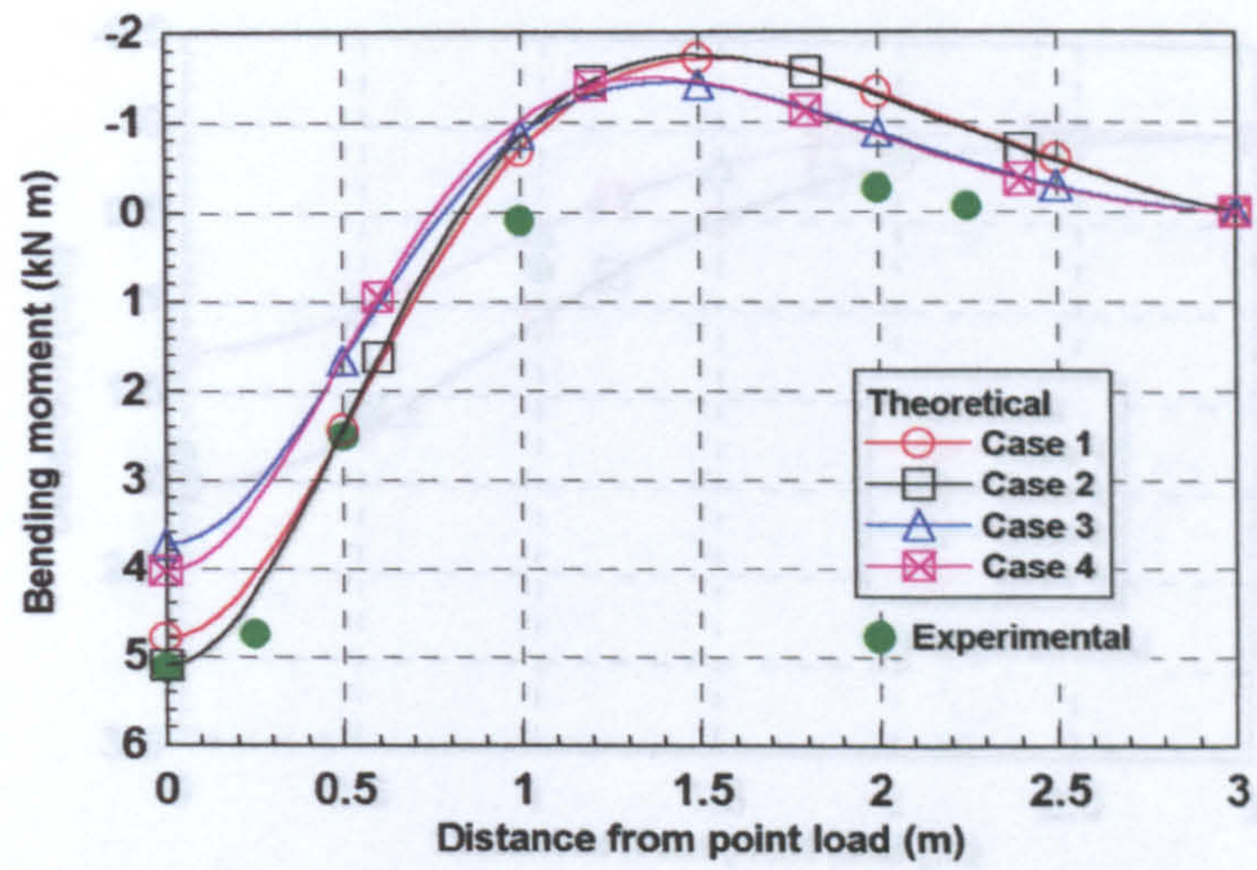

Fig. (8.21): Comparison between the experimental and theoretical bending moments of the concrete trough for test 1, (load = 43.27 kN).

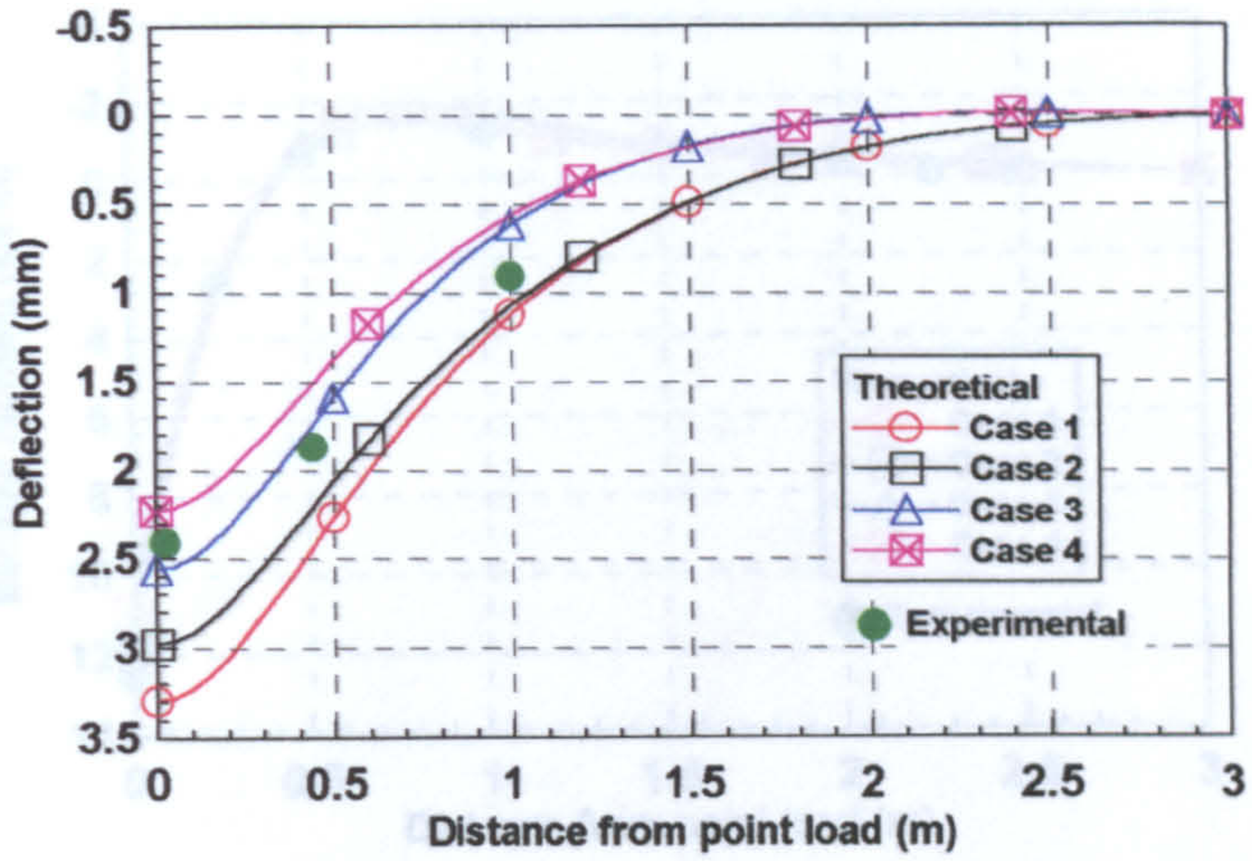

Fig. (8.22): Comparison between the experimental and theoretical deflections of the rail for test 2, (load = 95.48 kN).

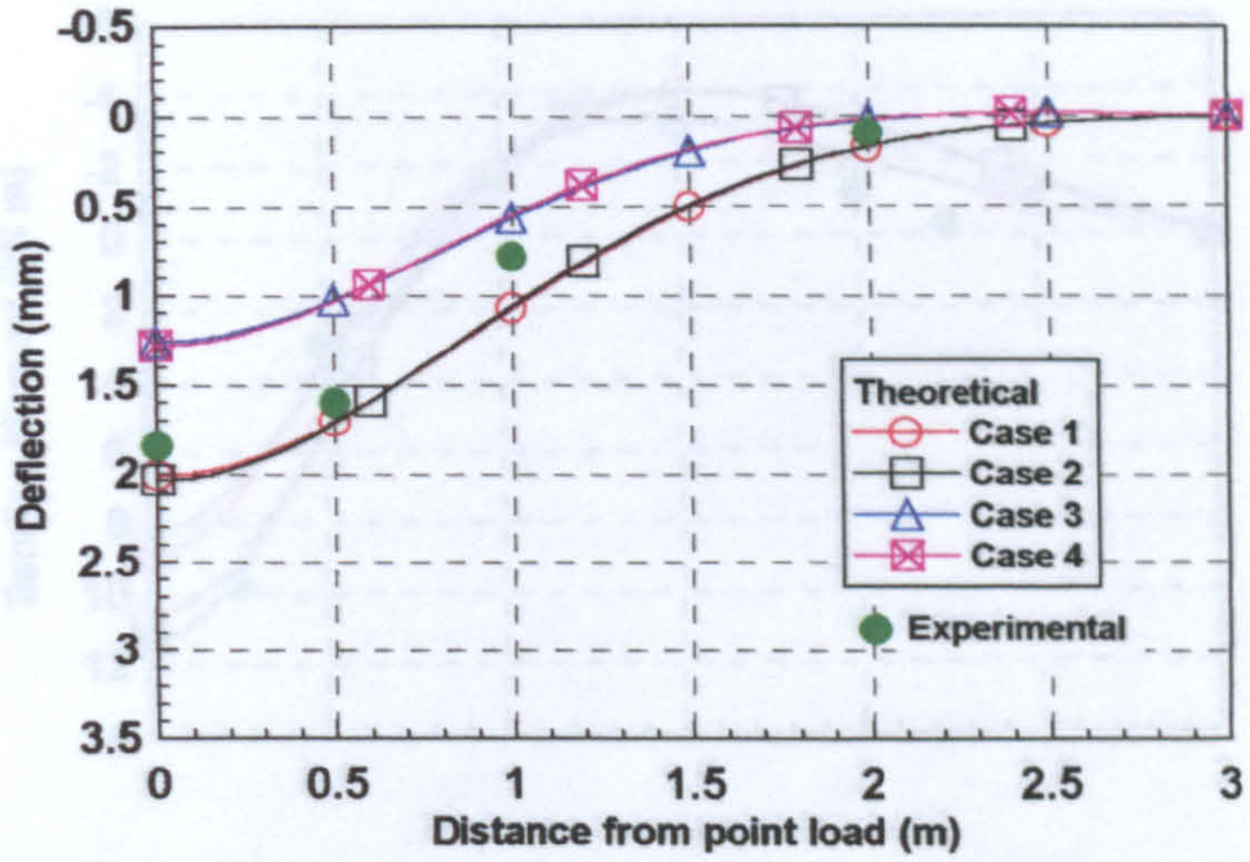

Fig. (8.23): Comparison between the experimental and theoretical deflections of the concrete trough for test 2, (load = 95.48 kN).

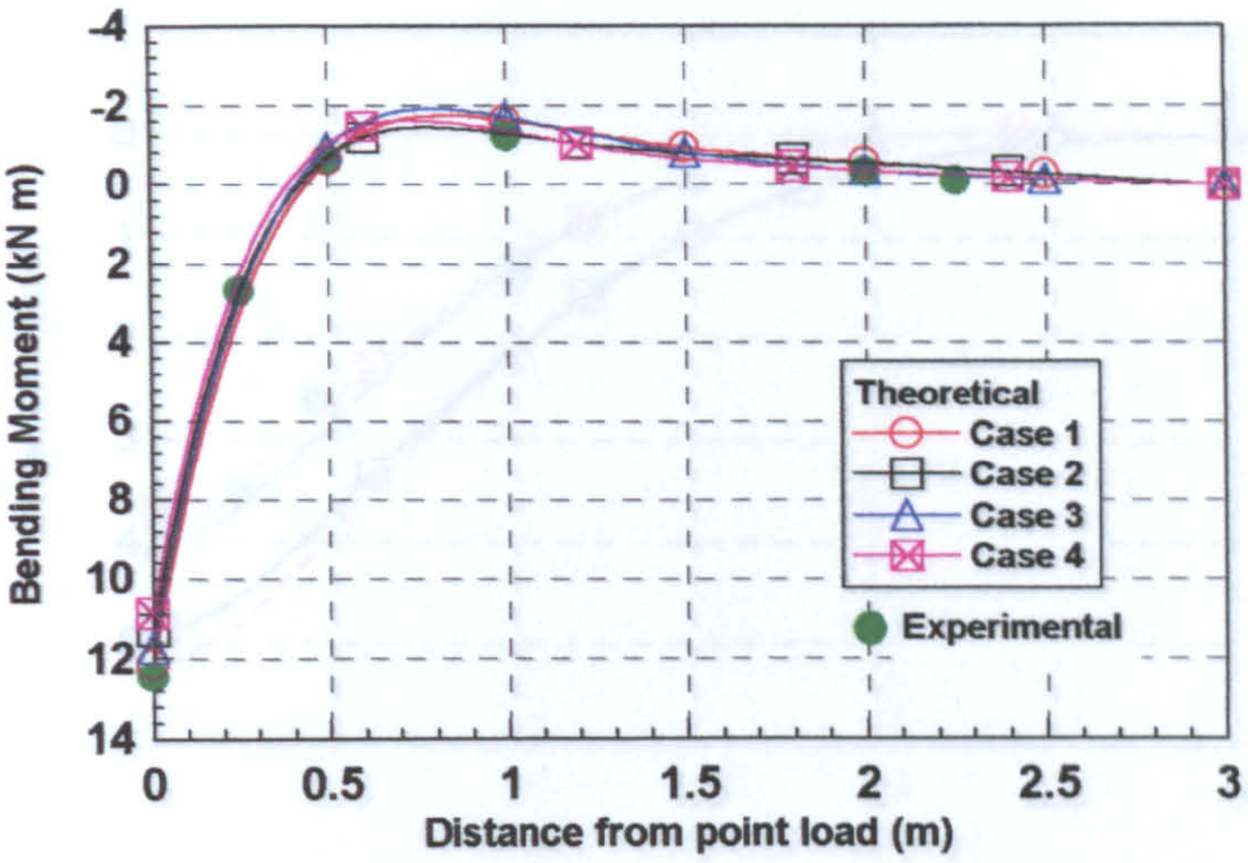

Fig. (8.24): Comparison between the experimental and theoretical bending moments of the rail for test 2, (load = 95.48 kN).

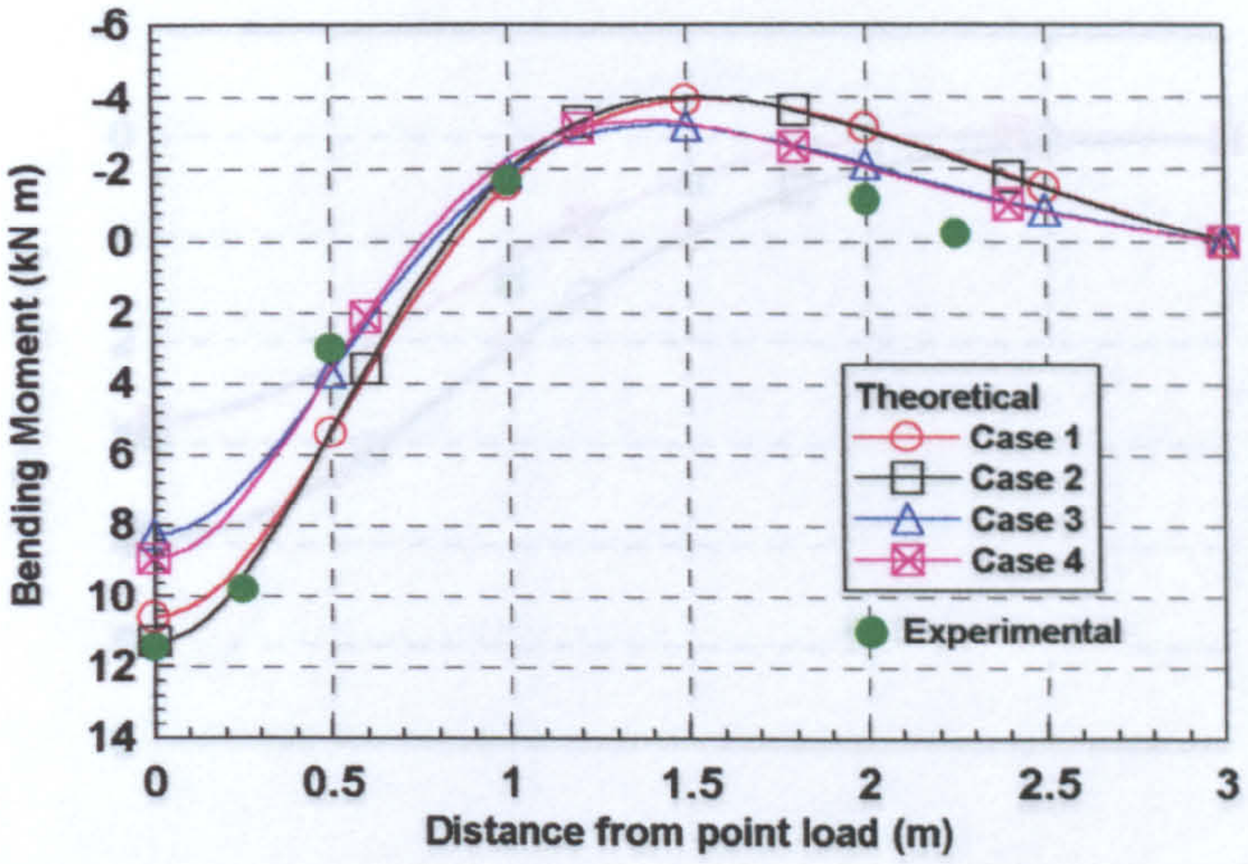

Fig. (8.25): Comparison between the experimental and theoretical bending moments of the concrete trough for test 2, (load = 95.48 kN).

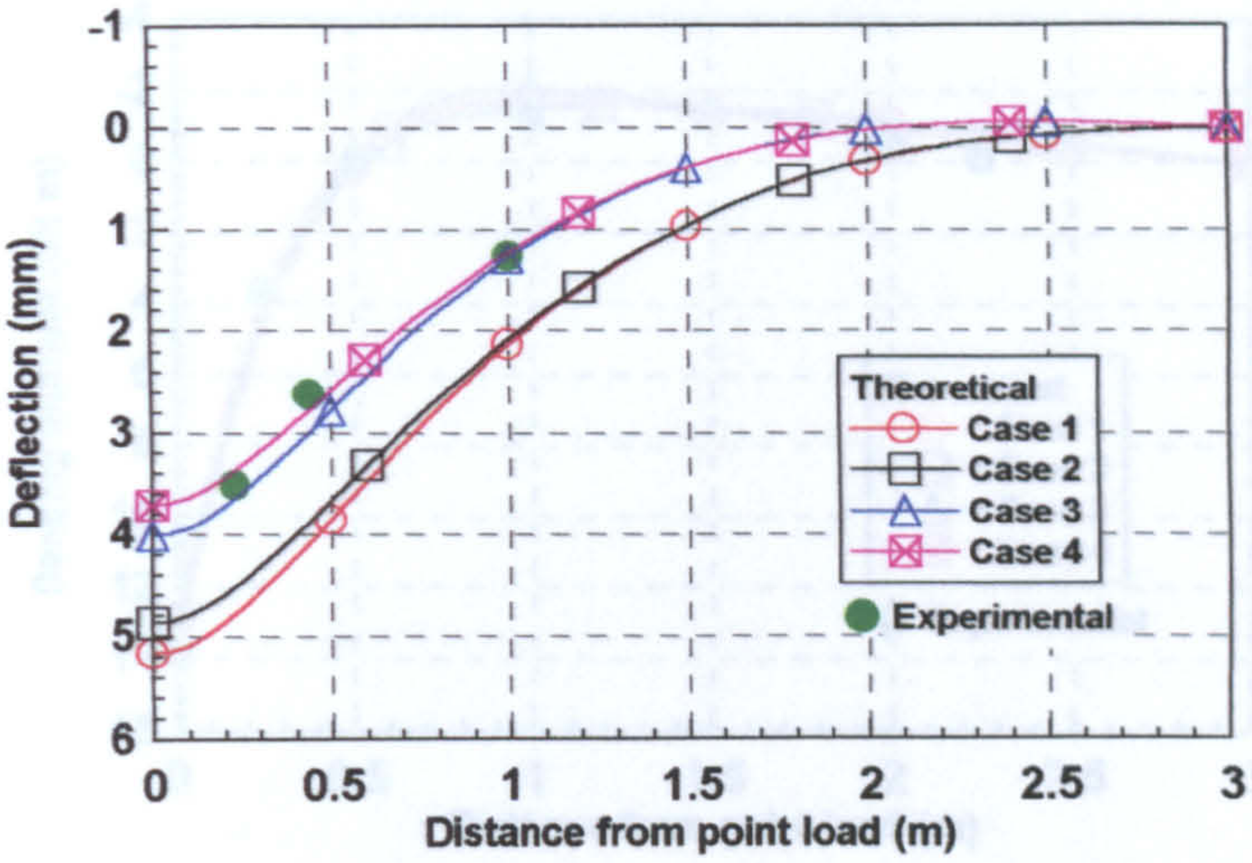

Fig. (8.26): Comparison between the experimental and theoretical deflections of the rail for test 3, (load = 98.38 kN).

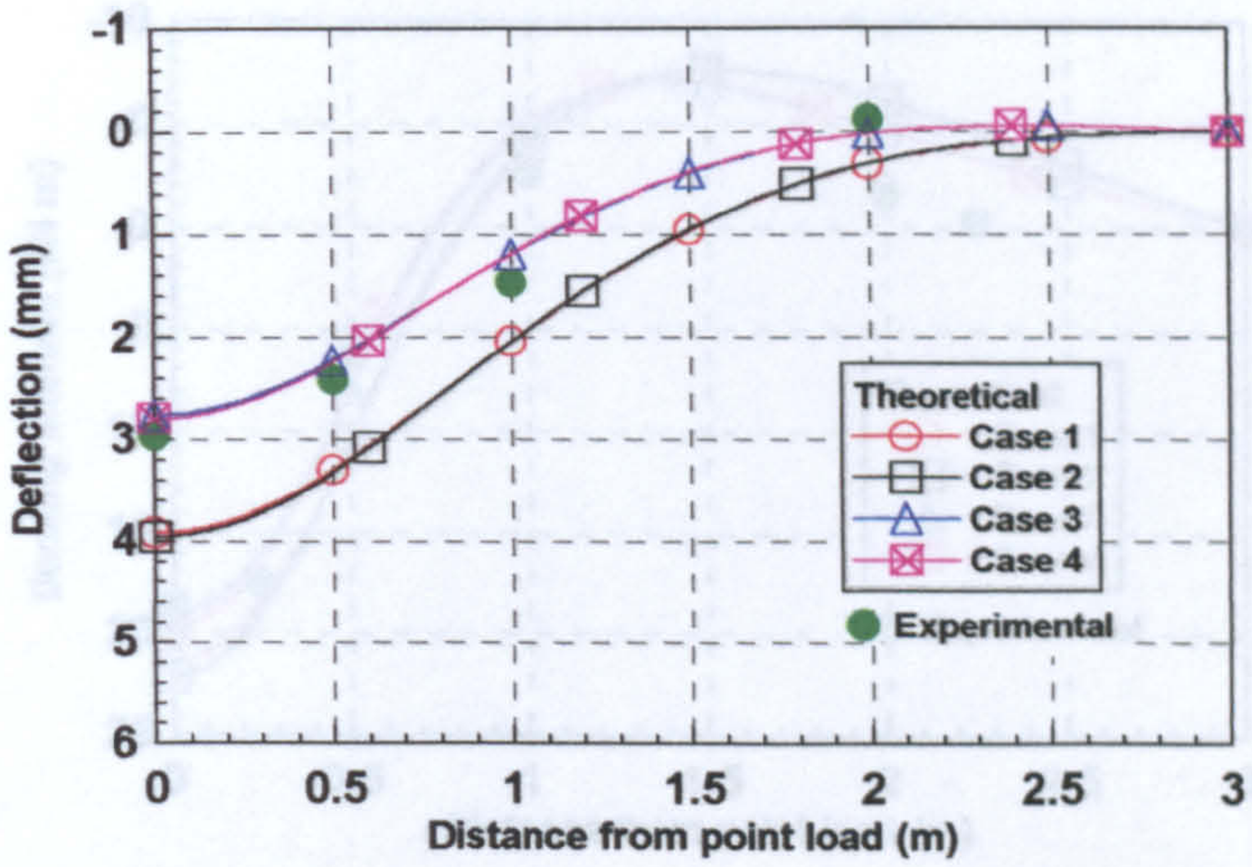

Fig. (8.27): Comparison between the experimental and theoretical deflections of the concrete trough for test 3, (load = 98.34 kN).

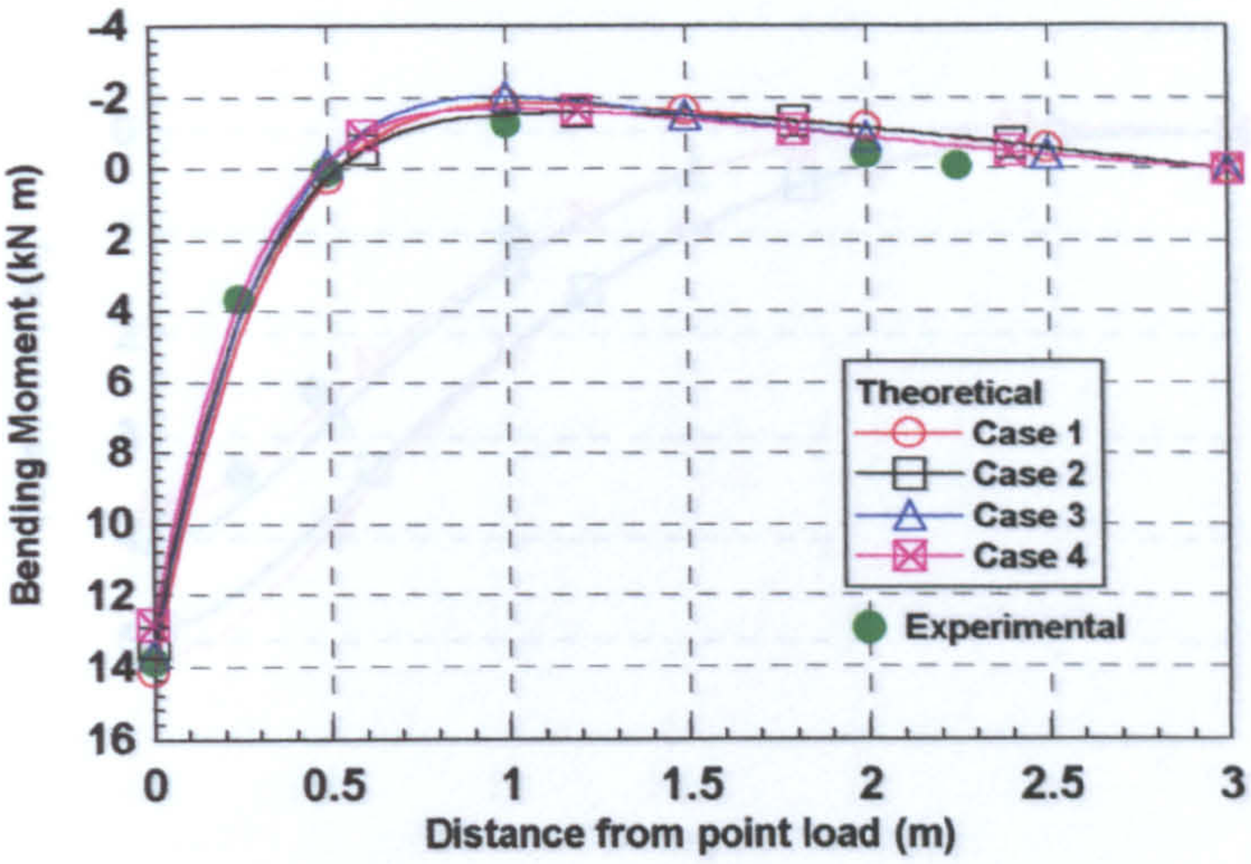

Fig. (8.28): Comparison between the experimental and theoretical bending moments of the rail for test 3, (load = 98.34 kN).

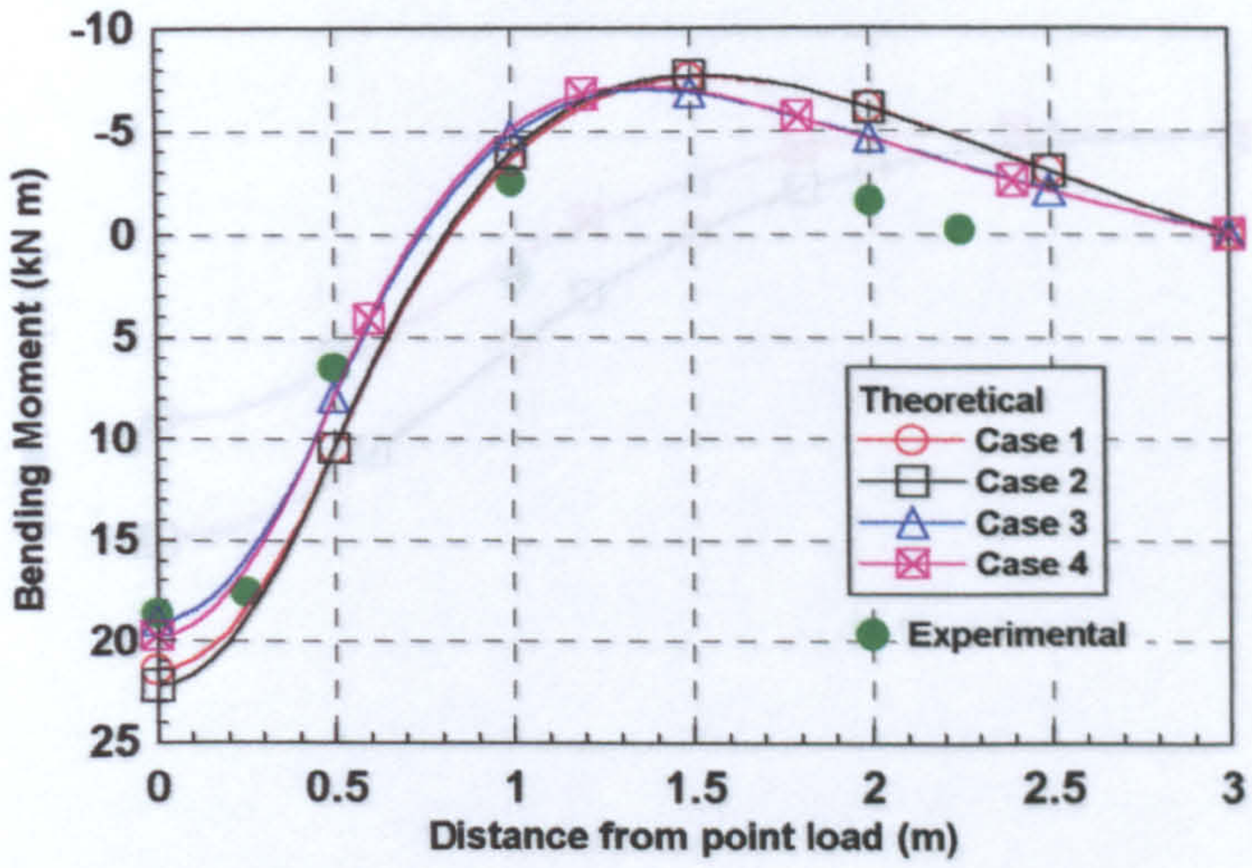

Fig. (8.29): Comparison between the experimental and theoretical bending moments of the concrete trough for test 3, (load = 98.34 kN).

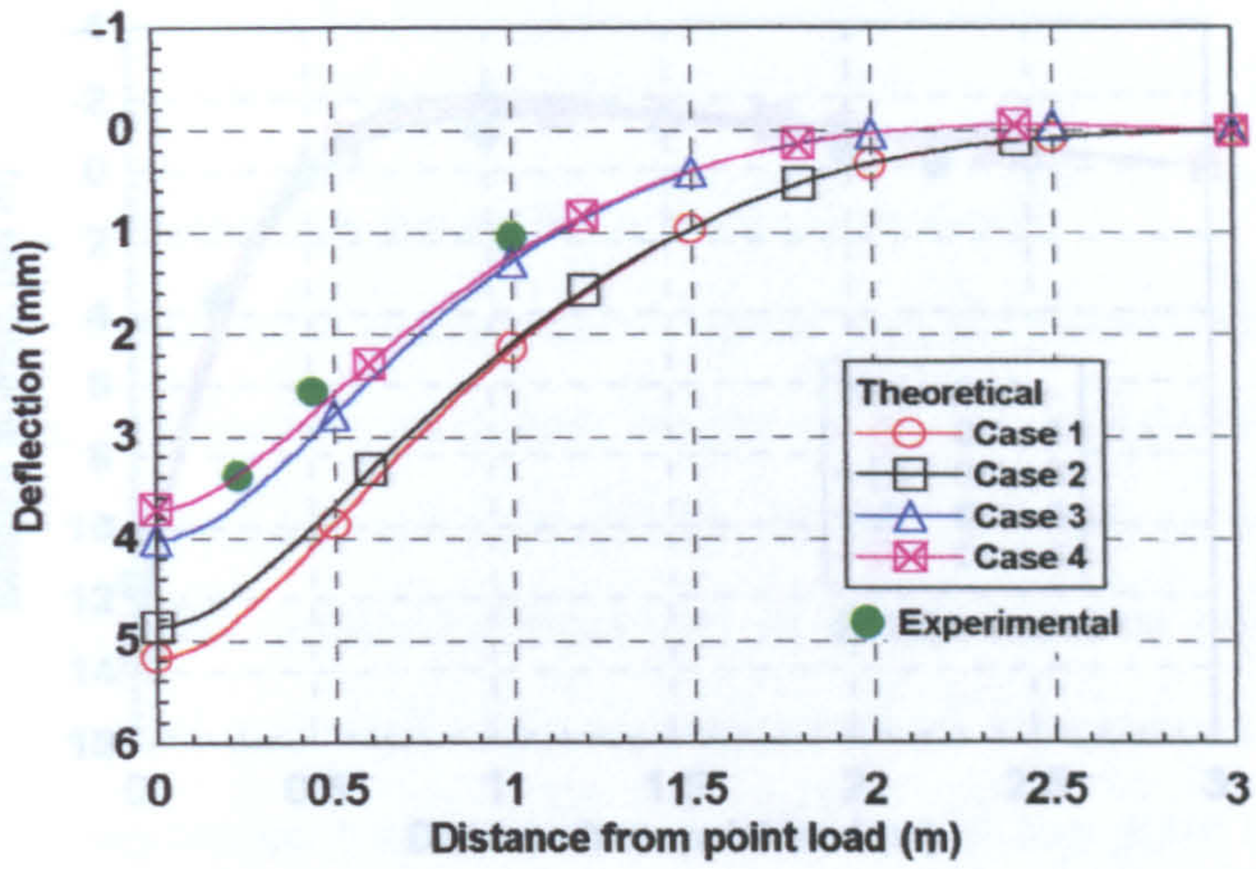

Fig. (8.30): Comparison between the experimental and theoretical deflections of the rail for test 4, (load = 98.21 kN).

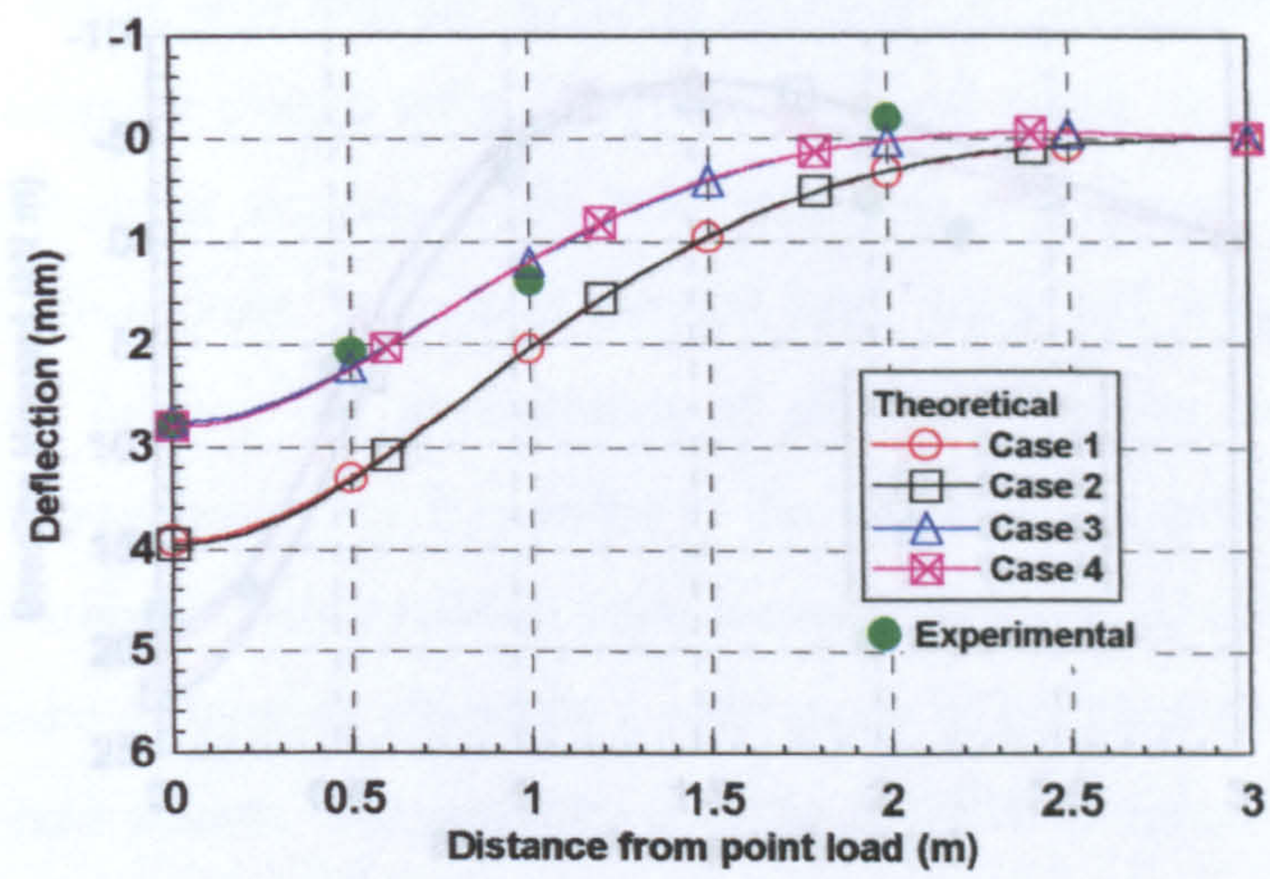

Fig. (8.31): Comparison between the experimental and theoretical deflections of the concrete trough for test 4, (load = 98.21 kN).

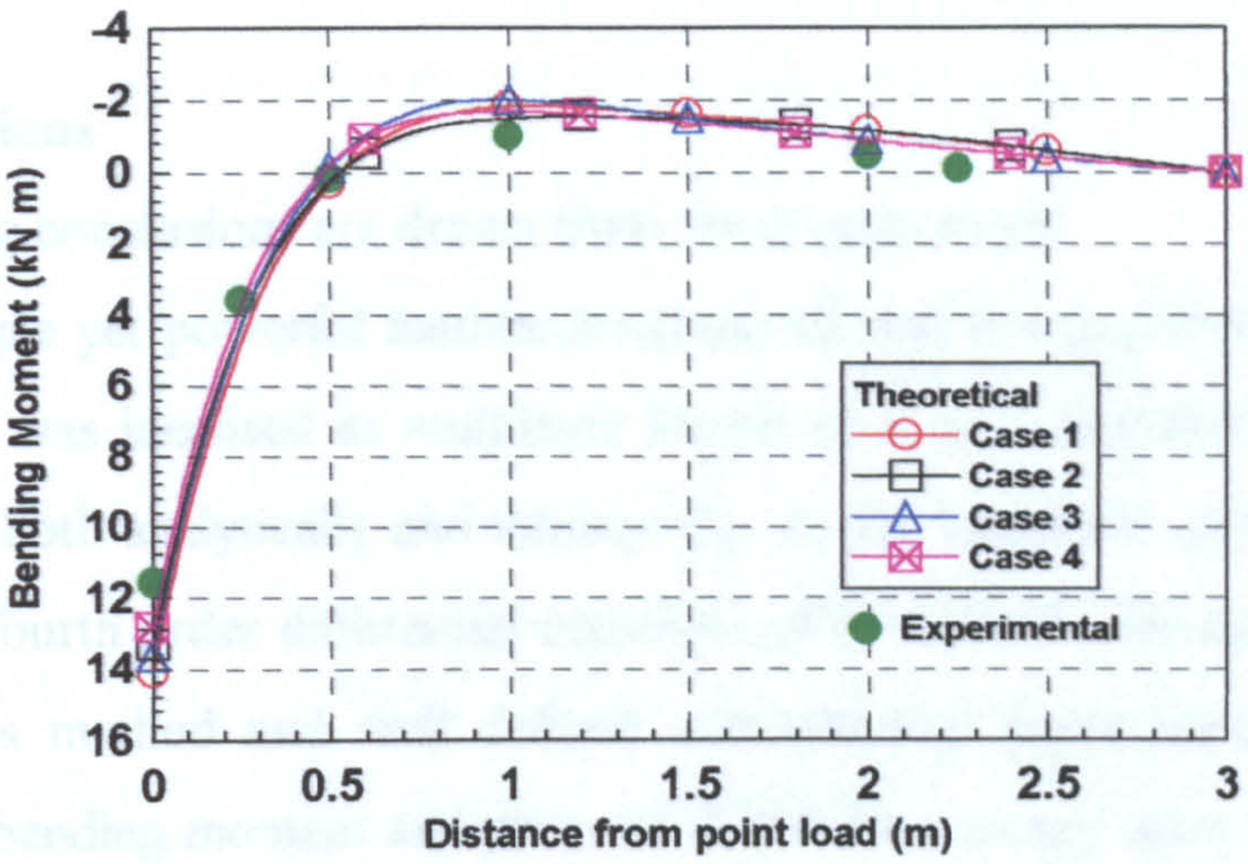

Fig. (8.32): Comparison between the experimental and theoretical bending moments of the rail for test 4, (load = 98.21 kN).

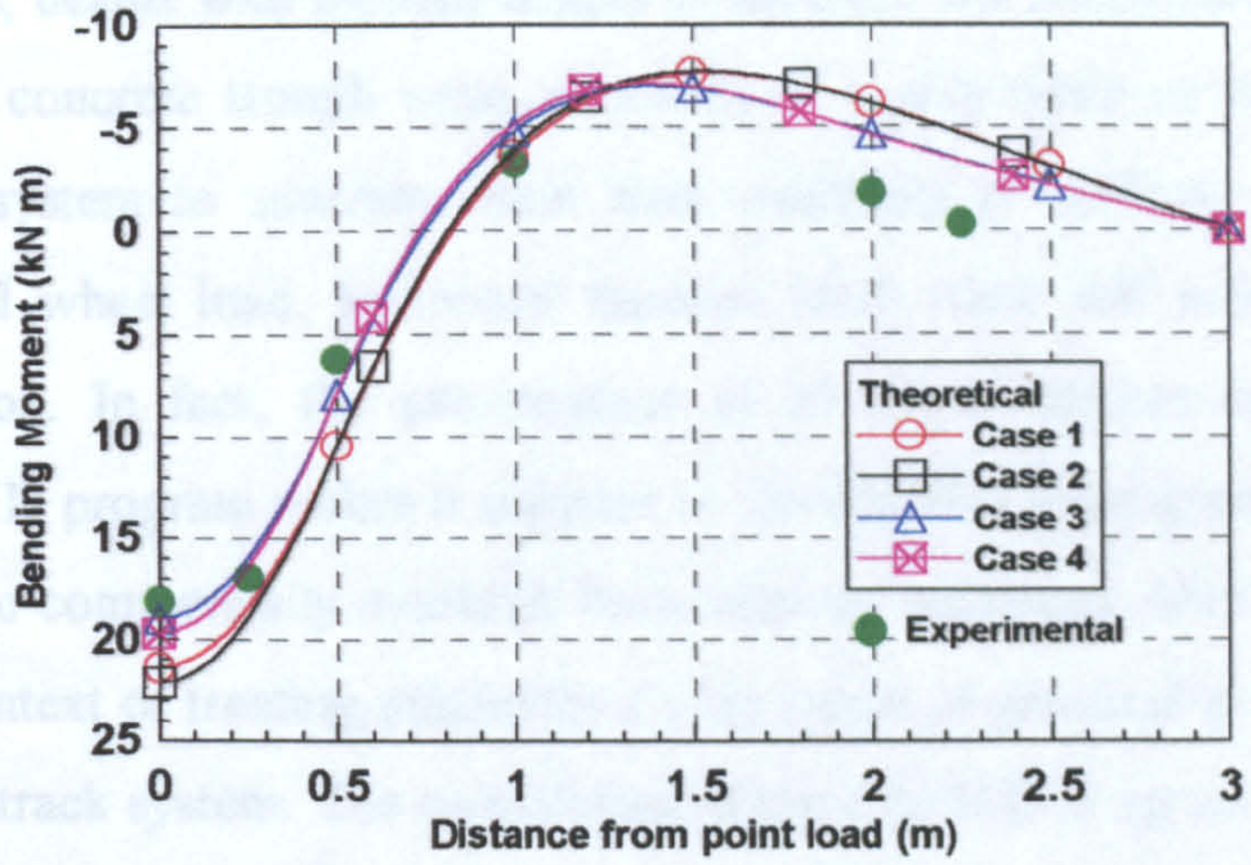

Fig. (8.33): Comparison between the experimental and theoretical bending moments of the concrete trough for test 4, (load = 98.21 kN).

CHAPTER NINE

CONCLUSIONS AND RECOMMENDATIONS

9.1 Conclusions

The following conclusions are drawn from the present work:

1. A simple yet powerful mathematical model was developed where the LR55 track system was idealised as multilayer beams on elastic foundations. This model was solved both analytically and numerically. In the analytical approach, the governing set of fourth order differential equations of the system was solved using a classical calculus method and well defined mathematical expressions for the deflection, shear, bending moment and pressure distribution at any point along the track were obtained. The computer program MLBOEF was developed for this purpose and it was coded in FORTRAN 77 for P.C. machines. In the numerical approach, a one dimensional finite element method was adopted where the rail and concrete trough were represented by conventional beam elements with three degrees of freedom per node, whereas the pad and track base were characterised by linear elastic springs. The computer program LR551D developed for this purpose was incorporated with special features namely: nonlinearity due to track base separation (uplift), beams with internal hinges to simulate the construction joints at the ends of the concrete trough units, existence of a soft patch or cavity underneath the track system to simulate track base weakness or collapse, combined effect of vertical wheel load, horizontal traction load, track self weight and temperature variation. In fact, the presentation of all these features simultaneously in the LR551D program makes it superior to the MLBOEF program (analytical solution) and the commercially available finite element packages ANSYS and ABAQUS in the context of treating efficiently a wide range of practical problems related to the LR55 track system. The correctness of the LR551D program was verified through comparing the results of a typical example with the MLBOEF, ANSYS and ABAQUS programs.

2. During the analysis phase, the behaviour of the LR55 track system was investigated under various boundary and loading conditions and for a range of pad and base moduli, from which the following points were concluded:

   a) The effect of wheel load is local and the deflection, bending moment and pressure distribution curves are only concentrated around a region where the load is applied and they diminish very quickly (exponentially) away from the load application. Consequently, multiple axle loads with axle spacing greater than 2.0 m have almost negligible effect on the track responses. As the modern rail vehicles have smaller axle load spacing around 2.0 m, examining the behaviour of the LR55 track system under a single wheel load might be regarded as sufficient and acceptable without affecting the accuracy of the results appreciably.

   b) The effect of track system self weight on the deflection, bending moment and pressure distribution of the track system is very insignificant. This is because the weight of the rail and concrete trough is so small compared to the applied wheel load. In addition, the self weight is uniformly distributed over the whole length, while the wheel load is concentrated at one point. However, the self weight of the track system, though small, is found to be very important whenever nonlinear analysis due to track base separation is to be taken into consideration, because the self weight acts as a precompression force that counteracts the uplift of the track. Otherwise the analysis gives incorrect results.

   c) In practice, the LR55 track system is very long, i.e. theoretically infinite. However, analysis of a 12 m track length for theoretical study or 6 m track length for experimental purposes is quite sufficient to give similar results to an infinite length.

3. A nonlinear optimisation technique based on the Complex method was adopted to find the minimum area of a pre-tensioned prestressed concrete trough section satisfying the serviceability and ultimate states requirements of BS 8110 (1985) and Tarmac Precast Concrete Limited for three critical loading and boundary conditions. These load cases are 1.0 m long cavity, 1.8 m length of soft base patch and combined effect of vertical load, horizontal traction load and temperature variation of ±25 °C. The design wheel load was 104.21 kN. The optimum concrete trough section was found to have a total width and depth of 390 and 180 mm respectively and provided with 6 tendons of 9.3 mm diameter 7-wire strand at the

bottom and similar 2 tendons at the top and shear links of 6 mm diameter at 100 mm centre to centre as. It was interestingly found out that the minimum area of the concrete trough section also resulted in a minimum cost of producing 1 m length of the concrete trough unit. The performances of the LR55 rail, elastomeric pad and track base were routinely examined and found to be satisfactory under the same critical load cases.

4. A number of static and non-destructive tests were carried out on a full-scale 6 m long track model including the case of 1 m collapsed foundation simulation. The results and information acquired from these experiments compared well with the theoretical solution using the purpose built one dimensional finite element analysis (LR551D program). The theoretical optimum design of the prestressed concrete trough section was also demonstrated through these tests since the induced tensile and compressive stresses remained within the allowable limits and hence no failure occurred to the concrete trough due to test load around 100 kN. The rail and elastomeric pad were found to behave adequately during all these tests. Therefore, this experimental work confidently ensured the safety of the proposed design of the LR55 track system and eventually validated the mathematical model developed for the LR55 track system as multilayer beams on elastic foundations. In addition, the experimental work provided a clear insight as to how the track system respond in practice through the general observation of the overall behaviour of the track model subjected to loading and boundary conditions that are similar to actual situation. Thus, the experimental work on a full-scale track specimen can be regarded as an invaluable extension and complementary to the theoretical study of the LR55 track system.

9.2 Recommendations

The recommendations for further research are summarised in the following in order to have a comprehensive coverage of the LR55 track system project:

1. The present work concentrates on the analysis and design of a straight and level LR55 track system. This implies that the effect of horizontal and vertical curvature is too small to be taken into consideration. However, it is common for the track system to negotiate sharp bends, tight curves and steep gradients in particular

within the city centre where road spaces are restricted. In such cases, the curvature of the track system cannot be ignored as significant centrifugal force and torsion will be induced in the track system due to its curvature and these forces might appreciably influence the response of the track components. The one dimensional finite element model developed in this work can be extended to tackle in and out-of-plane curved tracks. This can be achieved by using rail and concrete beam elements that have six degrees of freedom per node (three translations and three rotations) and attaching to each node up to six different type of springs (three translations and three rotations) to represent the pad and base resistances. An individual track element formed by the assembly of these elements is capable of taking into account the three dimensional effect of the load and track geometry, though it is one dimensional in nature, i.e. line element.

2. There is a need for research to investigate the behaviour of the LR55 track system at switches, crossings and turnouts which is believed to be a separate subject though it is part of the main LR55 track project. At these points, there are normally more than one rail seated on the same supporting concrete element. Therefore, a particular structure that will be different in shape, size and dimensions from the currently designed concrete trough section is required and hence needs to be designed appropriately.
3. The analysis of the LR55 track system carried out in this thesis is due to static loads only, in which the nominal axle load is augmented by a dynamic load factor to take into account the impact effect of the moving vehicles. Although this assumption is considered acceptable in the literature and is practised by various railway organisations due to its simplicity and the calculation time and space required, a dynamic analysis could provide more realistic results when the track system is subjected to various kinds of frequency excitations caused by traffic loads.
4. The existing mathematical model developed for the LR55 track system represents the base and pad resistances by linear elastic uniaxial springs. This only gives an indication of average stresses in the supporting pad and base foundations. Moreover, this model cannot determine the local effect of the load such as the stress concentration round the corners of the concrete trough or rail and the twisting effect due to eccentric load. However, such limitations can be addressed

by employing a three dimensional finite element method. In such cases, the material nonlinearity of the supporting soil due to stress-path dependent and visco-elastic behaviour of the elastomeric pad can be well represented using the actual material constitutive laws and the exact geometrical shapes of the rail and concrete trough can be utilised for better reflection of local effect of the load and stress distribution within the track component.

5. Fully instrumented field tests are required to conduct on a live trial of the LR55 track system to investigate the actual performance of the system under the running road and rail vehicles.
6. An investigation would be worthwhile to examine the formation and propagation of rail head corrugation in the LR55 track system, which is a major problem in conventional rail tracks, leading to uncomfortable riding of rail vehicles and the premature wear of the rail.
7. Among other important topics worth investigating are fatigue characteristics of the LR55 track components under repeated axle loads and the buckling behaviour (both elastic and elasto-plastic instability) of the LR55 track system in the vertical and lateral planes.

REFERENCES

Abeles, P. W. and Bardhan-Roy, B. K. (1981), "Prestressed Concrete Designer's Handbook", A Viewpoint Publisher.

ACI 318-71 (1971), "Building Code Requirements for Reinforced Concrete", American Concrete Institute Committee 318, Detroit, USA.

ACI 318-77 (1977), "Building Code Requirements for Reinforced Concrete", American Concrete Institute Committee 318, Detroit, USA.

Adegoke, C. W. (1979), "Elastic and Inelastic Response of Track Structures Under Train Loads", Ph.D. Thesis, State University of New York at Buffalo, USA.

ALH Systems Limited (1992), "Series Six: Polyurethane Encapsulated", Experimental Report, UK.

ALH Systems Limited (1996), "Series Six - Rail Embedment Material", Technical Data Sheet, Certificate No. 93./1965, UK.

Al-Khaiat, H. (1979), "Analysis of Beams on Elastic Foundations by the Initial -Value Method", M.Sc. Thesis, The Pennsylvania State University, USA.

Andam, K. A. and Knapton, J. (1980), "Optimum Cost Design of Precast Concrete Framed Structures", Engineering Optimisation, Vol. 5, pp. 41-50.

AREA (1980), "Stresses in Railroad Track – The Talbot Reports 1918-1940", Reprint of Progress Reports of Special Committee under the Chairmanship of Prof. A. N. Talbot, First Report 1918; Second 1920; Third 1923; Fourth 1925; Fifth 1930; Sixth 1934; Seventh 1942, American Railway Engineering Association, Washington DC, USA.

Arora, J. S. (1989), "Introduction to Optimum Design", McGraw-Hill Book Company.

Aydogan, M. (1995), "Stiffness Matrix Formulation of Beams with Shear Effect on Elastic Foundation", Proceedings of the ASCE, Journal of Structural Engineering, Vol. 121, No. 9, Sep., pp. 1265-1270.

Balfour, J. A. D. (1986), "Computer Analysis of Structural Frameworks", William Collins Sons & Co. Ltd.

Benham, P. P. and Warnock, F. V. (1976), "Mechanics of Solids and Structures", Pitman Publishing Limited.

Baxter, M. I. (1993), "Sleepers- Single or Twin?", Track Report, The Journal of Pandrol International, pp. 6-8.

Baxter, M. I. (1997), "Modern Non-Ballasted Track Design to Reduce Railway Noise and Vibration" Proceedings of the International Seminars on Improving Vehicle and Track Performance, Kuala Lumpur, Malaysia, 14-15 May, Paper 2.1, pp. 1-5.

Boak, J. G. (1995), "South Yorkshire Supertram: route and civil works", Proceedings of the Institution of Civil Engineers, Transport, Vol. 111, Feb., pp. 24-32.

Bowles, J. E. (1988), "Foundation Analysis and Design", 4th Edition, McGraw-Hill Book Company.

Box, M. J. (1965), "A New Method of Constrained Optimisation and a Comparison with Other Methods", Computer Journal, Vol. 8, pp. 42-52.

British Steel (1996), "Structural Sections to BS 4: Part 1 and BS 4848: Part 4, Sections, Plates and Commercial Steels", Published by British Steel plc, Cleveland, UK.

British Steel Track (1992), "The Track Handbook", Published by British Steel Track Products, Cumbria, UK.

Browne, F. J. (1988), "Concrete Sleepers", Journal of Permanent Way Institution, Vol. 106, Part 3, pp. 249-256.

BS 5896 (1980), "High Tensile Steel Wires and Strands for the Prestressing of Concrete", British Standards Institution, London, UK.

BS 11 (1985), "Railway Rails", British Standards Institution, London, UK.

BS 8110 (1985), "Structural Use of Concrete, Part 1: Code of Practice for Design and Construction, Part 2: Code of Practice for Special Circumstances", British Standards Institution, London, UK.

Buckner, C. D. (1995), "A Review of Strand Development Length for Pre-tensioned Concrete Members", PCI Journal, Vol. 40, No. 2, March/April, pp. 84-105.

Bunday, B. (1984), "Basic Optimisation Methods", Edward Arnold Ltd.

Chana, P. (1984), "An Evaluation of the Factors Contributing to Size Effects in Concrete", Proceedings of a Seminar on "Design of Concrete Structures - The Use of Model Analysis", Edited by Clarke, J. L., Garas, F. K. and Armer, G. S. T., Elsevier Applied Science Publishers, Building Research Establishment, Watford, UK, "9-30 Nov., pp. 105-116.

Chang, S. C., Clement, W. A. and Selig, E. T. (1980), "GEOTRACK Model for Railroad Track Performance" Proceedings of the ASCE, Journal of the Geotechnical Engineering, Vol. 106, No. GT11, Nov., pp. 1201-1218.

Cheung, Y. K. and Nag, D. K. (1968), "Plates and Beams on Elastic Foundation-Linear and Nonlinear Behaviour", Geotechnique, Vol. 18, No. 2, June, pp. 250-260.

Chou, K (1977), "Optimum Reinforced T-Beam Sections", Proceedings of the ASCE, Journal of the Structural Division, Vol. 110, No. ST8, August, pp. 1605-1616.

Clark, D. K. (1894), "Tramways: Their Construction and Working with Special Reference to the Tramways of the United Kingdom", Published by Crosby Lockwood Ltd.

Clarke, C. W. (1957), "Track Loading Fundamentals", Railway Gazette, Vol. 106, Part 1, pp. 45-48; Part 2, pp. 103-107; Part 3, pp. 157-160; Part 4, pp. 220-221; Parts 5, pp. 274-278; Part 6, pp. 335-336; Part 7, pp. 478-481.

Cohn, M. Z. and MacRae, A. J. (1984), "Optimisation of Structural Concrete Beams", Proceedings of the ASCE, Journal of Structural Engineering, Vol. 110, No. 7, July, pp. 1573-1588.

Cope, G. H. (1993), "British Railway Track, Design Construction and Maintenance", Published by The Permanent Way Institution, 6th Edition, UK.

Cope, R. J., Sawko, F. and Tickell, R. G. (1982), "Computer Methods for Civil Engineers", McGraw-Hill Book Company.

CSA/NBC (1977), "Code for the Design of Concrete Structures for Buildings", Joint Committee on Reinforced Concrete Design, (CAN3-A23.3-M77), Canadian Standards Association, Ontario, Canada.

Desai, C. S. and Siriwardane, H. J. (1982), "Numerical Models for Track Support Structures" Proceedings of the ASCE, Journal of the Geotechnical Engineering, Vol. 108, No. GT3, March, pp. 461-480.

Dixon, L. C. W. (1972), "Nonlinear Optimisation", The English Universities Press Ltd.

Dulacska, E. (1992), "Soil Settlement Effects on Buildings", Development in Geotechnical Engineering, 69, Elsevier Science Publisher.

Esveld, C. (1989), "Modern Railway Track", MRT-Productions.

Fastenrath, F. (1981), "Railroad Track, Theory and Practice, Material Properties, Cross Sections, Welding and Treatment", Translated to English by Walter Grant, Frederick Ungar Publishing Co.

Feiring, B. R. (1986), "Linear Programming: An Introduction", Series: Quantitative Applications in the Social Sciences, A Sage University Paper 60, Sage Publication Inc.

FIP (1987), "Concrete Railway Sleepers", Thomas Telford Ltd.

Friel, L. L. (1974), "Optimum Singly Reinforced Concrete Sections", ACI Journal, Part 11, Nov., pp. 556-558.

Frederick, C. O. and Round, D. J. (1984), "Vertical Track Loading", Proceedings of a Conference on Track Technology, Nottingham, UK, 11-13 July, pp. 135-149.

Gent, A. N. (1992), "Engineering with Rubber: How to Design Rubber Components", Hanser Publishers.

Gere, J. M. and Timoshenko, S. P. (1985), "Mechanics of Materials", 2nd Edition, PWS Engineering Publishers.

Goble, G. G. and Lapay, W. S. (1971), "Optimum Design of Prestressed Beams", ACI Journal, Vol. 68, No. 9, Sep., pp. 712-718.

Gregory, M. S. (1971), "History and Development of Engineering", Longman Group Limited.

Hanna, A. N. (1979), "Prestressed Concrete Ties for North American Railroads", PCI Journal, Vol. 24, Part 5, Sep./Oct., pp. 32-61.

Haque, M. I. (1985), "Optimal Design of Plane Frames by the Complex Method", Computers & Structures, Vol. 20, No. 1-3, pp. 451-456.

Harris, B. and Bunsell, A. (1977), "Structure and Properties of Engineering Materials", Longman Group Limited.

Harrison, H. B. (1973), "General Computer Analysis of Beams on Elastic Foundations", Proceeding of Institution of Civil Engineers, Vol. 55, Part 2, Sep., pp. 605-618.

Hay, W. W. (1982), "Railroad Engineering", 2nd Edition, John Wiley & Sons Inc.

Himmelblau, D. M. (1972), "Applied Nonlinear Programming", McGraw-Hill Book Company.

Hetenyi, M. (1946), "Beams on Elastic Foundation", University of Michigan Press.

Hulse, R. and Mosley, W. H. (1987), "Prestressed Concrete Design by Computer", Macmillan Education Ltd.

IS:1343 (1960), "Indian Standard Code of Practice for Prestressed Concrete", Indian Standard Institution, New Delhi, India.

IS:784-1959 (1970), "Indian Standard Specifications for Prestressed Concrete Pipes", Indian Standard Institution, New Delhi, India.

Iyengar, N. G. and Gupta, S. K. (1981), "Programming Methods in Structural Design", Edward Arnold Publishers Ltd.

Kirby, R. S., Withington, S., Darling, A. B. and Kilgour, F. G. (1956), "Engineering in History", McGraw-Hill Book Company.

Kirkland, C. J. (1995), "Engineering the Channel Tunnel", E & FN SPON.

Kirsch, U. (1973), "Optimum Design of Prestressed Plates", Proceedings of the ASCE, Journal of the Structural Division, Vol. 99, No. ST6, June, pp. 1075-1090.

Kirsch, U. (1981), "Optimum Structural Design", McGraw-Hill Book Company.

Kong, F. K. (1978), "Bending, Shear and Torsion", In Development in Prestressed Concrete, Edited by Sawko, F., Vol. 1, Applied Science Publishers Ltd, pp. 1-68.

Kong, F. K. and Evans, R. H. (1989), "Reinforced and Prestressed Concrete", 3rd Edition, Van Nostrand Reinhold International.

Lau, C. M., Fwa, T. F. and Paramasivam, P. (1994), "Interface Shear Stress in Overlaid Concrete Pavement", Proceedings of the ASCE, Journal of Transportation Engineering, Vol. 120, No. 2, March/April, pp. 163-191.

Laursen, H. I. (1978), "Structural Analysis", Second Edition, McGraw-Hill Book Company.

Lesley, L. (1989), "A New LRT Track System", Proceedings of Light Rail 89 Conference, Bristol, UK., Nov., pp. 205-212.

Lesley, L. (1991), "A New Light Rail Track System and the 'Lesley' Low-Profile Rail", Modern Tramway and Light Rail Transit, Vol. 54, No. 645, Sep., pp. 305-311.

Lesley, L. (1993), "Light Rail Transit Development in the UK", Rail Engineering International, Vol. 22, No. 3, pp. 2-4.

Lesley, L. (1994), "Light Rail Tracks - A World Review", Urban Transport Report.

Lesley, L. and Al-Nageim, H. (1996), "Static and Dynamic Load Testing of a New Low Height Rail System", Proceedings of the Institution of Civil Engineers, Transportation, Vol. 117, Feb., pp. 2-5.

Levy, R. and Lev, O. (1987), "Recent Developments in Structural Optimisation", Proceedings of the ASCE, Journal of the Structural Engineering, Vol. 113, No. 3, Sep., pp. 1939-1962.

Lin, T. Y. and Burns, N. H. (1995), "Design of Prestressed Concrete Structures", 3rd. Edition, SI Version, John Wiley & Sons Inc.

Lipson, S. L. and Gwin, L. B. (1977), "The Complex Method Applied to Optimal Truss Configuration", Computers & Structures, Vol. 7, pp. 461-468.

Liventon, Z. (1949), "Elastic Foundations Analysed by the Method of Redundant Reactions", Transactions of the ASCE, Vol. 114, pp. 40-52.

Livesley, R. K. (1965), "The Automatic Design of Structural Frames", Quarterly Journal of Mechanical Applied Mathematics, Vol. 9, pp. 257-278.

Lounis, Z. and Cohn, M. Z. (1993), "Optimisation of Precast Prestressed Concrete Bridge Girder Systems", PCI Journal, Vol. 38, No. 4, July/August, pp. 60-79.

Lund, S. (1974), "Application of Optimisation Methods within Structural Design-Problem Formulations", Computers & Structures, Vol. 4, pp. 221-232.

Macleod, I. A. (1990), "Analytical Modelling of Structural Systems", Ellis Horwood Limited, UK.

Majid, K. I. (1974), "Optimum Design of Structures", Newnes-Butterworth.

Malter, H. F. (1960), "Numerical Solution for Beams on Elastic Foundations", Transactions of the ASCE, Vol. 125, pp. 757-791.

Miranda, C. and Nair, K. (1966), "Finite Beams on Elastic Foundation", Proceedings of the ASCE, Journal of the Structural Division, Vol. 92, No. ST2, pp. 131-142.

Moe, J. (1974), "Fundamentals of Optimisation", Computers & Structures, Vol. 4, pp. 95-113.

Mohammad, F. A. (1997), "Some Experimental Work on Series Six Elastomer", laboratory Report carried out at Liverpool John Moores University on behalf of ALH Systems Limited.

Morgan, B. (1971), "Civil Engineering: Railways", Longman Group Limited.

Muhr, A. and Gough J. (1991), " Load Deflection and Dynamic Testing of 300 mm - 25 mm square pads to assess the effect of Shape Factor for ICOSIT KC 330/UK Material", Laboratory Report RC4290, Rubber Consultants, SIKA LIMITED, April.

Mûller, R. K. (1984), "Microconcrete for Structural Model Analysis", Proceedings of a Seminar on "Design of Concrete Structures - The Use of Model Analysis", Edited by Clarke, J. L., Garas, F. K. and Armer, G. S. T., Elsevier Applied Science Publishers, Building Research Establishment, Watford, UK, "9-30 Nov., pp. 1-9.

Naaman, A. E. (1976), "Minimum Cost Versus Minimum Weight of Prestressed Slabs", Proceedings of the ASCE, Journal of the Structural Division, Vol. 102, No. ST7, July, pp. 1493-1505.

Naaman, A. E. (1982), "Prestressed Concrete Analysis and Design, Fundamentals", McGraw-Hill Book Company.

Naaman, A. E. (1982), "Optimum Design of Prestressed Concrete Tension Members", Proceedings of the ASCE, Journal of the Structural Division, Vol. 108, No. ST8, August, pp. 1722-1738.

Nagdi, K. (1995), "Rubber as an Engineering Material: Guideline for Users", Hanser Publishers.

Nilson, A. H. and Winter, G. (1991), "Design of Concrete Structures", 11th Edition, McGraw-Hill Book Company.

Profillidis, V. A. (1986), "Applications of Finite Element Analysis in the Rational Design of Track Bed Structures", Computers & Structures, Vol. 22, No. 3, pp. 439-443.

Przemieniecki, J. S. (1968), "Theory of Matrix Structural Analysis", McGraw-Hill Book Company.

Rao, S. S. (1978),"Optimisation, Theory and Applications", Wiley Eastern Limited.

Raymond, G. P. (1991), "Analysis of Rail Track Structures (ARTS)", Computers & Structures, Vol. 41, No. 6, pp. 1403-1409.

Rees, D. W. A. (1990), "Mechanics of Solids and Structures", McGraw-Hill Book Company.

Reinschmidt, K. F. and Norabhoompipat, T. (1975), "Structural Optimisation by Equilibrium Linear Programming", Proceedings of the ASCE, Journal of the Structural Division, Vol. 101, No. ST4, April, pp. 921-938.

Roberts, D. (1996), "Ultimo Pyrmont Light Rail Project: Technical and Design Aspects", Internal Report, GHD - Transmark Pty Ltd, Australia, May, pp. 1-19.

Rolt, L. T. G. (1968), "Railway Engineering", MacMillan & Co Ltd.

Sabnis, G. M., Harris, G. H., White, r. N. and Mirza, M. S. (1983), "Structural Modelling and Experimental techniques", Prentice-Hall Inc.

Scott, D. B. (1979), "Concrete Support for Railway Track: Sleepers", Proceedings of the Institution of Civil Engineers, Part 1, Vol. 661, Nov., pp. 635-648.

Selig, E. T. and Waters, J. M. (1994), "Track Geotechnology and Substructure Management", Thomas Telford Services Ltd.

Selvadurai, A. P. S. (1979), "Elastic Analysis of Soil-Foundation Interaction", Developments in Geotechnical Engineering Vol. 17, Elsevier Science Publisher.

Sika Limited (1990), "SikaRail KC 330: LRT Grades", Technical Data Sheet, UK.

Sikka, N. K. and Singh, S. P. (1972), "Some Aspects of Design of Monoblock Prestressed Concrete Sleepers", Proceedings of International Symposium on Prestressed Concrete Pipes, Poles, Pressure Vessels and Sleepers, Madras, India, Vol. 1, pp. 1-24.

Siriwardane, H. J. (1980), "Nonlinear Soil-Structure Interaction Analysis for One-, Two-, and Three Dimensional Problems Using Finite Element Method", Ph.D. Thesis, Verginia Polytechnic and State University, USA.

Smith, G. N. (1990), "Elements of Soil Mechanics", 6th Edition, Blackwell Science Ltd.

Sperring, D. G. (1992), "Practical Track Design", Paper 4.3.4, Fourth R.I.A. Track Sector Course, UK.

Srinath, L. S. " (1983), "Linear Programming: Principles and Applications", MacMillan Limited.

Stewart, H. E. and O'Rourke, T. D. (1988), "Load Factor Method for Dynamic Track Loadings" Proceedings of the ASCE, Journal of Transportation Engineering, Vol. 114, No. 1, Jan., pp. 21-39

Tabatabai, H. and Dickson, T. (1993), "The History of the Prestressing Strand Development Length Equation", PCI Journal, Vol. 38, No. 6, Nov./Dec., pp. 64-75.

Tayabji, S. D. (1976), "Consideration in the Analysis of Conventional Railway Track Support Systems", Ph.D. Thesis, University of Illinois, USA.

Tayabji, S. D. and Thompson, M. (1976), "Consideration in the Analysis of Conventional Railway Track Support Systems", Proceedings the of ASCE, Journal of Transportation Engineering, Vol. 103, No. TE2, March, pp. 279-292.

Taylor, H. P. J. (1992), "Concrete Sleepers", Paper 4.4, Section 4: Procurement, Supply and Manufacture, Costain Dow Mac Ltd., Track Sector Course, UK.

Taylor, H. P. J. (1993), "The railway Sleeper: 50 Years of Pre-tensioned Prestressed Concrete", The Structural Engineer, Vol. 71, No. 16/17, Aug., pp. 281-295.

Thakkar, M. C. and Rao, J. K. S. (1974), "Optimal Design of Prestressed Concrete Pipes Using Linear Programming", Computers & Structures, Vol. 4, pp. 373-380.

Thompon, G. E. (1971), "Linear Programming: An Elementary Introduction", MacMillan Limited.

Timoshenko, S. and Krieger, S. W. (1959), "Theory of Plates and Shell", 2nd Edition, McGraw-Hill Book Company.

Timoshenko, S., and Langer, B., F. (1932), "Stresses in Railroad Track", Transaction of the ASME, Vol. 54, pp. 277-302.

Ting, B. Y. (1982), "Finite Beams on Elastic Foundation with Restraints", Proceedings of the ASCE, Journal of the Structural Division, Vol. 108, No. ST3, pp. 611-621.

Ting, B. Y. and Mockry, A. M. (1985), "Beam on Elastic Foundation Finite Element", Proceedings of the ASCE, Journal of the Structural Engineering, Vol. 110, No. 10, Oct., pp. 2324-2339.

Tulloch, M. (1997), "Soil Reinforcement under Building Foundations", Final Year Reassert Project (BLTCE327), School of Built Environment, Liverpool John Moores University, U.K.

Uzan, J., Livneh, M. and Eshed, Y. (1978), "Investigation of Adhesion Properties Between Asphalt Concrete layers", Proceedings of the Association of Asphalt Paving Technologists, Vol. 47, pp. 495-521.

Vandenbril, G. (1997), "The first LRT System in Kuala Lumpur, Malaysia", Internal Report, Sistem Transit Aliran Ringan Sdn. Bhd., Malaysia.

Vanderplaats, G. N. (1982), "Structural Optimisation - Past, Present, and Future", AIAA Journal, Vol. 20, No. 7, pp. 992-1000.

Weber, J. W. (1969), "Concrete Crossties in the United States", PCI Journal, Vol. 14, No 1, Feb, pp. 46-61.

Williams, K. (1969), "Linear Programming: The Simplex Algorithm", Longmans Limited.

Zia, P. and Mostafa, T. (1977), "Development Length of Prestressing Strands", PCI Journal, Vol. 22, No. 2, Sep./Oct., pp. 54-65.

Zienkiewicz, O. C. (1977), "The Finite Element Method", 3rd Ed., McGraw-Hill Book Company.